Table of Contents

Acknowledgements

List of Abbreviations

2-CA	2-Cyanoacetamide
µTAS	Micro total analysis system
[^{18}F]FDG	2-Deoxy-2-[^{18}F]fluoro-D-glucose
[^{18}F]FDM	2-Deoxy-2-fluoro-D-mannose
[^{18}F]FECH	N-(2-fluoroethyl)-2-hydroxy-N,N-dimethyl-, chloride
[^{18}F]EtOTs	1-Fluoro-2-(tosyloxy)ethane; 2-Fluoroethyl 4-methylbenzenesulfonate
[^{18}F]FLT	3'-Deoxy-3'-[^{18}F]-fluorothymidime
[^{18}F]FMISO	1-(2-Nitro-imidazolyl)-3-[^{18}F]fluoro-2-propanol
[^{18}F]SFB	N-Succinimidyl 4-[^{18}F]-fluorobenzoate
[^{18}F]Flumazenil	Ethyl 12-fluoro-8-methyl-9-oxo-2,4,8-triazatricyclo tetradeca-1(10),3,5,11,13-pentaene-5-carboxylate
[^{18}F]Dopa	3-(2-Fluoro-[^{18}F]-4,5-dihydroxyphenyl)-L-alanine
A	Activity (s^{-1})
A$_s$	Specific activity (Bq·g^{-1})
ACN	Acetonitrile
AE	Anion exchange
APTES	(3-Aminopropyl)triethoxysilane
B	Magnetic flux density (T)
Bq	Becquerel
C	Coulomb (A·s^{-1})
CE	Cation exchange
Ci	Curie

c	Speed of light in vacuum (2.997925×10^8 m·s^{-1})
d	Depth of a channel (m)
DNA	Deoxyribonucleic acid
CCD	Charge-coupled device
CEC	Capillary electrochromatography
CIDG	2-Chloro-2-deoxy-glucose
CT	Computed tomography
d.c.y.	Decay corrected yield
DMAE	*N,N*-dimethylaminoethanol
diMM	*N,N*-dimethylmorpholinium
diMMCl	*N,N*-dimethylmorpholinium chloride
EtDt	1,2-Bis(4-methylbenzenesulfonyloxy)ethane
EOF	Electroosmotic flow
eV	Electron Volts ($1.602\ 189 \times 10^{-19}$ Joules)
fRe	Coefficient of friction
FEMM	Finite Element Method Magnetic
FDTS	Trichloro (1*H*, 1*H*, 2*H*, 2*H*-perfluorooctyl) silane
FID	Flame ionisation detection
GC	Gas chromatography
H	Magnetic field (A m^{-1})
HPAEC	High performance anion exchange chromatography
HPLC	High performance liquid chromatography
IC	Ion chromatography
IR	Infra-red spectroscopy
IV	Intravenous

K2.2.2	4,7,13,16,21,24-Hexaoxa-1, 10-diazabicyclo [8.8.8]-hexacosane (kryptofix)
L	Characteristic length (m)
m	Mass (kg)
M	Molar concentration ($mol \cdot L^{-1}$)
M	Magnetisation ($A\ m^{-1}$)
M$_r$	Magnetic remanence ($A\ m^{-1}$)
Mannose triflate	1,3,4,6-Tetra-*O*-acetyl-2-*O*-trifluoro-methanesulfonyl-beta-*D*-mannopyranose
m$_u$	Mass unit ($1.660\ 566\ 10^{-27}$ kg)
meq	Milliequivalent
N.C.A.	Non Carrier Added
N$_{AV}$	Avogadro's number ($6.022 \cdot 10^{23}$)
Nd-Fe-B	Neodymium-iron-boron
J	Joule ($kg \cdot m^2 \cdot s^{-2}$)
OTS	Octadecyltrichlorosilane
Δp	Pressure drop (Pa)
PBS	Phosphate buffered saline
PDMS	Polydimethylsiloxane
PEEK	Poly(ether ether ketone)
PET	Positron Emission Tomography
ppb	Parts per billion
ppm	Parts per million
PS	Polystyrene
PS-DVB	Polystyrene - divinylbenzene

P.T.C.	Phase transfer catalyst
PTFE	Poly(tetrafluoroethylene)
QAS	Quaternary ammonium silane (Dimethyloctadecyl [3-(trimethoxysilyl)propyl]ammonium chloride)
QC	Quality control
r	Radius of a particle (m)
rh	Hydraulic diameter of a channel (m)
R	Gas constant (8.314472 J K^{-1} mol^{-1})
R_Φ	Flow resistance in a microchannel (kg m^{-4} s^{-1})
RCY	Radiochemical yield
RCP	Radiochemical purity
Re	Reynolds number
SPE	Solid phase extraction
SAM	Self assembled monolayer
SPECT	Single photon emission computed tomography
t	Time (s)
T	Temperature (K or °C)
TLC	Thin layer chromatography
$TBAHCO_3$	Tetrabutylammonium bicarbonate
w	Width of a channel (m)
V	Volume (m^3)
υ	Velocity (m·s^{-1})
λ	Decay constant (s^{-1})
x	Distance (m)
Φ	Volume flow rate (m^3 s^{-1})

μ   Permeability (H m^{-1})

Abstract

Positron Emission Tomography (PET) is a non-invasive imaging method which enables to obtain both molecular and biochemical information of physiological processes *in vivo*, which means that PET imaging shows the chemical functioning of organs and tissues in a living subject. In recent years microfluidic lab-on-a-chip devices have been explored as a promising alternative for radiotracer synthesis due to benefits such as (i) superior control over reaction conditions leading to high yields and conversion rates, (ii) reduced reagent consumption and radioactive waste production as well as (iii) potential for automation with minimised shielding requirement. That said, most devices presented so far have focused on the synthesis of the radiotracer, with relatively little emphasis on the integrated devices that perform activation, synthesis and purification steps in an automated fashion. FDG (fluorodeoxyglucose) is one of the most widely used radiopharmaceuticals in Positron Emission Tomography (PET). Moreover the availability of several other PET radionuclides makes fluorine-18 (^{18}F) the most predominant in the fields of oncology and neuroscience.

The aim of the Radiochemistry on chip (ROC) project was to develop such an integrated lab-on-chip device and, in particular, here results for on-chip pre-concentration of fluoride, together with some preliminary results on the removal of Kryptofix (K2.2.2) and the purification of fluoroethyl-dimethyl-2-hydroxy-ethylammonium (FECH) are presented. Here in, three microfluidic modules for fluoride pre-concentration are described, the first employs a dam structure, the second and the third magnetic forces. In the final part of the thesis, preliminary results on the purification of fluoroethylcholine (FECH) and a suitable detection method for Kryptofix (K2.2.2) are reported.

Firstly, the design, fabrication and implementation of a glass microfluidic device for recovery of [^{18}F] and [^{19}F]fluoride ions is described. The device was initially tested with non radioactive [^{19}F]fluoride ions and shown to repeatedly trap and elute > 95% fluoride over 40 successive experimental runs with no decrease in efficiency. The same device was then tested for the trapping and release of [^{18}F]fluoride ions, again over 20 experiments were executed with no measurable decrease in performance. Finally, the [^{18}F]fluoride ions were eluted as a K^{18}F/K2.2.2 complex, dried by repeated dissolution in acetonitrile and evaporation of residual water, and reacted with EtDT leading to the formation of the desired product ([^{18}F]fluoroethyltosylate) with 96 ± 3 % yield (RCY). The overall time needed for conditioning, trapping, elution and regeneration was less than 6 minutes. This approach will be of great benefit towards an integrated platform able to perform faster and safer radiochemical synthesis on the micro-scale.

In the following chapter, magnetic microparticles are described as a method for the trapping and elution of [$^{18/19}$F]fluoride ions *via* formation of a magnetic plug inside a glass microdevice. Even though the method was found to be not as fast and efficient as the packed bed of microparticles (Chapter 3), and still requires several manual steps which are time and labour consuming, the proof of principle illustrates an alternative process not yet reported in the literature, with potential for future on-chip pre-concentration of fluoride. The results showed that by employing positively charged magnetic particles, fluoride could be trapped in yield of > 50 % and elution achieved with approximately 90 % recovery of fluoride. A subsequent method for reducing the inefficiencies of the plug of magnetic particles is described where a multilaminar flow microreactor was investigated in which functionalised magnetic particles can be deflected through streams of reagents with the final aim to perform trapping and elution of fluoride in continuous flow. In the final chapter preliminary studies into the detection

and removal of K2.2.2 and FECH are described. Two detection methods for K2.2.2 analysis and detection of K2.2.2 in FDG are proposed and assessed towards real sampling of FDG. Also a suitable detection method for FECH and DMAE and TBAHCO$_3$ was also optimised, with separation of the three analytes achieved with an isocratic IC method. Trapping of FECH was also achieved with cation exchange material trapped in micro-chamber, and the capacity of the material was found to be 5.5 µg mg^{-1}.

In a final study the integration of different micro-chambers modules was assessed for potential towards FECH purification to establish an alternative method whereby all the by-products are trapped and only FECH is released; results on this study showed that it was not possible to completely purify FECH due to DMAE presence found in the purified solution in high trace (only 30 % was trapped and the rest released together with FECH).

1 Introduction

1.1 Positron Emission Tomography (PET)

Positron Emission Tomography (PET) is a molecular *in vivo* imaging technique with very high resolution and sensitivity compared to single photon imaging (planar and single photon emission computed tomography (SPECT))[1] which requires the labeling with positron emitting radioisotopes, also referred to as radiotracers. It covers a wide range of applications in the fields of oncology, cardiology and neurology. PET scans can be applied for diagnosis of malignancy, grading of malignancy, staging of diseases, detection of residual disease, detection of recurrence, measuring the response to therapy and identification of the site of disease. The reason why PET is so successful compared to other techniques, such as X-rays and MRI scan and single photon imaging compared to single photon imaging (planar and single photon emission computed tomography (SPECT))[1], is that PET not only shows the anatomy of the body, but also the chemical and metabolic aspect of any eventual disease with the added benefit of sensitivity and specificity. Furthermore, specificity and sensitivity can be increased when combined with computed tomography (PET CT SCAN) as shown in Figure 1 where CT and PET images are taken sequentially showing the anatomy and metabolic aspect within the same image [2]. The development of positron emission tomography illustrates how advances in basic science translate into benefits for human beings. In 1930 Ernest Lawrence and co-workers [3, 4] realised the first cyclotron. By 1938 Lawrence and Livingston [4] had designed a "medical cyclotron". In the mid-1950, while looking for a method to examine the oxygenation of tumors, Ter-Pogossian and Powers investigated C-11, N-13, O-15, and F-18 and found many uses in medical and physiological research [5]. These early experiments stimulated interest in the use of short-lived radioactive

gases, and led, in 1955 to the construction of the first medical cyclotron, located on the grounds of the Hammersmith Hospital in London. The introduction of fluorodeoxyglucose (FDG) represented another major step towards practical clinical use of positron-emitting tracers. In 1977, after a decade of development, Sokoloff *et al.* described in a classical paper the use of carbon-14 deoxyglucose for measurement of local cerebral glucose utilization [6]. Shortly afterwards Reivichv *et al.* extended the carbon-14 radiographic method to measurements of regional glucose utilization with fluorine-18 deoxyglucose [7], a tracer developed by Ido and colleagues [8]. It was a significant accomplishment not only the development of this tracer but also the modeling of its use to reveal regional cerebral glucose utilization, which gave birth to functional mapping of the human brain[9].
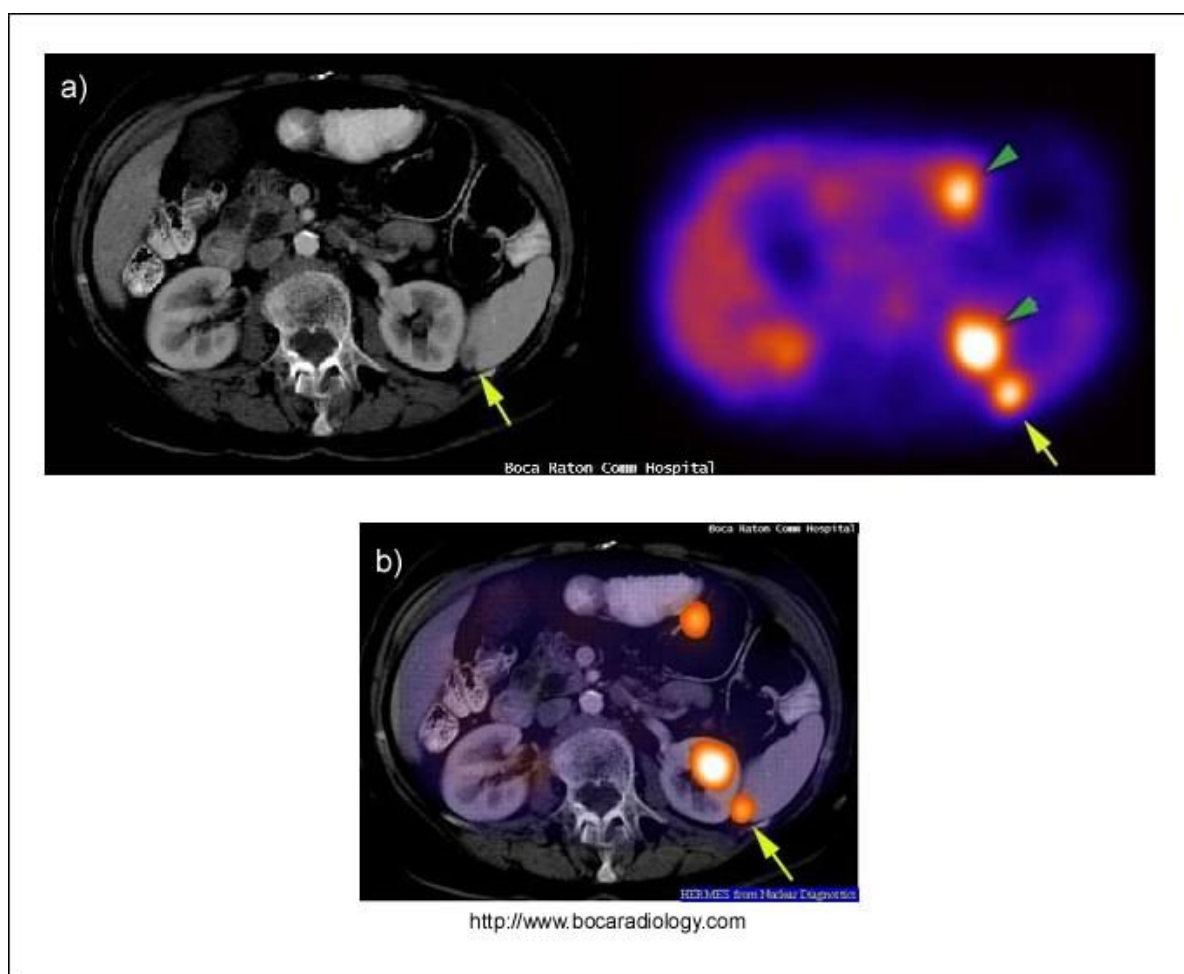
Figure 1 (a) CT scan showing the anatomy of the brain (left), on the right PET scan showing the metabolic process of the brain. b) Fusion of CT and PET scan increasing sensitivity and specificity.

1.2 Basic principles of PET imaging

Several steps are required in the PET process, from the selection of a suitable molecular probe labelled with a positron emitting radionuclide, administration either by injecting into the vein, swallowing or inhaling, to imaging the distribution in the patient. Positron emitters are isotopes, which are neutron-deficient and reach their stability by conversion of a proton to a neutron. Figure 2 is a schematic representation of the positron emitted from the nucleus and the subsequent formation of two photons or gamma rays.
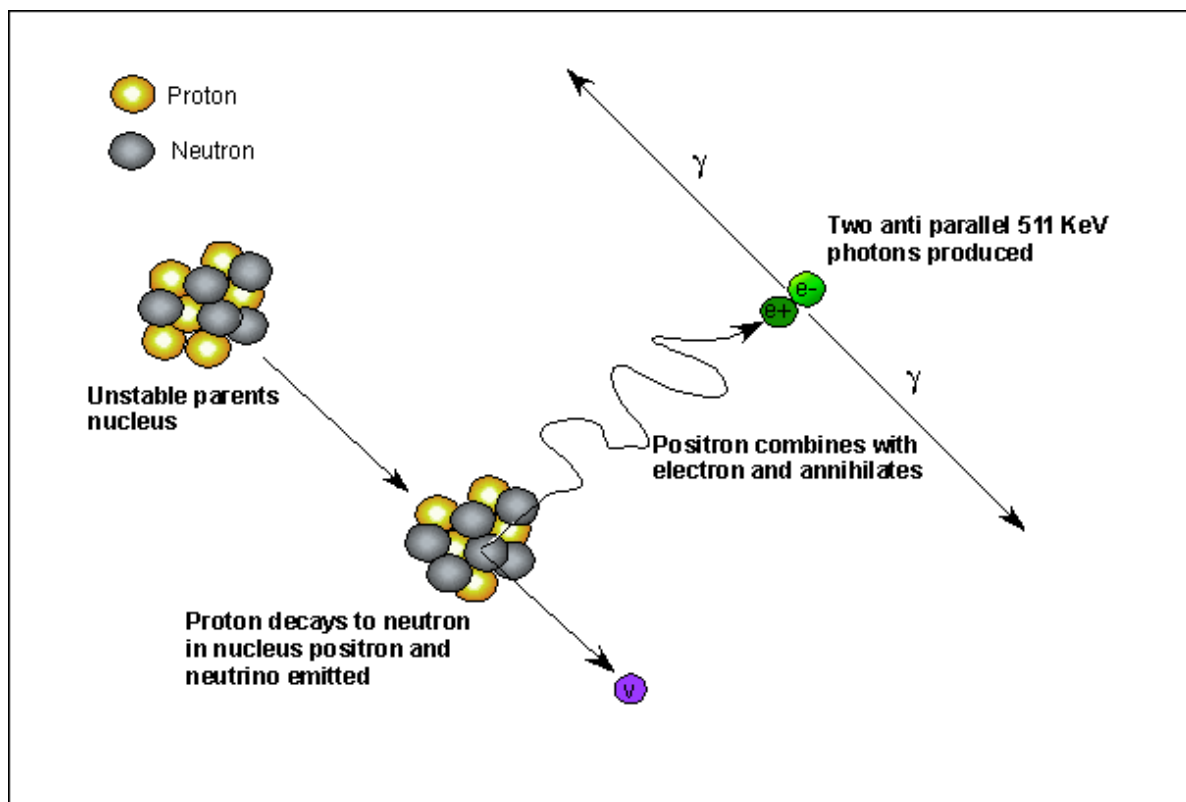
Figure 2 Schematic representation of positron emission and formation of 2 photons (gamma rays).

Once the positron is emitted, energy in form of β^+ radiation is given off. Once the radionuclide is emitted, annihilation process takes place, which is the energy produced between positron-electron and is produced outside the nucleus which takes place outside the positron emitting atom and gives rise to two photons or gamma rays (γ). Each of them has an energy of 0.511 MeV, given off at 180° opposite directions in order to maintain their momentum. This is the crucial phenomenon of the detection in PET where two photons are detected simultaneously by a circular array of detector in the PET scanner. The process of positron emission is described in more details below. There are two ways to produce a positron, by pair production and by nuclear transmutation. The general equation in positron decay is shown in equation 1:

$$_Z^A X \rightarrow _{Z-1}^A Y + _1^0 \beta^+ + v + Q(+e^-)$$
Equation 1
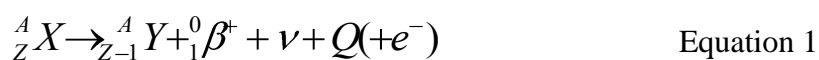
Where Q is energy, the atom X is a proton rich and achieves stability by converting a proton to a neutron [10]. The positive charge is carried away with the positron and to balance the charge an electron is ejected from the outer orbital (internal conversion); initially the positron has energy similar to the β^- decay, but it loses its kinetic energy by interaction with the surrounding matter *via* four types of interactions:

- Inelastic collisions with atomic electrons.

- Elastic scattering with atomic electrons, where positron is deflected but maintains energy and momentum.

- Inelastic scattering with a nucleus, positron deflected emission of radiation.

- Elastic scattering with a nucleus where positron is deflected but not transfer any energy to the nucleus.

When a positron and electron combine and annihilate giving off electromagnetic radiation in the form of two photons as described above, in some cases three photons can be emitted ($< 1\%$ probability) [2, 11].

Once the positron is ejected from the nucleus, it loses energy by collision with other atoms and combines with another extra nuclear electron so the total mass of $\beta^+ + e^-$ is converted to energy according to Einstein equation (2): [11]

$$\text{Total mass of } \beta^+ + e^- = 18.219 \times 10^{-31} \text{ kg}$$

$$\text{Speed of light} = 2.998 \times 10^8 \text{ ms}^{-1}$$

$$E = mc^2 = 1.6375 \times 10^{-13} \text{ kg m}^2 \text{ s}^{-2} \text{ (J)} \qquad \text{Equation 2}$$

$$= \frac{1.6375 x 10^{-13}}{1.6022 x 10^{-19}} \text{ eV}$$

$$= 1.022 \times 10^6 \text{ eV} = 1.022 \text{ MeV}$$

Examples of isotopes which undergo decay *via* positron emission are shown in Table 1:

Table 1 Properties of commonly used positron emitting radioisotopes [12].

Isotope	Half-life (min)	Maximum positron energy (MeV)	Positron range in water (mm)	Decay product	Production method
^{11}C	20.3	0.96	1.1	^{11}B	Cyclotron
^{13}N	9.97	1.19	1.4	^{13}C	Cyclotron
^{15}O	2.03	1.70	1.5	^{15}N	Cyclotron
^{18}F	109.8	0.64	1.0	^{18}O	Cyclotron
^{68}Ga	67.8	1.89	1.7	^{68}Zn	Generator
^{64}Cu	762	3.15	1.7	^{64}Ni	Cyclotron

1.3 Radiation detector

Radiation detectors measure the energy lost or deposited by ionizing radiation when they pass the detector, typically they convert the energy into an electrical or charge signal. They are generally divided into three categories: gas chambers, semi-conductors and scintillation detectors. The latter one is the most used and successful for the detection of 511 KeV photons in PET imaging. They consist of an inorganic crystal (scintillator) which emits visible (scintillation) light photons after the interactions of the photons with the detector, a photo detector measures the number of scintillation photons during the interactions which is proportional to the energy deposited within the crystal [13].

1.4 Fluorine, ^{18}F and its production

The non radioactive ^{19}F$^-$ isotope is a group p-block element (electron configuration: [He] $2s^2$ $2p^5$) has natural abundance of 100% and reacts readily with almost every element and compound when present in its gaseous form. This basically means that

neither any radioactive fluorine isotope nor gaseous fluorine will be found in nature. Fluorine is the most electronegative element present with a Sanderson electronegativity of 4.0. The most common oxidation number is -1.

[^{18}F]Fluorine itself is one of many known radioactive isotopes, and it consists of 9 protons and 9 neutrons with a half life between 109.8 – 109.7 min. All other known radioactive positron emitting fluorine isotopes (there are three) have short half-lives for *in vivo* imaging purposes (*e.g* ^{17}F, $t_{1/2}$= 64.8 s) and their production is of relatively of little interest [14].

1.5 [^{18}F]Fluorine radiopharmaceuticals

[^{18}F]Fluorine as part of the radiohalides is becoming increasingly the radionuclide of choice not only due to its physical and nuclear characteristics as described earlier but also due to the successful use in clinical oncology of 2-[^{18}F]fluoro-2-deoxy-D-glucose [^{18}F]FDG, which is currently the most widely used PET radiopharmaceutical. [^{18}F]fluorine it decays in 97% of the cases by positron emission and 3% by electron capture to the stable isotope ^{18}O [15]. In general it can react either as electrophile or nucleophile but due to its reactivity in the electrophile reaction, regioselectivity which makes the nucleophilic reaction of [^{18}F]fluoride the preferred method. The most common method to produce nucleophilic [^{18}F]fluoride is the ^{18}O (p, n) ^{18}F nuclear reaction, i.e. the reaction of an accelerated proton with ^{18}O to produce a neutron and ^{18}F^{-}. A variety of chemical reactions are available for ^{18}F^{-}, but they can be divided mainly in two categories; S_N2-type (nucleophilic substitution bimolecular) reactions with the substrate containing a leaving group, and aromatic nucleophilic substitution reactions, which utilise an activated aromatic group. Its relative longer half-life makes it ^{18}F^{-} a suitable candidate both on synthesis time and longer imaging applications [16]. Nucleophilic substitution with no-carrier-added (N.C.A) [^{18}F]fluoride is still the only

way to obtain products with high specific activity which denotes the ratio of the radiotracer in question to the total amount of compound both labelled and unlabelled is expressed in GBq µmol^{-1} or mCi mmol^{-1}. Several developments in the synthesis of ^{18}F-tracers have been achieved, with some of the common radiotracers used in PET shown in Table 2; peptide synthesis *via* prosthetic group labeling [^{18}F]SFB, click chemistry formation of triazole between an azide and an acetylene, enzyme fluorination of adenosylmethionine but the three main methods of fluorination procedures are namely; i) direct fluorination (one step) [^{18}F] such as flumazenil ii) direct fluorination followed by cleavage either basic/acid hydrolysis or oxidative cleavage such as FDG, iii) synthesis of a ^{18}F-synthon (prosthetic group) either 2 or 3 steps such as FECH [15].

Table 2 Common ^{18}F radiotracers for PET with their application and structure [17-21].

Radiotracer	Applications	Structure	References
[^{18}F]Fluoroethylcholine (FECH)	Prostate, brain tumors		[17]
[^{18}F]Fluoromisonidazole (FMISO)	Hypoxia		[18]
[^{18}F]Fluorothymidine (FLT)	Cellular proliferation		[19]
[^{18}F]2-Deoxy-2-fluoro-D-glucose (FDG)	Glucose metabolism and tumors		[20]
[^{18}F]Fluorodopa (FDopa)	Parkinson's disease		[21]
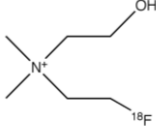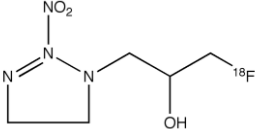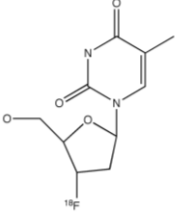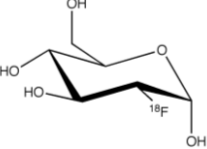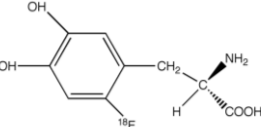
1.6 [18F-]Fluorine radiochemistry systems for synthesis

Currently the synthesis of radiocompounds is performed in a variety of formats depending on the type of chemistry and their requirements, commonly these platforms are referred to as radiosynthesisers or radiochemistry systems. Radiochemistry systems are able to perform a number of operations such as chemical reactions, neutralisation, purification and dilution. These are mainly used to synthesise radiopharmaceuticals, where due to the large amount required for clinical purposes, automation is an essential requirement in order to minimise handling of these high energy emitters which would be dangerous for the operators. There are many commercially available systems, a

classification of these will be presented below, but it will be restricted to systems for [^{18}F] labeling.

Radiochemistry systems can be divided in three main categories:

- Systems to be charged with reagents (1.6.1),

- Systems with disposable cassettes (1.6.2),

- 'Modular' systems (1.6.3),

Functionality also varies between systems depending of their use; single dose FDG, and multi-dose where both nucleophilic substitutions and electrophilic reactions can be performed on the same system. Depending on the chemistry performed, the system can also be divided in two further categories; substitution in a reactor or in a loop as well as whether acid or basic hydrolysis is performed on reactor or on cartridges.

From a technical point of view, they differ depending on the number of reactors available, their detector functions, and if they integrate a HPLC – preparative for their purifications [22].

1.6.1 Radiochemistry systems to be charged with reagents

The first group of system are characterised by the fact that reagents and products are loaded onto reactor vessels either manually or in some cases by robotic arms. Common materials for vessels are plastic, glass or glassy carbon, with volumes reagents from 1 mL to 10 mL. Reaction temperature are controlled by electrical resistance (25 – 250 °C) or *via* Peltier technology (-180 – 300 °C). In the next paragraphs some of the commercially available systems are described.

Three synthesisers are available from GE (GE Healthcare, United Kingdom) under the name of TracerLab as shown in Figure 3: the "FX-FDG double" for FDG synthesis (Figure 3a) with a 60 % radiochemical yield (R.C.Y.) is able to perform two independent runs and it comes with three radiation detectors. The "FX-FN" or "FX-FE"

(Figure 3b), for both nucleophillic and electrophilic substitution which features built-in preparative radio / UV HPLC and the "FX-Dopa" (Figure 3c) which enable the synthesis of Fluoro-Dopa with a 20 % radiochemical yield in less than 40 min with 99% enantiomeric purity.

FX-FDG double   FX-FN or FX-FE   FX-Dopa
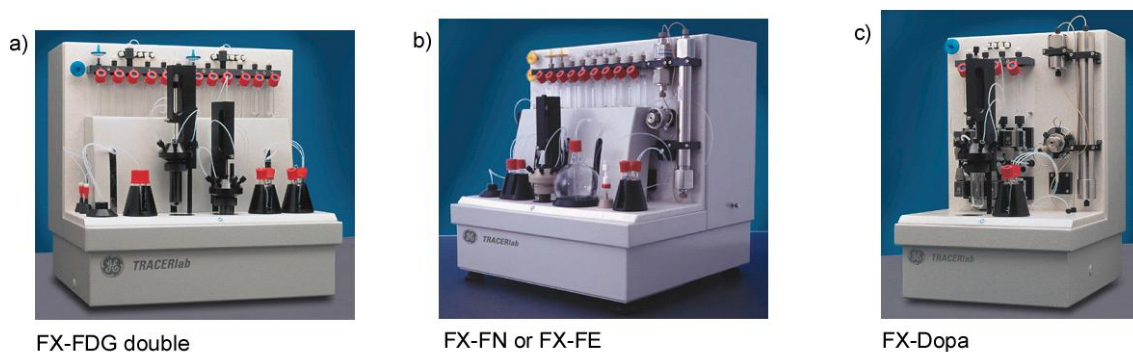
Figure 3 a) GE Tracer Lab FX-FDG for synthesis of FDG which allows two consecutive runs without opening the hot-cell [23]. b) The TracerLab FX-FN/FE a versatile system for multiple ^{18}F radio compounds[23, 24]. c) The TracerLab FX-DOPA for fully automated synthesis of [^{18}F]F-Dopa [25].

Raytest (Raytest GmbH, Germany) also produce a series of synthesisers under the name of "Synchrom" as shown in Figure 4; for single run FDG synthesis as shown in Figure 4(a) as well as a system for general radiosynthesis with an HPLC purification system built in as shown in Figure 4(c).

SynChrom FDG   SynChrom F2   SynChrom R&D

Figure 4 Images of different modular systems from Raytest a) the "Synchrom FDG", b) "Synchrom F2" and c) "Synchrom R&D" [26].

Furthermore there are Synthra synthesisers (Synthra GmbH, Germany) for FDG and F-Dopa as shown in Figure 5(a-b) both with integrated heating / cooling systems and three radiation detectors as well as a system with built-in preparative Radio / HPLC purification.

Figure 5 (a) The "Synthra FDG^{two}" a fully automated system for FDG synthesis[27]. (b) the synthra F-Dopa for routine production of 6-[18F]fluoro-L-Dopa[27].
(c) The "Synthra RN^{plus}" a completely automated radio synthesis system for routine production of a wide variety of [18F]fluorine labelled compounds by nucleophilic substitution[27].

1.6.2 Radiochemistry systems with disposable kits

Another category of radiochemistry synthesisers consists of systems with disposable cassettes where chemicals, cartridges and solvents are already included and loaded into the cassette, thus allowing multiple back-to-back production runs for ^{18}F-FDG, as well with the advantages of reducing maintenance and cross-contamination.

Figure 6 Image of a disposable cassette system with reagents and chemicals already loaded the image shows a cassette system for the GE "FastLab" [28].

Two systems are available from GE Healthcare (GE HealthCare, United Kingdom), the "MX Tracer Lab" as shown in Figure 7(a) for synthesis of FDG in 60 % radiochemical

yield in less than 27 min as well as the "Fast Lab" which allows different cassette systems to be used (FDG, ^{18}F-NaF) with a 70 % radiochemical yield for FDG in less than 23 min.

MX Tracer Lab
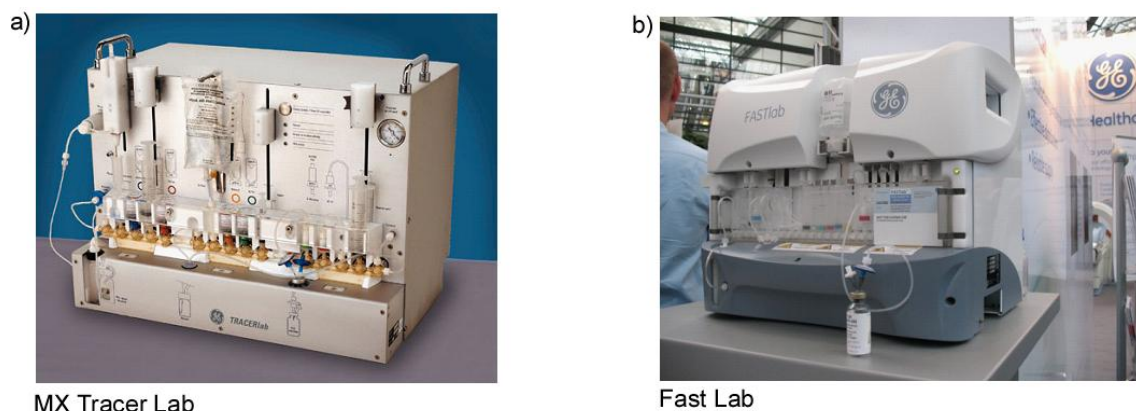
Fast Lab

Figure 7 (a) The "GE MX Tracer Lab" for FDG synthesis[29].(b) The "GE Fast Lab" a more versatile system for multiple synthesis of radiocompounds including FDG, FLT, FMISO [25].

Cassette systems are also produced by IBA (IBA Solutions, Belgium) with the "Synthera" family for both FDG and FLT as shown in Figure 8. The "Synthera FDG" in Figure 8(a) enables FDG synthesis with a yield of 55 % and an automatic ejecting of the cassette. The "Synthera FLT" (Figure 8(b)) allows synthesis of FLT in a 20% yield in less than 40 min also available with the "Synthera HPLC" for on-line purification.

Synthera FDG

Synthera ^{18}FLT
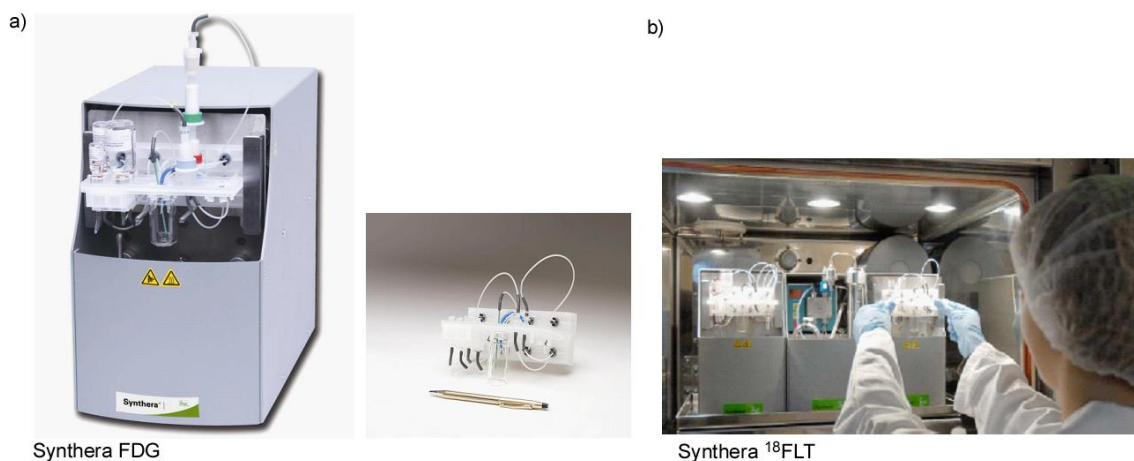
Figure 8 Images of two types of "Synthera" produced by IBA. (a) The "Synthera FDG" for synthesis of FDG and (b) the "Synthera FLT" for synthesis of FLT [30].

Also belonging to the category of the cassette systems is the Siemens "Explora" (Siemens Healthcare, Germany) with three different synthesisers; the "Explora FDG$_4$" for synthesis of FDG with a non d.c.y. of 65 % in 45 min which allows up to four sequential runs of FDG and includes up to five radiodetectors. In the same product family is the "Explora FM+LC" for synthesis of FLT which allows for reagents measurements and integrates a semi-preparative HPLC. This instrument supports two batches of automated synthesis before cleaning is needed.
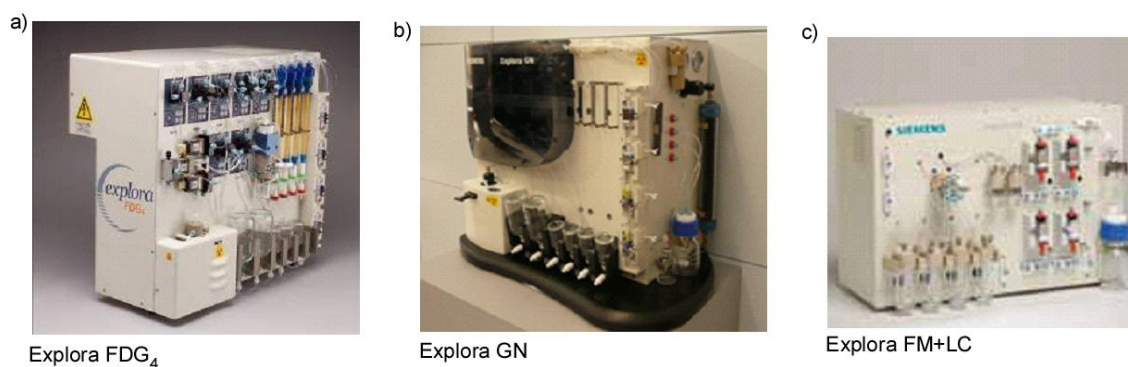
Figure 9 (a) The "Explora FDG$_4$" a disposable system for FDG synthesis[31]. (b) The "Explora GN" for multiple synthesis of FDG[32]. (c) The "Explora FM+LC", a fully automated system with built-in a semi-preparative LC system for purification [33].

Bioscan which has recently been acquired by Eckert and Ziegler (Bioscan Europe Ltd., France), offers two synthesisers one for FDG synthesis with a yield of 55% as shown in Figure 10(a) as well as an automated loop system for synthesis of ^{18}F-Choline and other alkylation syntheses like ^{18}F-FBrEt or ^{18}F-FBrMe which allows direct injection into the HPLC system.

a) FDG-Plus Synthesiser
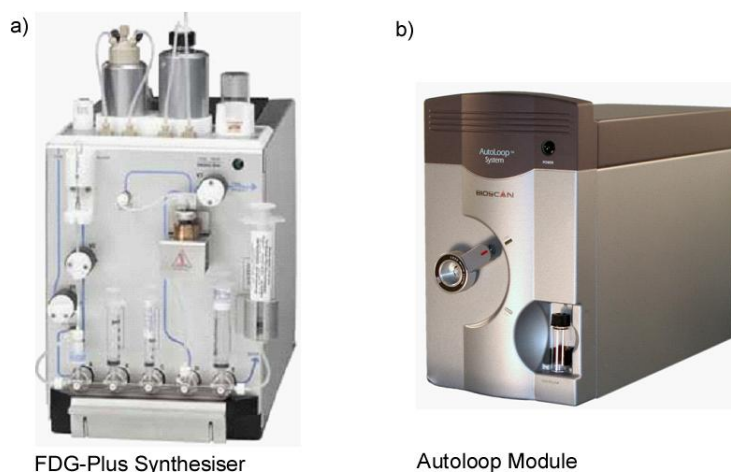
b) Autoloop Module

Figure 10 (a) The "FDG-Plus" synthesizer for multiple runs of FDG production[34].(b) "Autoloop" Module, a system that takes advantages of the 'loop technique' developed by Dr. Alan Wilson at the centre for Addiction and Mental Health in Toronto, where the reaction happen at room temperature in the closed loop [35].

1.6.3   Modular radiochemistry systems

This category of synthesisers consists of small, sealed, stainless steel modules stacked and connected by tubing and by a single electrical cable. The use of multiple, replaceable modules allow the system to be applied for various isotopes and many types of reactions. Due to its multifunctionality these systems can replace several single-purpose devices, which significantly reduce cost and lab space. Currently there are two companies that produce such systems. The first is by Eckert & Ziegler (Eckert & Ziegler Strahlen- und Medizintechnik AG, Germany) (Figure 11) where different modules (Figure 11(b)) can be assembled together for a custom synthesis process. Each individual modules are quite small (13 x 13 x 8 cm^3) in Figure 12(a-b) both the modular–Lab for FDG and FECH are shown which allow synthesis of FDG in less than 30 minutes and can produce up to four sequential FDG batches.
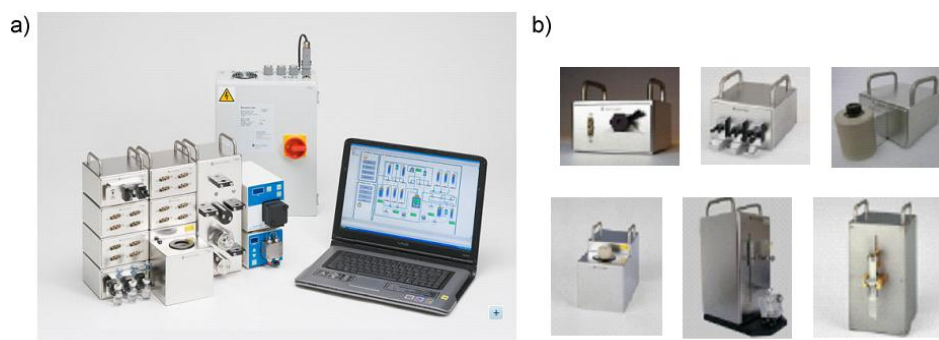
Figure 11 (a) Eckert & Ziegler modular system assembled and interfaced to a PC, (b) The individual components [36].

Modular Lab ^{18}F-FDG

Modular Lab ^{18}F-FECH
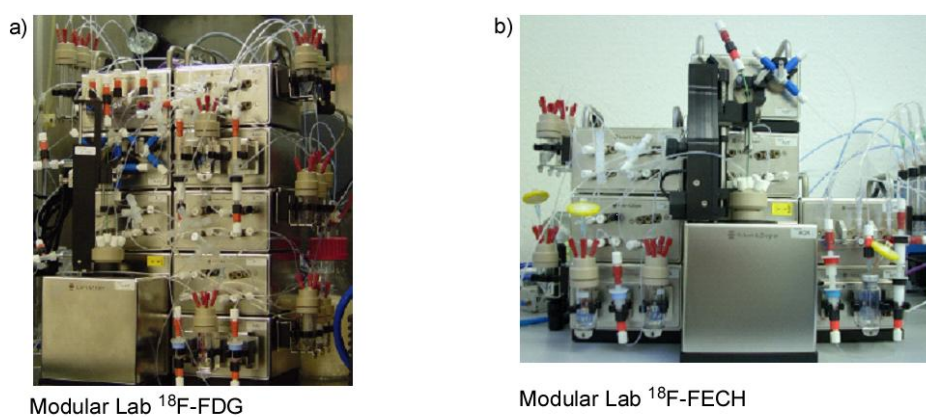
Figure12 The E&Z Modular Lab F-FDG for synthesis of FDG [37]. The Modular-Lab F-FECH for synthesis of FECH [38].

Also of similar concept are the Scintomics modular synthesisers (SCINTOMICS GmbH, Germany) with an example shown in Figure 13.
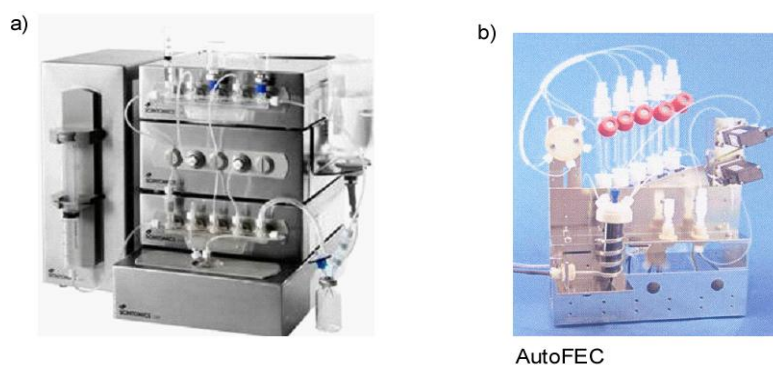
AutoFEC

Figure 13 (a) The Scintomics modular system, (b) The "AutoFEC" modular systems for synthesis of FEC [39].

1.6.4 "Microfluidic" radiochemistry systems

This category consists of modular, liquid-flow-based ^{18}F microchemistry system with the ability to combine both microscale and macroscale process steps in PET synthesis. The main difference to the modular systems is the integration of a microfluidic loop, commonly glass capillaries, for reactions [40, 41]. Current the only available system of this category is the Advion NanoTek LF (Advion, USA) as shown in Figure 14 which consists of a liquid flow reactor system, an auxiliary pump module as well as a concentrator and evaporator module, thus allows for a fast synthesis and enable production of multiple biomarkers from a single ^{18}F batch. It features lower reagent usage and can integrate a purification system. In Figure 14(b) the microfuidic reactor loop is shown which consists of a coiled fused silica capillary.
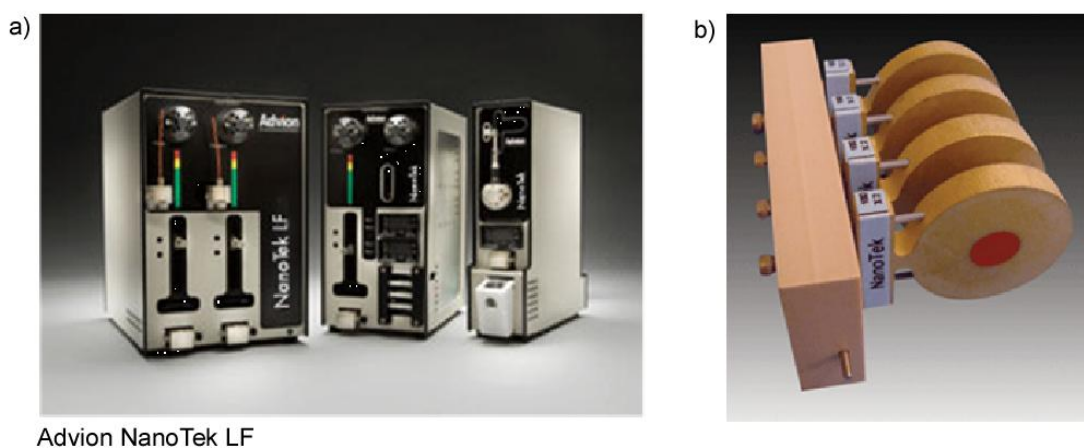
Advion NanoTek LF

Figure 14 (a) The microfluidic systems from Advion (Advion "Nanotek LF") which consists of a reactor module, a concentrator module and an evaporator module. (b) The microfluidic loops for reaction situated in the Advion "NanoTek LF" system which consists of a coiled glass capillary (approximately 2 m in length with a diameter of 150 μm)connected to a heating system [42].

Radiochemistry systems sizes comparisons

The paragraphs above show that there is an expansive line of radiochemistry modules for small to medium scale synthesis and production of different PET imaging biomarkers. In Figure 15 an image of the variety of the systems described above are

compared in terms of their size. In Table 3 few examples of each of the categories described above are compared in terms of their synthesis time and yield obtained

50 x 40 x 50 cm   30 x 25 x 50 cm   30 x 20 x 20 cm
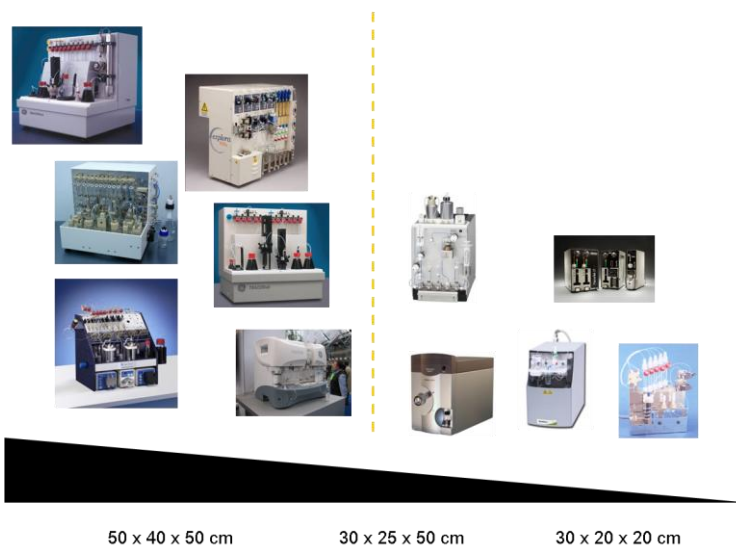
Figure 15 Comparison of the different radiochemistry modules described above in term of their size.

Table 3 some of the commercially available synthesisers compared in terms of their timing and synthesis yield

System	Company	Radiopharmaceutical	Time for synthesis (FDG)	R.C.Y	Advantages
1) **Charged**: "TracerLab" "Synthra FDG^{TWO}"	GE Healthcare Synthra	FDG, Fluoro Dopa FDG	< 30 min < 28 min	70 % 98 % R.C.P	Two production runs per loading High starting activity (555 GBq)
2) **Disposable**: "FastLab" "Explora FDG$_4$"	GE Healthcare Siemens	FDG FDG	25 min 45 min	74 % 65 %	Quick set-up (< 1 min) Automatic self-cleaning
3) **Modular**: "Modular Lab ^{18}F-FDG"	Eckert & Ziegler	FDG	<30 min	Not reported	Four sequential syntheses without user interaction
4) **Microfluidic**: "NantoTek LF"	Advion	FECH	< 90 s	60-85 %	"Dose on demand"

1.7 Preparation of nucleophilic [^{18}F$^-$] for radiosynthesis

In the following paragraphs an in depth description for the preparation of nucleophillic [^{18}F$^-$] radiotracers will be presented.

All radiosynthetic nucleophilic substitutions, to introduce [^{18}F$^-$] into molecules, start with a drying step, because the fluoride is obtained as an aqueous solution. This means that its nucleophilic properties are weak due to hydrogen bonding with water molecules [22, 43]. Therefore, prior to performing any synthesis, [^{18}F]fluoride is dried azeotropically under reduced pressure in the presence of acetonitrile. This step is commonly achieved in automated synthesis module or manually with a drying apparatus as shown in Figure 16 [15]. The first step after passing the [^{18}F]F$^-$ through an activated ion exchange cartridge is to remove the excess $H_2^{18}O$ water under vacuum with air or a gas such as helium or argon [44, 45]. Subsequently the [^{18}F]F$^-$ is eluted from the cartridge with a solution of K2.2.2 and K_2CO_3 in acetonitrile and collected in a second drying vial, the choice of acetonitrile is mainly due to its suitability to form an azeotropic mixture with water which facilitates the drying step [46]. Once the elution steps are complete, the drying vial is heated at about 90-95 °C with a constant flow of nitrogen (or helium or argon) under reduced pressure and stirring to help the evaporation of the azeotrope (water/acetonitrile); this drying step usually takes 3-5 min. As a small amount of water stays in the vial (about 10 - 20 μL), another portion of acetonitrile is added (about $0.5 - 1.0$ mL) and the drying continued. After the second drying step (another $2 - 3$ min) the complex is dried. Some researchers will add a third step to ensure complete drying of the complex, which finally leaves the [^{18}F] in the vial as a slightly yellowish film which is ready for use in the synthetic step. In the case of automated synthesis modules, the risk of contamination and the reduction of human errors make the drying procedure a convenient approach [47].

2) Elute the $^{18}F^-$ with K2.2.2/K_2CO_3/H_2O/CH_3CN into the reaction vessel

Gas

Vacuum

Equipment:
- reaction vial 5 mL + silicon septum lid
- Vacuum tubing
- gas tubing for He or N_2
- syringe 1 mL
- gas cylinder (He or N_2)
- oil bath or heating block
- heater with thermometer
- magnetic stirring bar
- QMA light cartridge

Chemicals:
- Kryptofix 2.2.2 or Cs_2CO_3
- K_2CO_3 or potassim oxalate
- Acetonitrile

^{18}F

1) Load the $^{18}F^-$/$H_2^{18}O$ onto the QMA- Cartidge

$^{18}F^-$

$H_2^{18}O$

Silicon septum

stirrer

Figure 16 Experimental setup to manually dry $^{18}F^-$: 1) The $^{18}F^-$ in $H_2^{18}O$ water has to be passed through the QMA cartridge (ion-exchange), the $^{18}F^-$ stays on the resin and the $H_2^{18}O$ water passes through; 2) a mixture of Kryptofix 2.2.2 (10-15 mg), K_2CO_3 (10-15 µL of a 1.0 M K_2CO_3 solution), water (40 µL) and acetonitrile (300-900 mL) elutes the $^{18}F^-$ from the resin into the drying (reaction) vessel. Adapted from [47]

FDG Synthesis

[^{18}F]FDG is a glucose analogue in which the hydroxyl group on the 2-carbon of a glucose molecule is replaced by a fluoride atom. Brown *et al.* [48] showed that the uptake of glucose was related to the expression of glucose transporter-1 (GLUT-1). After the transport of FDG across the cell membrane, it is phosphorylated to become FDG-6-phosphate. This compound is trapped intracellular and is resistant to further metabolic processes that would normally occur to glucose-6-phosphate. It is the increased number of glucose transporters located on the tumour cell membrane which allows an increased uptake of FDG and the trapping of FDG-6-phosphate in cancerous

tissue. This gradual accumulation of FDG in the malignant cells, allows the tumour to be visualised [49].

Step 1 **Aqueous** $^{18}F^-$ **(from cyclotron)** → anion exchange reaction / K2CO3/K2.2.2/MeCN → Activated ^{18}F

Step 2 **Azeotropic removal of H$_2$O and MeCN**

Step 3 Mannose triflate → MeCN / Fluorination → (product with ^{18}F)

Step 4 → HCl/NaOH / Hydrolysis → FDG + byproducts

Step 5 **Product purification:** removal of Phase transfer catalyst (K2.2.2) removal unreacted fluoride, removal of sugar precursor and acetylated by-products

Figure 17 Schematic synthesis of FDG step by step; Step 1 activation and isolation of fluoride. Step 2 solvent exchange from water to acetonitrile. Step 3 fluorination with mannose triflate. Step 4 hydrolysis. Step 5 product purification [50].

The first synthesis of FDG was carried out in Brookhaven National Laboratory by Wolf *et al.* [51] in 1976 by electrophilic fluorination (Figure 18 (a) shows the electrophilic mechanism); however, the first FDG trial in humans had a low yield and the synthesis time was long (several hours). Several improvements were made subsequently to try to incorporate other sugar precursors, but the main limitation was that the only 50 % of radioactive fluorine atoms were incorporated during the electrophilic fluorination step. Only several years later was there a breakthrough by Hamacher *et al.* [16] who through a nucleophilic substitution, with the use of Kryptofix 2.2.2 as phase transfer catalyst (P.T.C.), increased the yield over 50 % and reduced the synthesis times to 50 min.
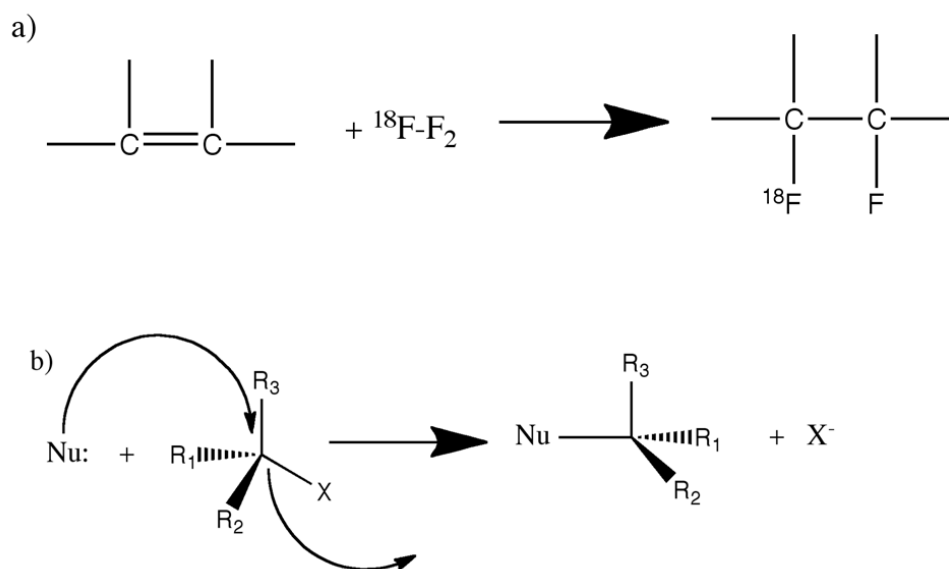
Figure 18 a) Electrophilic fluorination. b) Nucleophilic substitution.

In the synthesis, the F^- ion is the nucleophile and the precursor is mannose triflate in which the 1,3,4 and 6 positions are protected with an acetyl group and triflate is the leaving group at the second carbon (Figure 17). Since fluoride has high hydration energy, water is not a suitable solvent; hence a polar aprotic solvent like acetonitrile must be used to isolate the fluoride from the irradiated water. As previously discussed, this is achieved by anion exchange where the trapped fluoride is eluted with a solution

of ACN/K$_2$CO$_3$ and K2.2.2 [52]. The presence of the kryptand complexes the K$^+$ cations preventing the formation of KF and enhancing the reactivity of the fluoride [53]. Once the fluoride has been activated and isolated, it is necessary to evaporate any residual water from the solution, normally achieved by azeotropic distillation as described in Section 1.7. Then the fluorination takes place with the addition of the sugar derivative, mannose triflate, with acetyl protecting groups at position 1,3,4 and 6 preventing fluorination at these sites. The next step is to remove the acetyl protecting groups *via* either acid or base hydrolysis; whit the latter one being faster and taking place at room temperature [54]. The final step involves purification of the toxic compound K2.2.2 [55], removal of any unreacted fluoride and non-hydrolysed by-products or partially acetylated FDG. This is achieved using a series of SPE columns [56], where the by-products are retained and the FDG released. By this approach, FDG radiochemical yields of over 95% can be achieved and FDG is produced routinely in automated synthesis modules (ASMs) consisting of disposable cassettes with required chemical reagents as discussed in section 1.6 an example which is shown in Figure 19[57].

Figure 19 GE "FastLab" synthesiser by GE healthcare for synthesis of FDG [28].

1.8   Microfluidics and Micro Total Analysis System (µTAS)

Microfluidic devices consist of a network of channels etched in a solid substrate, the channels typically have dimensions in the range of 10 − 1000 µm. Such lab-on-a-chip devices are nowadays emerging as useful technology for the intensification and miniaturization of chemical processes. Microfluidic devices have found applications in a range of different research areas due to the advantages they offer over many of the bench top systems. Table 4 lists some of the key advantages of micro-reactors [58].

Table 4 General properties of microreactors and their benefits.

Property	Characteristics and benefits
Size	Heat transfer, diffusion and mass transfer, are improved. Better control over temperature and concentration gradients.
Volumes	Volumes in the range of nL-µL, reduced reagent consumption, increased safety.
High surface to volume ratio	More efficient heat transfer, increased rate of chemical reactions.
Short mixing time	Diffusion based mixing is in the s to min range, reaction time also reduced.
Mode of flow	Laminar flow where mixing is diffusion based can be regulated with hydrodynamic or electrokinetic controls.
Parallel process	Can be adapted for high throughput or combinatorial synthesis.

Several fabrication methods are available. Chips can be fabricated from polymers, metals, quartz, silicon or glass depending on the properties required for an application

such as the nature of the reaction, material cost and reliability. Glass is often the first choice because it is mechanically strong, compatible with a wide range of chemical solvents and is optically transparent. Alternatively polymer based devices especially PDMS give good flexibility in fabrication and valve control ability but are restricted to applications not involving organic solvents that cause swelling or damage [58].

With the development of MEMS (micro-electro-mechanical-system) technology and microfluidic systems, a number of groups have been working towards miniaturised PET radiosynthesis devices [59]. With the aim of offering exciting advantages such as low sample and reagent consumption, high reproducibility and automation. Furthermore, working with radioactivity requires special equipment such as lead-shielded cabinets (hot cells) and computerised systems. A few of the advantages of micro-PET tracer synthesis systems over conventional system are i) controlled transfer of small volumes of radioactive liquid, ii) increase in surface area which enhances heat and mass transfer (hence faster reaction), iii) better product selectivity, iv) reduced volume of reagents and v) reduced space requirement and easy shielding [60]. Overall, microfluidic reactors seem to be suitable for performing rapid radiolabeling reactions since they are ideally suited to handle small amounts of reagents (normally ng to μg), especially important when dealing with radiotracers where the supply can be limited. Some examples of radiolabeling in microfluidic device have been reported however most of them are only a proof of concept and few are discussed below.

The first example of [^{18}F]FDG synthesis in a glass based micro-reactor started with the conventional azeotropic method for drying aqueous [^{18}F] fluoride ions [61] where the dried K^{18}F with kryptofix was introduced into one micro-reactor through one of the two inlets and the precursor from the other inlet at a rate of 5-100 μL min^{-1}. Then the product was fed into another micro-reactor where the hydrolysis took place, and the

RCY obtained was 24% [61]. In 2006 Gillies *et a.l.* [46, 62] reported the use of a polycarbonate microfluidic reactor for radiolabeling using ^{18}F. Exploying two modules to achieve the synthesis of FDG, one for the fluorination of the triflate protected mannose in DMF, the second to carry out the deprotonation using sodium methanolate in methanol, but the result was incomplete deprotection of the mannose triflate precursor with a significant proportion of F$^-$ unreacted (Figure 20).
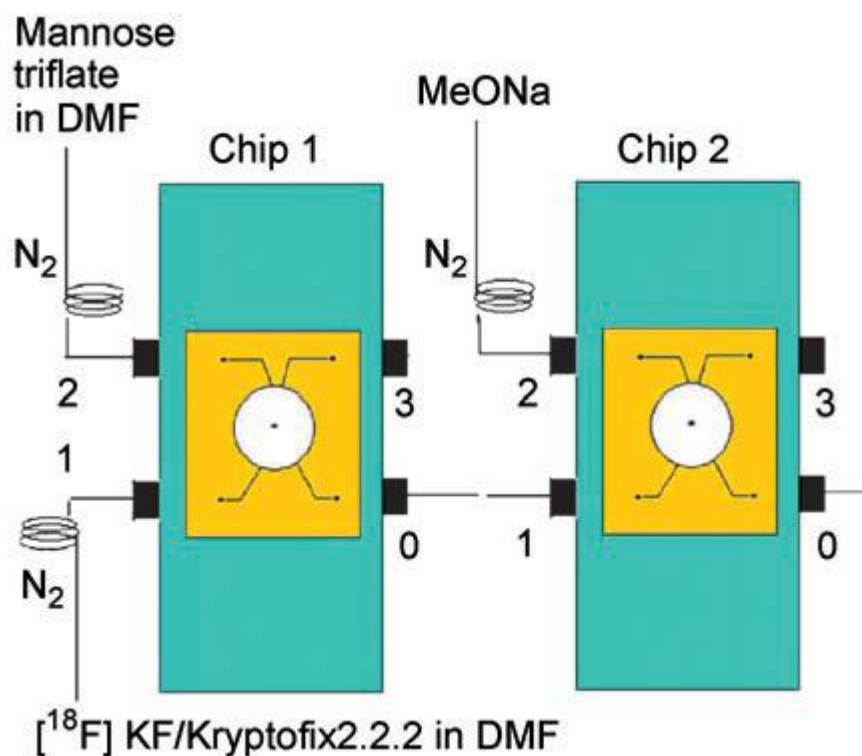
Figure 20 Schematic of the two microfluidic devices used by Gillies *et al.* Chip 1 radiolabelling of the mannose triflate, chip 2 base deprotonation [62].

A year later, Steel *et al.* [63] reported a two stage glass device for synthesis of FDG. This presented significant advantages over the previous devices in terms of total processing time, taking only 18 min compared to the 30-60 min of the previous systems. However so far, only a few of the five processing steps required for the synthesis of FDG were performed on a microfluidic device, mainly the fluorination and the acetyl deprotection. The first micro-reactor capable of performing the five chemical process

steps was reported by Lee *et al*. [64] in 2005 however the device only produced enough

FDG to conduct micro PET scans on a mouse model (Figure 21).
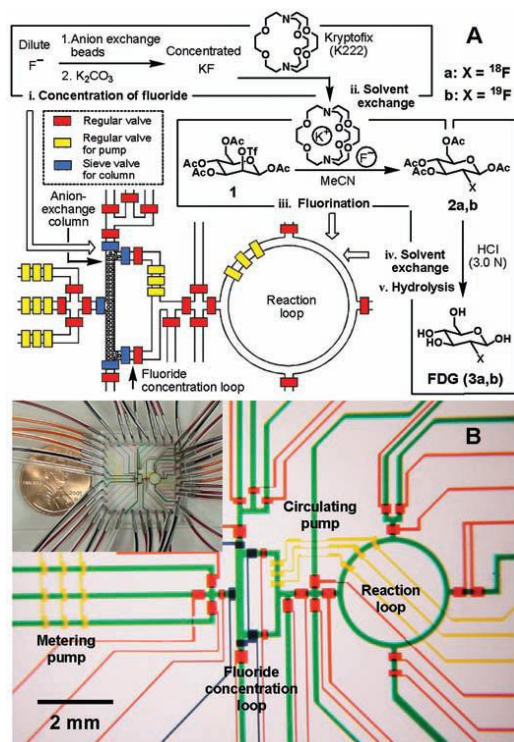
Figure 21 (a) Schematic representation of the microfluidic reactor circuit used for FDG production b) view of the device and optical micrograph from Lee *et al*.[64].

This was a PDMS device capable of performing the five steps with an integrated anion

exchange column for pre-concentration of fluoride. The main limitation of the device

was the PDMS elastomer and the poor resistance to chemicals and solvents. Recently, in

2010, the same group optimised a 5 μL coin-shaped reactor to produce sufficient

quantity of FDG to be validated by *in vivo* imaging; however, the complexity of the

system which consist of pressure valves and vacuum assisted mechanisms makes it still

a batch process that is not yet ready to produce multiple human doses [65]. Since then

not much has been achieved in terms of complete microfluidic synthesis due to the

complex nature of the chemistry involved however several groups have attempted a

different approach for the separation of [^{18}F]fluoride from water using EOF [66] and electrochemical separation [67, 68].

So far, all the process have not been united in one system capable of fulfilling the important requirements of a system that i) is fast and high yielding production of a broad range of biomarkers, ii) reducing reagent consumption, iii) is autonomous and self-shielding, iv) is located at the clinic, v) is reliable and capable of performing many cycles without involvement of technical help. The application of micro-reactors in radiochemistry is therefore still in its infancy with limited number of examples, most of them proof of principle studies or investigations [69] not yet ready to be transferred to a large scale production. Only two products using microfluidic flow reactors in some stages of radiosynthesis which have recently became available. Advion offers a system flow based system called "Nanotek LF". ScintOmics sells components for radiosynthesis system. These are described in Section 1.7.3-1.7.4 [59]. Nevertheless these so called 'microscale' systems still suffer from main limitations such as size, where apart from the micro-reactor (e.g the fused silica used in the Advion system) the rest of the components (pump, detector, heating system) still require a significant amount of space, as well extra engineering complexity (e.g. setting-up and stabilisation of the pressure pump) which make them only available to a specific group of experts.

Table 5 FDG synthesis in micro reactors and overview of the evolution.

Entry	Implementation of steps on chip	Micro reactor	Reference	Year
1	Solvent exchange Hydrolysis	Glass	[23]	2003
2	Fluorination Base deprotonation	Polycarbonate	[24]	2005
3	Fluorination Base deprotonation	Glass	[25]	2007
4	All five steps as batch process	PDMS	[15]	2005

1.9 [^{18}F]Fluoride ion activation on-chip

In order to address the challenges associated with performing the five steps, the first part of the thesis describes an investigation into the activation/isolation of [$^{18/19}$F]fluoride. Since the nucleophilic substitution was reported by Amacher *et al.*[16] two main advantages were reported i) the [^{18}F]fluorine is obtained as a solution in the irradiated water and ii) [^{18}F]fluorine is obtained "no-carrier-added" (NCA). This means the [^{18}F]fluoride ions has very high specific radioactivity, *i.e.* the ratio of [^{18}F] fluoride ions to mass of the carrier or total fluoride ion (^{19}F + ^{18}F). Highly specific radioactivity is essential for radiotracers, which are targeted at low density proteins, because low specific radioactivity (high carrier) would mean that non-radioactive tracers would annul any signal from radiotracer binding. Highly specific radioactivity also enables

radiotracers to be injected into human subjects in low mass doses (typically less than 1–10 nmol) without toxic or pharmacological effects [70].

1.9.1 Ion exchange process

The first step in many fluorine based radiosyntheses is the fluoride pre-concentration (as described in section 1.7) achieved *via* an anion exchange solid-phase extraction (SPE) process. In general Ion Exchange (IC) is a separation method based on an ion-exchange process occurring between the mobile phase and the ion exchange group bound to a solid material. The technique can be used for the separation of both organic and inorganic anions and cations, with the separation of anions accomplished either by a weak anion exchanger (NH_2 group bonded to a solid support) or strong anion exchanger (quaternary ammonium groups attached to the support), whereas sulfonate or carboxylic acid functionalities are used for the separation of cations. The solid support or resins employed in ion exchange chromatography carry the functional group with a fixed charge, and the counter ions are located near the functional group rendering the whole entity electrically neutral.

The anions in the mobile phase are exchanged for the counter anions in the stationary phase according to the reversible equilibrium process given by the Equation 3:

$$C - NR_3^+ X^- + B^- \longleftrightarrow C - NR_3^+ B^- + X^- \qquad \text{Equation 3}$$
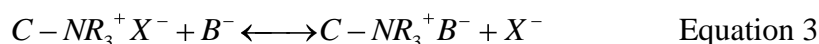
The separation of the ions is determined by their different affinities toward the stationary phase; the constant determining the equilibrium process is the selectivity coefficient K and is defined as follows:

$$K = \frac{\left[X^- \right]_s \left[B^- \right]_m}{\left[B^- \right]_s \left[X^- \right]_m} \qquad \text{Equation 4}$$

Where $[X^-]_{m,s}$ is the concentration of the sample ion in the mobile (m) or the stationary phase (s)

$[B^-]_{s,m}$ is the anion concentration in the mobile phase (m) or the stationary phase (s).

Selectivity provides a means for determining the relative affinities of ion-exchangers for different ions [71].

Some general rules can be offered to assist in the prediction of the affinity order [72] based on a number of properties:

   I.   The charge on the solute ion,

   II.   The solvated size of the solute ion,

   III.   The polarisability of the solute ion,

   IV.   The ion exchange capacity of the ion-exchanger,

   V.   The functional group on the ion exchanger,
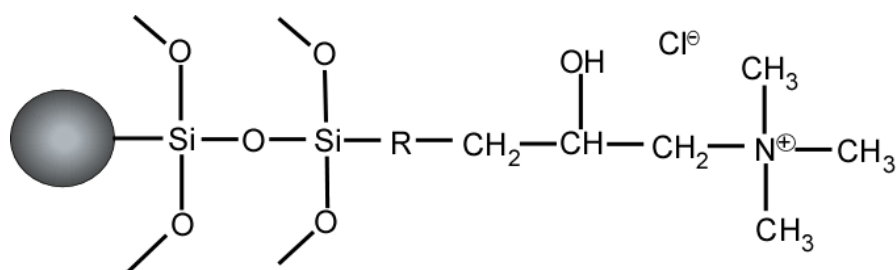
Figure 22 Example of a bound quaternary ammonium functional group with chloride as counter ion.

The first step of the synthesis of FDG and many ^{18}F based radiotracers is the pre-concentration (activation or isolation) of fluoride, and this is achieved by an anion exchange process by means of a solid phase extraction technique (SPE). There are four main phases in SPE as shown in Table 6:

Table 6 Different retention behavior between compounds for solid phase technique.

Name of Phase	Type of phase	Type of interaction	Application
Reversed phase	Polar liquid phase, non-polar modified solid phase	Non-polar interactions Van der Waals forces.	Process purification of active biomolecules, separation
Normal phase	Non-Polar liquid phase, polar modified solid phase	Polar-polar interactions Hydrogen bonding Π- Π interactions Dipole-dipole interactions.	Separation of small organic compounds with similar structures
Ion exchange	Anionic and cationic phase	Electrostatic attraction of charged group on the sorbent's surface.	Separation of charged compounds
Adsorption	Interaction of compounds with unmodified materials	Hydrophobic and hydrophilic interactions may applied depend on solid phase.	Separation of a wide variety of organic vapours and several types of inorganic gases.

1.9.2 Anion Exchange process

Ion exchange SPE can be used for compounds that are charged when in solution; the primary retention mechanism is mainly based on the electrostatic attraction of the charged functional group on the compound to the charged group that is bonded to the surface. For the purpose described herein anion exchange will be investigated. The material is comprised of an aliphatic quaternary amine group as illustrated in Figure 22. The pKa of such a quaternary amine is high (greater than 14) which renders the functional group charged at all pHs when in an aqueous solution making it ideal for the separation of [^{18}F]fluoride from [^{18}O]water. Several types of anion exchange support exist:

- Polymer based on PS-DVB (polystyrene crosslinked with divinyl benzene)
- Silica based
- Membrane based
- Monolith based

Release is achieved using a stronger eluent like high ionic strength salt like potassium carbonate (CO_3^{2-}) in the presence of phase transfer catalyst and acetonitrile. Other methods to isolate fluoride ions have been used recently, for example electrochemical procedures where an electrochemical cell was designed to allow anodic deposition of N.C.A. fluoride and recovery of deposited fluoride achieved in the presence of an aprotic solvent containing a phase transfer catalyst.[43] The use of the particles has been more a common choice due to surface area and volume ratios. There are three possibilities for the implementation of SPE in microfluidic device namely; i) to fill a channel with particles that serve as the extraction material, ii) to coat the channel wall with the functionality to act as the extraction material, iii) to fill a channel with a polymeric rod (monolithic phase) [73](Table 7).

The first example of wall coating was reported in 2000 by Kutter *et al*. [74] where the wall of a glass device was coated with C18 for enrichment of coumarin C460 but the method suffered from capacity problem due to the limited surface area. The implementation of beads in microfluidic was firstly introduced in 1995 by Ocvirk *et al*. [75]. This was a novel concept for liquid chromatography where a packed column was integrated in a silicon chip; a disadvantage of this early work was that the packing material could not be easily exchanged. Five years later, in 2000, Harrison *et al.* [76] reported the combination of solid phase extraction (SPE) and capillary electrochromatography (CEC) which allowed facile exchange of packing material.

Several improvements were made later with Ekstrom *et al.* [77] utilising a weir based silicon microextraction chip packed with reversed phase beads for the purification and enrichment of peptide mixtures. Subsequently Bergkvist *et al*. [78] improved the design and replaced the weir with a grid structure to contain the beads. In addition to beads, monolithic porous polymers prepared by photoinitiaton within the channel were reported by Yu *et al*. [79] in 2001, where an increase in concentration by a factor as high as 10^3 was achieved. Solid phase extraction on the chip was also later applied for DNA purification and extraction in 2007 by Wen *et al*. [80]. Even though the chip-based SPE method improved the sample treatment in terms of minimising sample loss and contamination problems, as well as reducing analysis time, the real benefit is in the development of an integrated system capable of miniaturising sample treatment, transportation, reaction, separation and detection provide the key to the success of microfluidic systems in chemical analysis and medical diagnosis.

Table 7 Different approaches for SPE technique and their evolution in the last decade.

Year	References	Type of SPE	Applications	Problems
1995	Ocvirk *et al*. [76]	Filled channel with particles	Liquid chromatography	Particles difficult to exchange
2000	Kutter *et al*. [75]	Coated channel wall with C18	Enrichment of Coumarin C460	Capacity problem due to limited surface area
2001	Yu *et al*. [80]	Photoinitiated monolith	Digestion of protein	Reproducibility
2002	Ekstrom *et al*. [78]	Weir based particle retention	Enrichment and purification of peptide mixtures	Not a complete integration of two steps
2003	Bergkvist *et.al*. [79]	Grid structure to contain the beads	Enrichment and purification	Not good extraction efficiency
2007	Wen *et al*. [48]	Sol-gel method	DNA extraction	Extraction efficiency not uniform

1.10 Product purification and analysis

As FDG is by far the most used radiopharmaceutical for clinical PET investigation, particular attention will be given to the purification of FDG, taking into consideration that the preparation of many other ^{18}F radiotracers is based on the same step by step approach. The potentially toxic chemical impurities resulting from the fluorination step and the hydrolysis step include: [^{19}F]FDG and FDM, K2.2.2, acetonitrile, together with radiochemical impurities of [^{18}F]FDM, [^{18}F] unreacted and partially or fully acetylated FDG. With this in mind, there are several quality controls and demands for FDG described in the European Pharmacopoeia which requires analysis for FDG and FDM by HPLC, K2.2.2 by colour spot test, ^{18}F by TLC and residual solvent by GC [81]. Based on these stringent guidelines, purification of FDG is performed on a series of

solid phase extraction cartridges including an anion exchanger cartridge for neutralisation of the acidic hydrolysis, alumina for removal of unreacted fluoride and a series of C18 cartridges for removal of starting materials or acetylated by products. An example of such a multifunctional cartridge is shown in Figure 23 [82]. The most widely used method for [^{18}F]FDG synthesis utilises the aminopolyether (K2.2.2 Kryptofix) as a phase transfer reagent to facilitate the nucleophilic [^{18}F]fluoride displacement of the triflate leaving group. Because of the toxicity of Kryptofix [IV rat $LD_{50} = 35$ mg / kg][83, 84] different method were developed to minimize the carryover of this reagent into the final product [85-87]; nevertheless verification for absence of K2.2.2 is still a mandatory requirement for quality control.

Thin-Layer Chromatography (TLC) is the most widely used quality control method for K2.2.2 in FDG injection. The method consists of spotting 2 µL samples of [^{18}F]FDG and K2.2.2 standard solutions on a silica gel plate and developing in methanol:NH_4OH (9:1). Following hot-air drying, the plates are exposed to iodine vapours for an additional 15 to 20 min for visualization [88]. Using an acidic iodoplatinate spray reagent Alexoff *et al.* [85] were able to increase the sensitivity of this method from 25 µg mL^{-1} to 2.5 µg mL^{-1} by spotting 5 µL samples [1 volume concentration hydrochloric acid to 4 volume colour reagent]; however, this method still requires the use of calibrated micropipettes and approximately 15-20 min to develop. A more rapid and sensitive method was developed by Mock *et al.* [55] where a colour spot test was able to confirm the presence of K2.2.2 in less than 5 min and utilised pre-treated strips of plastic-backed silica saturated with iodoplatinate reagent. Over spotting with the final product [^{18}F]FDG and Kryptofix standard solution, a blue-black circular spot is visible at K2.2.2 concentrations as low as 2 µg mL^{-1}; however as iodoplatinate is not specific for K2.2.2, it reacts with tertiary amines in general [89]. There is the possibility of a

false positive. If a negative colour reaction is observed however, this proves that Kryptofix is absent. Aside from techniques such as TLC a number of other analytical methods have been developed for detection of Kryptofix namely Gas Chromatography (GC) with a nitrogen-selective detector [90], HPLC with a conductivity detector [91] and Liquid Chromatography-tandem mass spectrometry (LC/MS/MS) which benefits from selective reaction monitoring [92]. Whilst the limit of detection for GC and HPLC are in the low µg mL^{-1} range, LC-MS/MS can be used to quantitatively detect ppb levels of K2.2.2 in radiopharmaceutical formulations.

Figure 23 Example of a solid phase extraction cartridge used for FDG purification from ABX, Germany.

1.11 FECH synthesis and purification

Another important radiotracer that is briefly discussed in Chapter 6 is 2-[^{18}F]Fluoroethyl choline ([^{18}F]FECH), a tracer used in oncology to image prostate cancer [93]. It represents one of the few examples of ionic radiotracers used in PET. Two synthetic approaches are currently employed and are as shown in Figure 24. In both methods ^{18}F-labelling can be carried out by ^{18}F-fluoroalkylation *via* small prosthetic groups. The most important ^{18}F-fluoroalkylating agent is 2-[^{18}F]fluoroethyl tosylate ([^{18}F]FETos), first introduced by Block *et al*. [94] [^{18}F]FETos can be synthesised easily in a

reproducible manner and purified using HPLC. In comparison 1-bromo-2-[^{18}F]fluoroethane ([^{18}F]BFE), synthesised by Chi *et al*. [95] is less commonly used because the synthetic route includes a final distillation step which makes the integration into an automated system difficult. The most common route is a two step approach which consists of the synthesis of the tosylated compound (EtDt) with subsequent addition of a large excess of *N,N*-dimethylaminoethanol (DMAE) to yield the desired final compound [^{18}F]FECH. In 2010 a one step approach was reported by Asti *et al*. [96] where the EtDt was reacted at the same time with DMAE in presence of ^{18}F$^-$/TBAHCO$_3$/ACN (after elution from the cartridge).

Purification of the final compound can be achieved using two routes. The first, reported by Hara *et al*. [97] utilised a semi-preparative HPLC, in the second approach by Asti *et al*. [96], the vial containing FECH was first washed with water, and the solution filtered through two C18 (reversed phase) cartridges connected with two anion exchange cartridges; finally the purified FECH was passed through a cation exchange cartridge and eluted with a solution of 0.9 % NaCl. Radiochemical purity (RCP) was assessed by TLC and chemical purity using an HPLC system equipped with a cation column and three different detectors (conductimetric, radiometric and UV detection at 206 nm). A GC with an FID detector was used to determine the concentration of volatile products such as ACN, EtOH. In both methods RCP of 99% was obtained.

a) Two step reaction
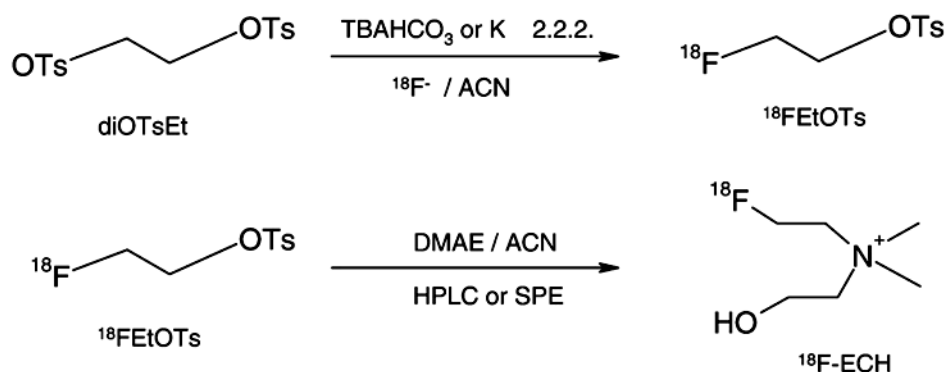
b) One step reaction
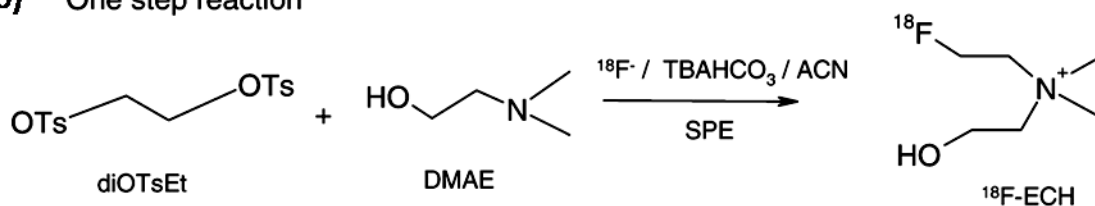
Figure 24 a) Two steps approaches for 2-[^{18}F]fluoroethyl choline (FECH) synthesis. b) One step approach for the synthesis of FECH. Adapted from [98].

1.12 Magnetism and magnetic particles

In this thesis two of the chapters are dedicated to the investigation of fluoride pre-concentration using magnetic particles. Such particles offer all of the advantages of polymeric particles some of which were described in Section 1.9 (*i.e.* high surface-to-volume ratio, variety of surface functional groups, range of sizes *etc.*), but with the added benefit of being easy to manipulate by the application of external magnets. Before describing these particles in more detail, it is worth discussing some of the relevant magnetic theory.

When an external magnetic field (**B**) is placed in proximity of a magnetic dipole moment (**m$_d$**), the dipole moment experiences a force (torque), τ, (in N m, or J), as the **B** field tries to align the dipole such that the moment (**m$_d$**) aligns parallel with the flux density (Equation 5).

$$\tau = m_d x B \qquad \text{Equation 5}$$

The extent to which a medium responds to the magnetic field (**H**) depends on the permeability of the material, μ, (in Henry per metre, H m^{-1}, corresponding to N A^{-2}). The relationship between the **H**, **B** and μ terms is given by Equation 6 [98]

$$B = \mu H$$
Equation 6

The field of magnetic flux density (**B**) consists of lines of magnetic flux, Φ_m (in Weber, Wb), within a unit area; hence a **B** field of 1 Tesla = 1 Wb m^{-2}. A greater number of lines per unit area give a greater value of **B**, indicating a stronger magnetic field. The value of **B** decreases rapidly with increasing distance from the surface of a magnet as the flux density lines move further apart, as shown in Figure 25 for a typical rectangular (bar) magnet.
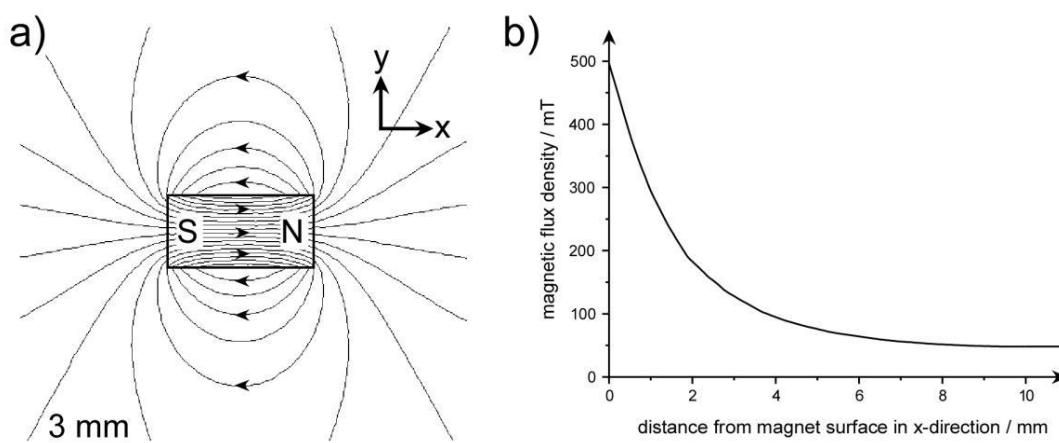
Figure 25 Characteristics of a typical rectangular magnet, illustrating a) the magnetic flux density, B, in and around the magnet, and b) the decrease in B with increasing distance from the magnet surface in the x-direction. Adapted from [99].

Additionally, when two permanent magnets are placed in proximity, different results are observed depending on their relative orientation. Figure 26a shows two magnets placed with their opposite poles facing, where the black lines represent the magnetic flux density, the colour shown indicates the relative magnitude of **B** field (where purple shows the highest value of **B** and blue the lowest). In the case shown in Figure 26 (a) the lines of magnetic flux density pass from the north pole of one magnet to the south pole of the other creating loop from one magnet to another. The flux lines between the

magnets are concentrated into a small space, and the result is an attractive force between them as shown in Figure 26 (a) [100]. In the case shown in Figure 26 (b) the field lines cannot cross, and they instead "push" against each other, generating a repulsive force between the magnets
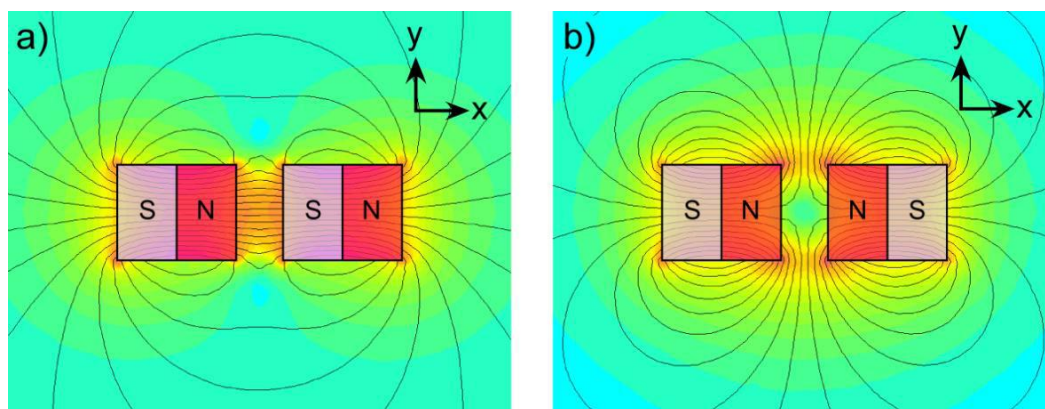
Figure 26 Magnetic flux lines and their density (B field) between two permanent magnets. a) When the opposite poles of two magnets are facing, the B field flows from the north pole of one magnet to the south pole of the other, and there is a resultant attractive force between the magnets. b) When the like poles of two magnets are facing, the field lines cannot cross, and they instead "push" against each other, generating a repulsive force between the magnets. Additionally, an area of low field is created between the facing poles. Adapted from [99].

Superparamagnetism

The main characteristic is that this materials exist as small, single domain nanoparticles [101, 102]. This means that all of the magnetic moments of the atoms in a particle align without the application of a magnetic field, forming a magnetic domain. However, due to the small size of the nanoparticles they are affected by thermal energy (k_BT), with the thermal motion continuously causing the moment of the particle to randomly flip. Hence, without an applied magnetic field the dipole moment becomes zero.
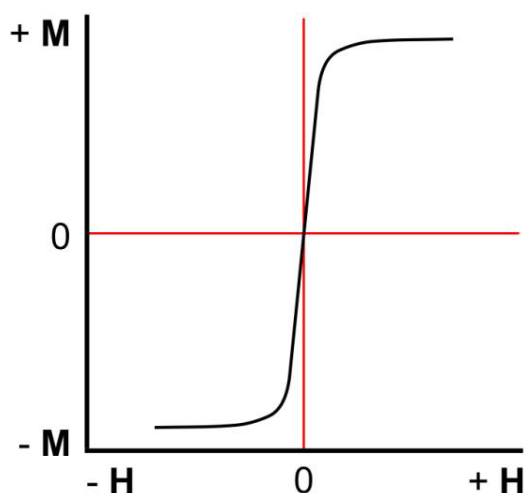
Figure 27 Magnetisation (M-H) curve for a superparamagnetic nanoparticle. As the applied field increases, so too does the particle magnetisation, until it is saturated. material, there is no magnetic remanence, meaning that upon removal of the field the particle essentially becomes non-magnetic.

When a magnetic field is applied, the moments of the particles align with the direction of the field, producing a magnetisation. However, when the field is removed, thermal energy is again able to affect the moments of the particles, returning them to their original state whereby they exhibit no magnetic moment. As a result, the particles lose their magnetisation and disperse back into the media they are present in. Hence, the particles act like paramagnets, except with very large magnetic susceptibilities and magnetic moments, and thus they are known as superparamagnetic particles. Figure 27 shows a typical **M-H** curve of a superparamagnetic nanoparticle, reaching saturation as seen in ferromagnetic materials but without the hysteresis, hence having no magnetic remanence (i.*e.* no magnetic "memory").

1.12.1 Superparamagnetic particles

Superparamagnetic particles can be fabricated or purchased in a range of sizes and with differing magnetic properties. The synthesis of superparamagnetic nanoparticles has been reviewed previously by Lu [103], Osaka [104], and Gijs [102, 105]. After the fabrication or synthesis of the magnetic particles, they can be coated with a layer of

material (such as a polymer, surfactant, silica, carbon, precious metal *etc.*) to prevent/reduce their agglomeration due to van der Waal's, magnetic and electrostatic forces. As well as these protective coatings, the surface can also be functionalised with a range of chemical or biological species (as with the microparticles in Section 1.2), including antibodies, antigens, DNA and chemical functional groups. Regarding their use in biomedicine, Osaka *et al.* [104] For their application to bioassays, and Palacek and Fojta [106] for their use in electrochemical DNA and protein biosensing. Additionally, reviews by Saiyed *et al*. and Safarik *et al.* [107] detail the use of magnetic particles (both nanoparticles and microparticles) in drug delivery and biomedicine, and for the isolation and purification of proteins and peptides. A review by Wu *et al.* [108] also summarises the most recent applications of magnetic nanoparticles in biomedicine, while a review by Krishnan [109] details their use in imaging, diagnostics, and therapy. Some of these applications include hyperthermia, drug targeting, MRI (magnetic resonance imaging) contrast enhancement and cell/particle separations [101, 110].

Two important uses of magnetic particles (both nanometre and micrometre sized) are their application to bioassays and particle/cell separations. Monodisperse magnetic microparticles can be purchased commercially from a number of sources and the brand names include Dynabeads (Invitrogen, Paisley, UK), Micromer particles (Micromod Partikeltechnologie GmbH, Rostock, Germany), Compel (Bangs Laboratorie, Inc., Indiana, USA), MACS MicroBeads (Miltenyi Biotec GmbH, Bergisch Gladbach, Germany), Adembeads (Ademtech, Pessac, France), SiMAG (Chemicell, Berlin, Germany), as well as Seradyn and MagnaBind particles (Thermo Fisher Scientific Inc., Illinois, USA).

Superparamagnetic microparticles (hereafter referred to simply as magnetic particles) are typically the same as polystyrene or silica microparticles, as described in Section

1.2, except that, crucially, they contain either a core of iron oxide (Figure 28a) or dispersion of iron oxide nanoparticles throughout the particle (Figure 28b). As well as polystyrene, various other polymer matrices can be used to fabricate the particles, and, in the case of SiMAG, a silicon matrix is also applied. The iron oxide core/nanoparticles are typically in the form of ferrimagnetic magnetite (Fe_3O_4) and maghemite (-Fe_2O_3), though sometimes other ferrites such as cobalt ferrite and manganese ferrite can be used.
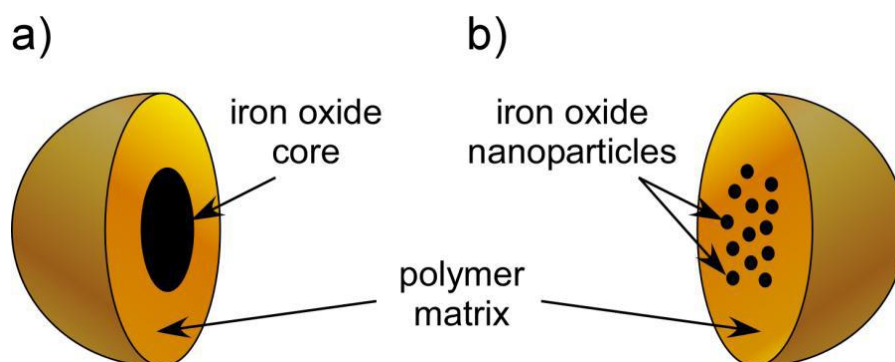
Figure 28 Cross-section of two types of superparamagnetic microparticle: a) an iron oxide core is encased in a polymer matrix, and b) iron oxide nanoparticles are dispersed throughout the polymer matrix, before being sealed inside with an extra layer of polymeric material.

Due to the size of the iron oxide nanoparticles, the microparticle as a whole displays superparamagnetic behaviour. Is due to its properties that superparamagnetic particles are becoming popular as mobile solid supports that can be easily manipulated with magnetic fields. The wide variety of possible surface functionalities, as with conventional polystyrene microparticles allows for their use in any number of reaction and/or separation procedures.
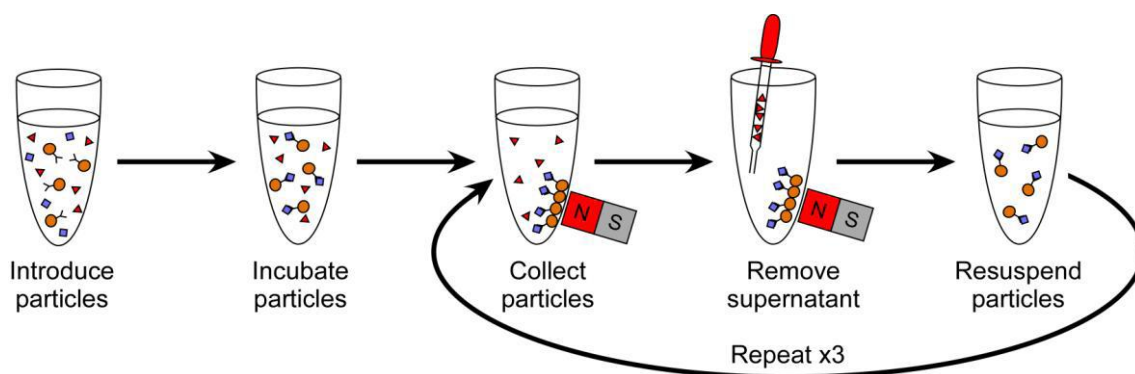
Figure 29 A typical reaction or separation using magnetic particles, where (1) the particles are introduced into the sample or reagent solution, (2) they bind to the target analyte/reagent, (3) the particles are collected using an external magnet, (4) the supernatant is removed and (5) the particles are resuspended in fresh buffer solution. Steps 3-5 are repeated several times to ensure any unbound material is removed from the particle surfaces. Adapted from [99]

A typical magnetic particle based bioassay or separation takes place in an Eppendorf tube or similar vessel, as shown in Figure 29. The tube contains the reagent or sample of interest into which the magnetic particles, featuring surface groups for binding specific targets, are introduced. The suspension is incubated with agitation, allowing the particles to bind to the target molecules, after which they are drawn to the side of the tube by application of an external magnetic field. The supernatant can then be removed, and fresh solution added. This washing step is repeated several times to ensure any unbound material are removed from the surface of the particles. Thus, the particles have successfully either removed the analyte of interest from the sample mixture, or been used to perform a bioassay or chemical reaction on their surface followed by their separation from the reagent solution.

This type of magnetic particles have gained particular attention in the field of microfluidics.some of their applications will now be presented.

The applications of magnetic particles in microfluidic devices have been reviewed in more detail by Pamme [111-113] and Gijs *et al.* [102] within a review of on-chip particle trapping methods by Nilsson *et al.* [114], and in reviews of on-chip continuous

flow particle separations by Pamme [115], Lenshof *et al.* [116], Gossett *et al.* [117], Kersaudy-Kerhoas *et al.* [118] and Tsutsui *et al.*[119].

1.12.2 On-chip magnetic trap and release procedures

Microfluidic methods of performing magnetic particle-based processes often employ a 'trap and release' technique (Figure 30). Here, functionalised particles are pumped through a micro-channel and trapped in a magnetic field, before having wash solutions or reagents flushed over them. A common use of the trap and release method is for the on-chip separation of magnetic particles that have been suitably functionalised to bind to a particular target analyte, from the original sample matrix. The particles are trapped and washed with buffer solution, which removes the unwanted non-magnetic material from the system and they are then released for collection or downstream analysis. Such processes have been achieved using permanent magnets [109, 120, 121] integrated micro-electromagnets [122, 123] external electromagnets [124, 125] and integrated metallic or microcircuit structures that are subsequently magnetised by an external applied field [126-128]. These set-ups have typically only been used to separate magnetic particles from their carrier fluid, but it has also been shown that different magnetic particle populations can be separated and trapped when combined with dielectrophoresis [121], along with the successful separation and detection of magnetically labelled dengue virus has been reported [120].
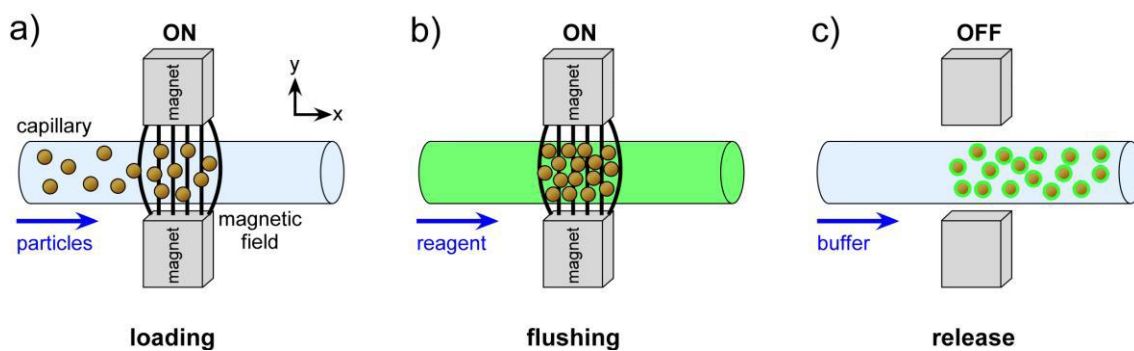
Figure 30 Trap and release method of magnetic particle handling in microchannels. a) Magnetic particles are loaded into the channel and trapped in a magnetic field, b) a sample or reagent is flushed over the trapped particles, allowing reactions to occur on the particles surface, before being washed with buffer solution, c) the field is removed and the particles released for downstream detection or further processing. Adapted from [99].

Here, functionalised particles are trapped in the micro-channel by a magnetic field, and a reagent solution is flushed over them, allowing the reagent to bind to the particle surfaces. The reagent is replaced with buffer solution in order to wash the particles, which are then released from the magnetic field for downstream detection, or other reactions and assays *i.e.* streptavidin-biotin and protein [129, 130], purification and enrichment of dengue virus samples for RNA amplification and detection [131], mRNA isolation [132], DNA hybridization [133, 134], separation [135] and protein digestion [136, 137]. The above examples show a selection of microfluidic 'trap and release' methods however, the 'trap and release' is a batch method, and as such suffers from the same inefficiencies as off-chip methodologies in that they can be laborious and time-consuming due to the number of reaction and washing steps that must be performed. One method of reducing these inefficiencies is to perform the separations, reactions and assays in continuous flow. This offers the advantages of combining all of the reaction and washing steps into one single process, thereby decreasing the amount of time and labour required and user intervention required, rendering the procedure relatively automated once developed.

1.12.3 On-chip magnetic particles separation in continuous flow

As previously mentioned continuous flow separations offer the potential to eliminate some of the inefficiencies associated with batch microfluidic methods, allowing continuous introduction and separation of the sample, as will be discussed in Section 4.2; magnets produce magnetic field gradients with respect to the distance from their surface. When in proximity to a micro-channel (~ few mm), these gradients are sufficient to exercise a pN force on a particle. An immediately obvious advantage of a magnetic force over other forces is its simplicity. Sorting of magnetic material is readily achievable with a very basic fluidic and magnetic set-up. For example, Kim and Park [138] presented a device with two inlets, a single channel and two outlets. Using a simple permanent magnet placed adjacent to the channel they were able to isolate fluorescent particles agglomerated with magnetic nanoparticles *via* an immunoassay procedure from a sample stream. The magnetic field gradient across the channel could be varied by simply moving the magnet closer or further from the channel edge[139-141].
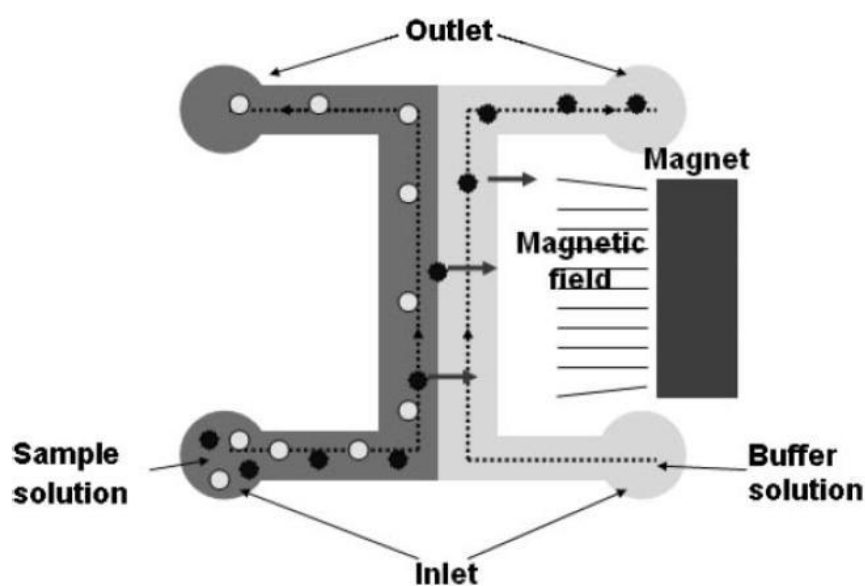
Figure 31 A common microfluidic method for continuous magnetic particle separation, known as a H-filter. A particle mixture is introduced into a wide channel alongside a buffer stream, and a

magnet used to deflect the magnetic particles into the buffer stream while the non-magnetic particles remain unaffected. The two particle populations are thus separated *via* two outlets. Adapted from [138].

In order to fractionate out material according to magnetic properties, a chamber with multiple outlets is required. The development of free-flow magnetophoresis using a small permanent magnet was first developed by Pamme *et al*. [142] in which a separation chamber was fabricated in glass with multiple exits. Magnetic particles were introduced and deflected from flow by the application of a magnetic field on the opposite side of the chamber, perpendicular to flow, as shown in Figure 32.
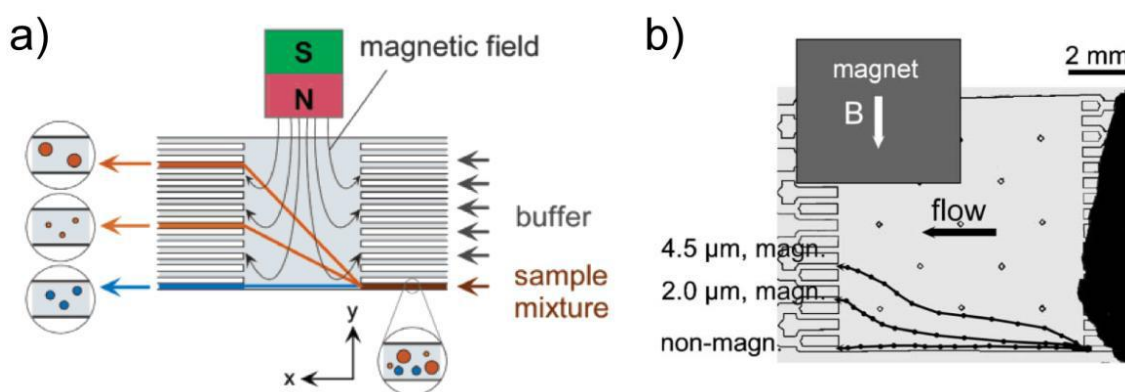
Figure 32 (a) Principle of on-chip free-flow magnetophoresis. A mixture of particles is introduced into a microfluidic chamber and deflected laterally by a magnetic field, allowing different particle types to exit the chip by different outlets [142]. (b) Experimental particle trajectories of 4.5 µm and 2.0 µm magnetic particles, as well as non-magnetic particles, demonstrating their separation as they traverse the chamber. Adapted from [113].

The on-chip free-flow magnetophoresis microfluidic device featured a wide chamber into which a mixture of particles was introduced into the bottom corner (Figure 32). A series of inlets allow the introduction of a buffer stream parallel to the sample stream, with the two streams flowing side-by-side due to laminar flow, and a series of outlets provide a number of potential exit points for the particles; as well as allowing the removal of sample and buffer waste. An inhomogeneous magnetic field was generated across the chamber, perpendicular to the direction of laminar flow, *via* an external

permanent magnet. When a mixture of magnetic particles of different sizes and magnetic susceptibilities was introduced into the chamber, they were deflected from the direction of flow by the magnetic field, traversing the chamber diagonally until they exited *via* one of the outlets. However, the different particle types deflected towards the magnet to different extents, such that the two particle populations exited through different outlets, thus achieving a continuous, simultaneous separation of two types of magnetic particles. Later, Pamme and Wilhelm [111] also used the technique to separate magnetically labelled cells. Thus, the technique of on-chip free-flow magnetophoresis has been demonstrated for the simultaneous separation of different magnetic particle types, and for the deflection and separation of magnetically labelled cells.

1.13 Aims of the project

The aim of this project was to develop an integrated modular microfluidic platform for the pre-concentration of [^{18}F]fluoride and purification of ^{18}F fluorine based radiopharmaceuticals employed in Positron Emission Tomography (PET). Micro Total Analysis Systems (µTAS) have been applied to the synthetic pathways typical for radiotracers in order to improve the traditional approach in terms of efficiency and safety. The work of this thesis was part of a European Union Radiochemistry on Chip project (CP-FP 213803-2 ROC as part of the FP7 Theme 4-NMP/Nanosciences, Nanotechnologies, Material and new Production Technologies) which consisted of a collaboration of industrial and academic partners as shown in Figure 33. The objective of this work package (WP4) was to implement microfluidic modules for ^{18}F pre-concentration (the starting material for radiosynthesis) and the final product purification.

The work performed throughout the PhD is split into different sections in this thesis. Firstly, the materials and methods used will be detailed in the **Experimental** Chapter.

This will be followed by several **Results** Chapters, which are divided into two main sections describing those experiments performed for the fluoride pre-concentration using *magnetic and non-magnetic particles* followed by the experiments on the investigation of the *product purification*. A **Conclusions** Chapter summarises the work performed along with recommendations for future of the work. **References** will then be listed, followed by an **Appendix** containing publications related to the work described here.
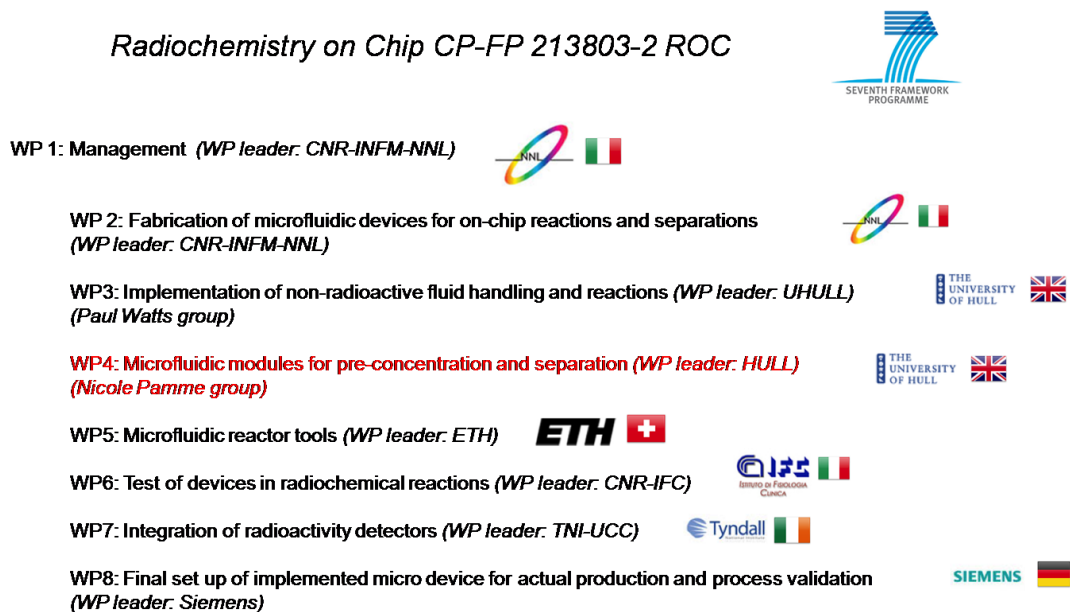
Figure 33 Image showing the different work packages (WP) involved in the FP7 EU project, with their deliverable and task.

2 Experimental

This Chapter describes the experimental set-up and procedures utilised for work in this thesis, detailing (Section 2.1) the chemicals, particles and instrumentation employed, the design of the microfluidic chips, the chip set-up and the particle visualisation (2.2, 2.3, 2.4), the off-chip fluoride pre-concentration experiments (2.5), on-chip fluoride pre-concentration *via* dam-structure experiments (2.6), on-chip fluoride pre-concentration *via* plug of magnetic particles experiments (2.7), on-chip fluoride pre-concentration *via*

free flow magnetophoresis (2.8), Kryptofix 2.2.2 detection and removal (2.10), FECH detection and purification (2.11).

2.1 Chemicals, particles and instrumentation

Solvents and reagents were purchased from the distributors shown in Table 7. All chemicals were of analytical grade. Aqueous solutions were prepared in water with a resistivity of 18.2 MΩ cm at 25 °C, obtained from an ELGA Option 4 that fed into an ELGA UHG PS water purification system (both devices from ELGA Process Water, Marlow Buckinghamshire, UK), unless otherwise stated. Prepared solutions were filtered through 0.20 µm syringe filters (Whatman, VWR, Lutterworth, Leicestershire, UK) prior to introduction into microfluidic devices.

Table 7 Chemicals, solvents and reagents used in the experiments described herein.

Chemical	Supplier
Solvents	
Acetone	Fisher Scientific, Leicestershire, UK
Acetonitrile	Fisher Scientific, Leicestershire, UK
Chloroform	Fisher Scientific, Leicestershire, UK
Cycloexane	Fisher Scientific, Leicestershire, UK
Ethanol	Fisher Scientific, Leicestershire, UK
Hexadecane	Fisher Scientific, Leicestershire, UK
Methanol	Fisher Scientific, Leicestershire, UK
Propan-2-ol	Fisher Scientific, Leicestershire, UK
Toluene	Fisher Scientific, Leicestershire, UK
2,2,4-Trimethyl pentane (isooctane)	Fisher Scientific, Leicestershire, UK
Acids and Bases and buffers	
Hydrochloric acid (36%)	Fisher Scientific, Leicestershire, UK
Methanesulfonic acid (MSA)	Sigma-Aldrich, Dorset, UK
Potassium carbonate	Sigma-Aldrich, Dorset, UK
Phosphate buffered saline tablets (PBS)	Sigma-Aldrich, Dorset, UK

Potassium bicarbonate	Sigma-Aldrich, Dorset, UK
Potassium fluoride	Sigma-Aldrich, Dorset, UK
Potassium hydroxide	Sigma-Aldrich, Dorset, UK
Sulphuric acid (98%)	Fisher Scientific, Leicestershire, UK
Sodium fluoride	Sigma-Aldrich, Dorset, UK
Sodium hydroxide	Sigma-Aldrich, Dorset, UK
Sodium chloride	Sigma-Aldrich, Dorset, UK
Surface treatments and silanising agents	
Agarose (low melting point)	Sigma-Aldrich, Dorset, UK
(3-Aminopropyl)triethoxysilane	Sigma-Aldrich, Dorset, UK
Dimethyloctadecyl[3-(trimethoxysilyl)-propyl]ammonium chloride (42 % wt. in MeOH) (QAS)	Sigma-Aldrich, Dorset, UK
Octadecyltrichlorosilane (OTS)	Sigma-Aldrich, Dorset, UK
Trichloro(1*H*,1*H*, 2*H*,2*H*-perfluorooctyl)silane (FDTS)	Sigma-Aldrich, Dorset, UK
Surfactants and additives	
Tween 20 (polysorbate 20)	Sigma-Aldrich, Dorset, UK
Sodium dodecyl sulphate (SDS)	Sigma-Aldrich, Dorset, UK
Fluoride pre-concentration	
Kryptofix 2.2.2 (K2.2.2) (4,7,13,16,21,24-hexaoxa-1,10-diazabicyclo-[8.8.8]-hexacosane)	Sigma-Aldrich, Dorset, UK
12-Crown-4 (1,4,7,10-Tetraoxacyclododecane)	Sigma-Aldrich, Dorset, UK
Tetrabutyl ammonium bicarbonate (TBAHCO$_3$)	ABX, Radeberg, Germany
FDG synthesis	
Mannose triflate, 1,3,4,6-tetra-*O*-acetyl-2-*O*-trifluoro-methanesulfonyl-beta-D-mannopyranose	ABX, Radeberg, Germany
2-Deoxy-2-fluoro-D-glucose (FDG)	ABX, Radeberg, Germany

2-fluoro-2-deoxy-glucose tetraacetate (ACY- FDG)	ABX, Radeberg, Germany
2-Fluoro-2-deoxy-D-mannopyranose (FDM)	ABX, Radeberg, Germany
FECH synthesis	
1,2-Bis(tosyloxy)ethane (Ethylene glycol ditosylate)	ABX, Radeberg, Germany
N-(2-Fluoroethyl)-2-hydroxy-*N*,*N*-dimethyl-chloride (FECH chloride)	ABX, Radeberg, Germany
2-(Dimethylamino)ethanol (DMAE)	Sigma-Aldrich, Dorset, UK

2.1.1 SPE with non magnetic particles

Several commercially available solid phase extraction (SPE) chromatography cartridges were investigated. The particle content was extracted from the cartridges; the specific details are reported in the Tables 8-11:

The most popular method for the purification of proteins and other charged molecules is ion exchange chromatography as described in Section 1.10.1. In cation exchange chromatography, positively charged molecules are attracted to a negatively charged solid support. Conversely, in anion exchange chromatography, negatively charged molecules are attracted to a positively charged solid support.

Anion exchange particles:

For a comparative study, the following commercial anion exchange cartridges and resins, commonly used in the pre-concentration of fluoride during the FDG preparation, were obtained; QMA Sepak light particles, (Waters, Massachusetts, USA), Chromabond PS-HCO$_3$ (Macherey-Nagel, Duren, Germany), Strata SAX particles (Phenomenex, Macclesfield, UK) and Source 15Q (GE Healthcare, Uppsala, Sweden) details of which are reported in Table 8. The cartridges were delivered in sealed packages except for the

source 15Q delivered as suspension of particles in 20% ethanol and 80% water. Before

use, each cartridge was washed with purified water to remove any residual contaminants

that may have been present.

Table 8 Commercially available SPE cartridges for anion exchange chromatography used in this work.

Cartridge / Particles type	Application	Particle diameter / μm	Functional group and counterion	Protein Binding capacity* (mg g^{-1})	Matrix core material
Sep-Pak Accell Plus QMA (Waters UK)	Strong anion exchanger	60	Quaternary ammonium (Cl-)	222	Silica
Chromabond PS-HCO$_3$ (Macherey–Nagel)	Strong basic anion exchanger	100	Quaternary ammonium (HCO$_3^-$)	0.90	PS-DVB
Chromabond PS-OH$^-$ (Macherey–Nagel)	Strong basic anion exchanger	100	Quaternary ammonium (OH$^-$)	0.53	PS-DVB
Strata SAX (Phenomenex)	Strong anion exchanger	57	Quaternary ammonium (Cl$^-$)	30	Silica
Source 15Q (GE Healthcare)	Strong anion exchanger	15	Quaternary ammonium (Cl$^-$)	40	PS-DVB

* As reported from the manufacturers MSDS

Reversed phase particles

Separation *via* reversed phase chromatography arises from the adsorption of

hydrophobic molecules onto a hydrophobic solid support in a polar mobile phase.

Decreasing the mobile phase polarity, using organic solvents, reduces the hydrophobic

interaction between the solute and the solid support resulting in desorption. The more

hydrophobic the molecule the more avidly it will adsorb onto the solid support. This

requires a higher concentration of organic solvent to promote desorption. Reversed phased cartridges were therefore investigated for removal of K2.2.2 (Table 9).

Table 9 Reversed phase chromatography cartridges investigated during the removal of K222.

Particles Type	Application	Particle diameter / μm	Functional group	Binding capacity* / mg g^{-1}	Matrix core material
Chromabond HR-P (Macherey–Nagel)	Reverse phase chromatography	85	Octadecyl carbon chain	300 ± 100 (caffeine)	PS-DVB
Strata-X 33u Polymeric reversed phase (Phenomenex)	Reverse phase chromatography	33	Octadecyl carbon chain	Not reported	Polymer
SEP-PAK C18 (Waters UK)	Reverse phase chromatography	55-104	Octadecyl mono functional silane	Not reported	Silica

* As reported from the manufacturers MSDS

Cation exchange particles

Table 10 Commercially available SPE cartridges for cation exchange chromatography.

Particles type	Application	Particles diameter / μm	Functional group	Binding capacity* / mg g^{-1}	Matrix core material
SEP-Pak Accell Plus CM (Waters UK)	Strong cation exchanger	53	Sulfonic acid	201	Silica
Chromabond PS-H (Macherey-Nagel)	Strong acid cation exchanger	100	Sulfonic acid	0.35	PS-DVB

* As reported from the manufacturers MSDS

Normal Phase particles

Neutral aluminum particles were also used for removal of fluoride during the purification step in the FDG synthesis (Table 11).

Table 11 Commercially available SPE cartridge for unreacted fluoride removal during purification of [^{18}F$^-$]fluorine based radiocompounds.

Particle name	Application	Particle diameter / μm	Functional group	Binding capacity*/ mg g^{-1}	Matrix core material
ALOX-N Macherey-Nagel	Normal phase	100	Aluminum oxide	0.29[143]	Aluminium oxide

2.1.2 Magnetic particles

Dynabeads superparamagnetic particles of 1 μm and 2.8 μm diameter were purchased from Invitrogen (Paisley, UK) and featured a variety of surface functionalities, as detailed in Table 12, and were supplied in a buffer suspension. Others particles were purchased from Chemicell (Chemicell, Germany). Table 12 lists the magnetic particles used during the work in this thesis with their characteristics and specifications.

Table 12 List of superparamagnetic particles employed in this work. Details are given of particle sizes, surface groups, number of particles, all as stated by the manufacturer.

Particle Type	Application	Particles diameter / μm	Surface group	Particles concentration / particles g^{-1}	Matrix core material
Dynabeads SAX (Invitrogen)	Strong anion exchanger	1.0	Quaternary amine (Cl$^-$)	1.8 x 10^{12}	PS
Dynabeads M-270 Amine (Invitrogen)	Weak anion exchanger	2.8	Amine (-NH$_2$)	2 x 10^9	PS
Dynabeads MyOne Carboxylic Acid (Invitrogen)	Weak anion exchanger	1.05	Carboxylic acid (-COOH)	7 - 12 x 10^9	PS
SiMAG –Q (Chemicell)	Strong anion exchanger	1.0	Quaternary ammonium (Cl$^-$)	1.8 x 10^{12}	Silica
SiMAG –Q (Chemicell)	Strong anion exchanger	3.0	Quaternary ammonium (Cl$^-$ counter ion)	6.8 x 10^{10}	Silica

Dynabeads RPC 18 (Invitrogen)	Reversed phase chromatography	1.0	Octadecyl carbon chain	2.3 x 10^{10*}	PS
SiMAG-DEAE (Chemicell)	Weak anion exchanger	1.0	Diethylamin oethyl	1.8 x 10^{12}	Silica
SiMAG-Carboxyl (Chemicell)	Weak cation exchanger	1.0	Sodium carboxylate	1.8 x 10^{12}	Silica
SiMAG-Phosphonate (Chemicell)	Weak cation exchanger	1.0	Sodium phosphonate	1.8 x 10^{12}	Silica
SiMAG-Sulfon (Chemicell)	Strong cation exchanger	1.0	Sodium sulfonate	1.8 x 10^{12}	Silica

*the only value given by the particles supplier was 12.5 mg beads mL^{-1}, since the exact density of the particles is not known, an assumption can be made in which the density is an approximate to that of polystyrene particles, so the following calculation was performed to obtain the number of particles per mL:

$$V = \frac{4}{3}\pi r^3 \qquad\qquad \text{Equation 7}$$

Density of polystyrene particles approximate 1.07 g mL^{-1}, hence by knowing the volume and the density the number of particles was calculated.

2.1.3 Detection instruments

In this paragraph a detailed list of several detection methods for some of the common analytes used in the synthesis of FDG reported in the literature are presented (Table 13). It is worth noting that not all of the below instrumentations were used or described in more detail by the author of this thesis, but it should give a general overview to the

reader in understanding the variety of detection methods available with a comprehensive list of their detection limit when reported.

Table 13 Methods applied to the detection of product and impurities after the synthesis of 2-[^{18}F]fluoro-2-deoxy-D-glucose.

Analyte	Detection method	Limit of detection
[^{19}F]Fluoride	IC with conductivity detector [144]	0.05 µg mL^{-1}
	Fluoride selective electrode [145]	1.9 µg mL^{-1}
[^{18}F]fluoride	Radio-TLC*	Not reported
[^{19}F]FDG	HPLC-PAD (IC-PAD or HPAEC-PAD)* [56, 82, 85, 146]	Not reported
		Not reported
	HPLC-RID[20]	Not reported
	GC [147]	0.31 µg mL^{-1}
	GC-MS [64]	0.02 µg mL^{-1}
	HPLC-UV (after derivatisation with 2-CA) (276 nm) [148]	Not reported
	HPLC-UV (after derivatisation with PMP) (210 nm) [149]	Not reported
[^{18}F]FDG	Radio-TLC* [16, 22, 62, 65, 67, 85, 150, 151]	Not reported
	Radio-HPLC* [20, 50, 82, 152]	Not reported
Kryptofix 2.2.2	Colour spot test on TLC plate* [22, 55, 57, 82, 153]	2 µg mL^{-1}
	TLC [85, 86, 88]	25 µg mL^{-1}
	GC with nitrogen selective detector [90]	0.25 µg mL^{-1}
	LC-MS-MS [154]	1 ng mL^{-1}
	Titration with lead (II) perchlorate [155]	1×10^{-5} M

	UV-Vis (after forming a lead (II) complex) (250 nm) [156]	< 10 µg mL^{-1}
	HPLC-UV (210 nm)[149]	0.5 µg mL^{-1}
	NMR [157]	Not reported
	IR [157]	Not reported
Acetonitrile	GC-FID* [22, 151, 158]	0.1 µg mL^{-1}
	GC-MS [159]	< 10 µg mL^{-1}
	HPLC-RID [20]	< 30 µg mL^{-1}

* Denotes recommended method of analysis according to the European Pharmacopeia [160].

2.1.4 Detection of [^{19}F]Fluoride ions

For detection of cold fluoride [^{19}F] three systems were compared namely; ion selective electrodes (ISE), Colourimetric detection and ion chromatography (IC).

In the first part of the project the fluoride ion detection was investigated using an ion selective electrode (Jenway 924-305 Fluoride (F$^-$), Jenway, Dunmow, Essex, UK). This is the most commonly used ion-electrode, responding to a wide range of fluoride concentration with little interference. The sensor is a crystal of lanthanum fluoride, whose surface potential changes when placed in solutions of different concentrations. The experiment was carried out to evaluate the dynamic range of fluoride concentration. The relationship between potential and fluoride concentration is given in the modified Nernst equation.

$$E_{F-} = E_{F-}{}^* - 0.0591 \log a_{F^-} \qquad [145] \qquad \text{Equation 8}$$

Where: E_F^- is a constant. A change in electrode potential of 59.16 mV will be associated with a ten-fold change in fluoride concentration.

A calibration graph of potential (mV) vs. log [F$^-$] could be plotted from which the concentration of the unknown could be determined.

The mV-reader was a Horiba pH/COND Meter D-54 (Horiba, Japan). A magnetic hot plate stirrer was used to stir the solutions before taking the measurement and to keep the temperature constant (20 ± 3 ℃). All the solutions were placed in a plastic beaker before the measurement. The electrode was clamped in a vertical position so that the sensor was immersed in a beaker and was washed and dried when transferring between solutions. The electrode was immersed in the solutions for 7 min to obtain a steady reading. Due to its sensitivity, the electrode was immersed in the most dilute standard first.

For the colorimetric detection of fluoride, two different spectrophotometers were employed: i) Perkin-Elmer UV/vis Spectrometer Lamba Bio 10 (Perkin-Elmer, Cambridge, UK) with UV win lab software and ii) Camspec M508 UV/vis Spectrophotometer (Camspec Analytical Instrument Ltd., Leeds, UK). The first was used to scan the wavelength range between 200 – 800 nm and the second for single wavelength calibration experiments. Optically transparent polystyrene disposable cuvettes (Fisher, UK) of 1000 μL volume and 10 mm pathlength were used for wavelength below 400 nm.

Later on an ion exchange chromatograph was set-up and used for detection of fluoride. The system employed was an ICS 2000 (Dionex, USA) with a conductivity detector and a self-regenerating suppressor AS11-HC column (250 mm column length, 2.5 mm diameter, 0.25 mL min^{-1} flow rate, 15 mM KOH as eluent) which was employed to quantify the trapping and elution of fluoride and was used in isocratic mode. Due to the

interferences of carbonate ions with the IC detector only concentrations lower than 0.001 M (mol L^{-1}) were employed to elute the fluoride

2.1.5 Detection of K2.2.2

All experiments for the detection of Kryptofix by HPLC-MS were performed with a Varian MS 500 (Varian, USA) quadruple ion trap mass spectrometer equipped with an atmospheric pressure ionization interface of electrospray ionization and dual gradient pump with an autosampler (Varian, USA). Electrospray ionization was performed in positive ion mode and the data were processed using Xcalibur software. HPLC analysis was performed on an analytical column HS C18, 150 mm x 2.1 mm, 3 µm particles, (Supelco, UK), with an isocratic mobile phase consisting of 50% water, 50% acetonitrile at a flow rate of 0.4 mL min^{-1} and an injection volume of 10 µL. Under these conditions the total run time was 10 min and the retention time of Kryptofix was 1.46 min. For the colorimetric detection of Kryptofix, two different spectrophotometers were employed; i) Perkin-Elmer UV/vis Spectrometer Lamba Bio 10 (Perkin-Elmer, Cambridge, UK) with UV win lab software, ii) Camspec M508 UV/vis Spectrophotometer (Camspec Analytical Instrument Ltd., Leeds, UK). The first to scan the wavelength range between 200 – 800 nm and the second for single wavelength calibration experiments. Optically transparent polystyrene disposable cuvettes (Fisher, UK) of 1000 µL volume and 10 mm pathlength were used.

2.1.6 Radioactive detection instrumentation

^{18}F Fluoride was produced at a cyclotron in Pisa (PETrace, GE, USA) by proton bombardment (Ep = 16.7 MeV, 5-10 min at 20-25 µA) of a 1.3 mL ^{18}O-water (enrichment >98 %) silver target. Radio HPLC was performed on a Waters Delta 600 pump system equipped with a RaytestGabi Star Gamma detector connected in series to

a Waters 996 Photo Diode Array (PDA) detector and a Synergi Fusion-RP C-18 column (4 x 150 mm) (Phenomenex, UK).

Radioactive tests and labeling reactions were conducted using an Advion Nanotek system (Advion, USA) as shown in Figure 34. The chips were connected to the system by modifying the standard plumbing whereby the inlet of the chip was interfaced to a port of an 8-way bridged valve bearing a 0.5 mL high pressure syringe. Three radiation detectors were integrated in the system in order to follow the distribution of the radioactive species during the experiments.

The operation for trapping and elution was software controlled, minimising direct intervention of the user. Solutions employed were; i) for conditioning 1.0 M $NaHCO_3$; ii) for trapping and release of irradiated target water containing the fluoride, Kryptofix 2.2.2 10 mg in 1 mL acetonitrile and 80 µL of 5 % w/v K_2CO_3. Trapping of fluoride took place at 500 µL min^{-1} and elution of fluoride at 250 µL min^{-1}.

Figure 34 Image of the modular, liquid-flow-based "NanoTek LF" microfluidic synthesis system [42].

2.1.6.1 [19F]Fluoride pre-concentration

All chemicals were of analytical grade and used without further purification. Ultrapure water (18 MΩ cm^{-1}) was employed unless otherwise stated. A solution of [19F] (1 µg mL^{-1}) prepared from sodium fluoride was used as a reference standard. The elution

solution consisted of 10 mg of Kryptofix 2.2.2 (K2.2.2) dissolved in 900 µL anhydrous acetonitrile (MeCN) and 100 µL of 0.01 M aqueous potassium carbonate (K_2CO_3).

Required amount of fluoride: The amount of [^{19}F]fluoride ions used for experiments and the amount of ion exchange packing used in the device were chosen according to the amount of [^{18}F]fluoride ion routinely used for FDG tracer synthesis. The radioactivity of 1-2 mL "hot water" used for FDG production can be as high as 150 GBq. Considering a specific activity between 300 GBq µmol^{-1} and 43,000 GBq µmol^{-1} (maximum theoretical activity = 63,000 GBq µmol^{-1}), it was calculated that the maximum amount of [^{18}F]fluoride ions present in cyclotron irradiated water should not exceed 9.5 µg, with a typical average of 0.5 µg [156, 161, 162]. The experiments with the radioactive fluoride isotope were carried out with hot water as would routinely be used for FDG synthesis. Experiments involving standard solutions of fluoride were carried out with 1 µg of fluoride ions.

On-chip procedure: The on-chip particle bed was activated prior to trapping by flushing with 2 mL ethanol and 2 mL purified water at a flow rate of 1000 µL min^{-1}. For trapping, 1 mL of fluoride standard solution was pumped through the particle packing at a flow rate of 500 - 1800 µL min^{-1}, this was followed by flushing with 1 mL water. The trapped fluoride was subsequently eluted with the K2.2.2/acetonitrile/K_2CO_3 solution at a flow rate of 500 µL min^{-1}. The particle bed was then regenerated by flushing the chip with 2 mL of 1.0 M $KHCO_3$, followed by 3 mL of purified water at 1000 µL min^{-1}.

Fluoride detection: Eluted solutions were collected after both the trapping and elution steps for the quantification of fluoride. 25 µL of each collected solution was injected into an ion chromatography system (ICS-2000, Dionex, USA) equipped with an AS-11HC analytical anion exchange column and a conductivity detector. The flow rate was 0.25 mL min^{-1} and 15 mM potassium hydroxide was used as the eluent.

2.1.6.2[^{18}F]Fluoride pre-concentration

<u>Chemicals and solutions</u>: High-purity solvents were stored on molecular sieves and vented through a sodalime molecular sieve trap during radiochemical experiments. [^{18}F]Fluoride ion was produced at a cyclotron (PETtrace, GE, USA) by proton bombardment (Ep = 16.7 MeV, 5-10 min at 20-25 µA) of 1.3 mL ^{18}O-water (enrichment > 98%) using a 1.5 mL silver target-holder. The produced target water with a starting activity of 5-7 GBq was diluted with pure water to a volume of 4 mL. Ethyl ditosylate (EtDT) was synthesized as published [93, 163].

<u>Fluorination mixture analysis</u>: HPLC with radioactivity detection was performed using a Delta 600 pump (Waters, USA) equipped with a Synergi Fusion-RP C-18 column (Phenomenex, UK) (4 µm, 3 mm x 150 mm) and a Gabi Star gamma detector (Raytest, Germany) connected in series to a 996 Photo Diode Array detector (Waters, USA).

<u>Microfluidic chip set-up for fluoride trapping test</u>: The microfluidic chips were connected to an Advion Nanotek radiotracer synthesis system (Advion, USA) by modifying the standard connections (Fig. 35). The inlet of the chip was interfaced to a port of an 8-way bridged valve bearing a 0.5 mL syringe on the common port and was operated under negative or positive pressure as required. The remaining vials were connected to vials containing (i) a solution of aqueous 1.0 M sodium bicarbonate (NaHCO$_3$) or H$_2$O, (ii) (K2.2.2) solution which was prepared by adding a solution of 10 mg K2.2.2 in 1 mL acetonitrile to 80 µL aqueous K$_2$CO$_3$ (5% w/v), (iii) air for drying the particle bed and (iv) irradiated target water. The remaining ports on the valve were blocked off. The chip outlet was connected to software controlled solenoid valve (SV) to direct the fluids towards either a waste or a collection vial.
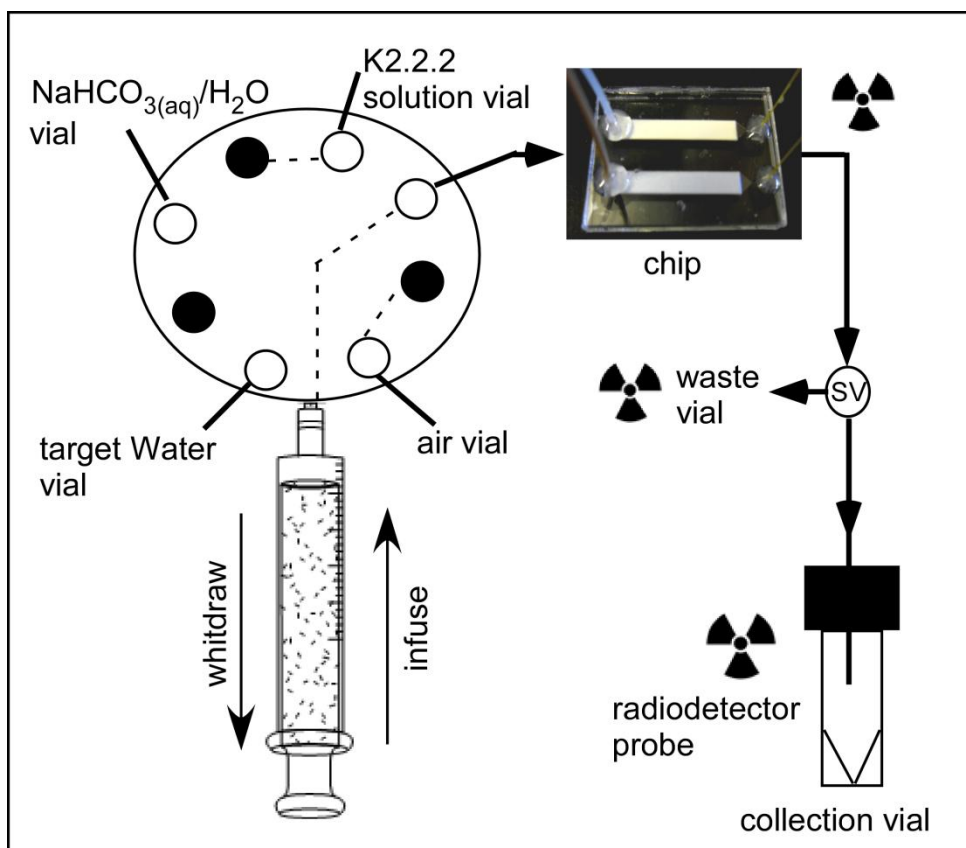
Figure 35 Schematic representation of the microfluidic chip integrated with the Advion synthesis system, showing the 8 way valve connected to a driving syringe, vials with target water (containing aqueous radioactive [^{18}F]fluoride ions), aqueous carbonate solution or water, K2.2.2/acetonitrile elution solution, air and finally the microfluidic anion-exchange chip. The chip outlet was connected to a solenoid valve (SV) which could direct liquid either to a waste vial or a collection vial. Radioactivity detectors were placed on the anion-exchange chip, next to the waste vial and next to the collection vial.

Figure 36 Image of the microchip device (packed bed microchip) integrated with the Advion Nanotek LF, showing the microchamber glass device and one of the three radiodetector probes placed on top the device for real time monitoring of the radioactivity.

<u>Procedure for trapping and releasing of fluoride</u>: A flow rate of 500 μL min^{-1} was employed for all steps. 0.5 mL of target irradiated water (activity ranging from 620-875 MBq) was delivered into the microfluidic chip packed with Chromabond PS-HCO$_3$ particles followed by 1 mL of air to dry the particles. The solenoid valve was then turned off/on to direct liquid to the collection vial. 0.5 mL of K2.2.2 solution was pumped through the chip followed by 1 mL of air to ensure recovery of the [^{18}F]fluoride complexed solution. The solenoid valve was turned back to direct liquid to the waste vial and additional 0.5 mL of pure H$_2$O was delivered to waste. The entire procedure took 6 min.

<u>Procedure for regeneration of the ion-exchange particles</u>: The packed chip was rinsed with 2 mL of NaHCO$_3$ and subsequently with 2 mL of H$_2$O, both at a flow rate of 500 μL min^{-1}, the reconditioning procedure lasted 4 min.

Three radiation probes were employed for continuous on-line count rate monitoring at different locations of the hardware; one was placed on top of the microfluidic chamber (Figure 36) to measure the radiation in the particle bed, the second for measuring radioactivity in the waste vessel and the third for measuring radioactivity in the collection vessel. The hardware operations for the trapping and releasing of [^{18}F]fluoride ions, as well as regeneration of the particle bed, were programmed using Advion's software (Version 1.4) in order to minimise direct intervention of the operator. At the end of each trap, release and reconditioning cycle, the waste vials and collection vials were counted and replaced with empty ones. The cycles were repeated for as long as target water was available; a maximum of eight consecutive runs was possible from the same batch of [^{18}F]fluoride ion solution.

2.1.6.3 Fluoride labeling reaction

When the fluoride solution was used for labeling reactions, the whole volume of target water (1.5 mL), containing [^{18}F]fluoride ion, was trapped in the chip and the elution step was performed at a slower flow rate, thus allowing the delivery of 100 μL drops directly into separate 3 mL V-vials (preheated at 110 °C) while applying nitrogen flow (1.2 bar) and a vacuum to aid evaporation. Azeotropic evaporation of the excess water was achieved by dropwise addition of 0.5 mL acetonitrile under the same nitrogen flow, leading to a bubble-free evaporation. This last step was done alternating the recovery of a 100 μL drop in the collecting vial to a 20 s pause allowing evaporation; this confined the entire radioactivity to the bottom of the V-shaped vial. The dry residue was then reconstituted with 0.5 mL of acetonitrile, and the labeling medium was charged into a 403 μL storage loop. A solution of EtDT (25 mg mL^{-1} in acetonitrile) was pumped into a second 429 μL storage loop. Finally, several labeling reactions were conducted by employing 10 μL aliquots of both reactants dispensed at 20 μL min^{-1}, each into a 15.7 μL fused silica reactor preheated to 150 °C. The fluidic scheme for this procedure is shown in Figure 37.
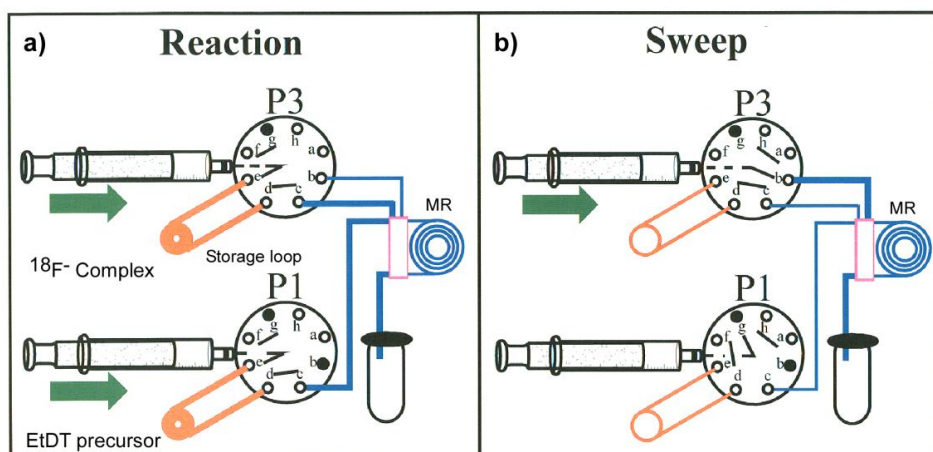
Figure 37 Schematic representation of the EtDT labeling reaction process within the Advion automated system after drying of excess of water has been performed. The precursor solution was pumped into the loop of pump 1 (P1) while the labeling solution was introduced into the sample loop of pump 3 (P3). (a) In the reaction step, fluoride complex and precursor solution aliquots were delivered into the capillary micro-reactor (MR) preheated at a temperature 150 °C from the storage loops by pushing with pure solvent (acetonitrile); in this phase the fluids moved through the

lines indicated in bold. (b) In the sweep step, the micro-reactor system was rinsed with pure solvent through the lines indicated in bold and prepared for a further reaction with other aliquots of reagents.

2.2 Microchip designs

Several chip designs were used throughout the experiments described here; 1) a dam structure chip design for fluoride pre-concentration, K2.2.2 removal and FECH purification, 2) four different glass devices with parallel channels for the pre-concentration of fluoride *via* plug of magnetic particles and 3) two different devices one with four inlets and four outlets the second with five inlets and five outlets for the magnetophoresis experiments.

2.2.1 Parallel channel chip

Four different chip designs were investigated (Figures 38-39) the difference between them was the number of parallel channels and the width of each individual channel. All of them were fabricated in glass with a depth between 20-30 μm. Preliminary experiments as described in Section 4.3 were carried out using the designs in Figure 38 featuring 16 parallel channels (PC16) of 200 μm width and 32 parallel channels (PC32) with a width of 100 μm each. The 64 channels (PC64) had a width of 200 μm for each individual channel whilst the 128 channels (PC128) had a width of 100 μm each channel.
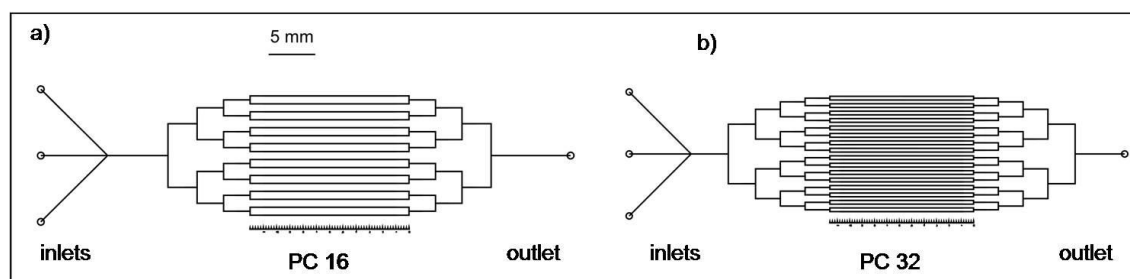

Figure 38 Schematic view of chips design for investigation on magnetic plug left device featuring a) PC16 and b) PC32.
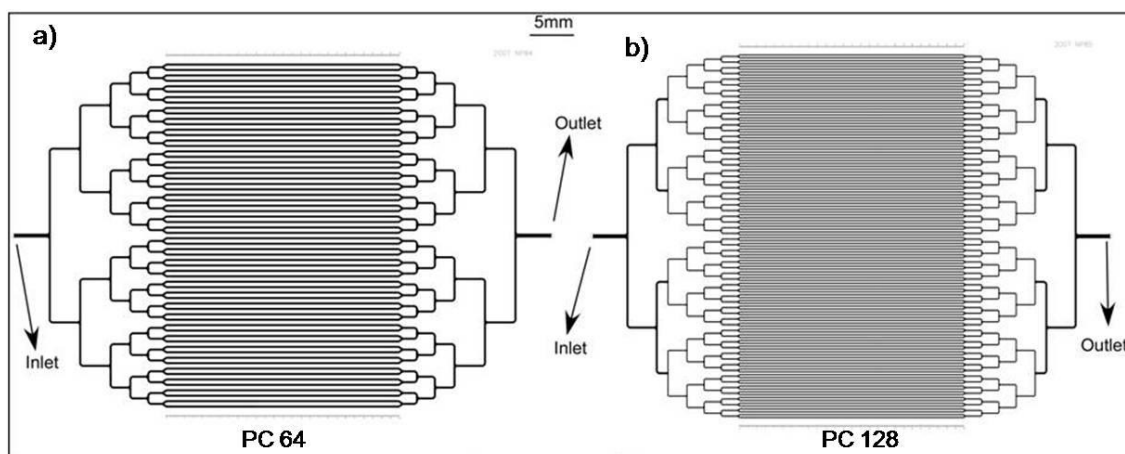
Figure 39 Schematic of chips design, featuring a) 64 parallel channels (PC64) and b) 128 channels (PC128).

2.2.2 Dam structure device

The chips design were patterned onto glass wafers using the photolithography technique and wet etching method of chip fabrication [164]. For the dam structure a double etched design was used to obtain 2 different depths to allow particles trapping, 3 mm glass wafers coated with chromium layer and photoresist layer were used (B270 glass, Telic, Valencia, CA, USA). The top plate was etched to a depth of 50 μm and the bottom 250 μm for a total depth of 300 μm. Particles were introduced *via* the larger hole (1.5 mm diameter) which was also the inlet for introduction of fluid. The outlet hole was drilled at 400 μm diameter. A schematic view as well as a photo of the empty chamber are shown in Figure 40.
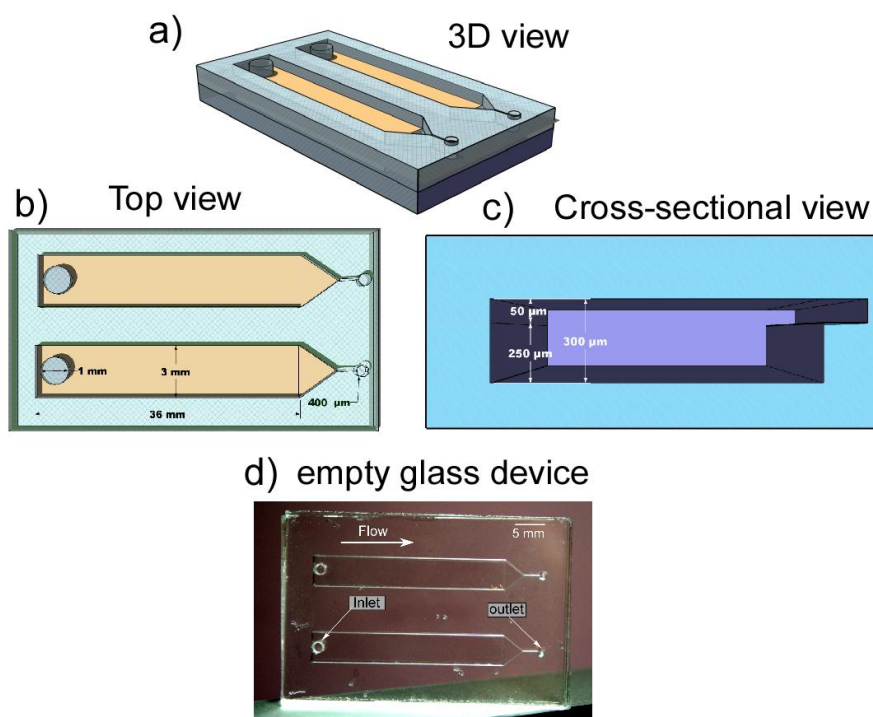
Figure 40 Schematic view of the dam structure chip device. a) 3D view, b) top view featuring dimension of the chamber and holes, c) cross sectional view featuring the depth of the double etched plates and d) a photo of the empty glass chip.

2.2.3 Free-flow magnetophoresis chip

Two different devices (FL1 and FL2) were used for the investigation of the free-flow magnetophoresis experiments. Both were fabricated in 1 mm thick B-270 glass to a depth of 20 µm. FL1 featured an 8 mm x 3 mm reaction chamber with a depth of 20 µm with a symmetrical inlet and outlet system of five channels (Figure 41). Each of the inlet and outlet channels was 240 µm wide, before branching into two 120 µm wide channels prior to the reaction chamber. Inlet 1 was used for the introduction of particles into the chamber, with inlets 2 to 5 used as reagent and buffer inlet channels, depending on the experiment being performed.

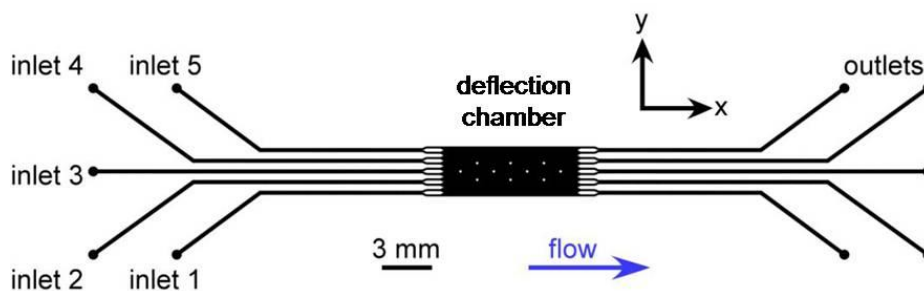**Figure 41 Schematic of chip design FL1, featuring an 8 mm x 3 mm reaction chamber, five inlets, and five outlets.**
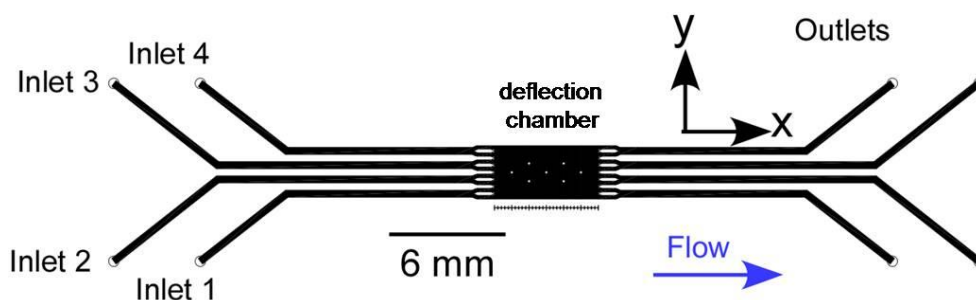
Figure 42 Schematic of chip design FL2, featuring a 6 mm x 4 mm reaction chamber, four inlets, and four outlets.

FL2 featured a reaction chamber of 4 x 6 mm etched at a depth of 20 μm with a symmetrical inlet and outlet system of four channels with a width of 200 μm.

2.3 Chip setup and interfacing

Chip designs FL1 and FL2 were utilised for the on-chip free-flow magnetophoresis experiments. Before the use of the pressure pump, glue was used for fixing capillaries into the inlets and outlets of the microchip. For most of the experiments described here, fused silica capillaries (150 μm i.d., 363 μm o.d., Polymicro Technologies LLC, Composite Metal Services Ltd., UK) were inserted into the inlet / outlets holes and glued in place using Araldite Rapid Glass & Ceramic epoxy resin. For the dam structure device where the inlet hole was 1.5 mm in diameter a piece of PTFE (0.3 mm i.d., 1.58 mm o.d., Supelco, UK) tubing was used and at the outlet a piece of poly ether ether ketone tubing (PEEK, 150 μm i.d., 360 μm o.d., Cole-Parmer Instrument Co., UK) was

glued using Araldite Rapid Glass & Ceramic epoxy resin, into the inlets and outlets holes of the chip and interfaced to a 5 mL syringe (Henke-Sass Wolf (HSW) polypropylene syringe, VWR), *via* Tygon tubing (1.0 mm i.d., 1.8 mm o.d., Cole-Parmer). A syringe infuse rate between 400 μL h^{-1} to 1.7 mL min^{-1} was applied using a syringe pump (Pump 11 Plus, Harvard Apparatus, UK).

Microfluidic chip interfacing with chip holder

Later in the project to avoid gluing issues with blocked channels when glue seeped into the inlet or outlet holes, a chip holder was used where chips could be fixed in place and the capillaries introduced and sealed without the need for glue. The chip holder was prepared in-house by the Engineering Workshop in the Department of Chemistry, and was fabricated from aluminium. The holder was built in two identical sections, each consisting of a bottom plate, onto which the chip was placed, with a top plate placed over the inlet holes of the chip and screwed into the lower plate (Figure 43). The top plate featured a matrix of holes, each 5 mm apart, such that the access holes of the chip could be aligned to allow capillaries to be connected to the chip.
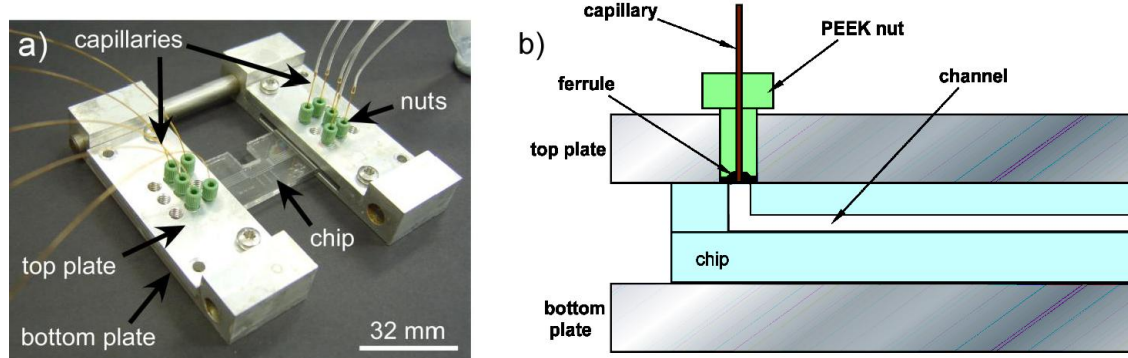
Figure 43 Photographs of the chip holders fabricated in-house, and the nuts used to connect the capillaries to the chip. a) Chip holder design, consisting of sliding sections to accommodate different sized chips. b) Schematic demonstrating the interfacing of capillaries to a microfluidic device when using a chip holder. The capillary is held by a ferrule that covers the inlet hole of the chip, and the ferrule is sealed against the chip by a PEEK nut that screws directly into the chip holder. The top and bottom plate are made of Aluminium and are held together in place by eight screws (four for the inlets side and four for the outlets). Adapted from [99].

Whether the capillaries were glued into a chip or a holder was used for the connections, the subsequent steps remained the same for each setup. Tygon tubing (0.254 mm i.d., 0.762 mm o.d., Cole-Parmer) was attached to each of the outlet capillaries and fed into a sample vial for waste collection. Tefzel ferrules (1/16 inch, Anachem Ltd., UK), with a sleeve of poly(tetrafluoroethylene) tubing (PTFE, 0.3 mm i.d., 1.58 mm o.d., Supelco, UK) inside them, and PEEK nuts (1/16 inch, Anachem Ltd.) were attached to the ends of each inlet capillary by inserting the capillary into the PTFE sleeve, and the chips then underwent a washing procedure. The washing solutions varied depending on the experiment. A PEEK syringe adaptor (1/4-28 Female to Female Luer adaptor, Anachem Ltd.) was screwed onto the nut of one of the capillaries, and the first washing solution was pumped through the chip via a 1 mL syringe (BD Plastipak, Becton Dickinson UK Ltd., UK). Positive pressure was used for all the experiments, syringes with the appropriate particle suspension and reagents were loaded onto a syringe pump with a multi-syringe rack (PHD 22/2000, Harvard Apparatus). The syringe pump was activated to start pumping the particle suspensions, reagents and buffers through the chip if using positive pressure. Flow rate between 10-30 $\mu L\ h^{-1}$ were employed unless the pressure pump was used.

2.4 Particle visualization

Chips were placed onto the stage of a Nikon Ti inverted fluorescence microscope (Nikon Instruments Europe B.V., Surrey, UK), equipped with 2x, 4x, 10x, 20x, and 40x objectives (Figure 56). Videos and images were captured using colour CCD camera (MTV-63V1N, Mintron Enterprise, Taiwan) and WinDVD Creator 2 software (InterVideo (Corel UK Ltd.), Berkshire, UK).

2.5 [¹⁹F]Fluoride pre-concentration off-chip

Initial investigations into non-radioactive fluoride pre-concentration were performed off chip in order to gain familiarity with the new detection methods and to optimize a suitable method for quantification of fluoride during the trapping and elution steps.

2.5.1 Preparation of anion standards for fluoride calibration

Seven anion standards were used to aid the analysis of fluoride by ion chromatography (IC) and to help identify the different peaks and their retention times. The standard was prepared by the dissolution of high purity salts in the concentration range between 10 - 100 ppm in high purity deionised water.

2.5.2 Preparation of stock solutions

A stock solution of NaF was prepared by dissolving 2.21 g of sodium fluoride (Sigma Aldrich, UK) in 1 L of water which gave 1000 ppm of F^- (1000 µg mL^{-1}). Fluoride standard solutions were prepared in the range $0.1 - 100$ ppm by serial dilution of the stock and stored in plastic beakers. A solution of 0.25 M K_2CO_3 (Sigma Aldrich, UK) was prepared by dissolving 6.9105 g in 200 mL water. A solution of 1.0 M $KHCO_3$ (Sigma Aldrich, UK) was prepared by dissolving 10.012g of potassium bicarbonate in 100 mL water.

2.5.3 Off-chip pre-concentration via non magnetic particles

The experiments were carried out by pumping solutions through the different cartridges listed in Table 8 using a syringe pump (Harvard apparatus 11 plus and Harvard apparatus PHD 2000, USA) with a disposable 1 mL plastic syringe (BD Plastipak, UK). Figure 44 shows the schematic procedures for trapping and elution of fluoride which includes the five steps cycle needed for the pre-concentration of fluoride; i) conditioning, ii) washing, iii) trapping, iv) elution, and v) regeneration.
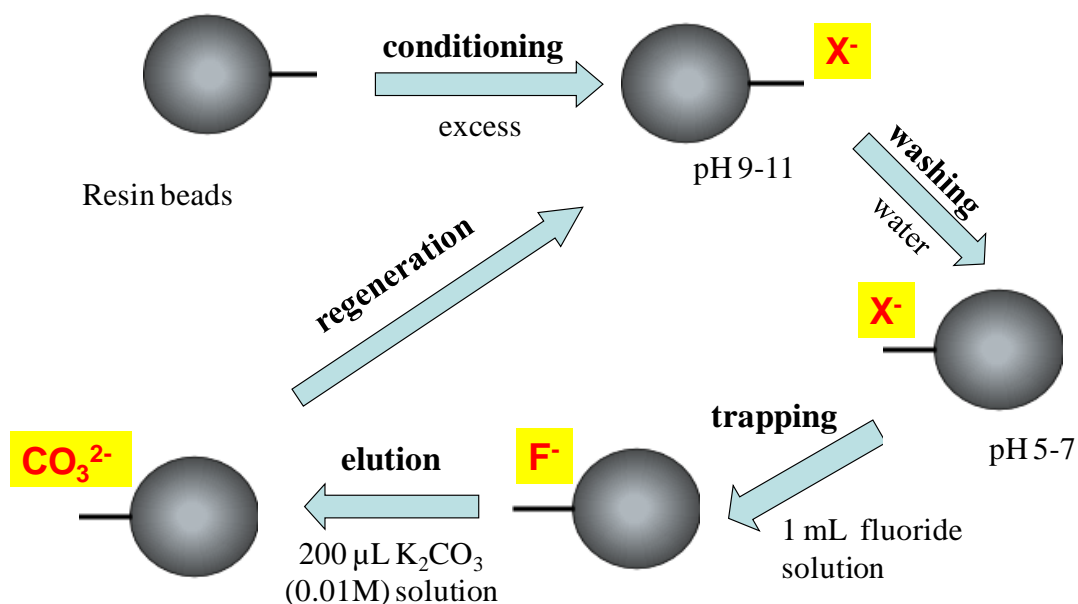
Figure 44 Schematic representation of fluoride activation; first conditioning of the resin, washing with water to neutralise the resin, trapping, elution and regeneration.

2.5.4 Off-chip pre-concentration via magnetic particles

Two different superparamagnetic particles, 1 and 3 μm diameter, featuring quaternary ammonium groups in the chloride form were tested during the off chip experiment to identify the binding efficiency of the particles to the fluoride ion in an aqueous environment. The particle suspension was vortexed for 20 s and the particles collected at one side of the Eppendorf tube (1.5 mL, VWR, UK) *via* an external magnet. The supernatant was removed and fresh water was added; the process was repeated twice. When loading of the counter ions was performed the last wash was replaced with a solution of NaCl (1.0 M). A schematic representation of the steps used during the magnetic approach for fluoride pre-concentration is shown in Figure 45.

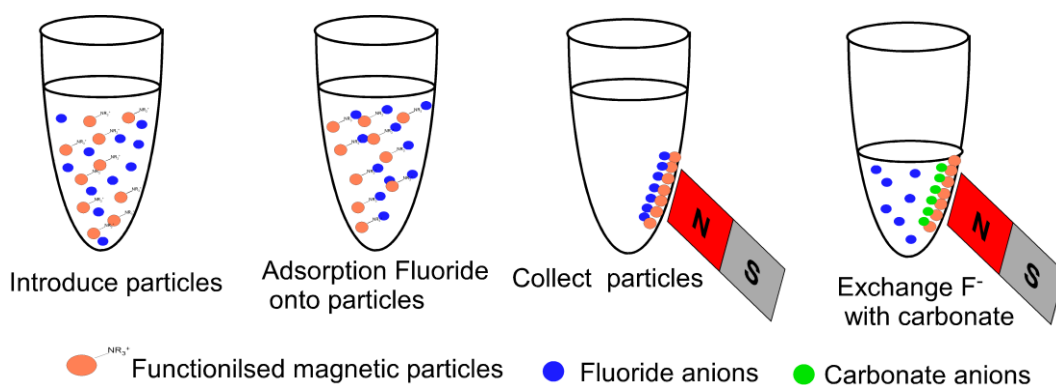**Figure 45 Steps by steps trapping of fluoride and elution. Step 1 fluoride solution was introduces into the Eppendorf containing the magnetic particles. Step 2 the adsorption of fluoride onto the particles surface takes place. Step 3 an external magnet is applied on the side of the Eppendorf and the particles with the fluoride ions collected on the side, a further washing step is sometimes performed with fresh buffer solution. Step 4 the carbonate anions in solution (less volume then the original solution is then introduced and the exchange between fluoride and carbonate takes place.**

2.6 Fluoride pre-concentration on-chip (dam structure)

The first part of the experiment was the preparation of the microchamber (described in 2.2.2) this was achieved by deconstructing the available cartridge and filling the chamber with the particles. For the pre-concentration of fluoride, the chamber was filled with commercially available anion exchange particles, (PS-HCO$_3$ or Sep-Pak Light Plus QMA) as described in Section 2.1.2. The particles were introduced as a dry powder from the larger hole by using a micro spatula and constantly tapping the device in a vertical position to obtain a homogenous packing, as shown in Figure 46 a). 20-30 mg of ion exchange particles could be trapped in the chamber. It has to be noted that during the gluing of the inlet tubing the tube was insert into the inlet hole (in top plate) in such a way that it will be in contact with the chamber (bottom plate) in order to ensure that when solution was pumped through the particles bed was fully wet. The on-chip particle bed was activated prior to trapping by flushing with 2 mL ethanol and 2 mL purified water at a flow rate of 1000 μL min^{-1}. For trapping, 1 mL of fluoride standard solution was pumped through the particle packing at a flow rate of 500 - 1800 μL min^{-1}, followed by flushing with 1 mL water. The trapped fluoride was subsequently eluted

with the K2.2.2/acetonitrile/K_2CO_3 solution at a flow rate of 500 µL min^{-1}. The particle

bed was then regenerated by flushing the chip with 2 mL of 1.0 M (KHCO$_3$) followed

by 3 mL of purified water at 1000 µL min^{-1}.
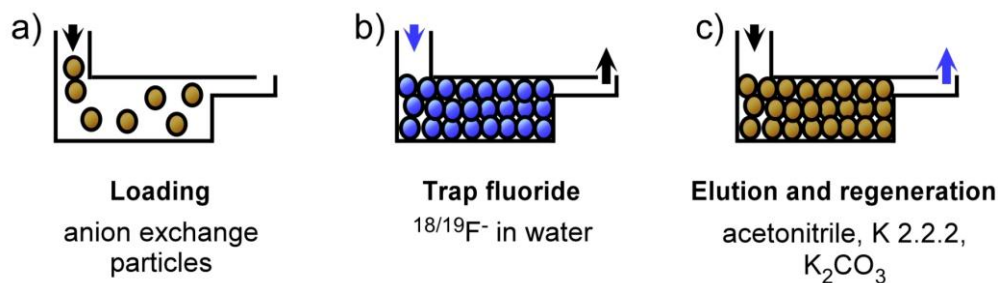
Figure 46 Pre-concentration of fluoride on trapped anion exchange particles, including (a) loading of the particles into a microfluidic device, (b) trapping of fluoride from solution and (c) elution of fluoride.
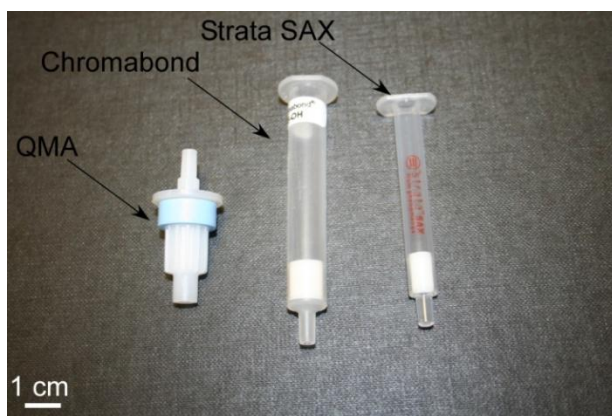
Figure 47 SPE cartridges commercially available. Silica based QMA from Water (50 µm average particles diameter), Chromabond polystyrene cross linked with divinyl benzene (100 µm average particles diameter) and silica based Strata SAX (60 µm average particles diameter).
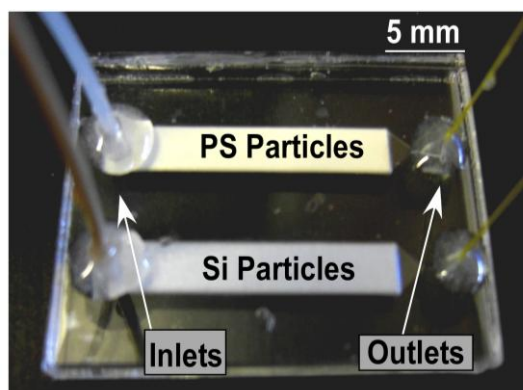
Figure 48 Dam structure device filled with two different anion exchange particles namely; silica (Si) and polystyrene (PS).

2.6.1 Pressure measurement on dam structure chip

Investigation on the maximum flow rate and pressure exerted on the dam structure chip were performed using a pressure meter DPG 120 (OMEGA Engineering INC., US) connected with PEEK tubing to the inlet of the chip allowing correlation of the pressure with the flow rate from the syringe pump; the experimental set-up for this study is shown in Figure 49.
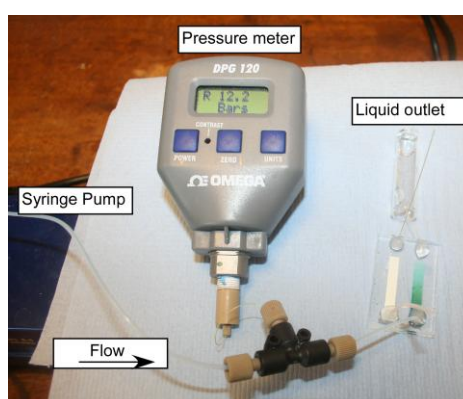
Figure 49 Set-up used to measure the pressure within the chamber of the packed bed device.

2.7 Fluoride pre-concentration on-chip via plug of magnetic particles

Magnetic microparticles can be captured on-chip with external magnets. As described in Section 1.13.2, fluoride can be trapped and subsequently eluted from the particle bed. The schematic representation for the pre-concentration of fluoride *via* magnetic plug trapping is shown in Figure 50, with the loading of the magnetic particles first and the trapping and release of the fluoride in the same device.
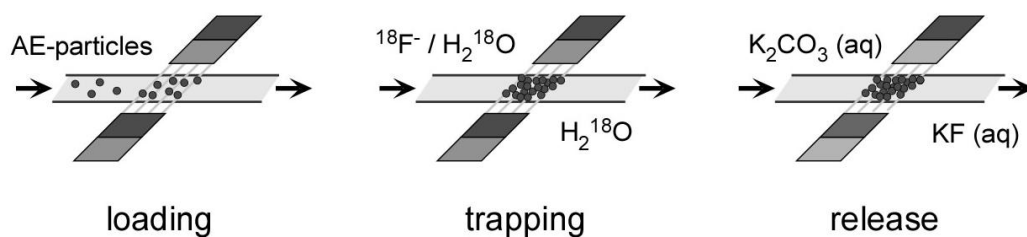
Figure 50 Schematic of the magnetic capture approach. Magnetic microparticles can be captured on-chip with external magnet; fluoride can be trapped and subsequently eluted from the particle bed.

Microchip pre-treatment

Before each experiment, the microchip was flushed with water to remove any air from the chamber and the channels by manual pumping. The microchip was then flushed with 100 mM NaOH using the syringe pump at a rate of 100 μL h^{-1} for 3 min. The NaOH was flushed out of the microchip with water, and EtOH was pumped through for another 3 min.

2.7.1 On-chip plug formation

1 μm and 3 μm Simag-Q superparamagnetic particles functionalised with a quaternary ammonium group in the chloride form were purchased from Chemicell (Berlin, Germany). The particles were received as a concentrated suspension (4.2 x10^{10} particles mL^{-1} for the 1 μm i.d. and 1.57 x 10^{9} particles mL^{-1} for the 3 μm i.d. particles); the stock suspensions was stored in a refrigerator at 6° C.

Fused silica capillary of ~ 8 cm length (100 μm i.d., 360 μm o.d., Polymicro Technologies LLC, Composite Metal Services Ltd, UK) was used. The polyimide coating was partly removed using a flame from a lighter to allow observation under the microscope. The capillary was then mounted onto a glass slide; tygon tubing (254 μm i.d., 762 μm o.d., Cole Parmer, UK) was pushed over the ends of the capillary. One end was dipped into the Eppendorf tube (1.5 ml VWR, UK) the other end the tubing was pushed over a 25G syringe needle (Terumo, Surrey, UK) which was luer locked to a 1

mL glass syringe (SGE Analytical Science, Australia). The sample was pulled from the sample tube through the capillary by application of negative pressure with a pump (Harvard Apparatus 11plus, Harvard application, USA). NdFeB magnets of 5 mm length and 2 mm diameter were purchased from Magnet Sales (Swindon, UK). A pair of magnets was glued to a glass support such that the opposite poles were facing each other over a 5 mm gap. The magnet holder was placed on the capillary support such that the capillary ran through the gap of the poles. Blu tac adhesive was used to fix the magnet holder. The whole set-up was placed on the stage of an inverted microscope (Nikon) with images captured and recorded with a CCD camera (PV10, Olympus, Japan) and Image pro capture software (Open source software http:\\rsb.info.nih.gov/ij.index.html). An image of the experimental set-up is shown in Figure 51.
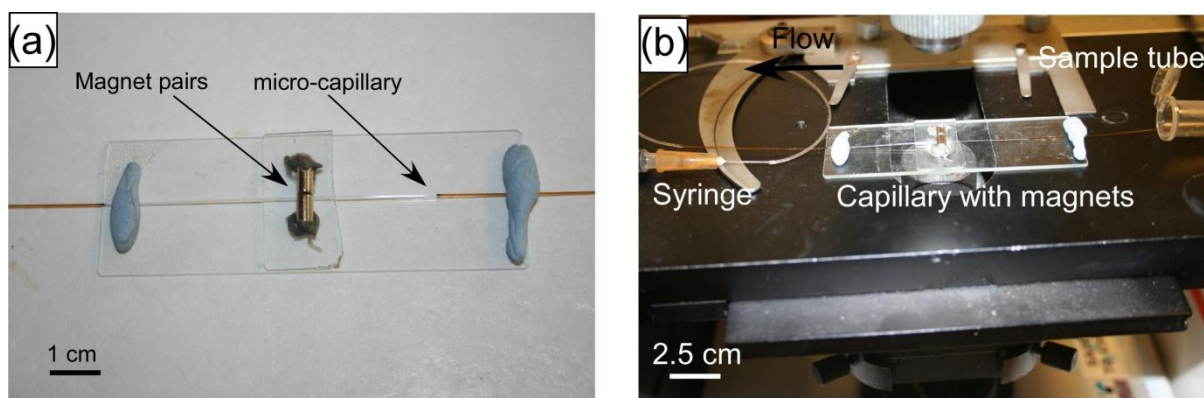
Figure 51 (a) Set-up of the glass capillary and the magnet pairs positioned on a glass slide, (b) Set-up of the microfluidic device under the microscope.

2.7.2 Magnet set-up for parallel channels experiment

For parallel channels experiments most commonly, a 10 x 10 x 5 mm^3 rectangular NdFeB magnet (Magnet Sales, UK) was placed on top of the chip, in the case when 128 or 256 parallel channels chip was used three magnets facing opposite poles were used.
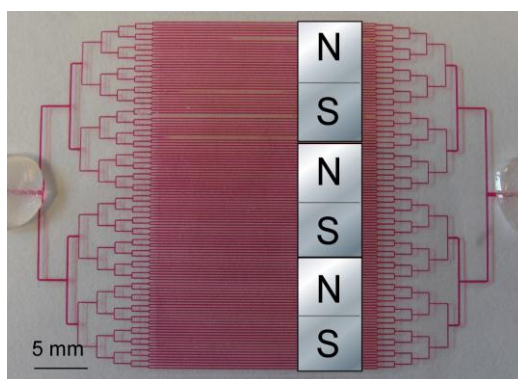
Figure 51 Image showing the device PC128 filled with red ink for visualization and the position and orientation of the NdFeB magnets.

2.8 Fluoride pre-concentration on-chip *via* free-flow magnetophoresis

This section describes the experimental parameters, chemicals, particles and set-up employed for the study of magnetic particle deflection behaviour in a microfluidic chamber with the aim of achieving the pre-concentration of fluoride *via* free-flow magnetophoresis.
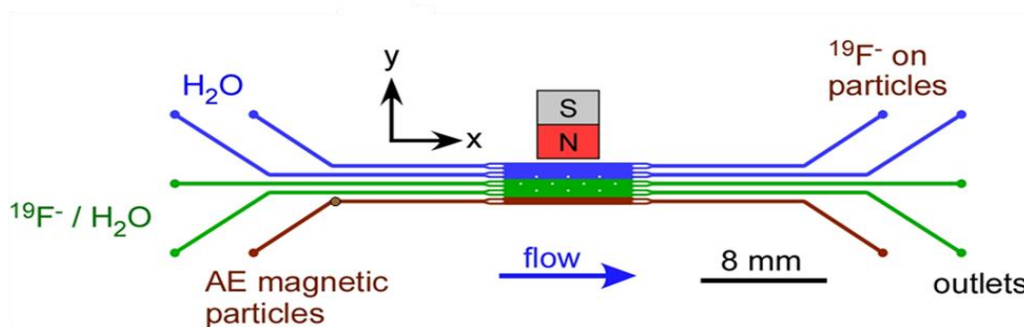
Figure 52 Schematic of the set-up of chip design for performing fluoride trapping in continuous flow. Magnetic particles were pumped into inlet 1, and fluoride ion in solution in inlet 2-3.

Dynabeads SAX particles (1 μm diameter), as described in Section 2.1.3, were purchased from Invitrogen and prepared as per the manufacturer's instructions. ~ 2 x 10^6 particles) were dispersed in 1 mL of PBS buffer in a 1.5 mL Eppendorf tube and underwent the following particle washing procedure; the suspension was vortexed for 20 s, the particles were collected at the side of the tube *via* an external magnet and the supernatant removed prior to the addition of fresh PBS. This washing process was

repeated twice more and once the supernatant had been removed for the last time the particles were resuspended in fresh PBS.

When a magnet was placed next to the deflection chamber, magnetic particles in the chamber experienced not only an attractive force in the y-direction but also upwards, in the z-direction, which could result in particles becoming stuck against the top surface of the chamber. Therefore, by positioning a magnet in the same horizontal plane as the particles, they would experience no upwards force and so should flow through the chamber without being pulled against the chip surfaces, thus helping to reduce 'sticking'. With this in mind, some of the chips had a section of glass cut out next to the chamber so that the magnet could be placed in line with the chamber. An example of a chip with a section of glass cut out is shown in the chip holder in Figure 53.
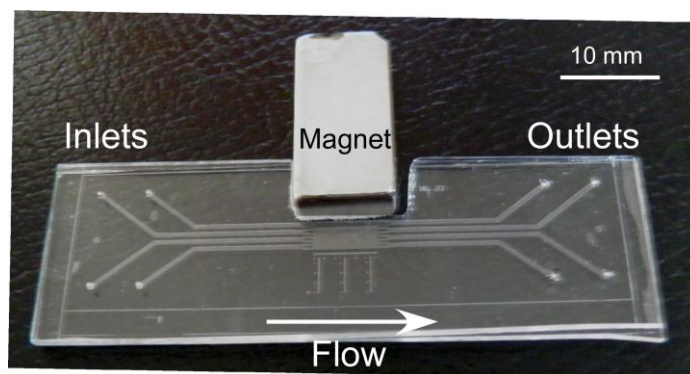
Figure 53 Glass chip featuring a box magnet 20 x 10 x 5 mm^3 within the glass cut out.
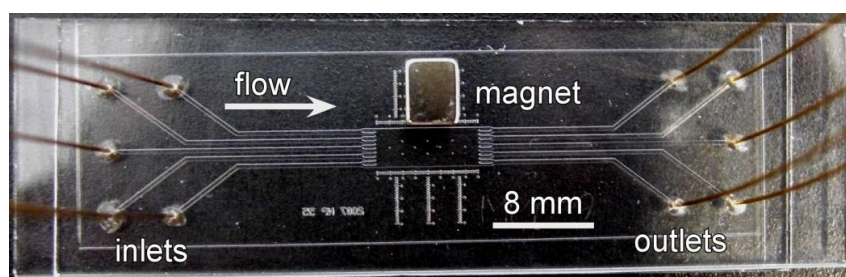
Figure 54 Chip design with the 4 x 4 x 5 mm^3 NdFeB magnet placed on top of the chip, next to the reaction chamber.

2.8.1 Pressure pump

In some experiment the syringe pump was replaced with a pressure control pump and the interface between the glass device and the tubing was substituted with a chip holder fabricated in house, the set-up of which is shown in Figure 56. The MicroFluidic Control System (MFCS) (Fluigent, France) is a high precision pneumatic pressure controller designed to handle fluid in microfluidics systems. It allows a stable and pulsation free flow with short response time (100 ms) and a stabilisation time a low as 1 s. With the MFCS it is also possible to control several independent channels at the same time as shown in Figure 55 thanks to the individually controlled vials. The user friendly software allows you to create scripts for complex flow patterns or dynamic coupling for user-controlled dependence between channels.
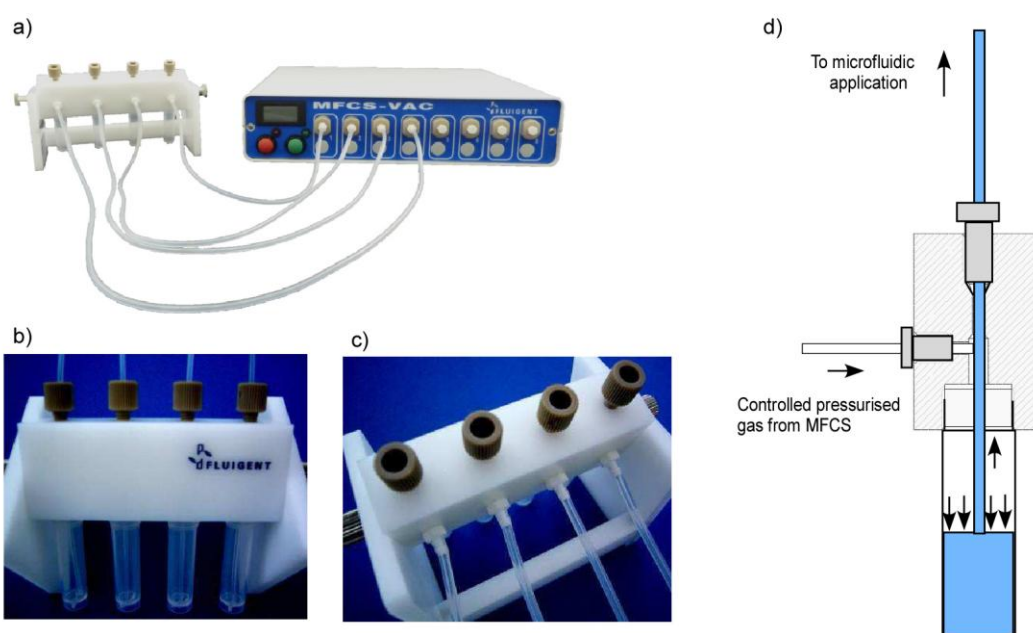
Figure 55 a) Schematic of the Fluigent pressure pump with the fluiwell + the reservoirs, b-c) image showing the front and back of the fluiwell (vials rack), d) showing the principle of the flow of the liquid via pressurized gas [165].
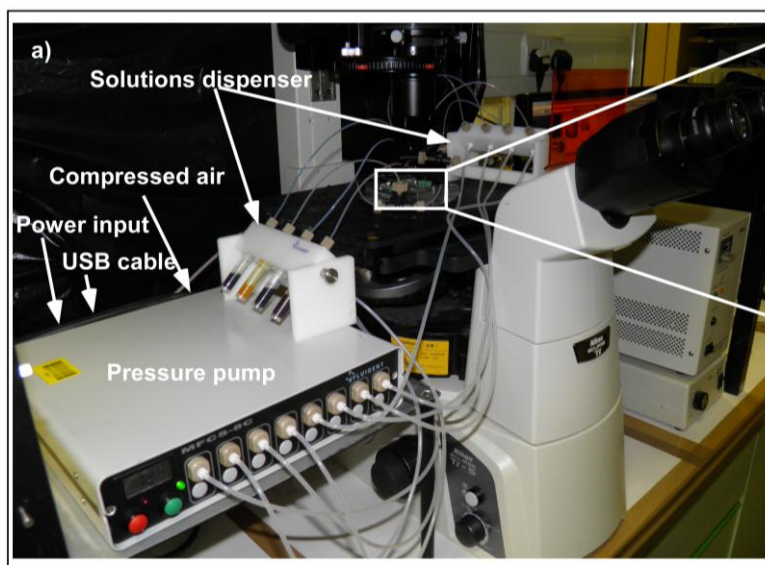
Figure 56 Full system set-up comprising of pressure pump connected to the chip and microscope for visualization.

2.8.2   Magnet setup for magnetophoresis experiment

Most commonly, a 4 x 4 x 5 mm^3 rectangular NdFeB magnet (Magnet Sales UK) was placed on top of the chip, next to the chamber, as shown in Fig 54. When a magnet was placed onto the chip surface, magnetic particles in the chamber experienced not only an attractive force in the y-direction but also upwards, in the z-direction, which could result in particles being drawn towards the top of the chamber and becoming stuck against the surface of the chamber. Therefore, by positioning a magnet in the same horizontal plane as the particles they would experience no upwards force, and so should flow through the chamber without being pulled against the chip surfaces, thus helping to reduce sticking. With this in mind, some of the FL2 design chips had a section of glass cut out next to the chamber so that the magnet could be placed in line with the chamber. An example of a chip with a section of glass cut out is shown in the chip holder in Figure 57. When this setup was used, a 20 x 10 x 5 mm^3 NdFeB rectangular magnet was placed in this position rather than the smaller magnet used above.
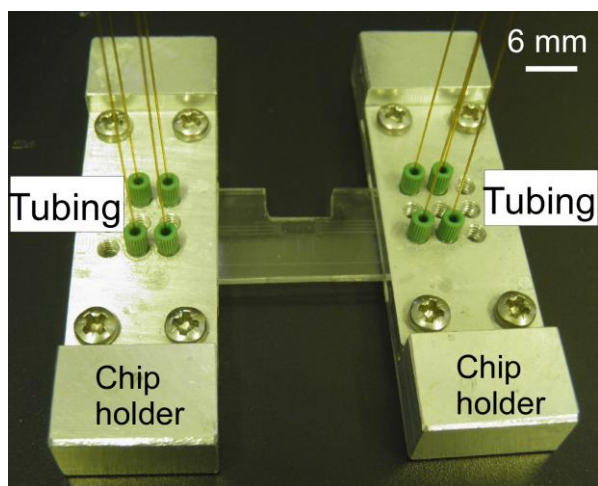
Figure 57 Chip holder featuring a glass device with cut out for magnet.

2.9   Surface treatment

In an effort to reduce the sticking of particles to the glass surfaces of the microfluidic channels, several treatments were performed to modify the glass. Initial attempts to perform surface treatments involved the introduction of chemicals through fused silica capillaries. However, it was found that this also treated the capillaries themselves, and always resulted in increased back pressure and difficulties in introducing particles into the chips. It was hypothesised that this was due to the presence of water (possibly from moisture in the air) that reacted with the silanising agent to form residues that partially blocked the capillaries. Silanisation of a glass surface requires a small amount of water to be present, but too much water will cause the formation of powdery residues, and were typically only used for $2 - 3$ weeks after being opened. Due to the suspected blocking of the capillaries, subsequent attempts to treat the chips involved pumping the required solutions directly into the chip *via* one of the following methods.

Table 14 Silanising agents and their properties. References show where the application methods for each agent were adapted from.

Silanising agent	Abbrev.	Leaving group	Solvent	Effect on the glass surface
Octadecyltrichlorosilane [166, 167]	OTS	- Cl	4:1 Hexadecane: Chloroform	Hydrophobic uncharged
Trichloro(1*H*,1*H*,2*H*,2*H*-perfluorooctyl)silane [168, 169]	FDTS	- Cl	Isooctane (2,4,4-trimethyl-pentane	Hydrophobic; fluorophilic; lyophobic; uncharged
2-[Methoxy (polyethyleneoxy)propyl] [170]	PEG-silane	- OMe	Toluene	Hydrophilic; uncharged
(3-aminopropyl) triethoxysilane [171]	APTES	- OEt	Ethanol	Positively charged at low pH
Dimethyloctadecyl[3-(trimethoxysilyl)propyl] ammonium chloride [172]	QAS (quaternary ammonium silane)	- OMe	Methanol	Positively charged

A chip, having been cleaned *via* a furnace (500 °C for 6 h) and/or in piranha (80:20 H_2SO_4:H_2O_2) solution, and with no tubing attached, was flushed with acetone by placing a syringe directly over one of the inlet holes, then a syringe filled with air used to remove the acetone. The chips were placed in a 60 °C oven overnight to ensure that the surfaces were dry. These steps were to ensure that no water was present in the chips ahead of silanisation treatments, where the presence of water can produce unwanted by-products and cause blockages. For the silanisation procedure, solutions were prepared by dissolving the silanising agent in an appropriate solvent to a concentration of 1 % v/v (Table 14).

Table 15 Chemical structures of the silanising agents.

Silanising Agent	Chemical Structure
OTS	
FDTS	
PEG - Silane	
APTES	
QAS	
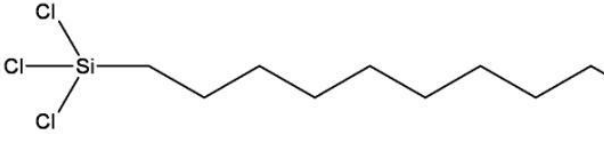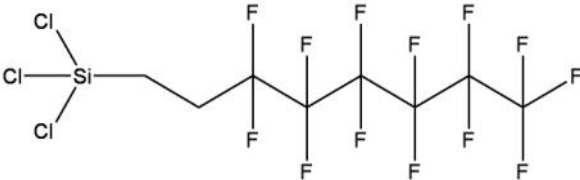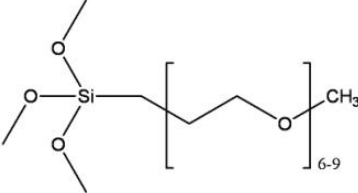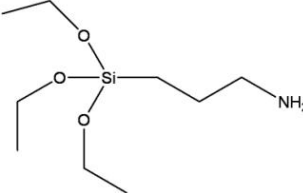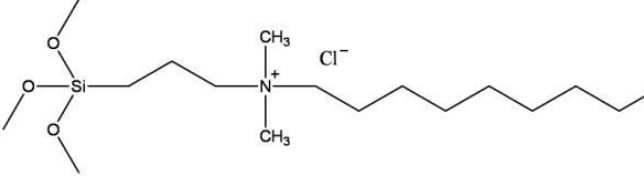
The chips were flushed first with the pure solvent *via* a syringe, before filling them with the silanisation solution list of the different surface treatment compounds is reported in Table 14 and leaving it to react for 10 min. Finally, the chips were flushed with the solvent again, followed by acetone and then water, leaving the chip ready for use in experiments. The silanising agents were used to render the glass chip surfaces hydrophobic, hydrophilic (more so than native glass), or positively charged, depending on the type of agent used. Each agent featured a silane group with four substituents, one of which was the group (-R) responsible for conferring the desired physical effect on the

system, and the other three of which were hydrolysable leaving groups of either methoxy (-OMe), ethoxy (-OEt) or chlorine (-Cl), used to link the silane to the glass surface. Table 14 shows the different silanising agents used in this work, together with their abbreviations, the effect on the glass surface, the leaving group, and the solvents used to prepare the 1 % v/v solutions. Table 15 shows the chemical structures of each of the silanising agents. Figure 58 shows the mechanism by which silane modification takes place on a surface featuring hydroxyl groups (-OH), such as the surface groups on glass [173, 174]. Firstly, the alkoxy (methoxy, -OMe, or ethoxy, -OEt) leaving groups of the silane are hydrolysed by water to form silanols. Hence, a small amount of water is typically required in the system to perform the surface treatment, and may come from the atmosphere or be present in small quantities on the surface of the glass. For those silanising agents featuring chlorine leaving groups, anhydrous alcohols are usually used as the solvent, and the chlorosilane reacts with the alcohol to produce an alkoxysilane and hydrochloric acid. Some of the hydrochloric acid then reacts with the alcohol to produce small quantities of alkyl halide and water, the latter of which causes the formation of silanol groups from the alkoxysilanes. Thus, whether an alkoxysilane (with methoxy or ethoxy groups) or a chlorosilane (with chlorine groups) is used as the starting material, both become silanols as a result of hydrolysis, albeit by slightly different mechanisms. In general, the reactivity of the silanising agents with the hydroxylated groups of the substrate surface is greater for the chlorosilanes than the alkoxysilanes, but nevertheless the latter type are the most widely used due to the non-corrosive and volatile byproducts, and for the methoxysilanes there is the advantage that they are able to modify surfaces under dry condition.

Figure 58 The deposition of silanising agents onto a glass substrate. The example shows an alkoxysilane featuring three hydrolysable methoxy groups.

Once hydrolysis of the silanes has been performed, the silanols produced undergo condensation to form oligomers, which in turn hydrogen bond with the hydroxyl groups of the substrate. Finally, a covalent bond is formed with the substrate due to loss of water by drying or curing, securing the silane and the properties of its R group to the glass surface. These steps are described sequentially, but can actually occur simultaneously after the hydrolysis step. Chips silanised with a hydrophobic treatment were tested by examining the water-air interface in a channel to observe the contact angle, where it was found that hydrophobic surfaces gave a contact angle of around 90 while untreated surfaces exhibited contact angles of < 30.

2.10 Kryptofix detection and removal

This section describes the experimental parameters, chemicals, particles, and set-up for the study of detection and removal of K2.2.2 in a microfluidic chamber.

2.10.1 Preparation of stock solution

Kryptofix standards were prepared in water by serial dilution of 1.0 mg mL^{-1} in acetonitrile. Kryptofix standards between $1 - 100$ µg mL^{-1} were used in this study.
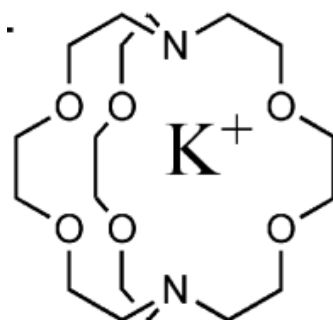
Figure 59 The chemical structure of Kryptofix K2.2.2 when complexes with K$^+$ ion.

2.10.2 TLC silica for detection of K2.2.2

Thin Layer Chromatography (TLC) is the most widely used quality control method for K2.2.2 in FDG injection. The method consists of spotting 2 µL samples of [^{18}F]FDG and K2.2.2 standards solution on silica gel plate and developing in methanol:NH$_4$OH (9:1). Following hot-air drying, the plates are exposed to iodine vapors for an additional 15 to 20 min for visualization [88]. When the Alexoff *et al.* [85] method was used an acidic iodoplatinate solution was prepared as described in Section 2.10 and the stock solution was applied to strips of plastic-backed silica gel 60 thin-layer chromatographic plates (Sigma-Aldrich, UK).

2.10.3 Colourimetric test for Kryptofix detection

4,7,13,16,21,24-Hexaoxa-1,10-diazabicyclo [8.8.8]-hexacosane, Kryptofix (98%), chloroplatinic acid 6 hydrate, potassium iodide and hydrochloric acid 36 % were purchased from Sigma Aldrich, UK.

Following the published method [55], stock iodoplatinate reagent was prepared by mixing 5 mL of 5% chloroplatinic acid in water with 45 mL 10% potassium iodide in water and diluting with an additional 100 mL of water. Acidic iodoplatinate was prepared by mixing 1 part conc. HCL with 10 part stock reagent.

Figure 60 Image of the setup for of the colour change reaction between K2.2.2 and iodoplatinate reagent.

2.10.4 HPLC–MS for Kryptofix detection

Owing to its increased sensitivity, an HPLC-MS-MS method was investigated which enabled quantitative experiments for the purification steps to be performed such as the amount of resin needed to remove the Kryptofix. The method of Ma *et al.* [92] was slightly modified as the use of ammonium acetate as mobile phase was found to be detrimental for the LC pump causing several stalling and blockages; consequently ammonium acetate was replaced with water (50:50 water: acetonitrile). The standard

stock solution of K2.2.2 was prepared in acetonitrile, from which the working solution of K2.2.2 was diluted to give a range of concentrations from 1.0 –100 ng mL^{-1}, all solutions were stored in a refrigerator.

2.11 FECH detection and on-chip removal

For the detection and analysis of FECH experiments, starting materials and by-products were purchased; EtDt, [^{19}F]Fluororethylcholine (FECH) was delivered in 20 mg vials and prepared from a stock solution by serial dilution in the concentration range 1-100 ppm in water, DMAE, dry acetonitrile (ACN) and tetrabutylammoniumbicarbonate delivered as liquid (TBAHCO$_3$). Kryptofix 2.2.2/K$_2$CO$_3$ solutions were prepared in the same concentration as used during the pre-concentration of fluoride experiments described in the experimental chapter Section 2.1.5.1. The microchamber glass device was prepared in the same way as described in Section 2.6 with the difference being the type of particles introduced in this case both CM cation exchange particles, as well as reversed phase particles were used. The on-chip particle bed was activated prior to trapping of FECH and K2.2.2 by flushing with 2 mL ethanol for the reversed phase particles and NaCl 0.1 M solution for the CM cation particles and subsequently washed with 2 mL purified water at a flow rate of 1000 µL min^{-1}. For trapping of FECH, 1 mL of FECH (10 µg mL^{-1}) standard solution was pumped through the particle packing at a flow rate of 500 - 1000 µL min^{-1}. This was followed by flushing with 1 mL water. The particle bed was then regenerated by flushing the chip with 2 mL of 1.0 M NaCl, followed by 3 mL of purified water at 1000 µL min^{-1}.

FECH and by-products detection: Solutions of DMAE, FECH and TBAHCO$_3$ were analysed by IC. Different mixtures at different concentrations between 1-100ppm were injected into the ion chromatography system (ICS-2000, Dionex, USA) equipped with a

CS18 IonPAC analytical cation exchange column and a conductivity detector. The flow rate was 0.25 mL min^{-1} and 20 mM potassium hydroxide (KOH) was used as the eluent.

3 On-chip pre-concentration of [$^{18/19}$F]fluoride *via* regenerable anion exchange resin

This Chapter describes the on-chip pre-concentration of fluoride with both [$^{18/19}$F]fluoride *via* a packed bed of anion exchange chromatography resin, this work has been published in the Journal of Chromatography A [1].

3.1 Introduction

As previously reported in Section 1.5 the most common reaction with radioactive fluoride is the nucleophilic substitution. When this reaction was described by Amacher *et al*. [16] two main advantages were reported i) the [^{18}F]fluorine is obtained as a solution in the irradiated water and ii) [^{18}F]fluorine is obtained "no-carrier-added" (NCA). This means the [^{18}F] fluoride ion has very high specific radioactivity (*i.e.*, ratio of [^{18}F] fluoride ion to its mass of carrier or total fluoride ion ^{19}F + ^{18}F). The nucleophilic substitution is achieved in the presence of a phase transfer catalyst, in this case K2.2.2, in Figure 46 and 61 the mechanism of the pre-concentration and activation of the [$^{18/19}$F]fluoride ions in the presence of K2.2.2 *via* a packed bed of anion exchange chromatography particles is described.

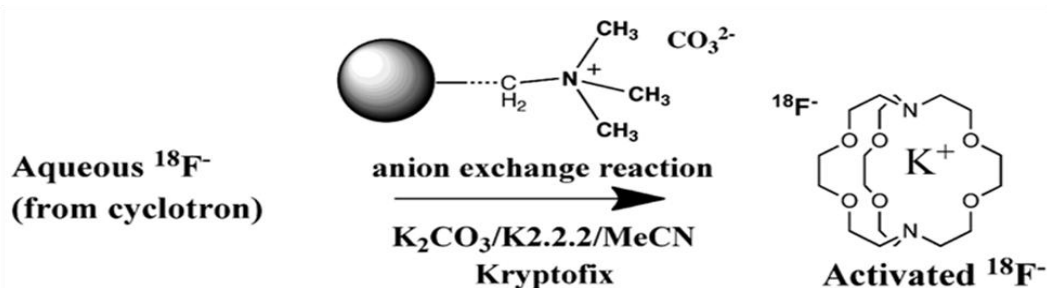**Figure 61 Principle of anion exchange process after the production of ^{18}F$^-$ from proton bombardment of ^{18}O water in a cyclotron. The fluoride ions are exchanged with the counter anions (CO$_3^{2-}$) and subsequently eluted with high ionic strength salt (K$_2$CO$_3$) in the presence of acetonitrile and Kryptofix as phase transfer catalyst, to obtain the activated fluoride.**

In Figure 62 is shown the schematic of the chip design already described in Section 1.2.2 as well as a photo of a glass device filled with two different types on AE particles. The amount of particles contained in the individual chamber was between 20-30 mg.
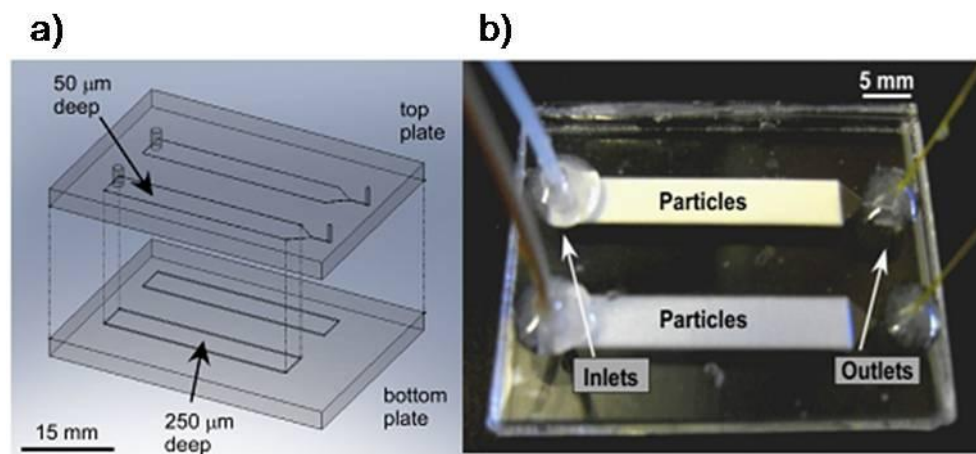
Figure 62 (a) Schematic representation of the chip design. The bottom plate features two chambers (3 cm long, 5 mm wide, 250 μm deep). The top plate, etched to a depth of 50 μm, also featured two chambers (3 cm long, 5 mm wide). This top plate also featured a triangular section (2.5 mm long), leading to a channel of 100 μm width that formed a shallow section for bead trapping when the top and bottom plates were thermally bonded. On the inlets side, 1.5 mm diameter holes were drilled into the top plates, while on the outlets, 400 μm diameter holes were drilled for the outlets. (b) Photograph of the glass device. One chamber was filled with polystyrene (Chromabond PS-HCO₃) particles and the lower chamber filled with silica (Sep-Pak Light Plus QMA) particles.

3.2 Non-radioactive [¹⁹F]fluoride ion detection methods

The first part of the work was dedicated to the investigation and optimisation of a low limit of detection method for non-radioactive fluoride, [^{19}F]fluoride. Three methods were investigated namely, (i) ion selective electrode, (ii) spectrophotometric detection and (iii) ion exchange chromatography with conductivity detector.

3.2.1 Ion Selective Electrode (ISE)

The fluoride electrode (described in 2.1.5) was first tested due to its ready availability and ease of use. The aim of this experiment was to prepare a series of standards in the range 1 x 10^{-2} M to 1 x 10^{-7} M of [^{19}F]fluoride and plot a calibration graph to measure the concentration of fluoride in an unknown solution.
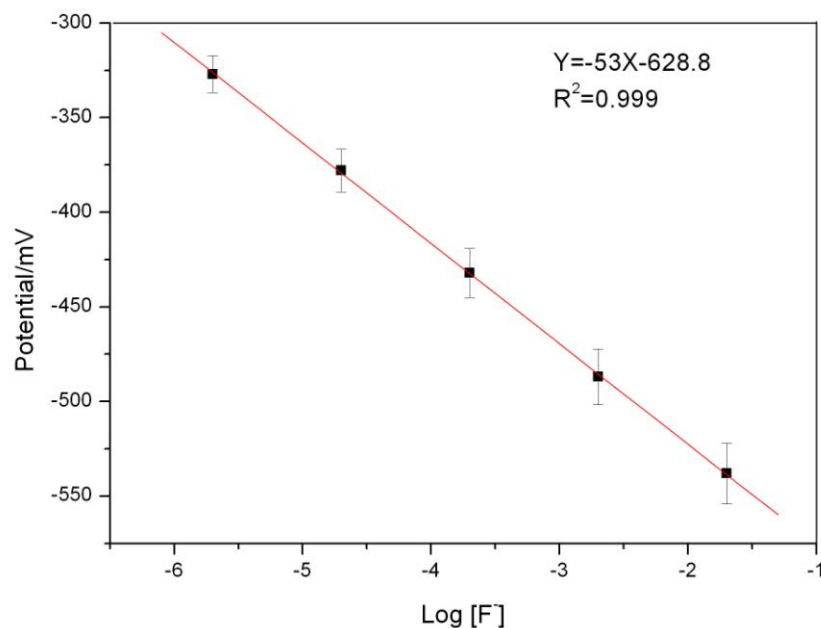
Figure 63 Calibration graph of Potential/mV versus the logarithm of [F⁻].

Table 16 Table showing the values of the potential /mV and the concentration of fluoride.

[Fluoride] /M	Potential /mV (mean n=3)	Log [F⁻]
0.000001	-238	-6
0.00001	-292	-5
0.0001	-334	-4
0.001	-397	-3
0.01	-458	-2
0.1	-513	-1

From the results shown in Figure 63 it can be seen that there was a linear response. However, the working range was limited between 1×10^{-2} to 1×10^{-6} M. The volume required for the measurement was around 200 µL and the error found while measuring the potential was found to be ±15 mV possibly due to factors such as temperature, time needed to take the reading, differences in volume and dilution factor. Owing to the limit of detection of only 1×10^{-6} M (19 µg mL^{-1} of fluoride), as well as the amount of volume required for analysis, >200 µL, the method was not optimised further.

3.2.2 Spectrophotometric detections: Alizarin fluorine blue

A spectrophotometric method was also considered with the intent to use it as a continuous on-line method for fluoride detection as described in experimental section 2.1.5. UV-vis spectra were obtained for each standard of fluoride in the range 10-50 ppm as shown in Figure 64. The maximum absorbance was at $\lambda = 625$ nm. As shown in Figure 65 a linear response was obtained, and it also shows that the absorbance was proportional to the concentration. Preliminary results obtained showed that the method had good sensitivity in the microgram range for the detection of fluoride. So was decided to carry out a further optimisation both for sensitivity and interferences.

Table 17 Mass of fluoride versus absorbance at 625 nm.

Mass [^{19}F]fluoride/(μg/mL) = ppm	Absorbance At 625nm (mean n=3)
40	1.1654
30	1.1071
20	0.9504
10	0.8362

Results of the concentration of [^{19}F]fluoride versus the absorbance found at $\lambda = 625$ nm are shown in Table 17. The spectra of a range of [^{19}F]fluoride concentrations are shown in Figure 64 and a calibration graph of the mass of fluoride versus the absorbance is plotted in Figure 65.
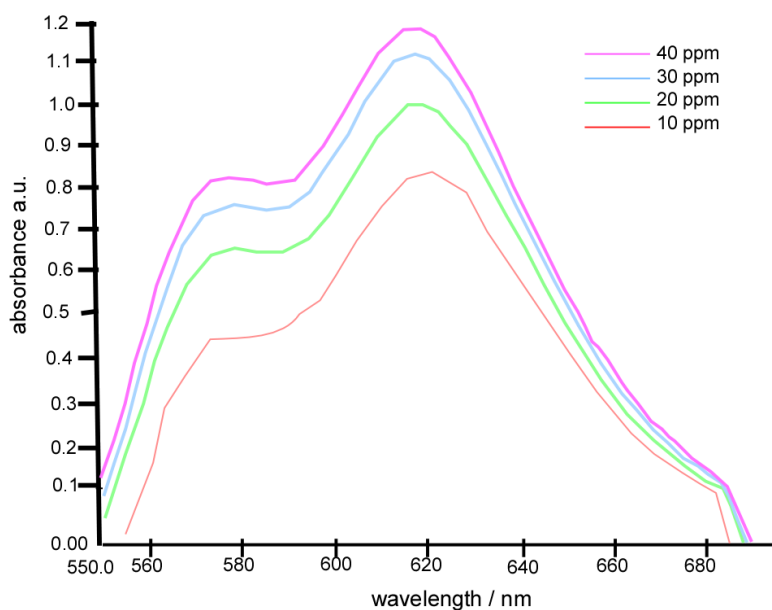
Figure 64 Absorption spectra at 625 nm of different fluoride concentrations (10-40 ppm).
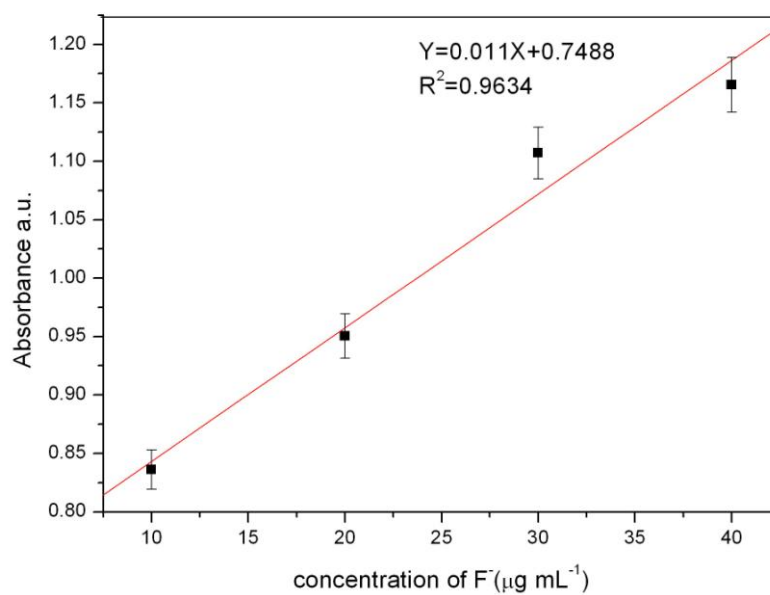
Figure 65 Calibration graph of absorbance vs concentration of fluoride.

A further test was performed to identify the effect of carbonate anions since pre-concentration of fluoride for radiosynthesis is performed in the presence of carbonate anions, introduced during the elution step as described in Chapter 1 Section 1.8. The results are shown in Table 18 and the graph plotted in Figure 67. The method was the

same as outlined previously. The only addition was a known amount of potassium

carbonate in each of standards, and the absorbance was measured at 625 nm.

Table 18 Effect of K$_2$CO$_3$ in the absorbance at 625 nm.

Concentration of [^{19}F]fluoride μg mL^{-1}	Volume of K$_2$CO$_3$(0.25 M) / ml	Absorbance At 625nm
40	2	0.1433
30	2	0.5221
20	2	0.5710
10	2	0.8045

As shown in Figure 66 there is no linearity between the peaks and the maximum

absorbance recorded, as compared with the spectra in Figure 64.
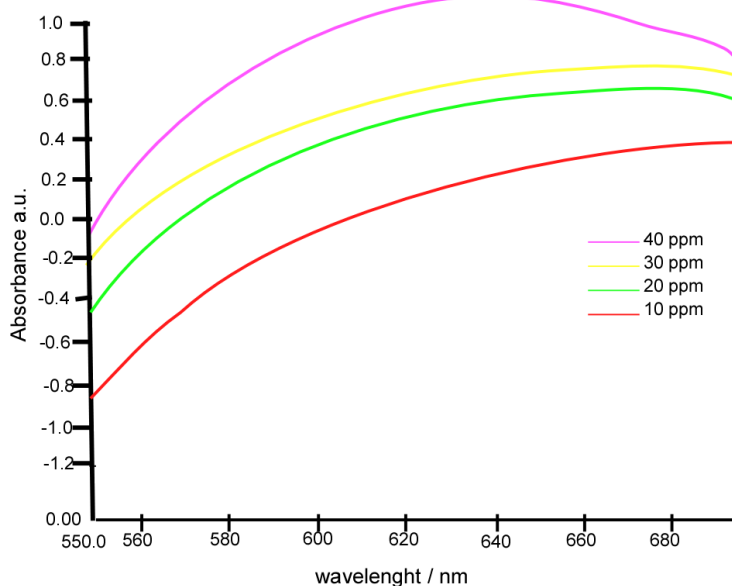
Figure 66 Absorption spectra of fluoride (10-40 ppm) and K$_2$CO$_3$ (0.25 M) at 625 nm.

When potassium carbonate was added to the reaction mixture, it can be seen that there is

no maximum absorbance as shown in Figure 66, possibly due to the carbonate (CO$_3^{2-}$)

anions reacting with the alizarin solution. Hence no proportionality between absorbance

and fluoride concentration was observed. The method could not be used further for this

research since most of the detection of fluoride will be in the presence of carbonate anions as the eluting agent; as reported in Section 1.8.

3.2.3 Ion exchange chromatography (IEC)

Ion Chromatography (IC) is one of the most common detection methods for the determination of anions in solution. A series of standard solutions, with $[^{19}F]$fluoride concentration between 1 and 40 ppm was injected *via* an injection loop of the instrument, and the area in µs min^{-1} was obtained. Subsequently a calibration graph was plotted from which unknown concentrations could be determined.

Table 19 Values of Area/µs min^{-1} *vs* concentration of fluoride/ppm.

Concentration/ ppm	Area /µs min^{-1} (mean n=3)
1	3.703
10	7.892
20	19.149
30	26.244
40	32.762
50	40.375
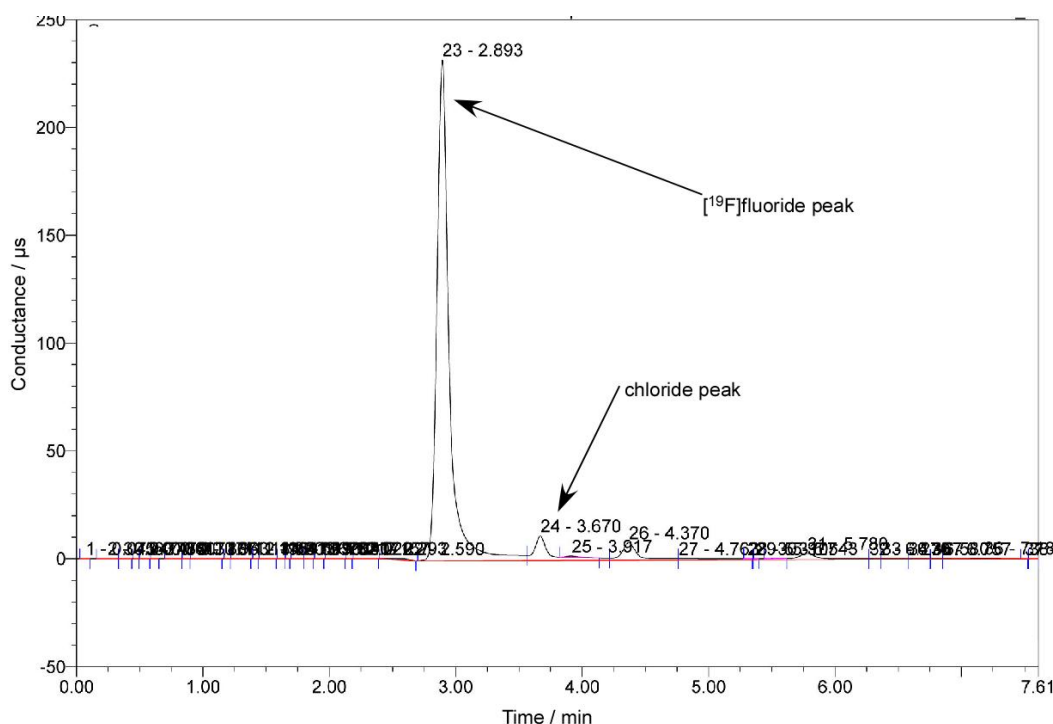
Figure 67 Chromatogram of a 30 ppm $[^{19}F]$fluoride standard showing the retention time for $[^{19}F]$fluoride at 2.893 minutes.
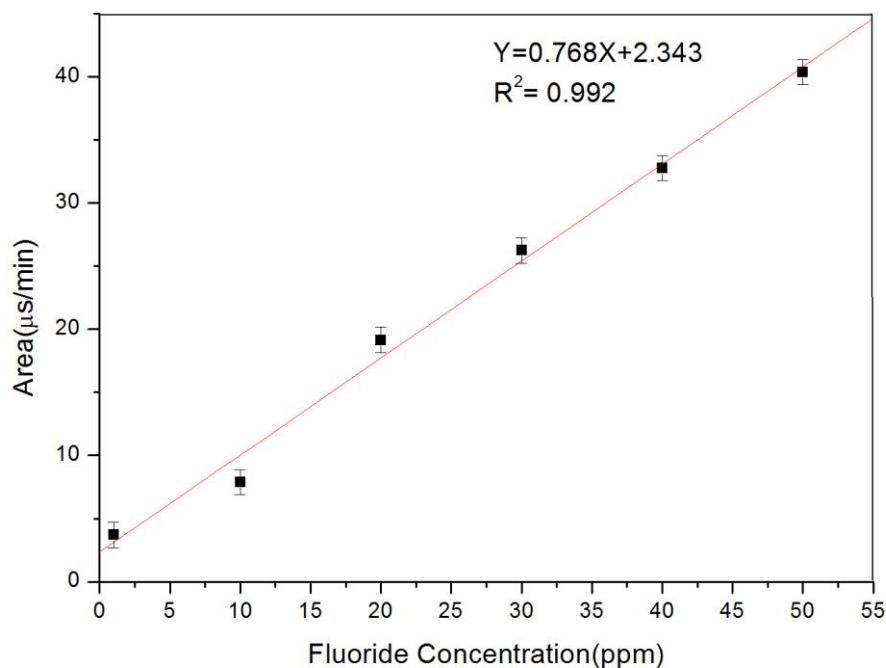
Figure 68 Calibration graph of area μs min^{-1} *vs* series of concentrations of fluoride in the range 1-50 ppm.

As shown in Figure 68 there is a good linearity with an R^2= 0.992, so for this reason a further investigation to determine the limit of detection was carried out, and the results are shown in Figure 69. For further calculation the slope of the graph in Figure 68 was used for subsequent studies. A series of standard solutions of fluoride were prepared in the range between 1 ppm to 10 ppb. The average of a series of repeated concentrations was plotted and the limit of detection calculated using the formula: (equation 9)

(Limit of detection = (3 x standard errors)/gradient)   Equation 9

Table 20 Average area/ μs min^{-1} with errors of different concentration of fluoride.

Concentration / ppm	Area1/μs min^{-1}	Area2/ μs min^{-1}	Area3/μs min^{-1}	Mean	STD
0.5	3.079	2.996	3.255	3.11	0.1322
0.1	1.517	1.456	1.689	1.554	0.1208
0.01	0.265	0.298	0.369	0.310667	0.0531

$$y=5.1592+0.6092$$
$$R^2=0.9205$$
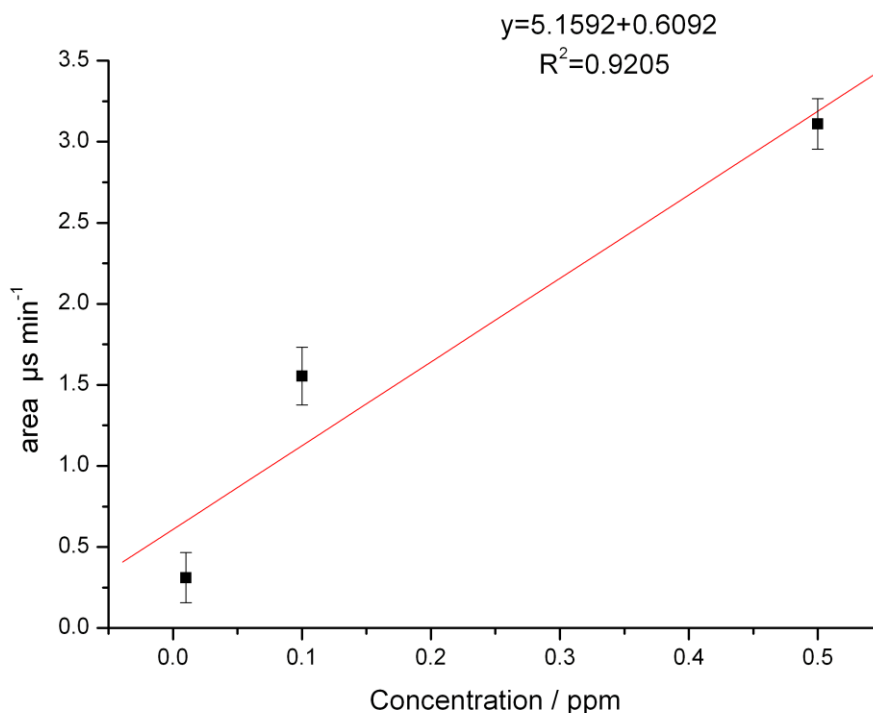
Figure 69 Determination of the LOD for [^{19}F]fluoride using ion chromatography.

The average standard error was calculated to be 0.102 ppm which gives a limit of detection of 0.06 ppm (3.15 x 10^{-6} mol L^{-1}). For the purpose of this research this was a good starting point for the detection of [^{19}F]fluoride since it was very close to the concentration of fluoride ions in water after the cyclotron bombardment (6.25 x 10^{-7} mol L^{-1}) as explained previously in Section 1.10.

The detection method was tested for interferences with carbonate anions. Three different experiments were carried out to investigate the minimum amount of carbonate that was possible to inject in the IC without affecting the resolution of the other anions in particular the fluoride anion. Three different solution were injected into the IC with the fluoride amount kept constant at 30 ppm (30 µg / mL^{-1}), only the carbonate (K$_2$CO$_3$) concentration was varied, 0.1, 0.01 and 0.001 M.
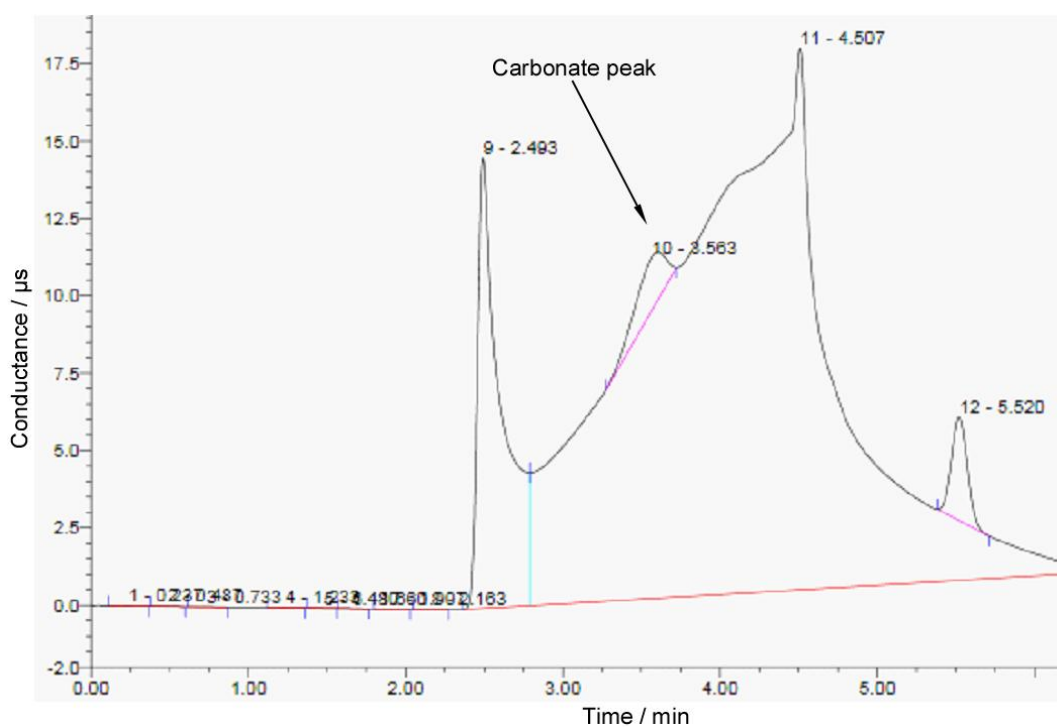
Figure 70 Chromatogram showing the effect of the carbonate ions on the resolution of the analytes at 0.1 M K$_2$CO$_3$.
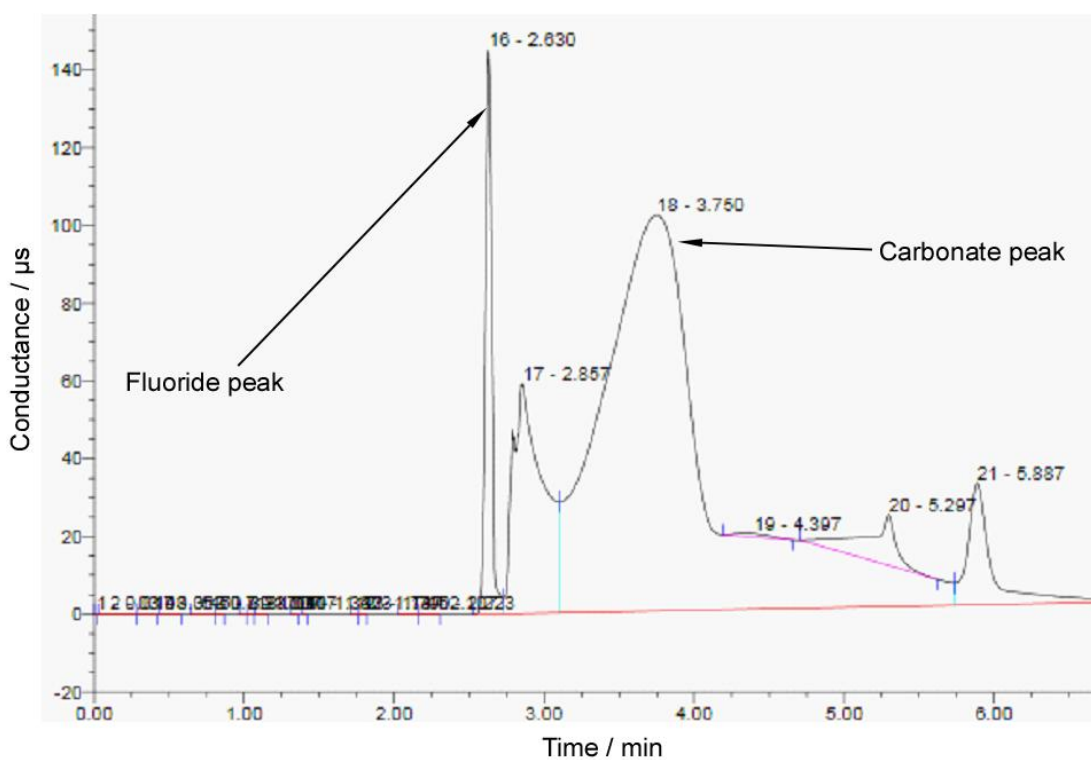
Figure 71 Chromatogram showing the effect of the carbonate ions on the resolution of the peaks. With 0.01 M K$_2$CO$_3$ the fluoride peak is resolved, but the interference is still present for further detection of other ions.
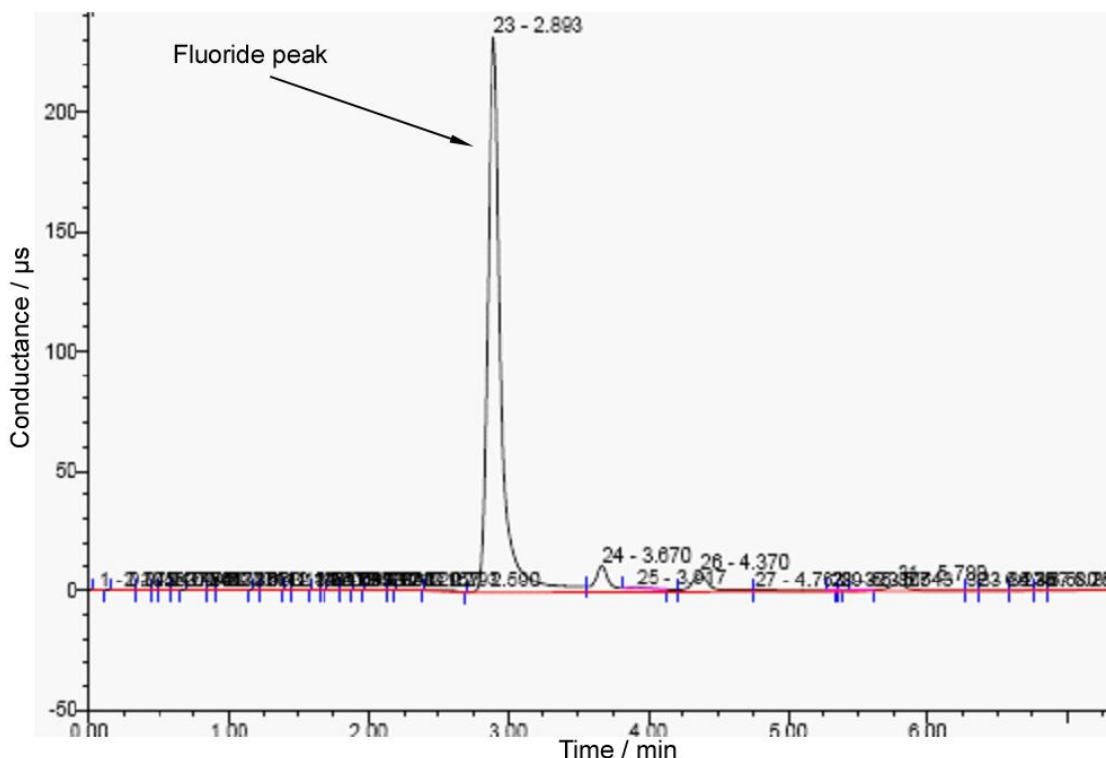
Figure 72 Chromatogram showing the effect of the carbonate ions on the resolution of the peaks. With 0.001 M K$_2$CO$_3$ fluoride peak and other peaks present in water fully resolved without interference of carbonate.

As can be seen from the chromatogram in Figure 70, in the presence of carbonate anions at high concentration (0.1 M) the fluoride peak cannot be resolved. When lower concentrations of carbonate were tested (0.01 M) it was possible to observe the fluoride peak as shown in Figure. 71, but the area and the height of the fluoride peak was not the same as the area observed when the same concentration of fluoride was run without carbonate; (Figure 67). Only when the carbonate concentration was lowered to 0.001 M the fluoride peak and the other anions were fully resolved. The experiment showed that IC could be used as a detection method for fluoride in the presence of carbonate anions without use of any buffer. Therefore this detection method seemed to be best suited in terms of the detection limit and volume required for analysis particularly when compared to the fluoride electrode.

In summary a suitable detection method for fluoride ions in solution at low concentration and in the microliter range volume was investigated. Three commonly used methods were compared; a colourimetric assay, an anion selective electrode and ion exchange chromatography. The first one proved not to be suitable for our purpose due to the volume required for the measurement (1 mL) and the interferences of other anions with the measurement. The second technique featured improved sensitivity (0.20 -1 ppm) and the time for the measurement but still the volume required was considered high for the purpose described herein (200 µL). Ion exchange chromatography proved capable to detect fluoride as low as 0.001-1 ppm in a reasonable time same as electrode (5 min) with low sample volume required (>25 µL). Table 21 compares the three different detection methods in terms of their sensitivity, volume, interferences and time required for test.

Table 21 Summary of the detections method.

Detection	Sensitivity	Volume	Interferences	Time / min
Colourimetric	1 ppm	1 mL	CO_3^{2-}	9
ISE	1ppm	200 µL	pH	5
IEC	0.01 ppm	25 µL	High concentration salt (CO_3^{2-})	5

3.3 Initial test of [^{19}F]fluoride trapping off-chip

Prior to performing on-chip experiments, three different commercially available disposable cartridges were employed to ensure that fluoride could be quantitatively trapped and eluted. For these experiments, different resin forms were employed as described in 2.1.2, featuring chloride, bicarbonate and hydroxide as their counter ions. Detection of fluoride was achieved with Ion Exchange Chromatography (IEC), [^{19}F]fluoride was measured after collection at the outlet of the cartridge and after elution

with K_2CO_3. The first experiments were carried out to determine the minimum amount of K_2CO_3 where no interferences from the CO_3^{2-} with the fluoride peak were observed; as previously described this was found to be 0.001 M (mol L^{-1}). This amount was found to be sufficient to release 1 µg of [^{19}F]fluoride from the resin. A comparison of the three cartridges illustrated the bicarbonate form as being the most suitable resin for further experimentation. The hydroxide resin could not quantitatively trap and recover the fluoride as shown in Figure 73. Only 80% of fluoride could be trapped over a series of four regeneration steps. The chloride resin gave >90 % trapping efficiency over the four runs, but a significant amount of chloride ions were detected over the course of the experiments even after excessive washing of the resin with $NaHCO_3$. Chloride has been reported to compete in the FDG synthesis step by forming 2-chloro-2deoxy-glucose (CIDG) hence affecting the final FDG yield [82]. For this reason, the bicarbonate resin was chosen for all future experiments.
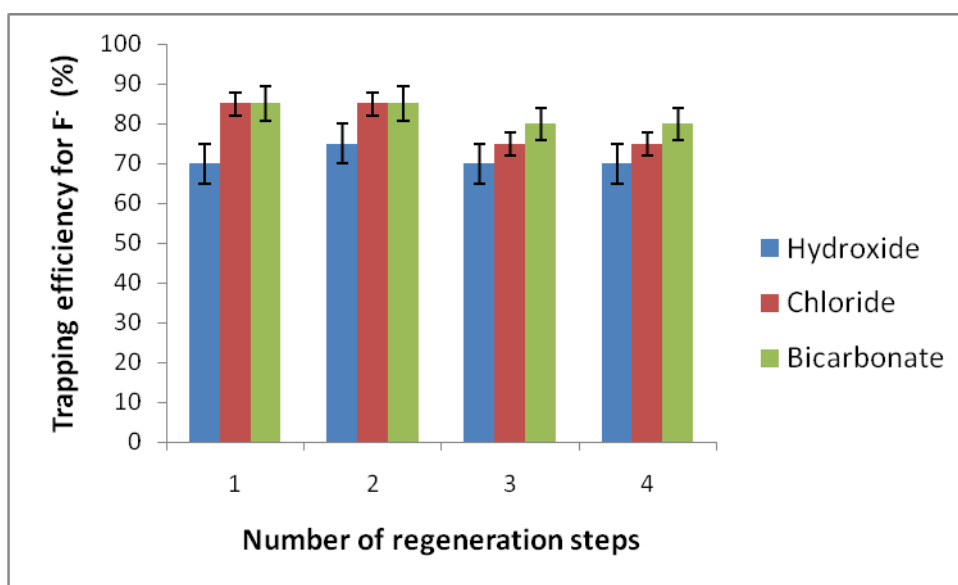

Figure 73 Graph comparing three different resin forms (hydroxide, chloride and bicarbonate) and their efficiency over a series of four runs.

3.4   [¹⁹F]Fluoride elution off-chip on QMA cartridge

This part of the work was carried out in collaboration with Dr. Victoria Hammond at the Chemistry Department, the University of Hull. During her research she investigated the on-chip fluorination of propylditosylate and mannose triflate using first a KF mixture, containing K2.2.2 : K_2CO_3 : KF (1.5 : 1.5 : 1) and consequently she assessed the activated [¹⁹F]fluoride solution obtained by the conventional trapping elution method as described in Section 2.1. Due to the higher concentrations needed in cold chemistry for detection purposes (HPLC-UV or HPLC with electrochemical detection) it was necessary to use the Sep-Pak QMA cartridges rather than the packed bed micro-reactors for the trapping of [¹⁹F]fluoride and its elution with K2.2.2 and potassium carbonate previously described in Section 2.5.3. When using the KF mixture a particulate formation was observed during the reaction, therefore the fluorination step was performed with the activated fluoride from the cartridge.

The [¹⁹F]fluoride trapping and release were carried out as outlined in Section 2.5.3. The [¹⁹F]fluoride solution was then used in a directly comparable experiment to those performed above with the KF mixture, and no fluorination of the expected compound was observed. The [¹⁹F]fluoride production was repeated a number of times (using freshly made solutions) and at no point was any fluorination observed. It was believed that there may not have been enough carbonate in the [¹⁹F]fluoride solution to promote the fluorination and to render the solution basic enough compared to the micro-reactor, as previous experiments have shown that some carbonate is required for efficient fluorination. The amount of carbonate was increased (up to 50 equivalents), however no fluorination was observed in the micro-reactor.

At this point it was speculated that there was a problem with the [¹⁹F]fluoride production. This was confirmed by testing the [¹⁹F]fluoride solutions by IC; it was

found that the [^{19}F]fluoride was being trapped on the cartridge but not being eluted in the K2.2.2 and carbonate solution. It is believed that this was a concentration effect, even though the method had been scaled up accordingly. It was thought that the most likely problem was the amount of water in the elution solution may not be enough to dissolve all the carbonate which is needed to replace the [^{19}F]fluoride on the cartridge. It is known that when the elution solution uses 100% water as the solvent, all the fluoride is eluted off the cartridge, but at the 8% water and 92% acetonitrile currently used resulted in no fluoride being eluted. The amount of water was doubled, and still no fluorination was observed. A study was then carried out to determine at which percentage of acetonitrile (required for the reaction) in the elution solution the fluoride stopped eluting from the cartridge. The results can be seen in Figure 74, showing that when the acetonitrile percentage rose above 60% the fluoride was no longer fully eluted from the cartridge the test was repeated twice in two different experimental days (n=1 each day) . Any drop in the concentration of fluoride in the final solution would have a direct effect on the amount of fluorination that would occur in the micro-reactor, meaning it is important to elute as much of the fluoride as possible from the cartridge
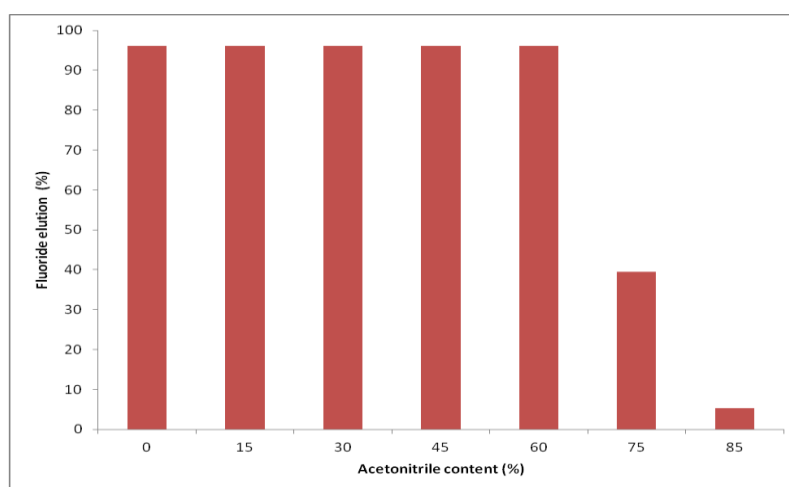
Figure 74 Percentage of fluoride eluted in respect to the acetonitrile content from 0-85%.

An experiment was then conducted to determine whether it was possible to use the elution solution (60% acetonitrile, 40% water) directly in the micro-reactor to perform the fluorination of the tosylate compounds system set-up used by Dr Victoria Hammond is shown in Figure 75. The experiment was done using a residence time of 30 s in the micro-reactor, over a temperature range of 60 to 180 °C. There was no fluorination observed in any of the samples, and it was also noticed that particles were forming in the channels of the micro-reactor. This shows that the elution solution was not suitable for direct use in the fluorination reaction and needed to undergo solvent exchange in a module between the fluoride production and fluorination reaction module. It should be noted that the particles forming could have been due to reactant insolubility in water and there may have been too much water present for it to remain in solution.
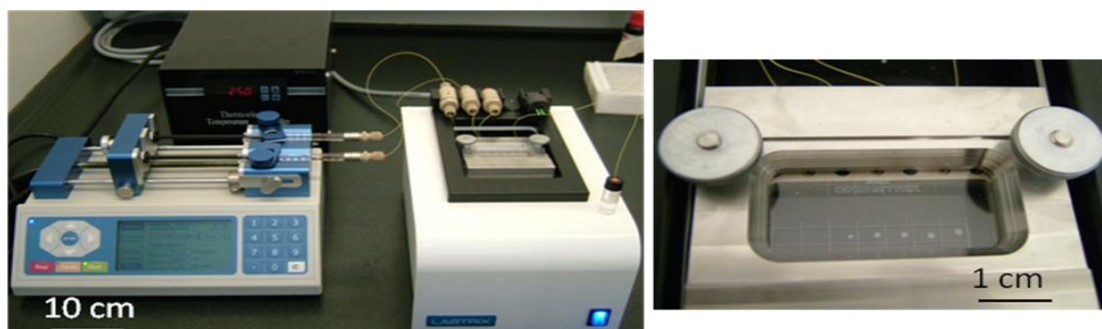
Figure 75 (left) Labtrix ® start system from Chemtrix BV. Temperature range -15ºC to 190 ºC for experiments. Pressure set to 15 bar. Also shown the microreactor (supplied with the instrument) in a holder that can be placed over the heated element. The tubing goes directly into the holder where it connected to the microreactor by `O` rings (made from Perlast®) so no leakage can occur. Courtesy of Victoria Hammond.

3.5 On-chip [¹⁹F]fluoride trapping, elution and regeneration

Optimisation of fluoride detection: The first step involved the calibration of the ion exchange chromatography instrument for fluoride detection in the lowest ppm region, which was sufficient for the amount of fluoride to be detected. It was found that carbonate, which was the eluent used for releasing the fluoride from the on-chip solid

phase packing at a concentration of 0.36 M, interfered with the fluoride peak. After the first trapping, another peak overlapping with the fluoride was observed and was found to be acetate which has a retention time close to that of fluoride, as shown in Figure 76 (top and middle). These species were probably formed *via* a reaction between $KHCO_3$ and acetic acid (present in the polymeric particle packing) during the regeneration step. For this reason, the height of the peak was used to determine the amount of fluoride trapped, rather than the area under the peak.

Initial tests on anion-exchange particle beds: Both silica (Sep-Pak Light Plus QMA) and polystyrene (PS) (Chromabond PS-HCO$_3$) particles were tested initially to compare their performance for the trapping and subsequent release of fluoride. In each case a microfluidic chamber was filled with particles as described in Section 2.1 and the fluoride standard ($1\mu g\ mL^{-1}$) was trapped and subsequently eluted, with no difference in performance observed between the two types of anion-exchange particles. However during the regeneration steps a significant chloride peak was detected in the eluate from the silica-based ion exchange material. This material was originally in the chloride form but was rinsed with 2 mL of 1 M $KHCO_3$ solution prior to its use in our experiment as previously discussed. The presence of chloride can interfere with the following radiofluorination reaction by forming undesired chlorinated by-products, affecting the synthesis of FDG [82]. Moreover, the silica particles were found to be difficult to remove from the device while the polystyrene particles (PS) could be easily removed by treating the chip in a furnace at 500 °C for several hours. For these reasons, the Chromabond PS-HCO$_3$ particles in the carbonate form were selected over silica in the chloride form for subsequent investigations.

<u>Trapping and elution efficiency</u>: The PS particle chip was then tested for the trapping and elution of fluoride. 1 µg mL^{-1} fluoride standard was pumped through the chip containing the PS particles in the bicarbonate form at a maximum flow of 1500 µL min^{-1}. Each collected aliquot was analysed for the presence of fluoride. The peak height of fluoride was normalised against the peak height of fluoride present in purified water and then converted to a percentage to give the amount of trapped fluoride. The fluoride was eluted with a 1 mL solution containing 10 mg K2.2.2 in 900 µL acetonitrile and 100 µL K$_2$CO$_3$ (0.01 M) pumped at 250 µL min^{-1} through the chip. The eluted solution was dried and reconstituted with 1 mL water, as acetonitrile is not a suitable solvent for ion chromatography, prior to being analysed for the presence of fluoride. This experiment was repeated up to 40 times, and it was found that the [^{19}F]fluoride could be trapped and released in all cases with more than 90 % efficiency.
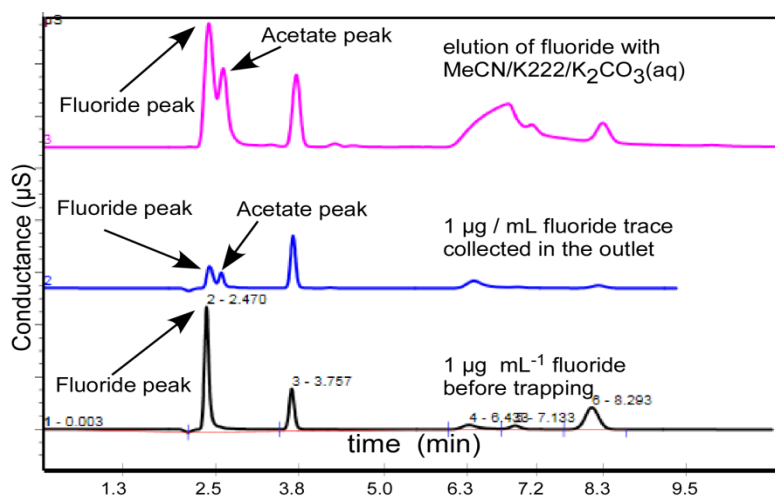
Figure 76 Chromatograms obtained for the trapping and elution of non-radioactive [^{19}F]fluoride ions, showing 1µg mL^{-1} fluoride before trapping (bottom), the diminished fluoride peak of waste solution collected during trapping (middle) and the full fluoride peak following elution (top).

3.5.1 Resin breakthrough for [^{19}F]fluoride

The full capacity of the particle packing with respect to the [^{19}F]fluoride ion was investigated by the determination of the breakthrough capacity. 1 mL aliquots of

fluoride solutions (1 µg mL^{-1}) were consecutively introduced into the chip, at a flow rate of 500 µL min^{-1}, until fluoride was detected at the outlet; the percentage of fluoride trapped versus the mass of fluoride introduced is shown in Figure 79. The amount of fluoride trapped was about 90 % over the first ten injections, before gradually decreasing down to 40 %, as expected due to the reduced number of binding sites present in the particle bed. The trapping capacity determined by breakthrough analysis specific for [^{19}F]fluoride ion was found to be 11 ± 4 µg of per 20 ± 5 mg of dry particles which is equal to 0.55 µg g^{-1} of particles (0.028 meq g^{-1}). This was found to be 28 times less than the maximum loading capacity provided by the manufacturer (0.80 milli-equivalents g^{-1}) to be noted that the manufactures protocols uses different binding molecules and detection method [175].
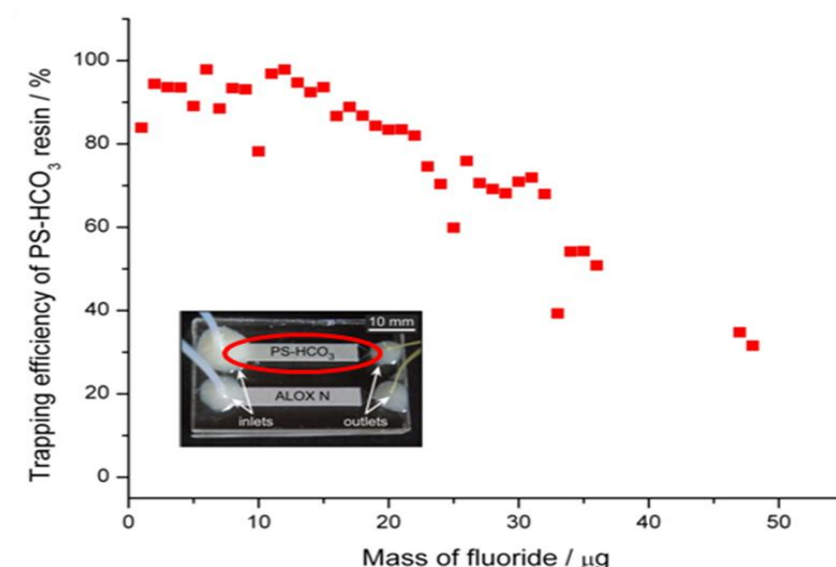
Figure 77 Breakthrough plot of the anion-exchange chip showing the trapping efficiency versus the amount of [^{19}F]fluoride ions introduced into the chip. As the mass of fluoride was increased, the trapping efficiency decayed linearly as the number of trapping sites on the particles decreased. The maximum capacity of the anion exchange particles (Chromabond PS-HCO$_3$) before loss of efficiency was determined to be 0.55 µg mg^{-1}.

3.5.2 [^{19}F]Fluoride trapping and regeneration at maximum flow rate

The reusability of the resin bed was accomplished by regenerating the particles at the end of each trapping and elution by pumping 2 mL of NaHCO$_3$ (1.0 M) at flow rate of 1 mL min^{-1} and subsequently washing extensively (3-5 mL) with purified water at the same flow rate. This would replace the original counter ion present on the resin by washing out all the other anions bound to the particles. A total of 40 runs were performed on the same resin bed, and no significant decrease in trapping of fluoride was observed (>90 % trapping efficiencies in all the runs). After establishing the reusability of the chip we investigated the maximum flow rate at which the fluoride could be quantitatively trapped. In this experiment the same chip was employed, and the detection of fluoride (%) towards different flow rate was plotted the results Figure 80 show significant decrease in trapping efficiency (< 80 %) at a flow rate 1850 µL min^{-1} and above. The same chip was used repeatedly for these experiments to confirm that the decrease in efficiency was due to the high flow rate rather than the decrease in capacity of the resin, to prove this, after the 2000 µL min^{-1} runs a standard fluoride of 1 ppm was introduced with flow rate of 700 µL min^{-1} and this resulted in trapping efficiency of 93 %.
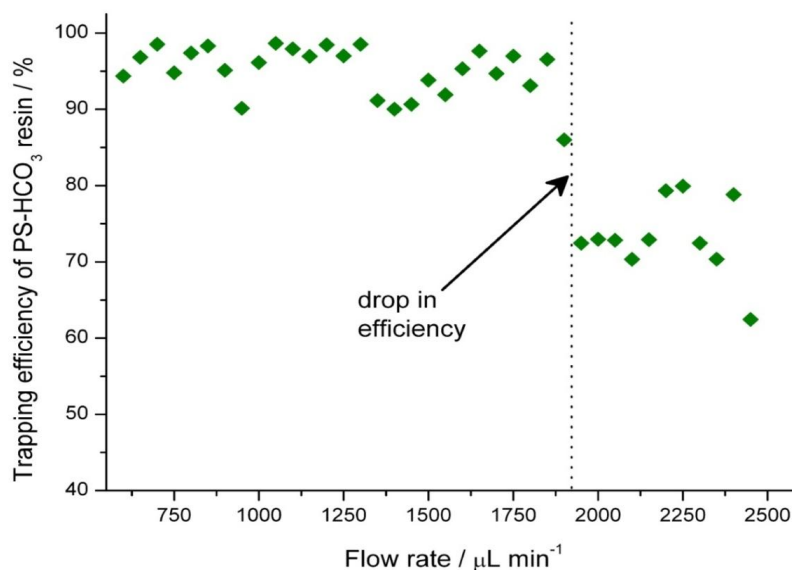
Figure 78 Graph showing the efficiency of the fluoride trapping onchip (%) vs flow rate µL min^{-1} showing a decrease in efficiency of about 15-20 % after flow rate of 1800 µL min^{-1}.

3.5.3 Pressure study on-chip

As part of a modular system which at the end will constitute an integrated platform for the synthesis of radiotracers together with four other modules, pressure testing was performed on the chip to ascertain a suitable pressure which the chip could withstand. A pressure gauge was employed to measure the back pressure resulting from the packed bed (typical set-up described in Section 1.6.1) and was found that the device did not leak or cracked at a maximum pressure of 12 Bar (188 psi) in Figure 81 a graph showing the relation between the pressure and the flow rate is plotted.
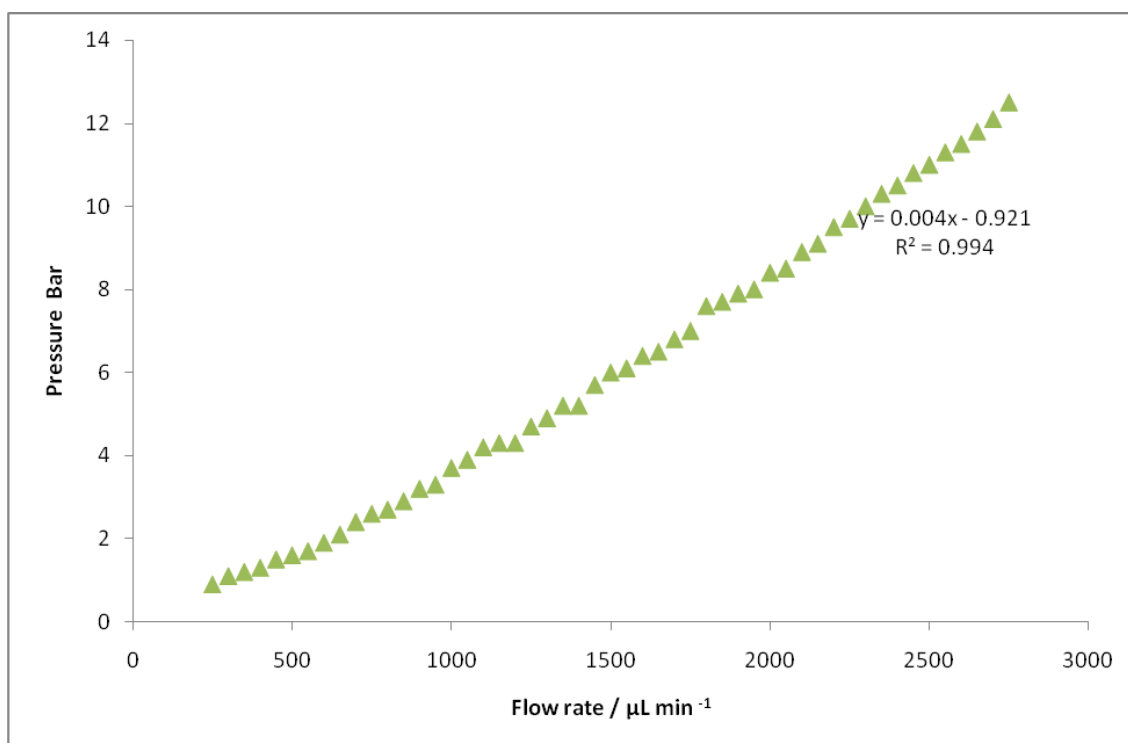
Figure 79 Calibration graph of the flow rate µL min^{-1} *vs* pressure / bar.

3.5.4 [^{19}F]Fluoride trapping and elution efficiency on-chip

Next the on-chip elution was investigated, 1 µg of fluoride was trapped on chip at a flow rate of 500 µL min^{-1} then the elution solution consisting of 1 mL (900 µl aqueous K$_2$CO$_3$ (5%) + 100 µL MeCN (10 mg K2.2.2)) was pumped. 50 µl aliquots were collected at different flow rates ranging from 10 to 200 µl min^{-1} and analysed for presence of fluoride. The area of the peak was used for quantification and calculated with respect to the reference peak area of the starting fluoride solution a graph of the results is shown in Figure 80 (n=1). Since it was not possible to exactly match the area of the starting fluoride against the sum of the areas of the different aliquots, to make sure that the fluoride was completely eluted the experiment was performed until no fluoride was measured in the eluent, this value was found constant between the different flow rates to be a volume of 250 µl; as shown in Figure 83 no fluoride was measured within the 300 µl aliquot. Furthermore, no linear trend or correlation was observed

between flow rates and percentage of trapped fluoride eluted, however it can be seen that at a higher flow rate fluoride is eluted quickly.
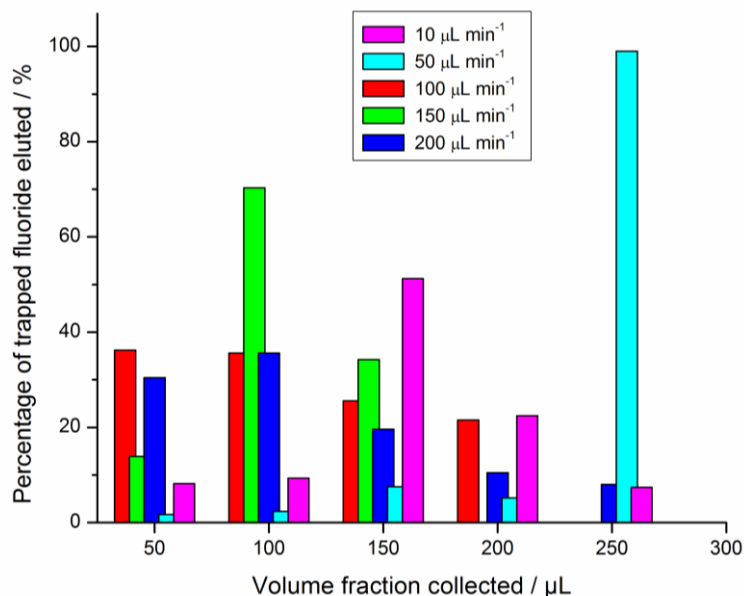
Figure 80 Elution of trapped fluoride from PS-HCO$_3$ particles at different flow rates. In all cases, 100 % of fluoride was eluted in the first 250 μL collected from the chip, with higher flow rates typically affording faster elution times of the total fluoride.

3.6 On-chip [^{18}F]fluoride trapping and release

<u>Conditioning and regeneration of the integrated anion-exchange chip</u>: After experiments carried out on the trapping procedure with non-radioactive fluoride, the method was tested for radioactive [^{18}F]fluoride ion as outlined in the experimental section 2.6. The possibility of trapping and releasing several aliquots of aqueous [^{18}F]fluoride ion was investigated. The first aspect to be considered was the set-up of a suitable procedure for pre-conditioning of the anion-exchange particle bed. Since the chosen polymer was polystyrene based, at the beginning of each experimental day 2 mL of 96% ethanol (EtOH) solution was flushed through the chip in order to fully wet the particle bed. However, before re-conditioning the counter anion with NaHCO$_3$, an additional rinse of the chip with 2 mL of pure water was required, since it was found that passing

bicarbonate solution immediately after EtOH caused copious salt precipitation in the hardware. After this first EtOH/H_2O pre-conditioning step, the system was ready for bicarbonate re-conditioning. This was performed by flushing the chip with 2 mL $NaHCO_3$ (1M), followed 2 mL H_2O and no further EtOH preconditioning cycles were required during the same experimental day. The trapping of [^{18}F]fluoride ions was conducted using 0.5 mL portions withdrawn from a batch of irradiated water, with total starting radioactivity ranging from 5 to 7 GBq, and whose volume was adjusted to 4 mL with pure water. This process was chosen for conducting as many experiments as possible with one batch of irradiated water.

3.6.1   [^{18}F]Fluoride trapping in the integrated chip

 [^{18}F]fluoride ion trapping in the integrated chip: Radioactivity, as indicated earlier, was monitored in three key positions of the hardware; the microfluidic chamber, waste vial and collection vial. As shown in Figure 81, complete trapping of the radioactivity was always observed in the chip, and during the delivery of [^{18}F]fluoride ion into the chip there was no radioactivity detected in the waste vial (Figure 81, red line/solid line). Experiments were also conducted by trapping the whole 4 mL of target water in order to determine whether volume or fluoride mass was detrimental for trapping, whereupon it was found that the performance of the chip remained excellent, and there was no escape of radioactivity. In this trapping step, as well as in the elution step, it was important to dry the system void volume by using 1 mL of air. We also tested flow rates from 50 to 500 µL min^{-1} to investigate any flow related effects and found that the total radioactivity was always trapped on the particles, independent of the applied flow rate.

3.6.2 [¹⁸F]Fluoride elution in the integrated chip

[¹⁸F]fluoride ion elution in the integrated chip: 0.5 mL of K2.2.2 in acetonitrile solution containing 5 % K_2CO_3 (0.36 M) was used for elution of the fluoride complex from the anion-exchange particle bed. This volume was sufficient for eluting more than 95 % of the radioactive fluoride trapped on the particles. As a matter of fact, by monitoring the signal from the radioactivity detector placed on the chip, we noticed that the first 200-250 µL of eluent already removed all of the radioactivity from the particle bed; the rest of the volume and the air served for emptying the tubing up to the collecting vial and drying the system. Also in this case, we tested various flow rates from 50 to 500 µL min^{-1} and found no decrease in the performance of the elution step. Hence, the maximum flow rate was adopted as the optimal working condition, in order to perform the fastest possible processing times.

After elution, 0.5 mL of H_2O was used to rinse the system and prepare it for the re-conditioning cycle, and also to avoid the previously described precipitation problems encountered when using concentrated bicarbonate solution. During this stage, a small decrease in radioactivity counts was observed in the chip; this was justified by the elution of fluoride residuals from the anion-exchange particles. This remaining radioactivity was completely recovered in the waste vial during the $NaHCO_3/H_2O$ reconditioning phase, as illustrated in Figure 81. The waste vial counting revealed that the amount of [¹⁸F]fluoride ions that could not be recovered as elution complex with this procedure was < 5 % of the total radioactivity. No radioactivity was detected in the particle bed at the end of the whole cycle, the on-chip detector always returned to background reading. The same chip was used for performing a total of 20 trap and release cycles over three experimental days, and the performance of the system was

always consistent in recovering >95% of the total radioactivity in the acetonitrile/K2.2.2 elution phase.
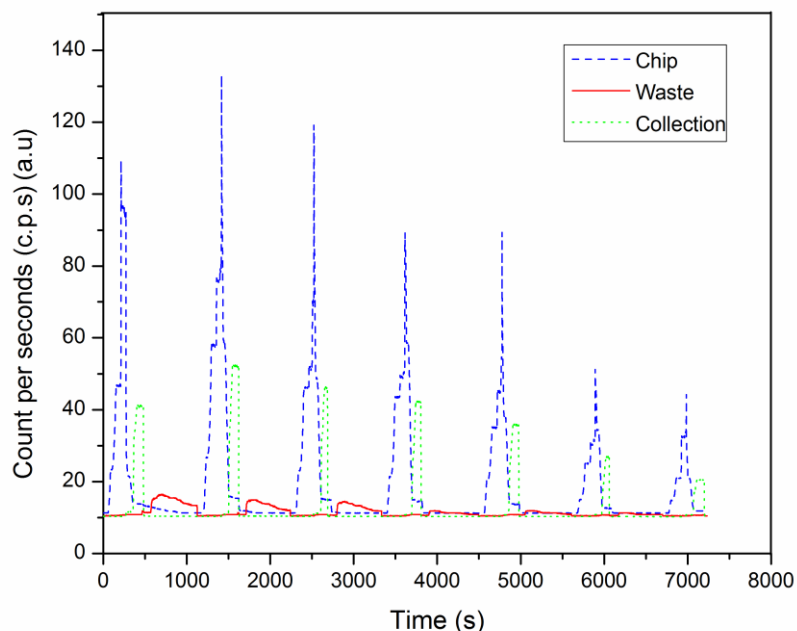
Figure 81 Seven consecutive runs of the trapping and elution of radioactive [^{18}F]fluoride ions. Counts per second (c.p.s) was measured by three independent radioactivity detectors: on the chip (blue / dashed line), in the collection vessel after elution (green/ dotted line), and in the waste vessel (red / solid line).

3.7 [^{18}F]Fluoride labeling reaction

<u>Labeling reaction</u>: To demonstrate the reactivity of the [^{18}F]fluoride ion solution produced *via* this process, its efficiency for labeling was tested in a model aliphatic substitution reaction frequently used in our laboratory, namely the fluorine substitution of the tosylate group of ethyl ditosylate (EtDT). The concentrated [^{18}F]fluoride solution eluted from the chip was collected and excess water was removed by azeotropic distillation as described in Section 2.4. The dried, activated labeling solution was used to perform sequential on-capillary reactions with EtDT precursor solution using a commercial Advion "NanoTek" microfluidic module. Briefly, the reactants were charged into small-bore PEEK loops of adequate volume and delivered, by pushing pure

solvent on the opposite head of the loops into the 2 m long micro capillary (100 μm i.d.) housed in a heater (Figure 82(a)). After each run, the system was cleaned with pure solvent (the sweep step, (Figure 83 (b)), and a further run performed in a similar manner. A sample from each consecutive run was analysed by Radio-HPLC and an average incorporation yield of 96 % (Figure 82 top) demonstrated very good chemical reactivity and high process stability over repeated runs.

Figure 82 Typical Radio-HPLC profile for the labeling of ethyl ditosylate (EtDT) to yield [¹⁸F]fluoroethyltosylate. The top trace represents the radioactivity , and it shows the percentage of unreacted fluoride against 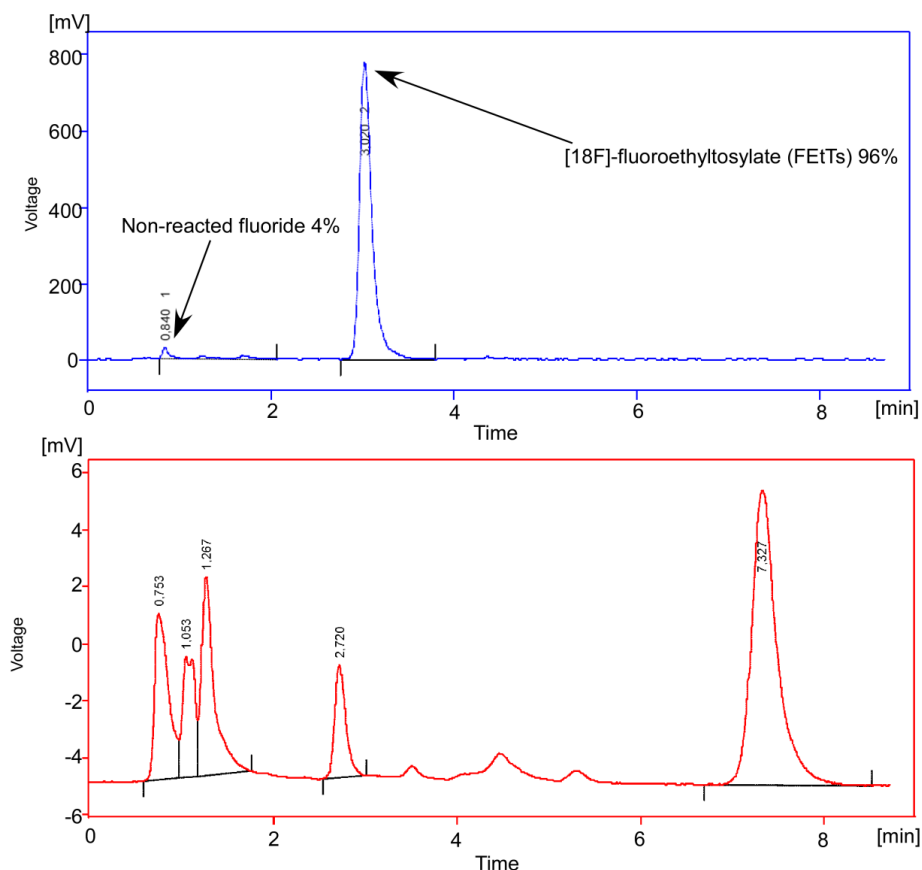the percentage of product formed, while the bottom trace represents the UV absorbance at 254 nm showing the unreacted EtDT peak (Rt = 7.3min).
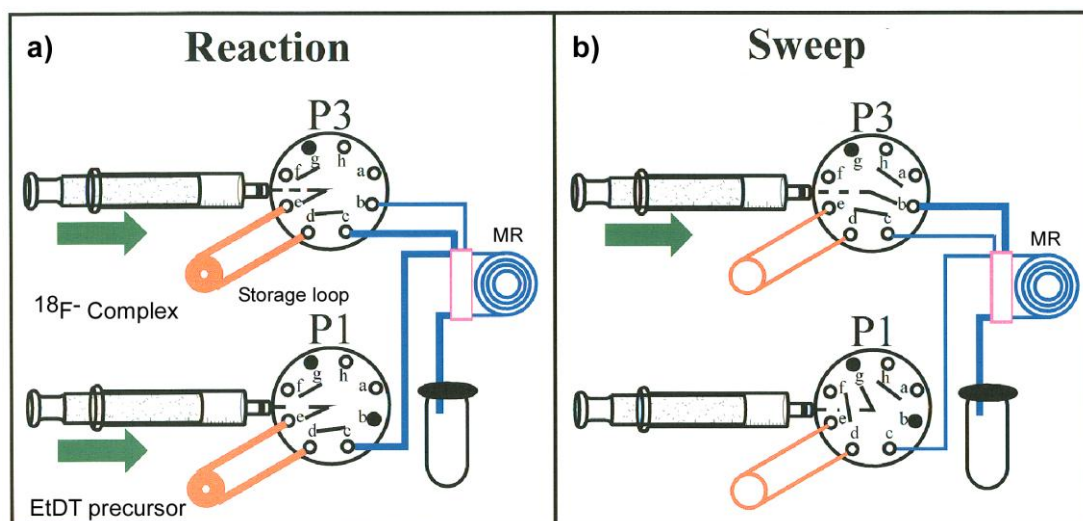
Figure 83 Schematic representation of the EtDT labeling reaction process within the Advion automated system after drying of excess of water has been performed. The precursor solution was pumped into the loop of pump 1 (P1) while the labeling solution was introduced into the sample loop of pump 3 (P3). (a) In the reaction step, fluoride complex and precursor solution aliquots were delivered into the capillary microreactor (MR) preheated at a temperature 150 °C from the storage loops by pushing with pure solvent (acetonitrile); in this phase the fluids moved through the lines indicated in bold. (b) In the sweep step, the microreactor system was rinsed with pure solvent through the lines indicated in bold and prepared for a further reaction with other aliquots of reagents.

3.7.1 Particle stability

After successfully demonstrating the reusability and the efficiency of the packed micro-chamber module with both non-radioactive and radioactive fluoride it was decided to see if in any way the particles were affected by the radioactivity or from the regeneration steps. A series of SEM pictures of the particles before and after treatment with both radioactive and non radioactive fluoride were taken as shown in Figure 84, (a) SEM pictures of the resin before any treatment showing the monodispersity of PS-DVB beads, (b) SEM picture after a series of trapping of [^{19}F]fluoride treatments which shows a slight formation of crystals possibly due to the salt washing ($NaHCO_3$) and (c) SEM picture of resin after a series of radioactive treatments showing a significant crystal formation identified as Na crystals by elemental analysis, due to a non extensively washing with water after the regeneration step.
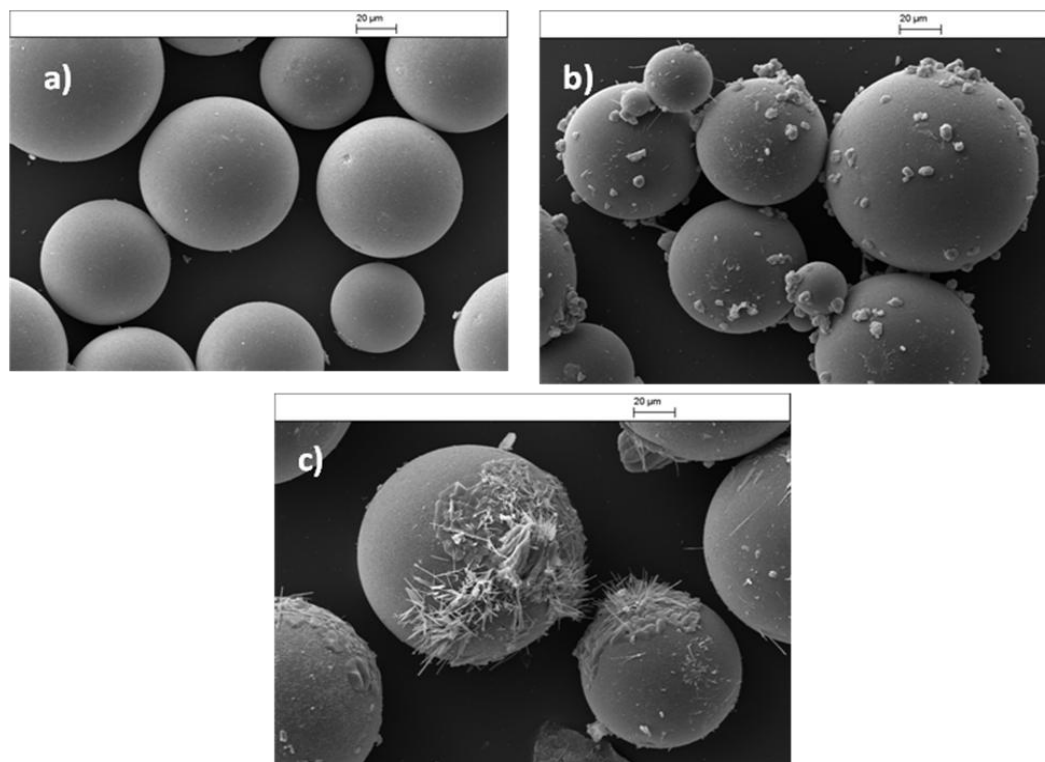
Figure 84 (a) SEM picture of PS-DVB particles. (b) SEM picture of PS-DVB particles after several treatment with [^{19}F]fluoride. (c) SEM picture of PS-DVB particles after a series of treatment with 18 F fluoride, showing some crystal formation which was identified to be Na by elemental analysis due to non sufficient washing after the conditioning and regeneration steps.

3.8 Summary

Both radioactive [^{18}F] and non-radioactive [^{19}F]fluoride ions could be repeatedly recovered by employing a chip containing a smaller amount of anion exchange particles than conventional cartridges. The entire process required less than 6 min and had a trapping efficiency >90%, while the particles could be repeatedly regenerated and reused up to 40 times *via* a multicycle approach, without loss of performance. The radioactive solution resulting from this innovative process was highly reactive and could be employed in the radiofluorination of EtDT. On this basis, the chip could easily be integrated into automated systems to provide highly reactive fluoride complexes for the production of fluorinated PET radiotracers in high yields. The ability to regenerate the anion-exchange chip would also allow many batches of radiopharmaceuticals to be

synthesized without requiring continuous manual interaction of personnel within the shielded synthesiser.

4 On-chip preconcentration of [$^{18/19}$F]fluoride via magnetic batch approach

In this chapter, proof-of-principle experiments are described in which plugs of positively charged superparamagnetic particles were formed inside a parallel channel glass device. Both [$^{18/19}$F]fluoride was trapped on the particles and subsequently eluted This initial study has been published in the proceedings of the MicroTAS 2010 conference [176].

4.1 Introduction

Microparticles are most commonly used as packing materials in microfluidic devices, acting as a high surface area solid-support for reactions. Magnetic particles can be formed into plugs of particles using simple magnetic set-ups, and this has already been demonstrated for many analytical applications [59, 64]. So far, to our knowledge, nothing has been reported for such a method for pre-concentration of [$^{18/19}$F]fluoride used for radiotracer synthesis that involves the use of magnetic forces. Here, we investigate this method. The schematic shown in Figure 85 describes the concept the loading of the magnetic particles which, under the influence of the magnetic forces, form a plug. Pumping of the fluoride ions in aqueous solution results in trapping *via* exchange reaction onto the magnetic particles and finally, elution can be performed *via* a high ionic strength salt (K_2CO_3).
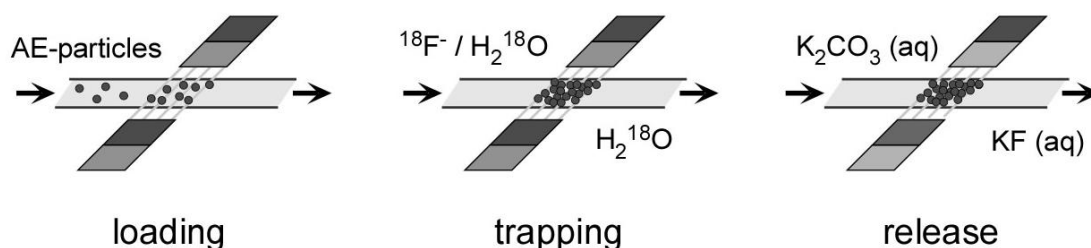
Figure 85 Schematic of the magnetic capture approach. Using an external magnet; fluoride can be trapped and subsequently eluted from the particle bed.

4.2 Off-chip test for [¹⁹F]fluoride trapping and elution

A series of off-chip tests were performed to ensure and quantify the trapping efficiency of the magnetic particles for fluoride. The main objective was to determine the number of particles needed to trap 1 µg of fluoride. From preliminary results using non magnetic particles (Chapter 3) it was known that trapping of fluoride was achieved *via* strong anion exchanger solid support, hence two different commercially available types of magnetic particles were employed as described in Section 2.1.3. Firstly the manufacturer's protocols were followed together with the method employed in Chapter 3 for the on-chip pre-concentration *via* packed bed. However it was not possible to measure any trapping of cold fluoride even with very high number of particles mL^{-1}. Even at 1×10^{10} particles mL^{-1}, no significant trapping efficiency could be measured in the ion exchange chromatography. A deviation from the manufacturer's protocol was then tested in which the magnetic particles suspension was firstly washed with high concentration of HCl in a way that the particles counter ions (in the case of Invitrogen SAX and Chemicell SiMAG-Q Chloride counter ion Cl$^-$) could be always be present in excess. By using 0.1 M of HCl during the last washing step of the stock preparation it was possible to observe and measure, trapping of fluoride. The number of particles needed to trap 1 µg of fluoride was found to be 1×10^7 particles mL^{-1} of Chemicell SiMAG-Q particles.

In Figure 86 the set-up for the off-chip experiment shows the magnet one on side and the particles attracted to it, and subsequently the supernatant solution is analysed *via* IC for presence of fluoride.
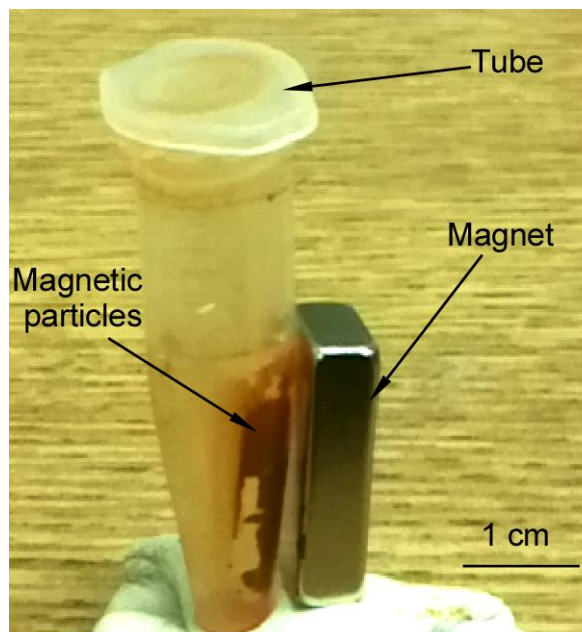
Figure 86 Photo of the off-chip set-up used to determine trapping and elution efficiency of fluoride, in this image is shown an Eppendorf tube with the box magnet placed on the side to allow the magnetic particles to be trapped on one side so that the supernatant can be analysed for presence of fluoride, Particles used in this image are Chemicell SiMAG-Q.

4.3 Optimisation of chip design

In parallel to studying the trapping efficiency of the magnetic particles, the formation of a magnetic plug in a capillary was investigated; the set-up is shown in Figure 89 and described in Section 2.7.1. Using a solution of 1×10^{4} particles mL^{-1}, particles were successfully trapped within the two magnets. Magnetic plugs were formed in the capillary according to the method described in Section 2.1.5, with different flow rates investigated. The maximum was found to be 60-120 µL hr^{-1} (1-2.5 mm s^{-1}); photographs of the plug formed can be seen in Figure 87.
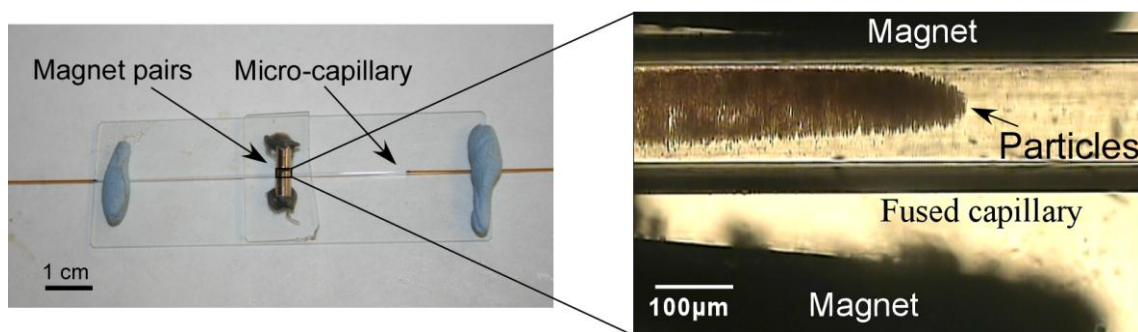
Figure 87 Single on capillary formation of plug at 120 µL h⁻¹.

However from the off-chip experiments it was known that the number of particles to trap 1 µg of fluoride was not sufficient. So a design with several parallel channels was fabricated, first a design consisting of 16 and 32 parallel channels as shown in Figure 38. The design with 32 parallel channels was tested, 1×10^8 particles were pumped through the chip at a flow rate of 350 µL h⁻¹ but this caused blocking and clogging of the device at several points. Finally a device with 128 parallel channels was used (PC128 section 2.2.1). Some sticking of the magnetic particles on the glass surface was observed possibly due to the negatively charged silanol groups interacting with the positively charged functional groups of the magnetic particles. However, formation of plugs on the channels was achieved by placing three box magnets on top of the device. Several flow rates were investigated to determine the maximum flow for the formation of plug with minimum particles escaping. This was found to be 900 µL h⁻¹. At this particular flow, most of the particles were trapped on chip, the exact number of particles was not possible to determine however as shown in Figure 88 the middle vial represent the solution collected at the outlet of the device during the trapping experiment and clearly can be seen the clear solution collected with a minimum amount of particles demonstrating successful trapping and plugs formation.
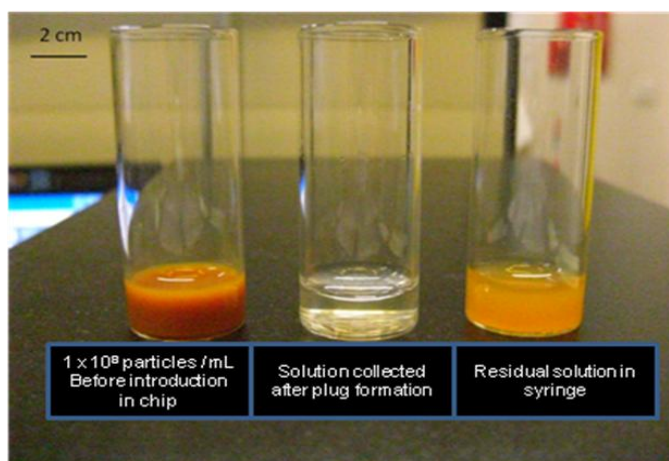
Figure 88 Magnetic particles suspensions (left) before introducing in chip as very dense concentrated solution, (middle) solution collected at the outlet of the 128 paralle channels showing the most of the particles have formed magnetic plugs, (right) residual particles at the end of the experiment found at the bottom of the syringe.
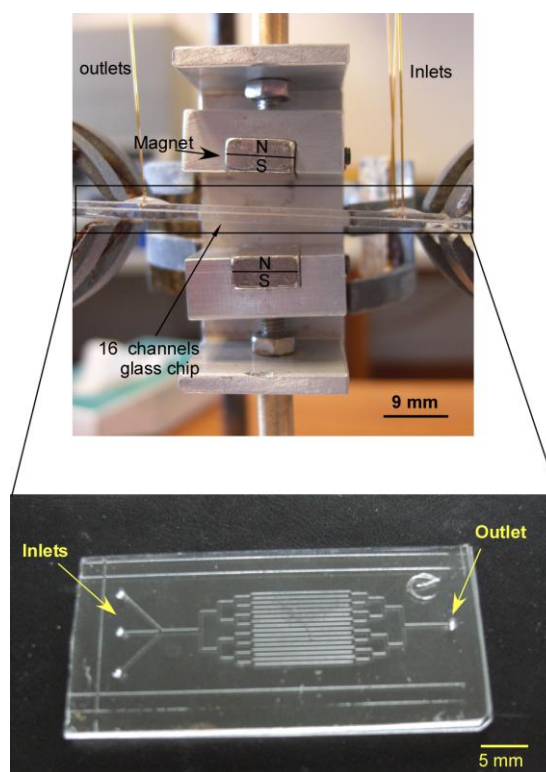
Figure 89 (top) Set-up of the magnet pairs to form plug, magnet held in place) by a clamp and placed on top and bottom of the glass device (at distance of 2 mm from the glass device for magnetic field improvement. (bottom) Image of the 16 parallel channels glass device.
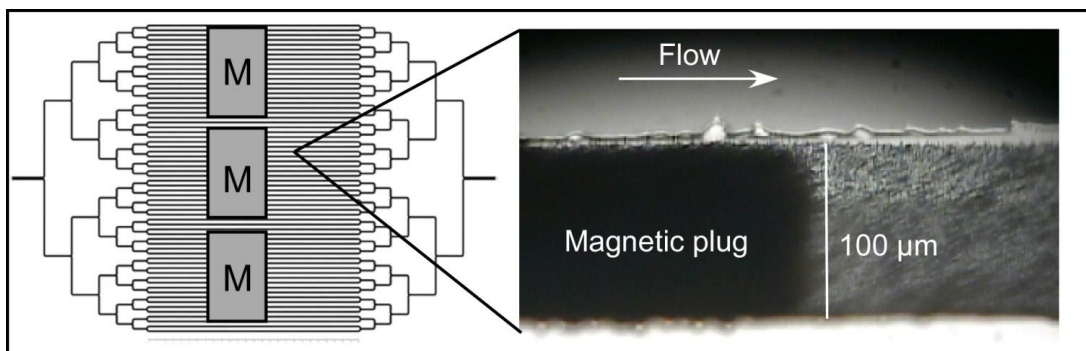
Figure 90 CAD image of the 128 parallel channels on the left and the formation of plug image downstream the magnet. Showing the position of the three magnets, which were always in the top middle of the glass device.

As shown in Figure 90 plugs were successfully formed on chip, even though not in all the channels was possible to observe a uniform and constant plug formation. A FEMM simulation was performed to model the magnetic field gradient across the parallel channels and as shown in Figure. 92. Interestingly was found that plugs formation was more readily formed at the edges of the series of magnets where the magnetic field gradient is stronger, and leaving some of the central channels with no plug formation as shown in Figure 91 (bottom area).
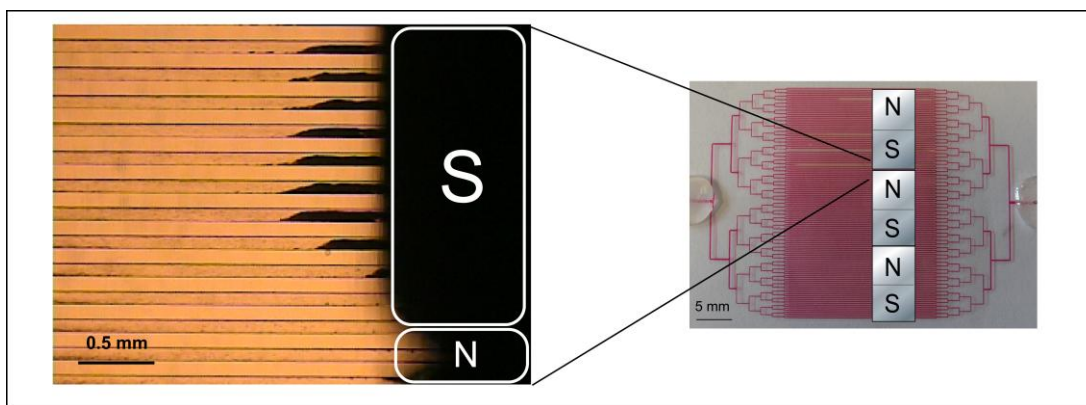
Figure 91 image of the plug formation on chip showing some of inner channels where no plug was formed possibly due to the weaker magnetic field gradient suggested using the FEMM simulation.

In Figure 92 two-dimensional simulation of the magnet flux density, B, over the 128 parallel channels glass device, as observed from a side-on view. FEMM software was used to generate the model. As shown in the simulation, the magnetic field is stronger at

the edges of the magnets and weaker in the middle magnet, possibly this explain why fewer particles were trapped between the border of the magnets as shown in Figure 90 between the south pole of one magnet and the north pole of the next magnet less particles plug formation is observed.
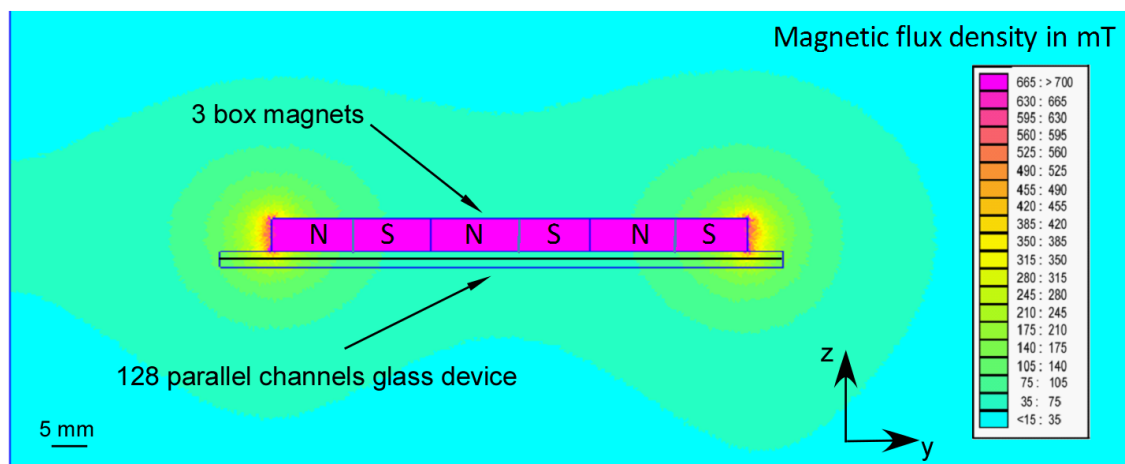
Figure 92 FEMM simulation of the magnetic flux density of 3 magnets facing opposite poles (10 x 10 x 5 mm^3 NdFeB magnets across the microfluidic chamber from a side-on cross-sectional view.

4.4 [^{19}F]Fluoride trapping and elution on-chip

After investigating the plug formation we performed an experiment where after forming a plug with 1×10^7 particles mL^{-1} at 900 μL h^{-1} (Figure 93) a solution of standard fluoride 1 μg mL^{-1} to was pumped to perform the trapping step. Initially the solution was pumped at low flow rate of 300 μL h^{-1} and by carefully observing under the microscope if any of the plugs were disrupted gradually it was increased up to 700 μL h^{-1} where some deformation of the plugs was observed so it was decided to pump all the remaining solution using this flow rate.
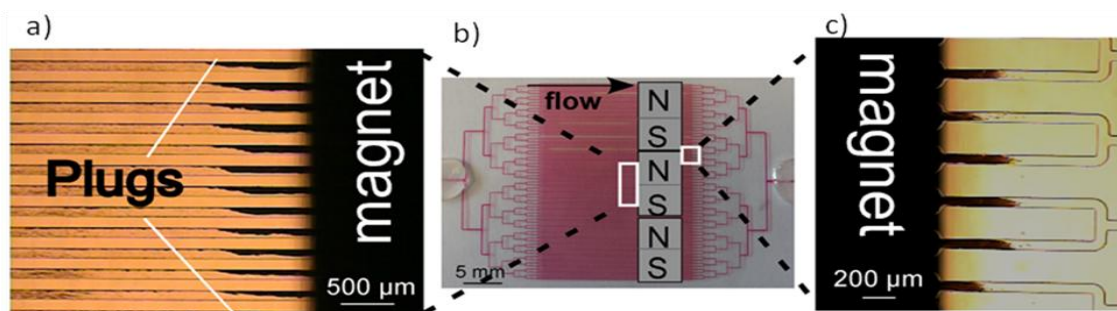
Figure 93 Photographs of magnetic particle plugs formed on chip (a) upstream from the magnet, (c) downstream from the magnets, (b) image of the 128 parallel channels device filled with red ink for visualization and showing the position and orientation of the NdFeB magnets.

Subsequently the solution was collected at the outlet and analysed using IEC for presence of fluoride. In this case we used the area of the fluoride peak and was found that 0.5 µg of fluoride was trapped on the magnetic beads. A significant amount of chloride was observed during the analysis, but there was no interference with the fluoride peak. In Figure 94 a series of four chromatograms representing the fluoride peak in the water background (d), the peak of the fluoride standard (e), the trapping of fluoride after passing through the magnetic plugs and finally the release of the fluoride with K_2CO_3 (0.001M) are illustrated. Subsequently, a third step for the release of the fluoride was performed, in this case 1 mL of solution of K_2CO_3 (0.001M) was pumped at a flow rate of 500 µL h^{-1} and the solution collected at the outlet was analysed with IEC, and as a result 70 % (3.5 µg) of the trapped fluoride was successfully released.
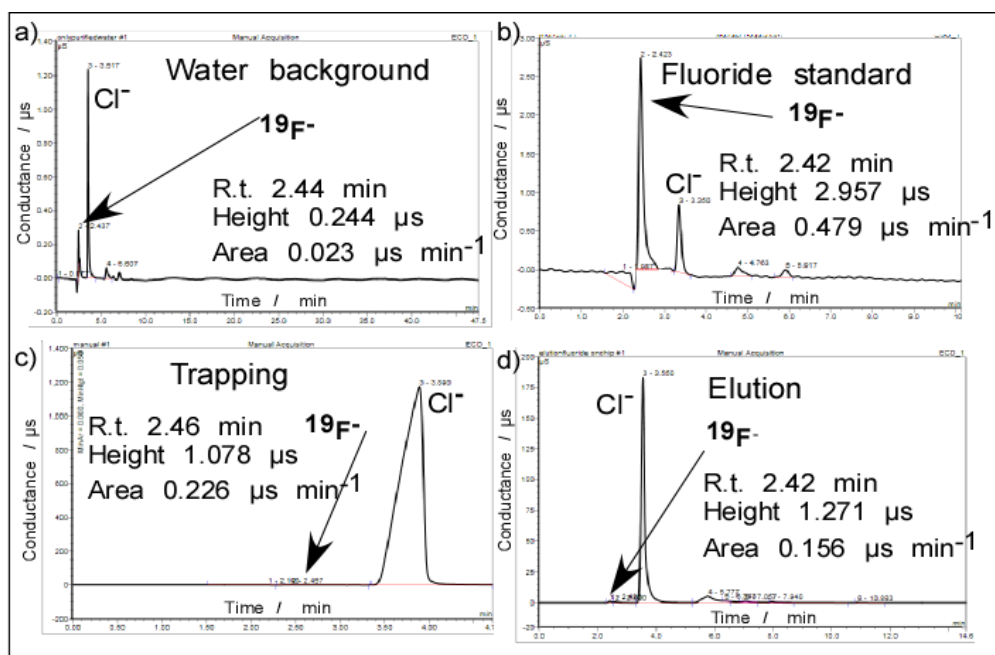
Figure 94 (a) Chromatogram of water (background signal), showing the presence of fluoride at very low concentration, (b) chromatogram of 1 µg mL^{-1} fluoride solution (reference standard). (c) Chromatogram after passing fluoride solution through the magnetic particles plugs, showing a small fluoride peak and a large chloride peak (the counter-ion on the resin) (d) Chromatogram of eluted fluoride solution featuring the fluoride peak and indicating that 70 % (3.5µg) of fluoride had been released.

With the proof of principle demonstrating that indeed cold fluoride could be trapped and eluted on chip *via* a formation of magnetic particles plugs, the set-up and experiments were transferred on the radioactive trapping and elution of fluoride.

4.5 [18F]Fluoride trapping off-chip

This work was carried out in collaboration with Dr Giancarlo Pascali in the radioactive facilities of the Institute of Clinical Physiology of National Research Council (IFC-CNR) in Pisa (Italy). In order to corroborate the experiments carried out in Hull with non radioactive fluoride. First off-chip tests were repeated in the same way as described in Section 2.7.1.
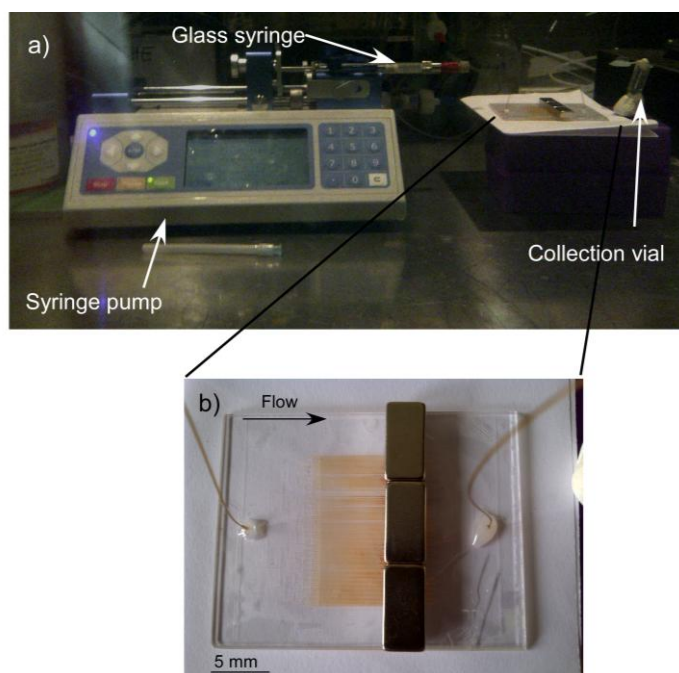
Figure 95(top) set-up of the on-chip trapping and elution of [^{18}F]fluoride *via* plug formation of magnetic particles, showing a syringe pump, glass syringe and glass device, through a glass window for radioactivity shielding. (bottom) image of the glass device at the end of the experiment showing the brownish color given by the particles on the left and the clear side after the magnet on the right.

100 µL of Chemicell particles (1 x 10^9 particles mL^{-1}) in 900 µL of solution of HCl in water (0.1M) was first prepared in the Eppendorf tube, vortexed for 30 s and the supernatant washed away, subsequently an activity of 63.4 mCi of [^{18}F]fluoride was added to the Eppendorf tube, with mixing by shaking for about 1 min. The magnet was then applied on the side, the supernatant washed away, and the activity was measured on the vial which now contained only particles without solution, it was measured as 8.4 mCi n.d.c, (8.6 d.c.) the washed solution also was measured and found to be 50 mCi n.d.c (52.25 d.c.). This procedure was repeated for three times, but no significant trapping and elution of activity was measured, the total activity trapped at the end was only 3 % of the starting fluoride. It was known from the non radioactive test that off chip experiment was not giving great results for fluoride trapping; in the case of the radioactive test it may be that the incubation time was not enough for the exchange mechanism between F$^-$ with Cl$^-$.

4.6 [¹⁸F]Fluoride trapping and elution on-chip

Despite the unsuccessful results with the off-chip radioactive fluoride the experiments was tested on-chip and the setup and procedure are described in Section 2.7.1. This time 30 µl of Chemicell particles (1×10^7 particles mL^{-1}) were loaded in the glass syringe and the plug was formed at 20 µL min^{-1} as shown in Figure 95. 500 µL of [¹⁸F]fluoride with activity of 38.3 mCi was pumped through the chip at a flow rate of 15 µL min^{-1}, at the end of the solution activity was measured first in the syringe and found to be 3.7 mCi as well as in the collection vial where was measured at 20.18 mCi which is equal to 45 % of radioactive fluoride successfully trapped on the plug. Subsequently a 100 µL solution of K2.2.2 + K_2CO_3 and MeCN was pumped at 10 µL min^{-1} for the elution steps, at the end of the solution, activity was measured in the vial, and only 50 % of the fluoride was eluted, this steps were repeated again with another 100 µL elution solution where finally another 40 % of fluoride was successfully eluted.

$$A = A_0 e^{-\left(\frac{0.693t}{T_{0.5}}\right)}$$ Equation 10

A_0 = Initial Activity

A = Activity

$T_{0.5}$ = half life of [¹⁸F]fluoride 109.7 min or 6586 s

t = time elapsed since initial activity

Since the activity at any given time was measured Equation 10 was rearranged in order to solve the initial Activity A_0:

$$A_0 = \frac{A}{e^{-(0.693t)/T_{0.5}}}$$ Equation 11

Activity of fluoride at the start of the experiments 38.3 mCi at time 0.

The amount of fluoride trapped was calculated by subtracting the amount of activity left in the empty syringe plus the activity at the outlet minus the starting fluoride activity, decay corrected using Equation 11.

Table 22 Values of the trapping and elution activity during the on-chip experiments.

	Initial activity	Activity N_0	Time / s	Efficiency / %
Glass syringe (A)	3.7	4.55	1980	
Collection vial (B)	13.18	16.23	1980	
Trapped activity D=(C-(A+B))		17.31	1980	45
Fluoride elution 1	3.3	4.49	2940	25
Fluoride elution 2	4	6.2	4200	35
Fluoride elution 3	2.6	6.33	8460	35

As reported in Table 22 the trapped activity was measured indirectly by difference. What has to be noted is first results of this experiment are based on the theoretical decay of the fluoride at different time points, especially within such a long experiment (elution step was after 141 minutes, 109.7 half life of fluoride) and is not considering any possibilities of fluoride sticking on the glass surface which is an issue already reported in literature [156]. The experiment was then repeated once more using the same settings with the difference being that between the trapping and the elution 200 µL of pure MeCN were pumped at 8 µL min^{-1} to actually prove if the fluoride was trapped onto the particles, or there was any sticking of fluoride in the tubing. Using this approach 35 %

trapping of fluoride and 60 % elution of fluoride, with another 30 % of the trapped fluoride being washed away by the MeCN was observed.

4.7 Summary

Investigations were performed into trapping and elution of [$^{18/19}$F]fluoride *via* formation of magnetic plug inside a glass micro-device even though the method was not as fast or as efficient as the packed bed of micro-particles (Chapter 3). The proof of principle showed that an alternative process that uses magnetic forces can be adapted for future on-chip systems for pre-concentration of fluoride. However by employing positively charged magnetic particles, fluoride could be trapped and eluted; although the efficiency and the volume throughput were not as high as expected. Further optimisation of the set-up however could have potential for any future dose-on-demand applications [177].

5 On-chip free-flow magnetophoresis: towards a continuous method for pre-concentration of [$^{18/19}$F]fluoride

The work described in this chapter concerns the determination of laminar flow and study of magnetic particle characteristics in a microfluidic device with the ultimate aim to develop a continuous method of [$^{18/19}$F]fluoride pre-concentration.

5.1 Introduction

As described in Section 1.5, the principle of on-chip free-flow magnetophoresis was further developed such that continuous flow trapping and elution of [$^{18/19}$F]fluoride be performed on mobile AE magnetic particles. Briefly, laminar flow is generated in the x-direction across a wide chamber, as in the magnetophoresis device, but with the flow now consisting of alternating streams of reagents and buffer solutions (Figure 96). Functionalised magnetic particles are then introduced into the chamber and deflected sequentially through each of the streams, allowing consecutive reactions to take place on the particle surfaces.

The principle of this method was a modification of a similar process currently under investigation in our Research group (Dr. Pamme, The University of Hull), three types of applications were investigated: (i) bioassays (by Sally Peyman)[178, 179],(ii) DNA hybridisation (by Martin Vojtisek) [180] and (iii) chemical reactions/depositions (by Mark D. Tarn) [181-183].

Here, a departure from the more bioanalytical assays was investigated, in which fluoride pre-concentration could be performed in continuous flow, possibly even combined with solvent exchange. One envisaged concept is shown in Figure 96, whereby magnetic particles with anion-exchange groups on their surface are deflected through a chamber

with several laminar reagent streams. The particles first pass through a fluoride-containing stream where the fluoride binds to the particle surface. The particles are then dragged into a stream which would elute the fluoride, either an aqueous solution of carbonate or, alternatively, an acetonitrile based solution containing some carbonate. The fluoride on the particle surface will be replaced by the carbonate. The fluoride ions will leave the micro-chamber and can be guided to the synthesis step, whereas the magnetic particles are further deflected for separate collection. Whilst the previous applications were already performed (immunoassays, DNA hybridisation), the capture of anions and the pulling of particles through interfaces of different solvents, has not yet been studied.
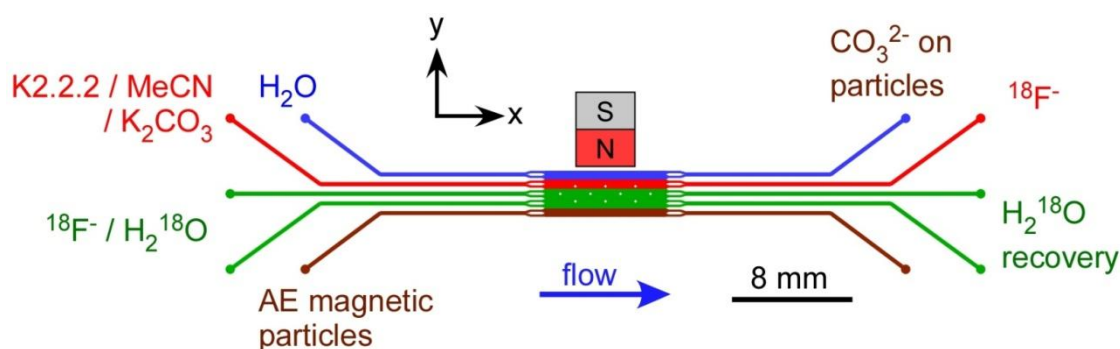
Figure 96 Continuous flow magnetic approach showing the principle of the multi laminar flow regime where AE particles are introduced into the reaction chamber and deflected *via* magnetic field (left). The green streams show the trapping while the red stream shows the elution of the fluoride.

5.2 Multilaminar flow approach

Before performing particle experiments in the multilaminar flow chips, the flow regimes were tested to confirm that they were laminar. Previous work by Peyman *et al.*[179] had already established that the diffusion between the laminar streams was not sufficient to cause cross-contamination between reagents; however the experiments and the set-up were repeated during the work herein, to gain confidence and practicality with such a precise and specific process. Figure 99 shows the laminar flow regime of

alternating streams of aqueous dye within two different chips designs. The figure clearly shows that laminar flow was obtained, with the coloured streams liquids flowing side-by-side through the microfluidic chamber. During this part of the work the previously used hydrodynamic pump described in experimental section 2.3 was replaced by a pressure driven pump as described in Section 2.8.1 and shown in Figure 55, where instead of having the liquid pumped through the chip by controlling the flow rate, a difference in pressures between the inlets and the outlets of the device allows the liquid to flow in the y direction. It is due to this pressure drop between inlets and outlets that the particles and liquid within the microfluidic chamber can be manoeuvred.
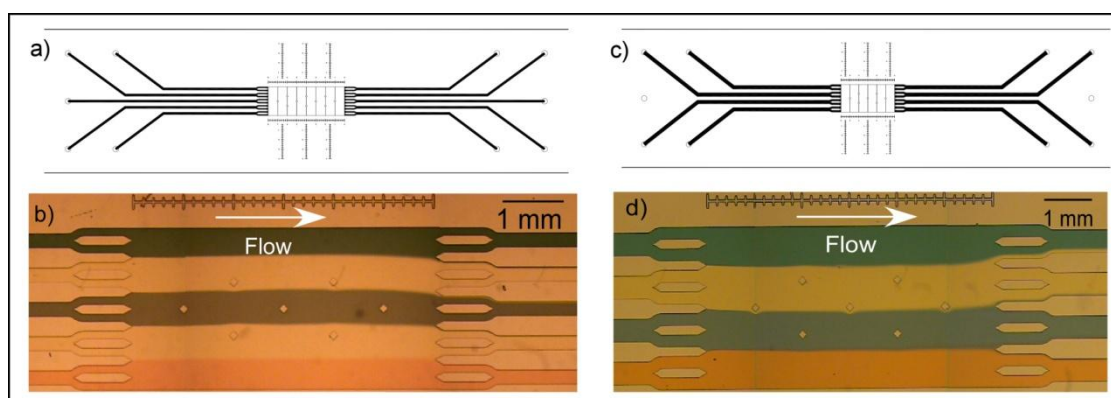
Figure 97 Laminar flow inside the chamber of two different chips design FDL1-FDL2, showing stable stream with minimal diffusion.

Pressure drop

As a liquid flows through a pipe or channel the pressure decreases from one end of the channel (the source of the pressure) to the other due to frictional forces, an effect known as the pressure drop. These frictional forces arise from a resistance to the flow exerted by a channel based on its dimensions and the viscosity η (N m s^{-1}) of the fluid flowing through it [3]. The pressure drop within the device chamber during the experiments was achieved by controlling the pressure at the inlets and outlets using the MFCS fluigent pump as described in Section 2.8.1. However it can also be calculated theoretically by first determining the flow resistance Rφ (Kg m^{-4} s^{-1}) as shown in Equation 12:

$$R_\phi = \frac{2fR_e l\eta}{wd\delta^2}$$
Equation 12

Where l = channel length (m), w = channel width (m), d = channel depth (m), fRe = the friction coefficient which is related to the shape of the microchannel (assumed to be 24 for a microfluidic chamber). The hydrodynamic diameter, δ (in m), can be calculated for a rectangular cross-section using Equation 13:

$$\delta = \frac{2wd}{w+d}$$
Equation 13

The pressure drop, Δp (Pa), is then determined from the flow resistance, R_ϕ, and the applied flow rate, ϕ (m^3 s^{-1}), using Equation 14. This can be also be likened to the calculation of the voltage, or potential difference (V), from the current (I) and resistance (R) in an electronic circuit according to Ohm's law, $(V = I\,R)$

$$\Delta p = \phi R_\phi$$
Equation 14

As in an electrical circuit, the flow resistance of multiple channels in a microfluidic chip may be treated like electrical resistors, and Kirchhoff's laws can be applied to find the total flow resistance, R_ϕ (tot), for the chip and its individual sections. When the channels in a microfluidic chip are in a serial arrangement (*i.e.* one channel follows another) the total flow resistance can be calculated using Equation 15, where $R1$, $R2$ etc. refer to resistance values for individual channels.

$$R_\phi = R_1 + R_2 + R_3 + ... + R_i$$
Equation 15

When the channels are in a parallel arrangement (*i.e.* when a single channel splits to give two parallel channels) in the case of the magnetophoresis chip the total resistance can be calculated by determining the value of $1/R$(tot) from each of the parallel channels as shown in Equation 16, before taking the inverse of this number to give R_ϕ(tot).

$$\frac{1}{R_{\phi (ot)}} = \frac{1}{R_1} + \frac{1}{R_2} + \frac{1}{R_3} + ... \frac{1}{Ri} \qquad \text{Equation 16}$$

The velocity of the laminar flow profile depends on the distance x from the centre of the chamber with a depth, d, and the length l, of the chamber. It also depends on the pressure drop, Δp, over the chamber and the viscosity, η; of the pumped medium:

$$v = \frac{\Delta p}{4L\eta}\left[\left(\frac{d}{2}\right)^2 - x^2\right] \qquad \text{Equation 17}$$

As an example, the theoretical flow velocity within the separation chamber was calculated for a pressure difference of 50 mbar in each of the 4 inlets of the glass device with 4 inlets 4 outlets with a depth of 20 um and a width of 3 mm and a length of 6 mm, assuming viscosity of 1.002 N s m^{-2} and x^2 = 0 at distance x due to the parabolic flow velocity. Then the total linear velocity was calculated to be 200 μm s^{-1} by using Equation 17 and the theoretical volumetric flow rate was calculated and found to be 43 μL h^{-1} using Equation 14. The calculated values were compared to the experimental results, in fact a different experiment was carried out to be able to determine the speed of the liquid inside the chamber, where a calibration of the particles speed against the pressure differences were plotted as shown in Figure 100, The particles were forced in the y-direction from the inlet pressure that was always kept constant at 200 mbar and series of video were recorded of the particles crossing the chamber whilst changing the pressure at the outlet from 195-140 mbar. The videos were then analysed by recording the time that a particle takes from point a to b and the particles speed was recorded. As shown in Figure 100, linearity was observed (n=20) however as expected due to the laminar flow profile a significant error especially at high pressure differences within 30-60 mbar, was observed.
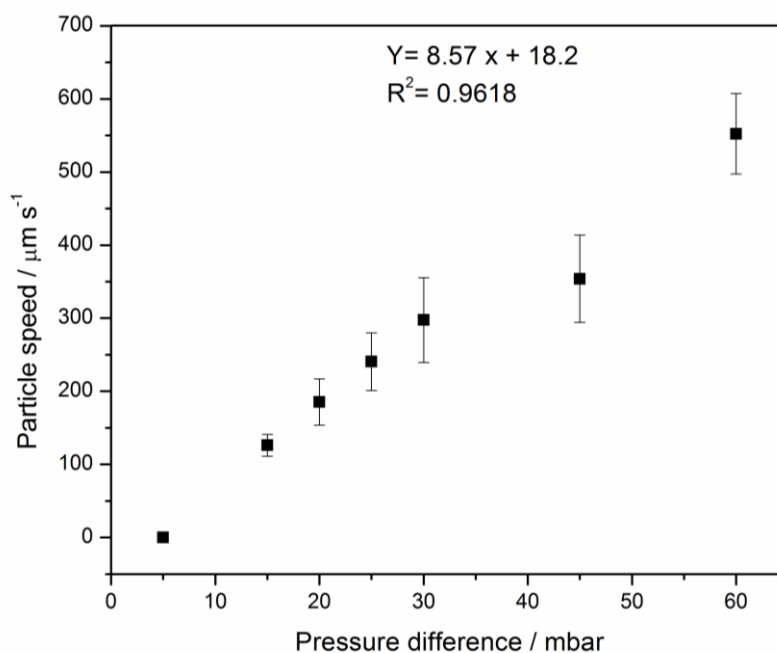
Figure 98 Plot of the particles speed µm s^{-1} *vs* pressur difference between inlets and outlet, particles used were Dynabeads M280.

As shown in Figure 98 at 50 mbar difference in pressure corresponds an average particle speed of 460 µm s^{-1} which surprisingly was nearly double the theoretical linear velocity calculated previously to be 200 µm s^{-1}, a possible explanation of this difference could be the fact that the particles anlaysed under the microscope were at a different distance within the parabolic flow regime, which means that particles at a different depth within the 20 µm structure could have experienced a variations in their velocity up to 50%, phenomena that are already reported previously [184]. Nevertheless 50 mbar was then used for all the further experiments.

5.3 Off-chip AE particles deflection

Once the laminar flow within the chamber was determined, an off chip experiment to pull particles through a water: acetonitrile interface was carried out (Figure 99). However since acetonitrile is a polar solvent and miscible with water, at first it was not possible to investigate the transfer of particles through the two interface layer especially off chip where mixing happens rapidly, nevertheless using a reported method it was possible to separate the two layers by adding excess of high ionic strength salt. In this case K_2CO_3 (3 g in 5 mL solution 80:20 ACN:H_2O) was added and the magnetic particles transported from the water layer to the acetonitrile layer using a small permanent magnet. As clearly shown in Figure 99(a-b) [185]. The experiment suggested that the particles can indeed be mobilised through this interface by means of the conventional small permanent magnets.
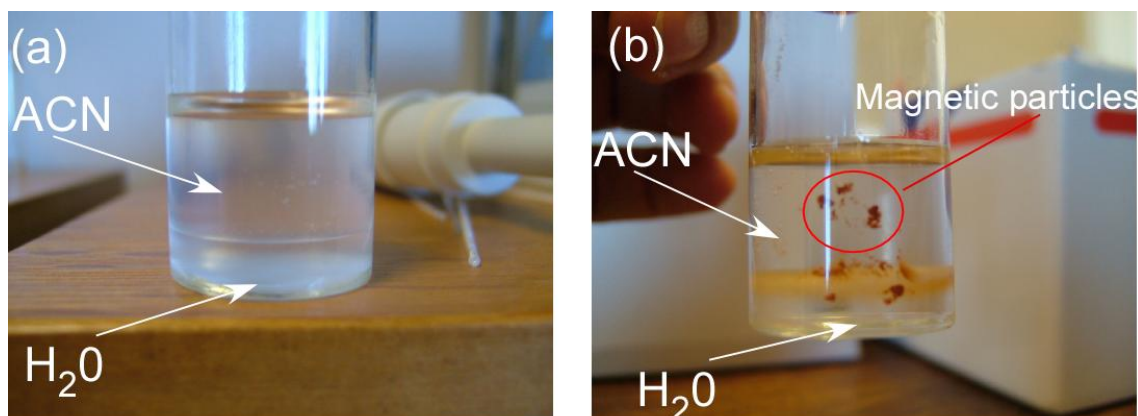
Figure 99 a) Separation of water-acetonitrile layers. b) Pulling of 3 μm particles from water to acetonitrile with small permanent magnet.

5.4 On-chip surface treatment optimisation

After the laminar flow optimisation and the study of solvent effects on the magnetic particles, an experiment with particles inside the device was carried out, as detailed in Section 2.7.4. Invitrogen SAX particles were introduced into the microfluidic chamber of chip design FDL1 *via* inlet 1, with a stream of water: MeCN: K222: K_2CO_3 in inlet 4,

and aqueous fluoride solution (1 µg mL^{-1}) from inlets 2 and 3. The principle of the experiment is shown in Figure 96. However, in initial experiments; the particles simply stuck to the surface of the glass upon entering the chamber and would not move thereafter as shown in Figure 100. This likely occurred as a result of two factors, the first being that the particles have experienced an upwards magnetic force due to the NdFeB magnet being placed on top of the chip, which would have drawn the particles towards the upper surface of the glass chamber. Secondly, the quaternary ammonium particles are positively charged (Figure 22 section 1.9) at pH between 2-14 and therefore experienced an electrostatic attraction to the surface of the glass chip which possessed a negative charge. Experiments with the magnet placed in-plane with the chamber by having a cut out to place the magnet were also carried out which gave similar effect without improving adhesion.When silanisation of the chip was performed that chip was only used for 1-2 experiments.
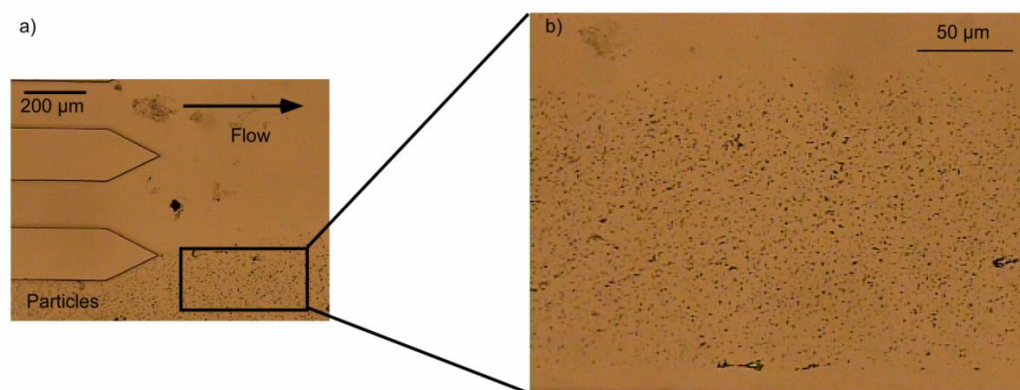
Figure 100 Image showing the Invitrogen SAX particles stuck in the glass device with no treatment.

In an effort to reduce this effect, the glass channels were treated with octadecyltrichlorosilane (OTS) as described in section 2.4 to render the chip surfaces uncharged, albeit hydrophobic, but no significant improvement was observed. An attempt to reduce the sticking was made using trichloro (1H,1H,2H,2H-perfluorooctyl) silane (FDTS) to treat the glass surfaces rather than OTS. FDTS features a

perfluoroalkyl chain (Table 15) that, when coated onto the glass surfaces, formed uncharged and hydrophobic surfaces that prefer to be wetted by fluorinated species. Tests to confirm the successful treatment of the hydrophobic coating were done by measuring the contact angles between at the air-water interfaces as shown in Figure 101.
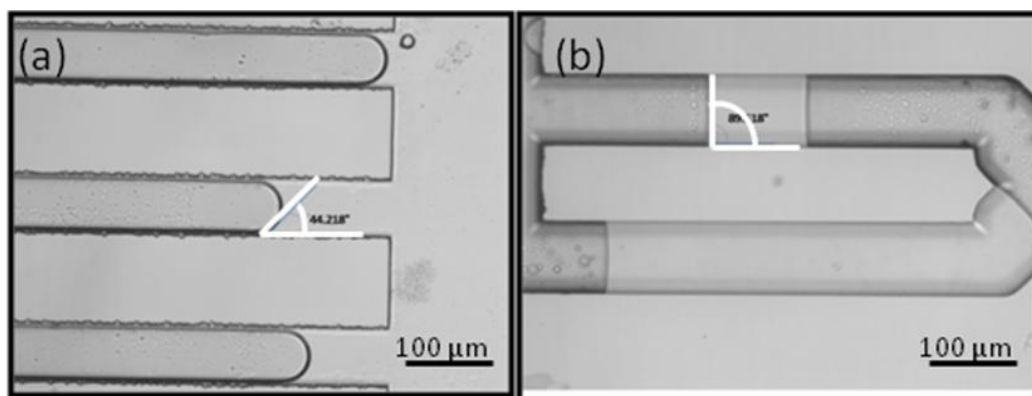
Figure 101 (a) Contact angle measurement using water/air interface without silanisation(°44.218), (b) after silanisation (°89.518).

As the chip design used to test the success of the surface treatment was a different design previously used for magnetic plug (Chapter 4), the coating method was then applied to the newer chip design. On chip contact angle measurements were performed *via* water-air interface, the value before treatment was 45 ° ±5 and after treatment was 90° ± 5. This proves that after the treatment the channels were hydrophobic, the negative charges on the glass surface were replaced by the silanol functional group as described in Figure 58. Further attempts to manoeuvre the particles through the chamber included a positively charged surface treatments (QAS, quaternary ammonium silane) that would actually repel the positively charged particles away from the surface and a primary amine such as APTES, however no significant improvement was observed, the different surface coating were compared by analysing the average percentage of particles sticking within a specific area in the chamber.

Table 23 Table showing the compounds name structure and functionality with their relative results for the particles sticking.

Compound name	Functionality	Adhesion
Trichloro-(octadecyl)silane	Hydrophobic	24%
Trichloro-(1*H*,1*H*,2*H*,2*H*-perfluorooctyl)silane	Hydrophobic	15%
(3-Aminopropyl)-triethoxysilane (APTES)	Positively charged	22 %
Quaternary ammonium silane (QAS)	Positively charged	29 %
Poly(allylamine)hydrochloride (PAH)	Positively charged	30 %

The different surface treatments as reported in Table 15, were tested using the same design chip of 5 inlets and 5 outlets with pressure difference of 15 mbar, the pressure was reduced to be able to visualize the particles during the video analysis. Using 1×10^6 particles mL^{-1} of Invitrogen SAX 1 µm, with no surface treatment and no magnet present, each individual chip was first treated and then particles pumped through the chamber from inlet 1, videos were taken and recorded for 5 min at inlet 1 and particles counted, the average particles per minute was recorded to be 120, then images were taken at the inlet and at the end of the chamber, with the aid of image J software the image of the inlet was subtracted to the outlet so that the difference will be only the particles stuck at the outlet, as shown in Figure 102(b) and103(b). Detailed results on percentages are reported in Table 23 with the FDTS showing the least number of particles stuck within the chamber.
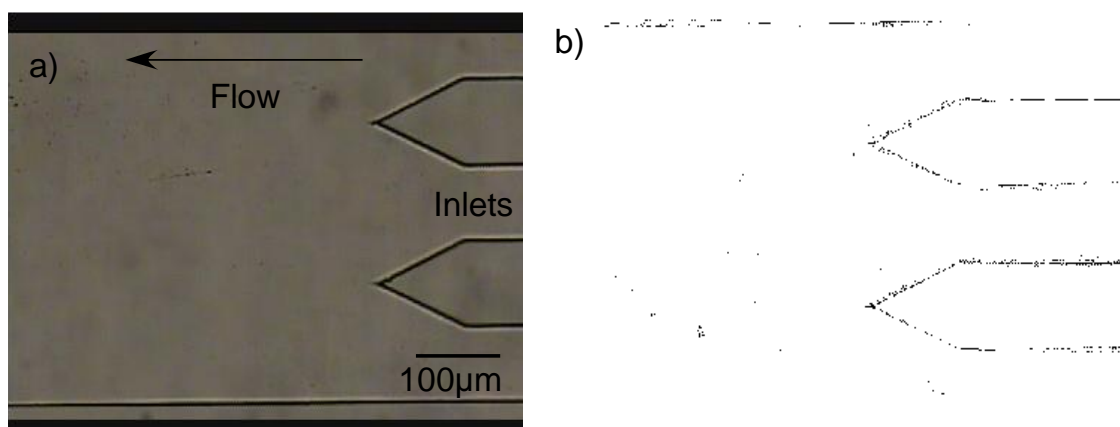
Figure 102 Image of the chip of the particles at time 0 showing very little sticking as proved by the back ground image (b) where the small black dots represent the particles stuck.
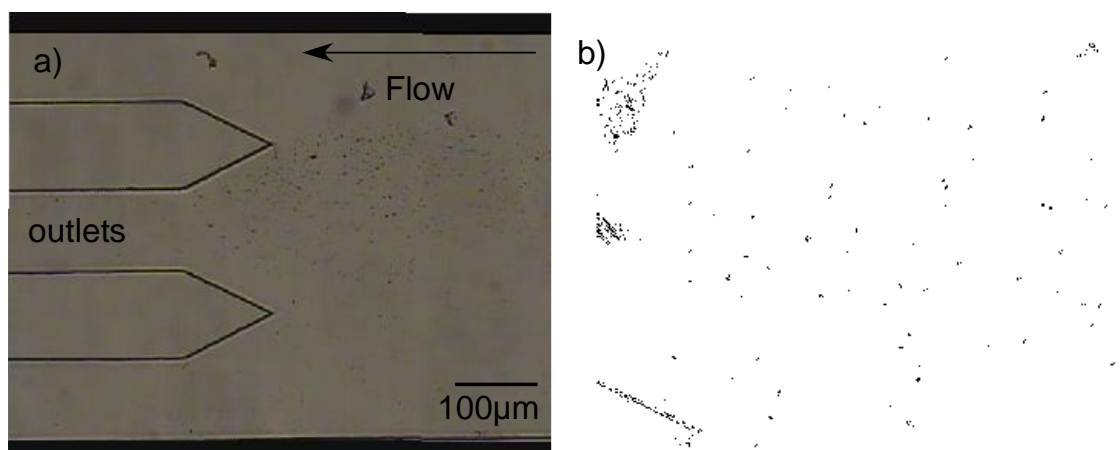
Figure 103 image of the video at the outlet of the chamber after 2 minutes showing particles stuck at the surface as proved by the background image, then the number of particles was counted before and after and percentage of sticking recorded.

However sticking of the particles was never completely resolved, furthermore what was observed was that the number of particles sticking within an experiment was increasing during the time, in fact there were approximately 120 particles per minute going through the inlet channel at a flow rate of 10-20 µL h^{-1} and in the best case only 15% of these were stuck on the glass surface, however during the same experiment after 60 min of pumping the solution the number of particles had increased from 15 to 900, as well as the number of particles sticking on the surface within the same experiments, it was observed that as the number of particles stuck increased, less particles were going

through the chamber and exit at the outlet. In fact each individual particle was acting as a small magnet sometimes forming cluster of two or more particles. An example of a device with particles stuck after 30 min is shown in Figure 104, to be noted the different sizes of the dots where the small dot represent one or two particles whilst the big dots are cluster of two or more particles.
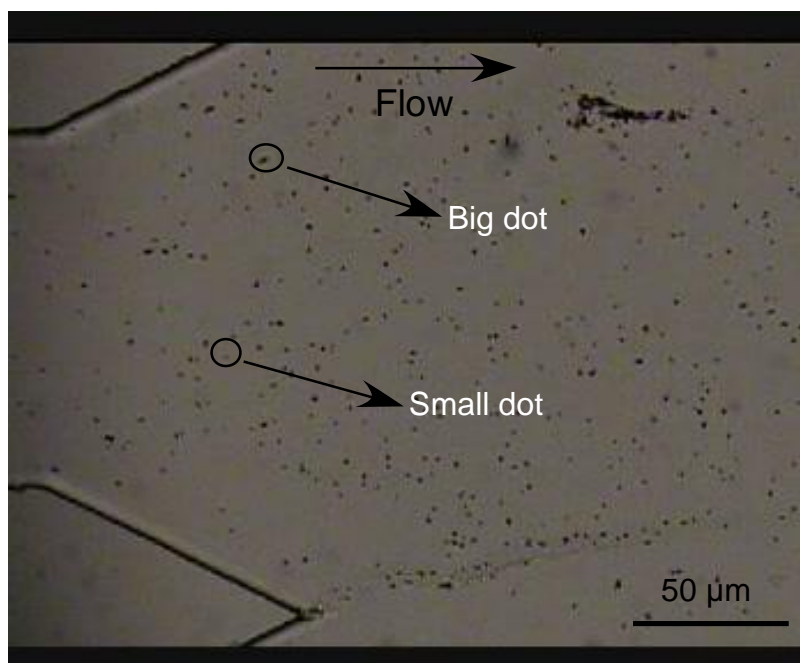
Figure 104 Image of a glass device inlet with APTES surface treatment where the different size of the dots represent the small one or two particles and the big dots a cluster of two or more particles agglomerate.

Once the optimum surface treatment was determined to be the FDTS a deflection experiment was attempted and to avoid the pulling of the particles towards the top of the glass device a chip with a cut out near the top side of the chamber was used as described in section 2.8, However with the first box magnet 10 x10 x 5 mm^3 placed at 1 mm from the chamber the particles could not deflect, possibly due to the strong field of the magnet, then the distance of the magnet from the chamber was changed, from 1 to 2, 3 and then 4 mm and in all the cases particles were not deflecting along the chamber, but they were stuck on the glass as soon as they enter the chamber. The smaller box magnet was tested 4 x 4 x 5 mm^3 and even when placed in the recess of the device no deflection

166

was observed and the particles were following the flow of the liquid and going out at the outlet, also it was placed on top of the chamber however no deflection or particles sticking was observed.

As such, the mechanism behind the sticking of the particles to the surface is not fully understood, other than to say that an apparent lack of repulsive forces causes the van der Waal's forces of attraction to dominate. Therefore, this remains an important factor to consider regarding the potential of the multilaminar flow system for applications in which solvents and charged particles are required, including many types of organic synthesis. To overcome this limitation as it is at present, future work should involve a rigorous study into the electrostatic, van der Waal's, hydration, and hydrophobic forces at work in the system from a more physical chemistry-based viewpoint. This would include characterisation of the particles in different media, the effect of the glass surfaces with different treatments (*e.g.* hydrophilic, charged, and hydrophobic silanisation), and the influence of different surfactants at varying concentrations. With this type of information, a wider range of practical uses for the multilaminar flow technique could become available, with the possibility of tailoring the type of chip surface, particle functionalisation, and liquid media to suit specific processes.

5.5   Particle deflection studies

A further test was carried out in order to understand if the surface functionality of the particles was the main reasons of this sticking issue, or others were the factor to consider, so other chromatography particles were tested with different functional groups, strong anion exchange particles, weak anion exchange particles, cation exchange particles and reversed phase particles specific details are reported in Section 2.1.2. The experiment was performed with chip design FDL1 with no surface treatment

with a pressure difference of 50 mbar without presence of magnet with 1×10^7 particles mL^{-1}, and as expected it was found that both cation and reversed phase magnetic particles could be deflected in some way along the chamber whilst the weak anion could be partially deflected, some particles would stop along the deflection trajectory, but they will continue their flow when disruption of the capillary was performed. Figure 105 shows a device with no magnet and a stream of MyOne weak cation exchange particles (with a carboxylic functional group, as shown in Table 12 experimental section 2.1.3) flowing from inlet towards the outlet with no major sticking observed, a box magnet 10 x 10 x 5 mm^3 was placed in the cut out of the glass and as shown in Fig 106 particles were deflected even though has to be noted some sticking at the tip of the inlet was observed most of which was due to a cluster of particles which observed a stronger magnetic field.
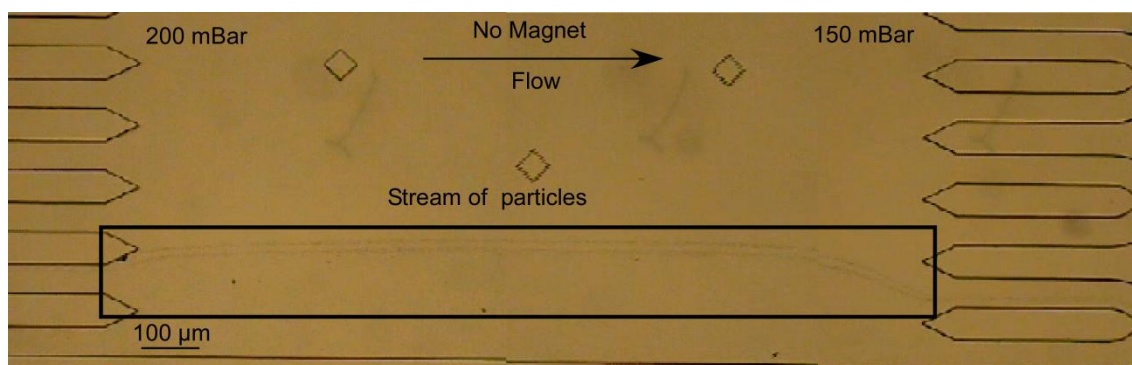
Figure 105 Image showing a stream of MyOne weak cation exchange particles flowing with very limited sticking from inlet to the outlet without magnet.
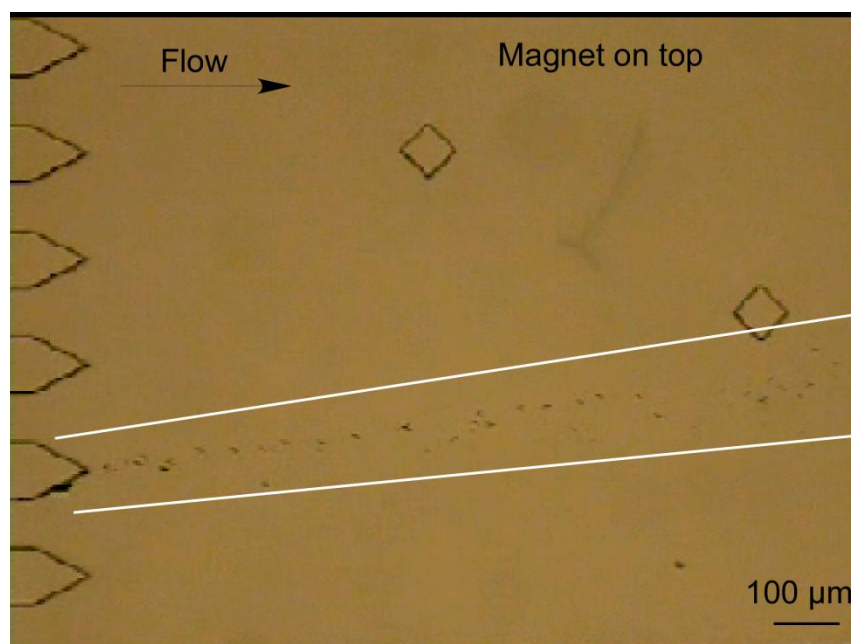
Figure 106 Image showing MyOne weak cation exchange particles deflected across the chamber towards the outlet in presence of a magnet.

The same experiment was repeated with reversed phase C18 particles, and similar deflection was observed. When weak anion particles (primary amine) were tested a different behaviour was observed where deflection could only be achieved if capillary were flicked at different interval demonstrating the electrostatic interactions between the negative glass surface and a partially positive charge of the primary amine was not too strong such as particles would stick on to the surface.

Table 24 Magnetic particles types with their size, showing that deflection was not possible to achieve with the strong anion magnetic particles.

Magnetic particle type	Size (μm)	Deflection across chamber
Strong anion ($-NH_3^+$)	1.0	No ($\approx$ 20% sticking)
Reversed phase ($-C_{18}$)	1.0	Yes
Weak cation ($-COO^-$)	1.0	Yes
Weak anion ($-NH_3^+$)	2.7	Yes (some sticking)

5.6 Summary

Investigations were performed into deflection of AE superparamagnetic particles with a view towards fluoride trapping and elution in continuous flow. However, due to the charge of the particles, the charge of the chamber surface itself, and perhaps further as yet unknown reasons, deflecting particles across the chamber proved difficult as they would stick to the surface, thus preventing them from crossing the reagent stream. Different surface treatments were also tested with no major improvement; however a more dedicated study would need to be carried on in order to understand the effect of variable like magnet size, distance from the chamber and speed of particles. To prove that most probably is the interaction between the strongly positive magnetic particles and the negatively charge of the wall surface was the reason of the sticking, other chromatography magnetic particles were also tested for deflection within the microfluidic device results are shown in Table 24.

6 Towards Radiotracer purification

In this chapter a suitable method for removal of Kryptofix as well as an investigation into the purification of FECH was investigated using the chip design for performing fluoride pre-concentration as described in Chapter 3.

6.1 Introduction

The vast majority of all ^{18}F-PET-tracers are purified after the reaction by means of HPLC or SPE, mostly using C18 reversed phase materials (RP) or ion exchange materials (an image of the cartridge used for FDG purification is shown in Figure 107) [82].

Resin	Type of phase
PS-H$^+$	Cation (+ve) exchange
PS-HCO$_3$	Anion (-ve) exchange
ALOX N (alumina)	Normal phase
HR-P	Reversed phase
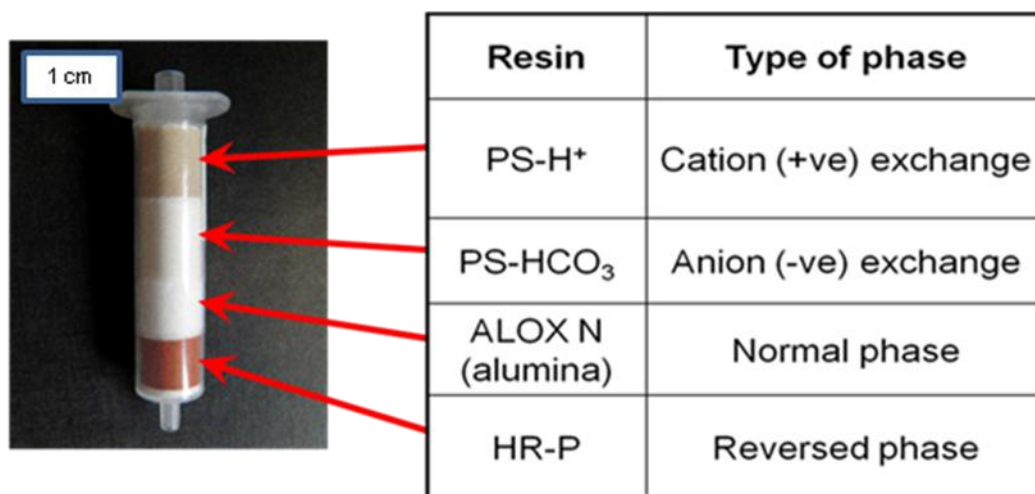
Figure 107 Image of an example of cartridge used for FDG purification and on the right the materials contained and the type of phase.

One of the compounds present in many radiotracers that needs to be removed is the phase transfer catalyst K2.2.2. In the following pages, two detection methods are examined, the first being the colourimetric detection, a modification of the colour spot test procedures by Mock *et al.* [55], the second a more sensitive method which consists of a modification of the LC-MS-MS method by Ma *et al.* [92].

Together with the investigation of Kryptofix removal a method for detection and removal of 2-[^{18}F]fluoroethyl choline [FECH] was also investigated, one of the few examples of ionic radiotracer for PET. The synthesis starts from the production of [^{18}F]fluoroethyltosylate which reacts with *N,N*-dimethylamino ethanol (DMAE) in presence of MeCN as described in Fig 108. As the FECH product is the only charged compound present in the reaction mixture the solution is passed through a cation exchange cartridge, where the un-reacted compounds will pass through while the FECH is trapped and subsequently eluted with a saline solution.
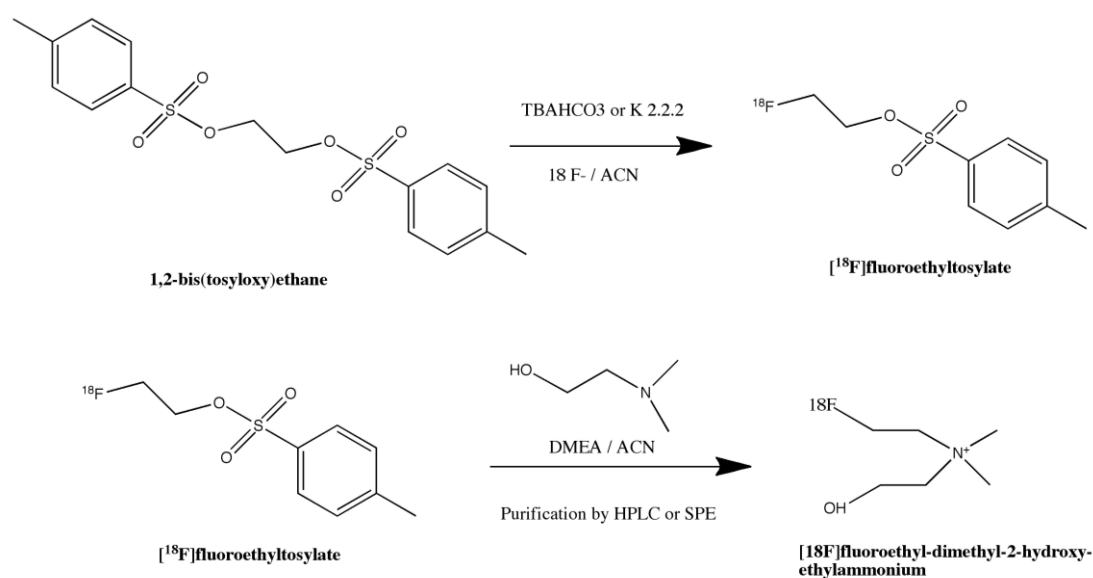
Figure 108 Synthesis of FECH in two steps reaction first fluoroethyltosylate is produced and then is reacted with excess of DMAE to yield the final FECH.

6.2 Kryptofix detection and removal

6.2.1 Colourimetric detection

In the first instance the method of the colour spot test was reproduced as reported by Mock *et al.* In this method however it was only possible to compare the colour of the spot between a reference standard and the unknown concentration of Kryptofix and by colour comparison determine if the solution was less than 20 μg mL^{-1}. This method is

based on TLC silica plate as described in Section 2.10.2. What was observed during the experiments was that when K2.2.2 in different concentration was reacted with the stock iodoplatinate reagent a different colour changes from orange / red colour to blue / purple with significant colour change at above 50 µg mL^{-1} was observed as shown in Figure 60. It was decided to investigate a semi-quantitative method for the determination of K2.2.2 by using a spectrophotometer to measure the absorbance. Firstly a quartz cuvette was used and investigated the minimum amount of K2.2.2 needed for the reaction with iodoplatinate to occur. It was found that 1:1 volume K2.2.2 : iodoplatinate was sufficient to obtain a color changes and all the experiment were carried out using 10 µL standards kryptofix with 10 µL iodoplatinate reagent made up in 800 µL water. Since this is a precipitation reaction the best method was found to be the addition of the reagents first, followed by the addition of water. A full spectrum of the different concentrations from 1 - 200 µg mL^{-1} was run and it was found that the absorbance increased with an increase in concentration of K2.2.2 as shown in Figure 109. Two major peaks were observed, at about 600 nm and the other at 365 nm, due to some overlapping issue with some standards at 600 nm, 365 nm was chosen to carry out a calibration.
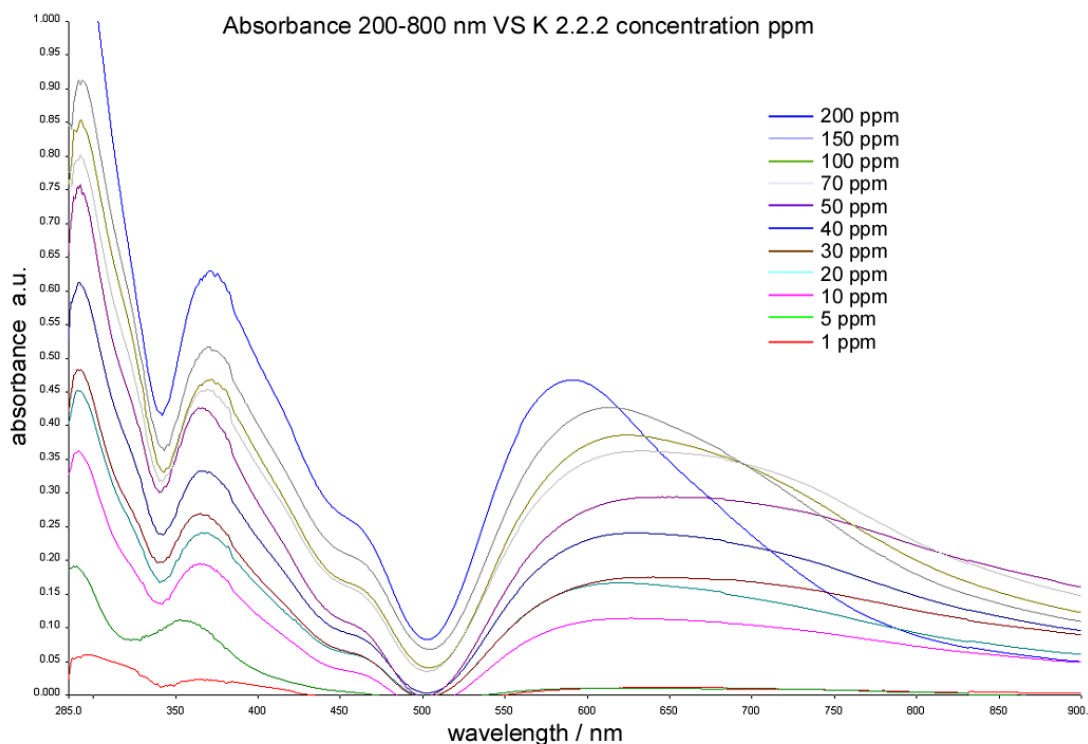
Figure 109 Spectrum range of Kryptofix standards (1 -200 ppm).

The absorbance was plotted against the log scale of the concentration ranges between 5 -200 ppm as shown in Figure110 (n=3). Below 5 ppm the method is not sensitive enough and the absorbance of the standards interfere with the blank sometimes giving a negative value. The method was tested with a real sample of FDG after purification; the absorbance value obtained was very close to zero so was not possible to quantify the K2.2.2 amount in FDG.
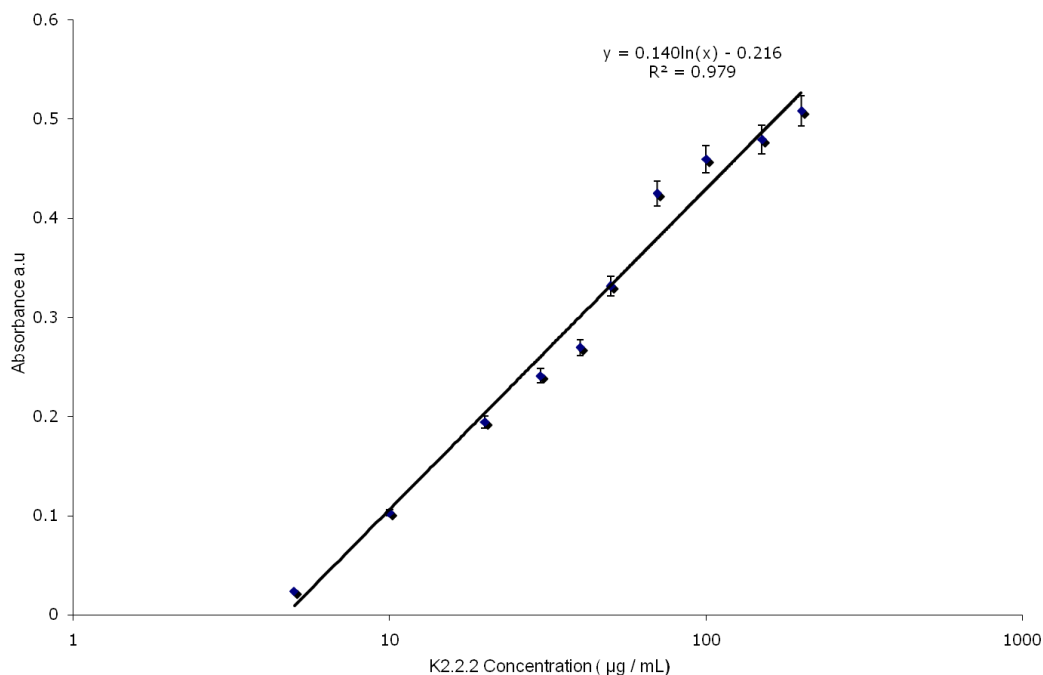
Figure 110 Calibration curve of the log scale of the concentration of standard Kryptofix solution (10 µL) + acidified iodoplatinate reagent (10 µL) and 800 µL water *vs* the absorbance measured at λ 365 nm.

6.2.2 HPLC-MS detection

A more sensitive method which uses an HPLC-MS-MS was investigated which would enable some quantitative experiments for the purification steps to be performed, such as the amount of resin needed to remove the K2.2.2. The method from Ma *et al.*[92] was slightly modified, the use of the ammonium acetate as mobile phase was found to be detrimental for the LC pump causing several stalling and blockages so the ammonium acetate was substituted with water (50:50 water:ACN), and it was still possible to identify the K2.2.2 standards peak. As shown in Figure 111 a typical HPLC mass spectrum of K2.2.2 in ACN solution with retention time of 1.46 min, illustrates some uncomplexed K2.2.2 and K2.2.2 with sodium. The standards were prepared in ACN solution since in the presence of water the two peaks were found to co-elute. Another interesting fact is that it could not be possible to see the K2.2.2 + K at 416 *m/z* even after spiking the standard with potassium fluoride; this was of particular interest since it

is known that K2.2.2 exhibits particular affinity for potassium ions amongst other alkali

metal cations [186].
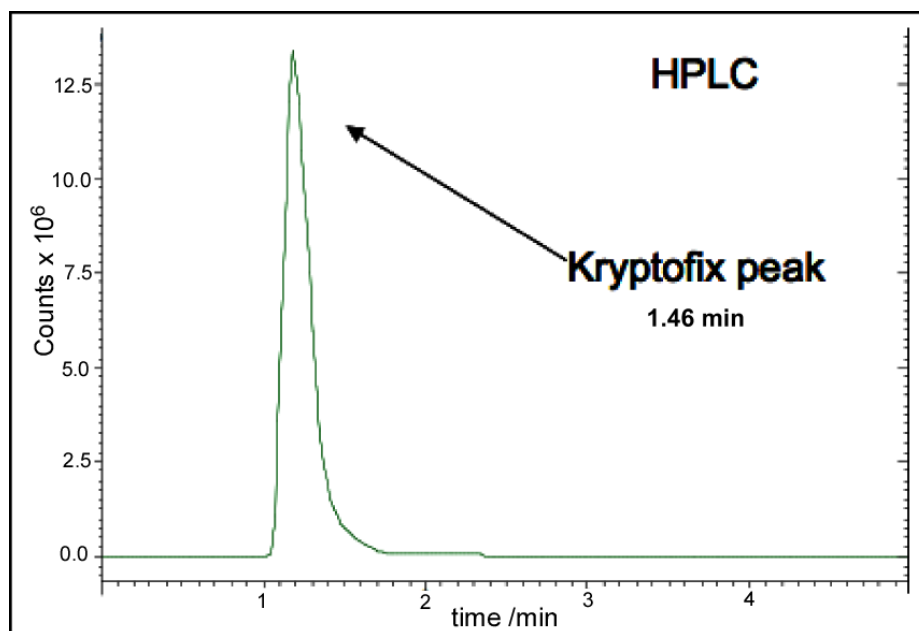
Figure 111 HPLC spectrum showing a typical chromatogram of Kryptofix.
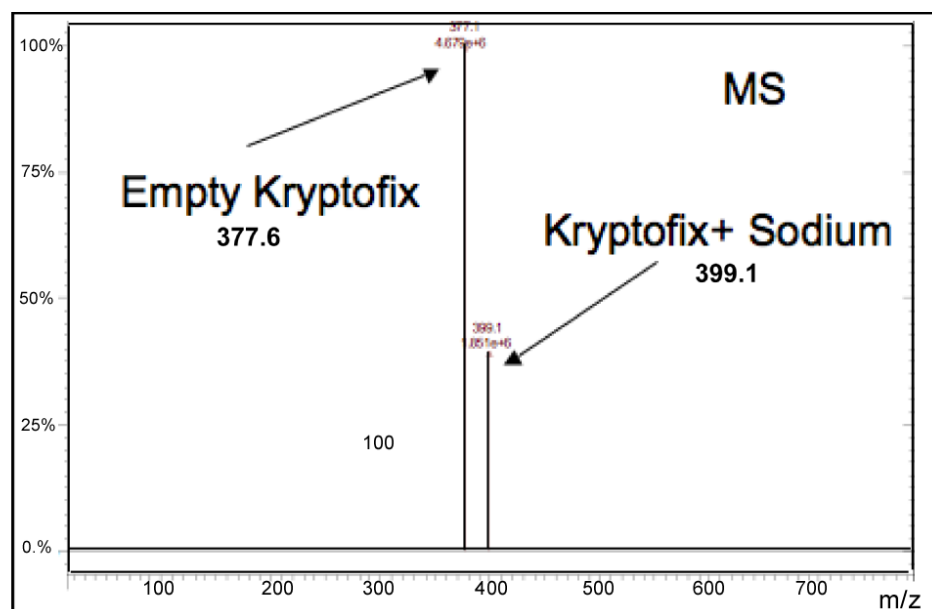
Figure 112 Typical MS spectrum of Kryptofix showing the empty kryptofic at 377 *m/z* **and the sodiated Kryptofix at 399** *m/z***.**

Once the feasibility of the detection method was established the limit of detection (LOD) was determined to be 0.59 µg mL^{-1} by plotting the peak area against the concentration of K2.2.2 standards as shown in Figure 113 (n=1) and was calculated using the formula:

LOD = (3.3 * standard deviation of the lowest value)/gradient of the slope) Equation 19
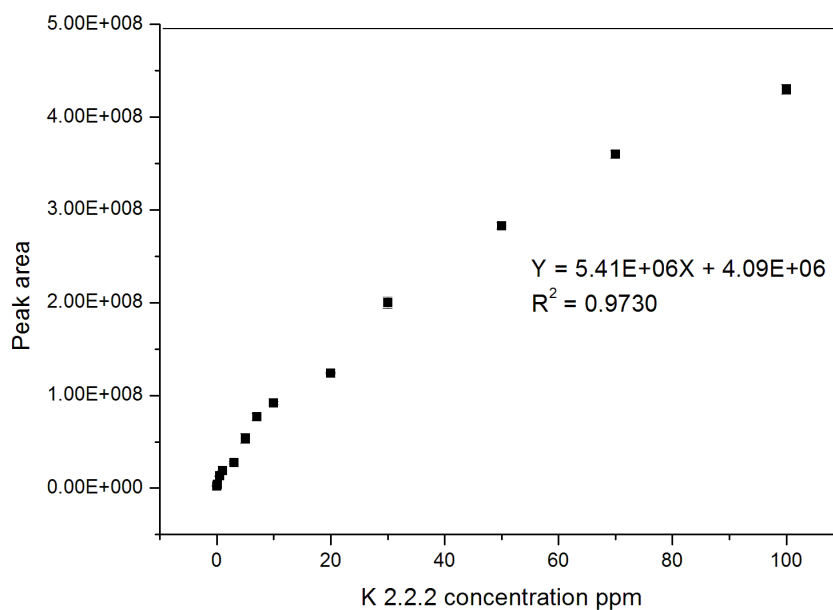
Figure 113 Concentration of kryptofix standards (0.1- 100 ppm) *vs* peak area measured with HPLC-MS.

Even though the method was not as sensitive as the one previously reported by Ma *et. al.* [92] it is suitable to quantify K2.2.2 below the required level which is 25 µg mL^{-1}.

In Table 25 the two methods for detection of K2.2.2 are compared, and the most accurate and specific for our experimentation was found to be the HPLC-MS.

Table 25 Comparisons between HPLC-MS and spectrophotometric detection

	HPLC -MS	**Spectrophotometric**
Run time	2-5 min	<2 min
Preparation time	< 2 min	10-30 min

Volume required	10 µL (injection)	10 µL
LOD	0.6 ppm	10 ppm
User friendliness	Commercial system	Wet chemistry
Advantages	Accurate	Inexpensive
Disadvantages	Expensive	Semi-quantitative

6.3 Removal of K2.2.2 in FDG

After establishing that HPLC-MS was the most suitable method for detection of K2.2.2 it was tested on a real sample of [^{19}F]FDG prepared according to Gomzina *et al*. [22] procedures The [^{19}F]FDG sample was provided by Dr Victoria Hammond and after the product was purified it was analysed for the presence of K2.2.2. Figure 114 shows the chromatogram of the peak identified during the run. This shows very low counts for K2.2.2 and in the spectrum below, the intensity of the K2.2.2 peak at 377 *m/z* together with some background ions. It was not possible to quantify, but it was concluded to be below our detection limit of 0.59 µg mL^{-1}.
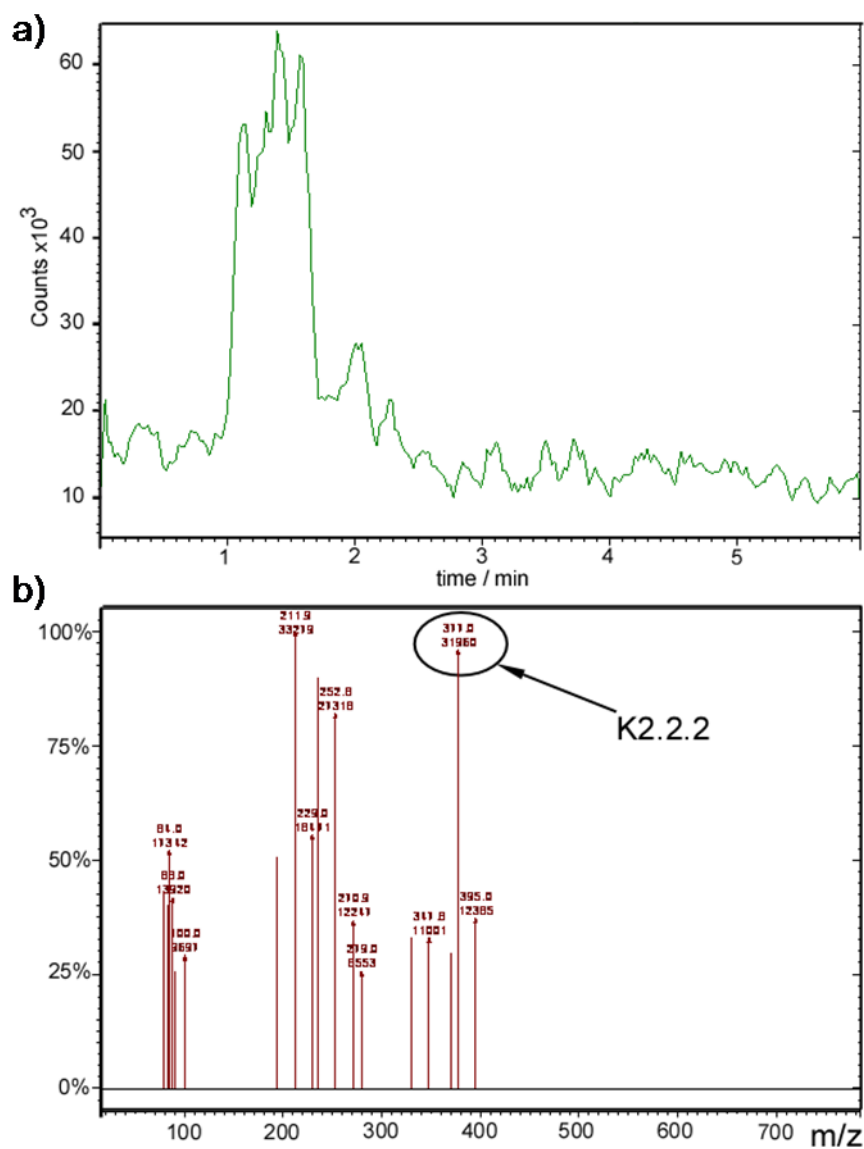
Figure 114. HPLC-MS spectrum of FDG showing very low count intensity for Kryptofix which was identified to be less than 100 ng.

6.4 FECH detection and removal

The next part of the chapter is focused towards the development of a new purification route for the synthesis of FECH. Since the purification of the FDG is already state of the art with single cartridges available to trap all the by-products and release only the final FDG product, it was decided to investigate a new approach for the FECH compound based on the same idea where all the by-products are trapped and the FECH released. Table 26 shows the compounds present in the FECH reaction. These include starting

materials, by-products and products with the corresponding type of purification

material, as well as the detection method used for analysis.

Table 26 Starting materials and products for the FECH synthesis with their solid phase material for extraction as well as the detection method.

Compounds	Resin	Detection
Ethyl-di-tosylate (EtdT)	C18	HPLC-UV
^{18}F-EtOTs	C18	HPLC-UV
DMAE	Cation	IEC
diMM	Cation	IEC
FECH	Cation	IEC
K2.2.2	C18	HPLC-MS / TLC
TBAHCO$_3$	Cation	IEC

The first step was the identification of a suitable detection method for the final product.

Since the final product is a positively charged compound the IEC instrument previously

used for fluoride detection was used, with the difference being a switch from anion to

cation exchange, which involved replacing the column, the mobile phase and suppressor

to be able to identify cations. The starting material and final compounds were purchased

from ABX compounds and not synthesized, one of the by-products (diMM) was not

readily available and for this reason was not analysed. A known amount of both FECH

(15 ppm) and DMAE (10 ppm) was injected into the IEC and it was possible to separate

and identify both compounds. However for some reason, when FECH was injected at a

concentration lower than 5 ppm, no peak was observed. It was proposed that this is due

to the sensitivity of the instrument, which was unexpected since typically LOD up to

ppb level can be analysed with the IC in cation mode. However further work to evaluate

parameters such as temperature of the column, injection volume or trying a gradient

elution could help to analyse lower concentration of FECH. Figure 115 shows an isocratic run where it was possible to separate DMAE and FECH within the same run.
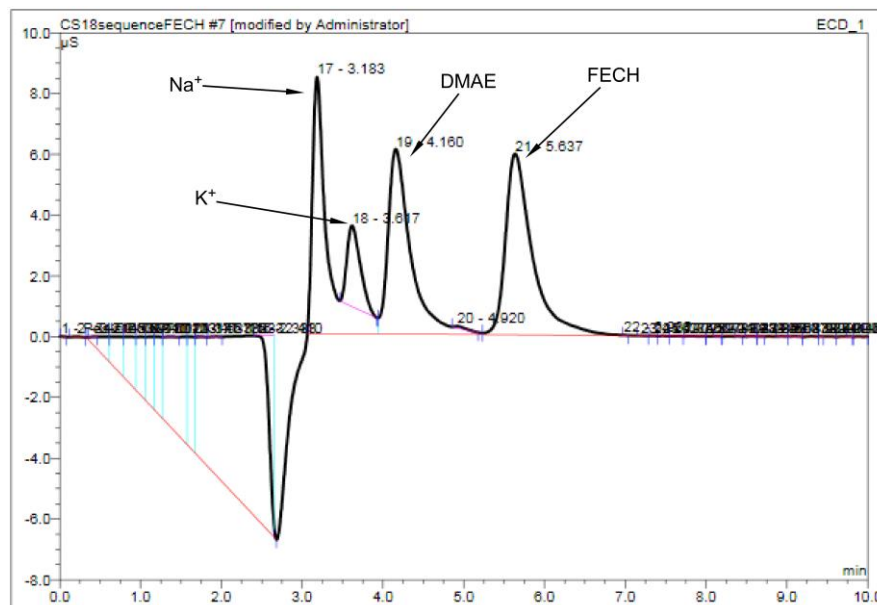
Figure 115 IC chromatogram of a mixture of DMAE and FECH separated with a CS18 cation column, 20 mM methanesulfonic acid 0.25 mL min^{-1}.

It is reported in the literature [96] that sometimes TBAHCO$_3$ is used during synthesis of FECH due to it being less toxic than K2.2.2 and easily removed with a cation cartridge. TBAHCO$_3$ was purchased from ABX. A mixture of FECH (10ppm) DMAE (10 ppm) and TBAHCO$_3$ (10 ppm) was injected in the IEC and surprisingly it was possible to separate the three compounds with an isocratic run. As shown in Figure 116, within 8 min the three compounds were eluted from the cation column. So far separation and identification of the three compounds was not reported in the same run. However, further studies in the limit of detection and quantification would need to be carried out in order to optimize the method to be able to analyse much lower concentration commonly obtained during radiotracer synthesis.
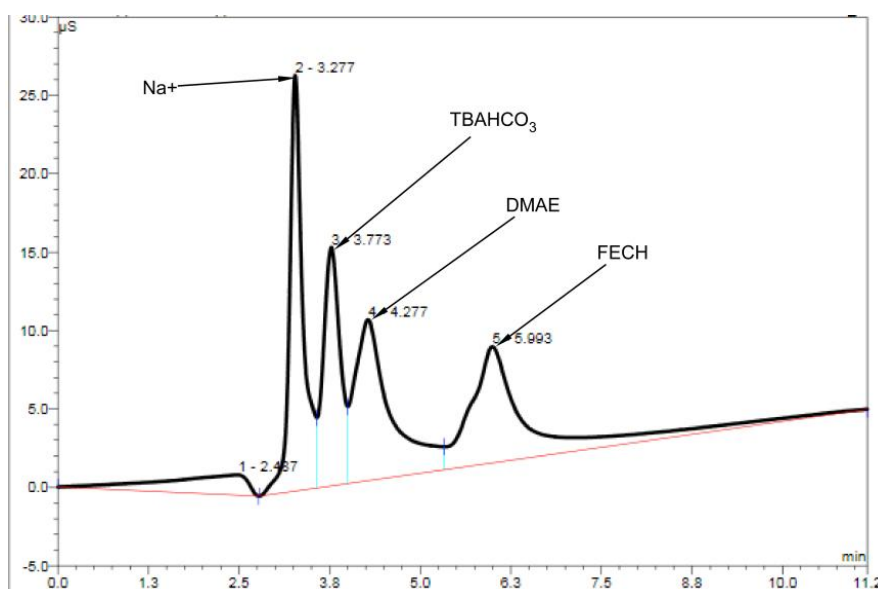
Figure 116 IC chromatogram of a mixture of DMAE and FECH and TBAHCO$_3$separated with a CS18 cation column, 20 mM methanesulfonic acid 0.25 mL min^{-1}.

Once the method for detection of FECH and DMAE was optimised, the chip design used for the pre-concentration of fluoride in Chapter 3 was prepared and filled with cation exchange particles from the CM cartridge (Waters, UK) describe in Section 2.1.2. Approximately 20 mg of dried particles were filled in each chamber of the chip as shown in Figure 117.
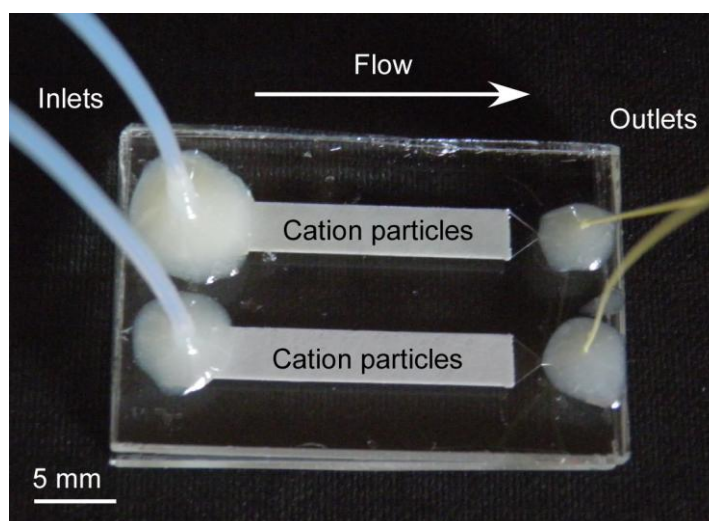
Figure 117 Image of glass device used for FECH removal showing the two chambers filled with approximately 20 mg each of cation exchange particles extracted from a CM cartridge from Waters UK

Once the device was prepared it was connected to a syringe pump as described in section 2.1.7.1. In detail 1 mL of 10 ppm of FECH (10 µg mL^{-1}) was pumped through the chip at 600 µl min$^-$1(n=1). The solution was collected at the outlet and analysed for presence of FECH, in order to measure the resin specific capacity for FECH trapping. As shown in Figure 118, the percentage of FECH trapped was plotted against the number of times that a 1 mL solution was pumped through the chip, which was equal to 10 µg mL^{-1} per run.
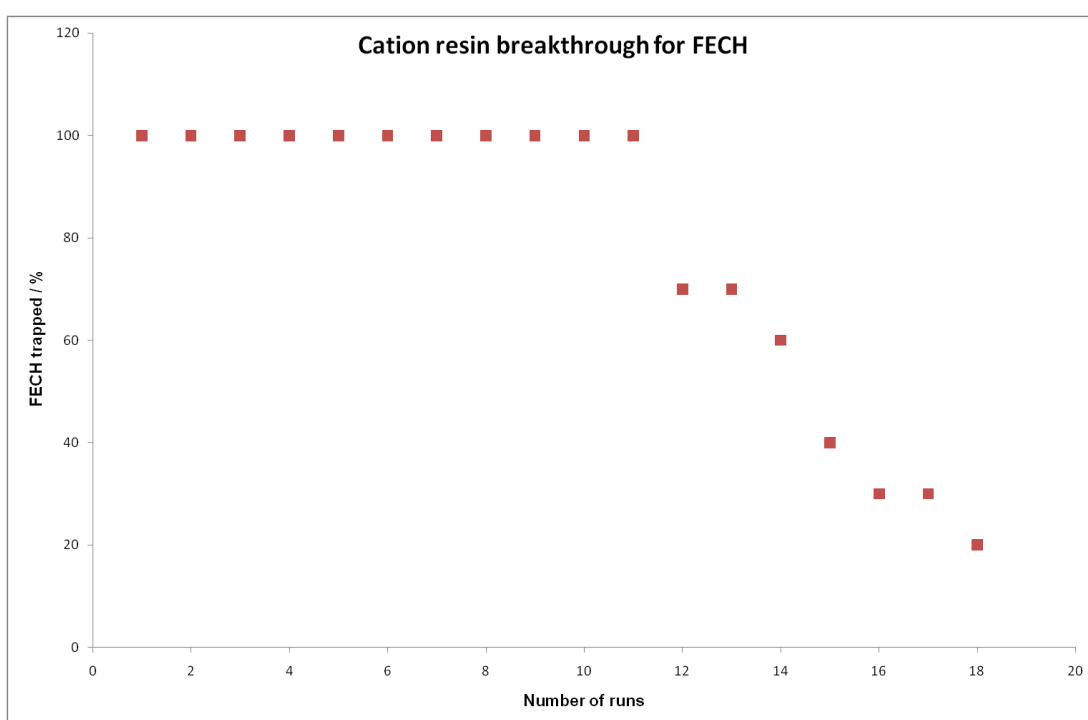
Figure 118 Graph showing the % of FECH trapped vs the number of runs which equal to 10 µg mL^{-1} per run.

The maximum trapping capacity where more than 90% FECH was trapped was found to be 110 µg of FECH per 20 mg resin, which is equal to 5.5 µg mg^{-1} of resin. Since the amount of FECH is much lower that the capacity determined using the method above, it would be possible to reduce the amount of resin, and as a consequence the design of the microchamber could be much smaller for real FECH purification during the

radiosynthesis. The next step was to investigate the possibility to have a single use system where different radiotracers could be purified. It has to be noted that in the current radiotracer synthesis there is no need of such a system. However many research groups are currently working on microfluidic modular platforms, with the final goal to be able to produce different doses of different radiotracers at the touch of a button, with the final aim to have a versatile, small and fully automated systems. By combining the need for such as a system as well as the knowledge that SPE purification of any product is basically performed on four different types of chromatography material together with the awareness that these materials could be regenerated as proven with the anion exchange resin during the pre-concentration of fluoride in Chapter 3. The concept was to fill four of the chamber micro-devices with the different materials (Alumina, Cation, Anion and Reversed phase resins). Describe in Section 2.1.2 of experimental chapter and be able to connect them with the use of tubing valve and T-connector. In this way the product could be directed into any of the four chambers, so that a product could be purified and collected at the outlet and each individual chamber could be regenerated independently; using its own regenerant solution. Figure 119 in more detail shows example how crude FDG could go pass through the four chambers for purification and be collected at the outlet. Subsequently the individual materials could be regenerated independently by introduction of separate solutions; such as, reversed phase with an excess of ethanol, cation and anion with an excess of salt/base (NaCl, K_2CO_3) and alumina could be stripped of its un-reacted fluoride by washing with acid. In this way the different materials could be ready to be used in the next purification step. In the case of FECH, the unpurified mixture could be passed first through the reversed phase where starting materials (tosylated by products, DMAE and K2.2.2) could be trapped, subsequently FECH will be trapped in the cation resin whilst un-reacted fluoride is

retained by the alumina and a final step would be the release of the FECH *via* chip 2 by washing with a saline solution. However, it will be difficult to integrate this system in any of the current platforms due to stringent quality requirements, with the possibilities of cross contamination. However this approach could not be used in the current cartridge approach where all the materials are in direct contact, as shown in Figure 109 with the FDG base hydrolysis cartridge which contains all the materials in the same tube. It would not be possible to pass, for example, a solution of strong acid through an anion exchange material or a strong base through the cation exchange materials.
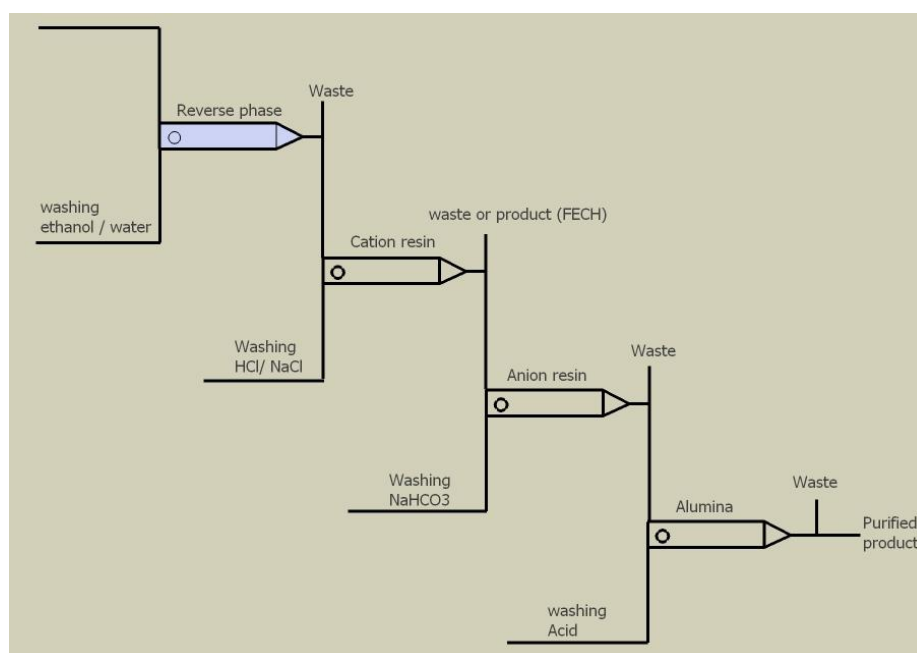
Figure 119 Schematic of four different micro-chambers independently connected where it will be possible to redirect the liquid solution in the desired chamber by using a valve or T junction to allow multiple radiotracers purification and subsequently the regeneration of each individual material.

The schematic shown in Figure 119 was investigated to prove the concept for FECH purification by trapping all the by-products and starting materials except the final FECH. This was achieved by connecting three different micro-devices with the three materials: i) reversed phase ii) anion resin and iii) alumina as shown in Figure 120. 2 mL solution containing 40 μg of FECH, 200 μg of K2.2.2. 3 μg ^{19}F, 200 μg DMAE

was pumped through the chip at a flow rate 600 µl min$^{-1,}$ the solution collected at the outlet of the T-valve and analysed for the presence of different compounds. The colourimetric method was used to prove that K2.2.2 was present in less than 10 µg, Ion selective electrode for fluoride which proved to be less than 0.5 µg, FECH analysed by IEC where it shows that more than 90% was released. However, DMAE was not fully trapped. Only 30 % was trapped in the chips with 70 % released, possibly there was not enough reversed phase resin for both DMAE and K2.2.2. Further work will be the study of DMAE and the reversed phase resins capacity.
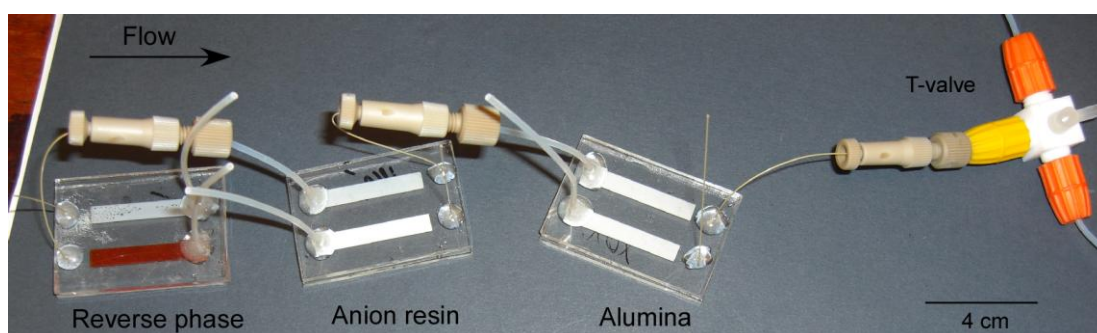
Figure 120 Image showing the three chips with different chromatography materials integrated and connected together used for FECH purification by trapping the byproduct and release the final product FECH.

6.5   Summary

Investigations were performed into the detection and removal of K2.2.2, with two detection methods identified for K2.2.2 analysis. Subsequently the method was applied to K2.2.2 in FDG samples to prove the suitability of the method. In addition, a suitable detection method for FECH, DMAE and TBAHCO$_3$ was also optimised by development of an isocratic IEC method. It was possible to achieve separation of three compounds in the same run. Trapping of FECH was also achieved with cation exchange material trapped in micro-chamber, and the capacity of the material was also studied and found to be 5.5 µg mg^{-1} of resin. Finally a study towards the integration of different micro-chambers was tested with FECH by integrating three different resin materials to

establish an alternative method for purification of FECH where all the by-products are trapped and FECH released. However, results of this study showed it was not possible to completely purify FECH, and DMAE presence was found in the collected solution in high traces (only 30 % was trapped and the rest released together with FECH.)

7   Conclusion

The aim of this work was to develop and implement a microfluidic platform for pre-concentration of $[^{18/19}F]$fluoride with possibilities to use it for further on-chip solid phase extraction purification techniques . In order to achieve this, the research employed three different approaches; 1) Anion exchange microparticles packed in micro-chambers, 2) characterisation of suitable magnetic particles and their optimisation for trapping and elution of fluoride in a micro glass device and 3) the investigation of a possible continuous flow trapping and elution of fluoride by means of free-flow magnetophoresis. In addition, preliminary studies and results on the on-chip removal of K2.2.2 as well as a new route for purification of FECH were also investigated. In this Chapter the achievements of the work will be summarised and discussed, along with considerations for future work on the project.

7.1   On-chip pre-concentration via packed bed (batch method)

While pre-concentration of $[^{18/19}F]$fluoride on-chip had been previously and extensively investigated one important factor in both the macro a micro scale method had not been considered yet, the regeneration of the solid phase extraction of the anion exchange material. Both radioactive $[^{18}F]$ and non-radioactive $[^{19}F]$fluoride ions could be repeatedly recovered by employing a chip containing a reduced amount of anion exchange particles than conventional cartridges. The entire process required less than 6 min and had trapping efficiency > 90 %, while the particles could be regenerated and re-used up to 40 times *via* a multicycle approach, without loss of performance. The radioactive solution resulting from this innovative process was highly reactive and could be employed in the radiofluorination of EtDT. On this basis, the standalone chip could easily be integrated into automated systems to provide highly reactive fluoride

complexes for the production of fluorinated PET radiotracers in high yields. The ability to regenerate the anion-exchange chip would also allow many batches of radiopharmaceuticals to be synthesised without requiring continuous user interaction within the shielded synthesiser. As a standalone chip, the design and optimisation was demonstrated to be a reliable and ready to use module for successful pre-concentration of [$^{18/19}$F]fluoride, however future work would need to include the possibility of integration with other microfluidic platform systems, where synthesis of radiotracers could be achieved in a series of micro-devices including synthesis, hydrolysis and purification steps. An effort towards this was currently under investigation by the ROC consortium and which preliminary results are shown in Figure 121, where indeed a platform was built in which four of the five steps required during the synthesis of FDG are integrated, (pre-concentration, solvent exchange, synthesis and hydrolysis) significant results were achieved (FDG was synthesised successfully) and they are currently been submitted to Proceedings of the National Academy of Sciences Journal (PNAS). Figure 121 shows an image of the prototype (http://www.roc-project.eu/site/)
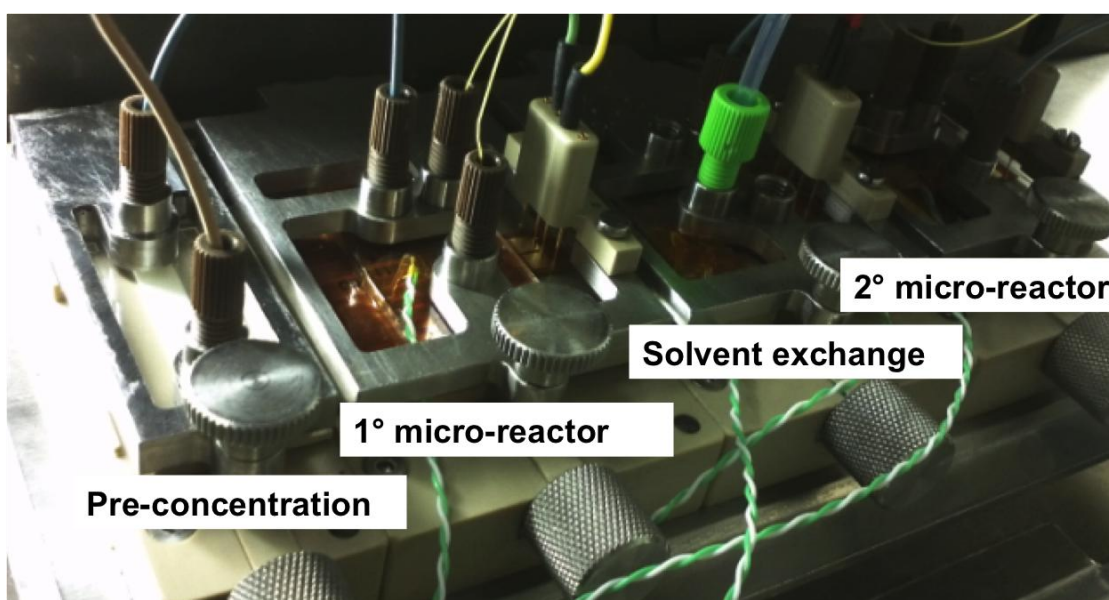
Figure 121 Image of the prototype modular system built by Siemens showing the four modules connected together in order the pre-concentration module, followed by the micro-reactor, the solvent exchange and the second micro-reactor.

7.2 On-chip pre-concentration via magnetic plugs (batch approach)

Many methods were reported on pre-concentration of fluoride however so far, there is no report in the literature for any trapping and elution of [$^{18/19}$F]fluoride *via* magnetic forces. Investigations were performed into trapping and elution of [$^{18/19}$F]fluoride *via* formation of magnetic plug inside a glass micro-device. Even though the method was not as fast as efficient as the packed bed of microparticles (Chapter 3) the proof of principle showed that an alternative process using magnetic forces can be adapted for future on-chip systems for pre-concentration of fluoride. Employing positively charged magnetic particles, fluoride could be trapped in yield of >50% and elution achieved with approximately 90% recovery of fluoride. However, this proof of principle was more labour intensive and time consuming than current methods for trapping and elution of fluoride, overall the process took nearly two hours (which includes loading of particles trapping of fluoride and elution of fluoride). Future work would therefore include optimisation of the number of magnetic particles required for trapping the fluoride, as well as a new chip design where number of channels and the depth could be increased in order to increase the volume throughput and the speed of the process. It also could be considered to investigate more accurate set-up including the magnets and the magnetic field.

7.3 Towards on-chip continuous method for pre-concentration

To further explore the use of magnetic forces in the pre-concentration of fluoride, a continuous method for the trapping and elution of fluoride was investigated, with the aim of having pre-concentration and solvent exchange performed on the same chip in continuous mode, which so far has not been reported in the literature. A multilaminar flow micro-reactor has been investigated and described in which anion magnetic particles can be deflected through streams of reagents with the final aim to perform

trapping and elution of fluoride in continuous flow. Previously, the platform had been applied to proof-of-principle bioassays [181, 187] and DNA hybridisation [180], to great effect. Herein, studies were undertaken to determine the possibility to deflect anion exchange superparamagnetic particles, with a view towards fluoride trapping and elution in continuous flow. However, due to the charge of the particles, the charge of the chamber surface itself, and perhaps further as yet not considered phenomena, deflecting particles across the chamber proved difficult as they would stick to the surface, thus preventing them from crossing the reagent stream. Different surface treatments were also tested with no major improvement however a more dedicated study would need to be carried on in order to understand the effect of variables such as magnet size, distance from the chamber, speed of particles as well as a more in depth study from a Physical chemistry point of view to understand the adhesion phenomena.

7.4 Towards radiotracer purification

Once the pre-concentration method *via* packed bed was optimised (Chapter 3), the same chip design was investigated for the purification, with the aim to have single independent chambers, where the different phase materials are connected, filled with different solid phase materials instead of individual cartridges (Figure 107), approach which is yet not reported in the literature and which would be beneficial since the independent materials could be regenerated and possibly reused for further purification experiments. Also an investigation was performed into the detection and removal of K2.2.2, with two detection methods identified for K2.2.2 analysis, with detection of K2.2.2 in FDG samples used to prove the suitability of the method. As suitable detection method for FECH and DMAE and TBAHCO$_3$ was also optimised by separation of the three compounds was achieved in the same run with IEC. Trapping of FECH was also achieved with cation exchange material trapped in micro-chamber and

the capacity of the material was also studied and found to be 5.5 µg mg^{-1} of resin. A subsequent study towards the possibilities of integrating different micro-chambers was tested with FECH. By integrating three different materials it was proposed that an alternative method for purification of FECH could be developed, where all the by-products are trapped and FECH released. Unfortunately, this study showed that it was not possible to completely purify FECH, with DMAE detected in the collected solution, with only 30 % trapped and the rest released with the FECH). Future work could include the optimisation of the device for removal of K2.2.2 with studies on the breakthrough of the reversed phase resin and tests on other radiocompounds rather than FDG. A more detailed study would need to be carried out for the purification FECH, first by repeating the experiments with a real sample of radioactive [^{18}F]FECH and a subsequent study on the breakthrough of each individual resin to identify the exact amount of solid phase materials required. Finally further work could be explored in which the series of micro-chambers could be used to purify different radiotracers.

List of Publications

Peer reviewed articles

1) Mark D. Tarn, Giancarlo Pascali, <u>Francesco De Leonardis</u>, Piero A. Salvadori, Paul Watts and Nicole Pamme

   Journal of Chromatography A, (2012) Accepted

   Purification of 2-[18F]fluoro-2-deoxy-D-glucose by on-chip solid-phase extraction

2) <u>Francesco De Leonardis</u>, Giancarlo Pascali, Piero A. Salvadori, Paul Watts and Nicole Pamme

   Journal of Chromatography A, 1218 (2011) 4714

   On-chip pre-concentration and complexation of [^{18}F]fluoride ions *via* regenerable anion exchange resin for radiochemical synthesis of Positron Emission Tomography tracers.

Conference proceeding

1) <u>Francesco De Leonardis</u>, Mark D. Tarn, Giancarlo Pascali, Piero A. Salvadori and Nicole Pamme

   Journal of Labelled Compounds and Radiopharmaceuticals, 54:S1 (2011) S46

   Microfluidic modules for the pre-concentration of [^{18}F]-fluoride for PET radiotracer synthesis, and its subsequent removal during product purification.

2) <u>Francesco De Leonardis</u>, Giancarlo Pascali, Piero A. Salvadori, Nicole Pamme

The Quarterly Journal of Nuclear Medicine and Molecular Imaging, 54:1 2010, 22

On-chip regeneration of anion exchange resins for [^{18}F⁻] pre-concentration in PET radiochemical synthesis.

Oral Conference Presentations

1) <u>Francesco De Leonardis</u>, Mark D. Tarn, Giancarlo Pascali, Piero A. Salvadori and Nicole Pamme

ISRS 2011- 19th International Symposium on Radiopharmaceuticals Sciences, 28th August – 2nd September **2011**, Amsterdam, The Netherlands.

Microfluidic modules for the preconcentration of [^{18}F]-fluoride for PET radiotracer synthesis, and its subsequent removal during product purification.

2) <u>Francesco De Leonardis</u>, Giancarlo Pascali, Piero A. Salvadori, Nicole Pamme

Analytical Research Forum 2011, 25th – 27th July **2011**, Manchester University, UK.

Microfluidic modules for pre-concentration and activation of [^{18}F]-fluoride for PET radiochemical synthesis.

3) <u>Francesco De Leonardis</u>, Mark D. Tarn, Nicole Pamme

Microfluidic for Molecular Imaging, 7th - 8th July **2011**, Area CNR Pisa, Italy.

Microfluidic modules for pre-concentration and purification.

4) <u>Francesco De Leonardis</u>, Giancarlo Pascali, Piero A. Salvadori, Nicole Pamme

   ESRR'10- 15th European Symposium on Radiopharmacy and Radiopharmaceuticals, 8th-11thApril**2010**, Edinburgh, UK

   On-chip regeneration of anion exchange resins for [^{18}F$^-$] pre-concentration in PET radiochemical synthesis.

Poster Presentations

1) Mark D. Tarn, Giancarlo Pascali, <u>Francesco De leonardis</u>, Paul watts, Piero A. Salvadori and Nicole Pamme

   16th International Conference on Miniaturized Systems for Chemistry and Life Sciences (µTAS), Oct 28th – Nov 1st **2012**, Okinawa, Japan.

   On-Chip Purification of [^{18}F]FDG in Positron Emission Tomography Radiotracer Synthesis

2) <u>Francesco De Leonardis</u>, Giancarlo Pascali, Piero A. Salvadori and Nicole Pamme

   14th International Conference on Miniaturized Systems for Chemistry and Life Sciences (µTAS), 3rd – 7th October **2010**, Groningen, The Netherlands.

   Microfluidic modules for [^{18}F]activation – Towards an integrated modular lab on a chip for PET radiotracers synthesis.

3) <u>Francesco De Leonardis</u>, Nicole Pamme

   Analytical Research Forum 2010, 26th – 28th July **2010**, Loughborough University, UK.

Microfluidic two-steps reactors for pre-concentration and purification in PET radiotracers synthesis.

4) <u>Francesco De Leonardis</u>, Giancarlo Pascali, Piero A Salvadori and Nicole Pamme

Clinical Biosciences Institute Research Day, 21st July **2010**,Cottingham, UK.

On-chip module for [^{18}F$^-$] activation for Positron Emission Tomography (PET) radiochemical synthesis.

5) <u>Francesco De Leonardis</u>, Paul Watts, Nicole Pamme,

SET for Britain 2010 Event at the House of Commons, 8th March **2010**, London, UK.

Pre-concentration of fluoride in a microfluidic device towards an integrate lab-on-a-chip synthesis device for PET labels.

6) <u>Francesco De Leonardis</u>, Nicole Pamme,

Biomagnetic Sensing Workshop, 25th Sep. **2009**, Cambridge, UK.

On-chip fluoride pre-concentration for integrated radiochemical synthesis.

7) <u>Francesco De Leonardis</u>, Paul Watts, Nicole Pamme,

Analytical Research Forum 2009, 21st – 23rd July **2009**, Kent, UK.

Pre-concentration of fluoride in a microfluidic device towards an integrate lab-on-a-chip.

References

1   Baley, D., Valk, P.E., Maisey, M.N. *Positron Emission Tomography Basic Sciences*. 2005: Springer. 381.

2   Valk, P.E., Bailey,D., Townsend D.W., Maisey, M.N. *Positron Emission Tomography Clinical Practice*. 2003: Springer. 473.

3   Anderson, C.D., Phys. Rev., 1932. **41**(4): p. 405.

4   Livingston, M.S., Henderson, M.C. and Lawrence, E.O., Proc. Natl. Acad. Sci. U.S.A., 1934. **20**(8): p. 470.

5   Terpogossian, M.M., Phelps, M.E., Hoffman, E.J., and Mullani, N.A., Radiol., 1975. **114**(1): p. 89.

6   Reivich, M., Kuhl, D., Wolf, A., Greenberg, J.*, et al.*, Acta Neurologica Scandinavica, 1977. **56**: p. 190.

7   Reivich, M., Kuhl, D., Wolf, A., Greenberg, J.*, et al.*, Circul. Res., 1979. **44**(1): p. 127.

8   Ido, T., Wan, C.N., Casella, V., Fowler, J.S.*, et al.*, J. Labelled Compd. Radiopharm., 1978. **14**(2): p. 175.

9   Wagner HN, *A brief history of positron emission tomography (PET)*, in *Semin. Nucl. Med.. 1998 Jul;28(3):213-20.* 1997.

10   Chopin,J.O., Liljenzin, JR.. *Radiochemistry and Nuclear chemistry*. 2nd ed. 1995: Butterworth-Heinemann Ltd. 707.

11   Geary, W., *Radiochemical Methods*. Analytical chemistry by open learning, ed. A.M. James. 1986: Wiley. 224.

12   Li, Z., Conti, P.S., Adv. Drug Delivery Rev., 2010. **62**(11): p. 1031.

13   Hamilton, L.V., *Oak Ridge Reservation Annual Site Environmental Report for 1996*. 1997.

14   Wester, H.J., Schoultz, B.W., Hultsch, C., and Henriksen, G., Eur. J. Nucl. Med. Mol. Imaging, 2009. **36**(4): p. 653.

15   Coenen, H.H., Elsinga, P.H., Iwata, R., Kilbourn, M.R.*, et al.*, Nucl. Med. Biol., 2010. **37**(7): p. 727.

16   Hamacher, K., Coenen, H.H. and Stocklin, G., J. Labelled Compd. Radiopharm., 1986. **23**(10-12): p. 1095.

17   Wyss, M.T., Spaeth, N., Biollaz, G., Pahnke, J.*, et al.*, J. Nucl. Med., 2007. **48**(4): p. 608.

18   Bejot, R., Kersemans, V., Kelly, C., Carroll, L.*, et al.*, Nucl. Med. Biol., 2010. **37**(5): p. 565.

19   Tang, G.H., Tang, X.L., Wen, F.H., Wang, M.F.*, et al.*, Appl. Radiat. Isot., 2010. **68**(9): p. 1734.

20   Koziorowski, J., Appl. Radiat. Isot., 2010. **68**(9): p. 1740.

21   Kumakura, Y., Cumming, P., Vernaleken, I., Buchholz, H.G.*, et al.*, J. Neurosci., 2007. **27**(30): p. 8080.

22   Gomzina, N.A., Vasil'ev, D.A. and Krasikova, R.N., Radiochemistry, 2002. **44**(4): p. 403.

23   GE HealthCare Life Sciences. [accessed 2012 January]; Available from: http://www.gehealthcare.com/euen/fun_img/products/radiopharmacy/products/tracerlab_tracercenter-2-fx-fdg.html

24   GE HealthCare Life Sciences. [accessed 2012 February]; Available from: http://www.gehealthcare.com/euen/fun_img/products/radiopharmacy/products/tracerlab_tracercenter-2-fx-f18nucleo.html.

25   GE HealthCare Life Sciences. [accessed 2012 March]; Available from: http://www3.gehealthcare.com/~/media/Downloads/us/Product/Product-Categories/PET-Radiopharmacy/TracerCenter/FastLab/GEHC-FASTlab-Multi-Tracer-ProductSpec.pdf.

26   Raytest GmbH. [accessed 2012, February]; Available from: http://www.raytest.de/pet/Synchrom/brochure_Synchrom.pdf.

27   Synthra GmbH. [accessed 2012 March]; Available from: http://www.synthra.com/production-f18-dopa-fdg-fluorine-fluorocholine.html

28   GE HealthCare Life Sciences. [accessed 2012 April]; Available from: http://www3.gehealthcare.com/~/media/Downloads/us/Product/Product-Categories/PET-Radiopharmacy/TracerCenter/FastLab/GEHC-FASTlab-Multi-Tracer-ProductSpec.pdf.

29   GE HealthCare Life Sciences. [accessed 2012 June]; Available from: http://www.gehealthcare.com/euen/fun_img/products/radiopharmacy/docs/TRACERlab_MX5.pdf.

30   Iba Solutions. [accessed 2012 March]; Available from: http://www.iba-cyclotron-solutions.com/products-cyclo/synthera

31   Siemens HealthCare. [accessed 2012 April]; Available from:
        http://www.medical.siemens.com/siemens/en_GB/gg_nm_FBAs/files/dash/FDG
        _Radiochemistry_DS_Final_1.19.11.pdf

32   Siemens HealthCare. [accessed 2012 February]; Available from:
        http://www.medical.siemens.com/siemens/en_US/gg_nm_FBAs/files/dash/ds_1
        0_explor_gn.pdf

33   Siemens HealthCare. [accessed 2012 May]; Available from:
        http://www.medical.siemens.com/siemens/it_IT/gg_nm_FBAs/files/dash/ds_09_
        explor_lc.pdf.

34   Bioscan [accessed 2012 January]; Available from: http://www.bioscan.com/pet-
        nuclear-medicine/pet-chemistry-synthesizers/fdg-plus-synthesizer.

35   Bioscan [accessed 2012 March]; Available from: http://www.bioscan.com/pet-
        nuclear-medicine/pet-chemistry-synthesizers/autoloop-carbon-11-fluorine-18

36   Eckert & Ziegler Strahlen- und Medizintechnik AG. [accessed 2012 March];
        Available from:
        http://www.ezag.com/home/products/radiopharma/radiosynthesis-
        technology/modular-lab-standard.html

37   Eckert & Ziegler Strahlen- und Medizintechnik AG. [accessed 2012 February];
        Available from: http://www.ezag.com/fileadmin/ezag/user-
        uploads/radiopharma/radiopharma/7131-0024_Fact_Sheet_ML_for_FDG.pdf

38   Eckert & Ziegler Strahlen- und Medizintechnik AG. [accessed 2012 May];
        Available from: http://www.ezag.com/fileadmin/ezag/user-
        uploads/radiopharma/radiopharma/7131-
        0002_Fact_sheet_ML_for_Fluoroethylcholine.pdf

39   Scintomics GmbH. [accessed 2012 March]; Available from:
        http://www.scintomics.com/en/production/grp-modules/index.html

40   Bouvet, V.R., Wuest, M., Wiebe, L.I., and Wuest, F., Nucl. Med. Biol., 2010.
        38(2): p. 235.

41   Chun, J.-H., Lu, S., Lee, Y.-S., and Pike, V.W., J. Org. Chem., 2010. **75**(10): p.
        3332.

42   Advion [accessed 2012 March]; Available from:
        http://www.advion.com/biosystems/nanotek/nanotek-positron-emission-
        tomography-references.php.

43   Hamacher, K., Hirschfelder, T. and Coenen, H.H., Appl. Radiat. Isot., 2002. **56**(3): p. 519.

44   Le Bars, D., J. Fluorine Chem., 2006. **127**(11): p. 1488.

45   Yu, S., Biomed. Imaging Intervention J., 2006. **2(4)**.

46   Gillies, J.M., Prenant, C., Chimon, G.N., Smethurst, G.J.*, et al.*, Appl. Radiat. Isot., 2006. **64**(3): p. 333.

47   Wester, H.-J., *Munich Molecular Imaging Handbook Series Pharmaceutical Radiochemistry (I)*. Vol. 1. 2011: Scintomics. 212.

48   Brown, R.S., Leung, J.Y., Kison, P.V., Zasadny, K.R.*, et al.*, J. Nucl. Med., 1999. **40**(4): p. 556.

49   Politis, M., Piccini, P., Pavese, N., Koh, S.B.*, et al.*, J. Neuropathol. Exp. Neurol., 2008. **214**(1): p. 112.

50   Hamacher, K., Coenen, H.H. and Stocklin, G., J. Nucl. Med., 1986. **27**(2): p. 235.

51   Fowler, J.S., Ido, T., Semin. Nucl. Med., 2002. **32**(1): p. 6.

52   Schlyer, D., Annual Accademic Medical Singapore, 2004. **33**(2): p. 146.

53   Kiesewetter, D.O., Cohen, R.M., International Journal Applied Radiation, 1986. **37**: p. 1181.

54   Saha, G.B., Macintyre, W.J.,Go, R.T., Semin. Nucl. Med., 1992. **22**(3): p. 150.

55   Mock, B.H., Winkle, W. and Vavrek, M.T., Nucl. Med. Biol., 1997. **24**(2): p. 193.

56   Kuge, Y., Nishijima, K., Nagatsu, K., Seki, K.*, et al.*, Nucl. Med. Biol., 2002. **29**(2): p. 275.

57   Kryza, D., Tadino, V., Filannino, M.A., Villeret, G.*, et al.*, Nucl. Med. Biol., 2008. **35**(2): p. 255.

58   Tabeling, P., *Introduction to microfluidics*. 2005: Oxford. 312.

59   Elizarov, A.M., Lab Chip, 2009. **9**(10): p. 1326.

60   Miller, P.W., J. Chem. Technol. Biotechnol., 2009. **84**: p. 309.

61   Brady F., Gillies GM, Geffrey NT, *Use of microfabricated devices*, in *WO/2003/078358*. 2003.

62   Gillies, J.M., Prenant, C., Chimon, G.N., Smethurst, G.J.*, et al.*, Appl. Rad. Isot., 2006. **64**(3): p. 325.

63   Steel, C.J., O'Brien, A.T., Luthra, S.K., and Brady, F., J. Labelled Compd. Radiopharm., 2007. **50**(5-6): p. 308.

64   Lee, C.C., Sui, G.D., Elizarov, A., Shu, C.Y.J.*, et al.*, Science, 2005. **310**(5755): p. 1793.

65   Elizarov, A.M., van Dam, R.M., Shin, Y.S., Kolb, H.C.*, et al.*, J. Nucl. Med., 2010. **51**(2): p. 282.

66   Lu, S., Clements, J.T., Gilde, M.J., Prak, A.*, et al.*, J. Labelled Compd. Radiopharm., 2007. **50**(5-6): p. 597.

67   Saiki, H., Iwata, R., Nakanishi, H., Wong, R.*, et al.*, Appl. Radiat. Isot., 2010. **68**(9): p. 1703.

68   Alexoff, D., Schlyer, D.J. and Wolf, A.P., Appl. Radiat. Isot., 1989. **40**(1): p. 1.

69   Lu, S.Y. and Pike, V.W., PET Chemistry, 2007. **62**: p. 271.

70   Cai, L.S., Lu, S.Y. and Pike, V.W., Eur. J. Org. Chem., 2008(17): p. 2853.

71   Haddad,P.R., *Ion chromatography principle and applications*. Journal of chromatography library. 1990: Elsevier. 775.

72   Weiss, J., *Ion chromatography*. Second edition ed. 1995: VCH. 465.

73   Landers, J.P., *Handbook of capillary and microchip electrophoresis and associated microtechniques*. third ed. 2007: CRC. 1567.

74   Kutter, J.P., Jacobson, S.C. and Ramsey, J.M., J. Microcolumn Sep., 2000. **12**(2): p. 93.

75   Ocvirk, G., Verpoorte, E., Manz, A., Grasserbauer, M.*, et al.*, Anal. Methods, 1995. **2**(2): p. 74.

76   Oleschuk, R.D., Shultz-Lockyear, L.L., Ning, Y.B., and Harrison, D.J., Anal. Chem., 2000. **72**(3): p. 585.

77   Ekstrom, S., Malmstrom, J., Wallman, L., Lofgren, M.*, et al.*, J. Proteomics, 2002. **2**(4): p. 413.

78   Bergkvist, J., Ekstrom, S., Wallman, L., Lofgren, M.*, et al.*, J. Proteomics, 2002. **2**(4): p. 422.

79   Yu, C., Davey, M.H., Svec, F., and Frechet, J.M.J., Anal. Chem., 2001. **73**(21): p. 5088.

80   Wen, J., Guillo, C., Ferrance, J.P., and Landers, J.P., J. Chromatogr. A, 2007. **1171**: p. 29.

81   Hung, J.C., J. Nucl. Med., 2002. **43**(11): p. 1495.

82   Lemaire, C., Damhaut, P., Lauricella, B., Mosdzianowski, C.*, et al.*, J. Labelled Compd. Radiopharm., 2002. **45**(5): p. 435.

83   Fang, C.F., Friedman, A.E., Lewis, R.J., and Tatken, R., Abstracts of Papers of the American Chemical Society, 1979(SEP): p. 3.

84   Baudot, P., Jacque, M. and Robin, M., Toxicology and Applied Pharmacology, 1977. **41**(1): p. 113.

85   Alexoff, D.L., Fowler, J.S. and Gatley, S.J., App. Radiat. Isot., 1991. **42**(12): p. 1189.

86   Moerlein, S.M., Brodack, J.W., Siegel, B.A., and Welch, M.J., App. Radiat. Isot., 1989. **40**(9): p. 741.

87   Chaly, T., Mattacchieri, R., Velez, J.W., Dahl, J.R.*, et al.*, App. Radiat. Isot., 1990. **41**(1): p. 29.

88   Chaly, T. and Dahl, J.R., Nucl. Med. Biol., 1989. **16**(4): p. 385.

89   Zweig, G. and Sherma, J., *CRC Handbook of Chromatography*. Vol. 2. 1972, Cleveland: CRC Press. 113.

90   Ferrieri, R.A., Schlyer, D.J., Alexoff, D.L., Fowler, J.S.*, et al.*, Nucl. Med. Biol., 1993. **20**(3): p. 367.

91   Kruse, M.A., Rees, S.E. and Watkins, G.L., J. Nucl. Med., 2000. **41**(5): p. 148P.

92   Ma, Y., Huang, B.X., Channing, M.A., and Eckelman, W.C., Nucl. Med. Biol., 2002. **29**(1): p. 125.

93   DeGrado, T.R., Coleman, R.E., Wang, S., Baldwin, S.W.*, et al.*, Cancer Research, 2001. **61**(1): p. 110.

94   Block, D., Coenen, H.H. and Stocklin, G., J. Labelled Compd. Radiopharm., 1987. **24**(9): p. 1029.

95   Chi, D.Y., Kilbourn, M.R., Katzenellenbogen, J.A., and Welch, M.J., J. Org. Chem., 1987. **52**(4): p. 658.

96   Asti, M., Farioli, D., Iori, M., Guidotti, C.*, et al.*, Nucl. Med. Biol., 2010. **37**(3): p. 309.

97   Hara, T., Kosaka, N. and Kishi, H., J J. Nucl. Med., 2002. **43**(2): p. 187.

98   Duffin, W.J., *Electricity and Magnetism*. 4th ed. 1990, Maidenhead, UK: McGraw-Hill Book Company Europe.

99   Tarn, M.D., *Continuous Flow Processes on Single Magneticand Diamagnetic Particles in Microfluidic Devices*. 2011, The University of Hull: Hull.

100   *Magnet Sales & Manufacturing*. [accessed 2011 November]; Available from: http://www.magnetsales.com/design/designG.htm.

101   Gijs, M.A.M., Microfluid. Nanofluid., 2004. **1**(1): p. 22.

102   Gijs, M.A.M., Lacharme, F. and Lehmann, U., Chem. Rev., 2010. **110**(3): p. 1518.

103   Lu, A.-H., Salabas, E.L. and Schueth, F., A Angew. Chem. Int. Ed., 2007. **46**(8): p. 1222.

104   Osaka, T., Matsunaga, T., Nakanishi, T., Arakaki, A.*, et al.*, Anal. Bioanal.Chem., 2006. **384**(3): p. 593.

105   Rida, A. and Gijs, M.A.M., Anal. Chem., 2004. **76**(21): p. 6239.

106   Palecek, E. and Fojta, M., Talanta, 2007. **74**(3): p. 276.

107   Morais, J., Azevedo, R.B., Silva, L.P., Lacava, Z.G.M.*, et al.*, J. Magn. Magn. Mater., 2004. **272**: p. 2400.

108   Wu, A., Ou, P. and Zeng, L., Nano, 2010. **5**(5): p. 245.

109   Krishnan, K.M., IEEE Trans. Magn., 2010. **46**(7): p. 2523.

110   Pankhurst, Q.A., Connolly, J., Jones, S.K., and Dobson, J., J J. Phys. D: Appl. Phys., 2003. **36**(13): p. R167.

111   Pamme, N. and Wilhelm, C., Lab Chip, 2006. **6**(8): p. 974.

112   Pamme, N., Lab Chip, 2006. **6**(1): p. 24.

113   Pamme, N., Eijkel, J.C.T. and Manz, A., J. Magn. Magn. Mater., 2006. **307**(2): p. 237.

114   Nilsson, J., Evander, M., Hammarstrom, B., and Laurell, T., Anal. Chim. Acta, 2009. **649**(2): p. 141.

115   Pamme, N., Lab Chip, 2007. **7**(12): p. 1644.

116   Lenshof, A. and Laurell, T., Chem. Soc. Rev., 2010. **39**(3): p. 1203.

117   Gossett, D.R., Weaver, W.M., Mach, A.J., Hur, S.C.*, et al.*, Anal. Bioanal.Chem., 2010. **397**(8): p. 3249.

118   Kersaudy-Kerhoas, M., Dhariwal, R. and Desmulliez, M.P.Y., IET Nanobiotechnol., 2008. **2**(1): p. 1.

119   Tsutsui, H. and Ho, C.-M., Mech. Res. Commun., 2009. **36**(1): p. 92.

120   Chang, W.-S., Shang, H., Perera, R.M., Lok, S.-m.*, et al.*, Analyst, 2008. **133**(2): p. 233.

121   Krishnan, J.N., Kim, C., Park, H.J., Kang, J.Y.*, et al.*, Electrophoresis, 2009. **30**(9): p. 1457.

122   Choi, J.W., Liakopoulos, T.M. and Ahn, C.H., Biosens. Bioelectron., 2001. **16**(6): p. 409.

123   Ramadan, Q., Samper, V., Poenar, D., and Yu, C., J. Magn. Magn. Mater., 2004. **281**(2-3): p. 150.

124   Sinha, A., Ganguly, R. and Puri, I.K., J. Magn. Magn. Mater., 2009. **321**(14): p. 2251.

125   Smistrup, K., Tang, P.T., Hansen, O., and Hansen, M.F., J. Magn. Magn. Mater., 2006. **300**(2): p. 418.

126   Chen, H., Kaminski, M.D., Caviness, P.L., Liu, X.*, et al.*, Phys. Med. Biol., 2007. **52**(4): p. 1185.

127   Deng, T., Prentiss, M. and Whitesides, G.M., Appl. Phys. Lett., 2002. **80**(3): p. 461.

128   Deng, T., Whitesides, G.M., Radhakrishnan, M., Zabow, G.*, et al.*, Appl. Phys. Lett., 2001. **78**(12): p. 1775.

129   Bronzeau, S. and Pamme, N., Anal. Chim. Acta, 2008. **609**(1): p. 105.

130   Hayes, M.A., Polson, N.A., Phayre, A.N., and Garcia, A.A., Anal. Chem., 2001. **73**(24): p. 5896.

131   Lien, K.-Y., Lin, J.-L., Liu, C.-Y., Lei, H.-Y.*, et al.*, Lab Chip, 2007. **7**(7): p. 868.

132   Jiang, G.F. and Harrison, D.J., Analyst, 2000. **125**(12): p. 2176.

133   Fan, Z.H., Mangru, S., Granzow, R., Heaney, P.*, et al.*, Anal. Chem., 1999. **71**(21): p. 4851.

134   Smistrup, K., Kjeldsen, B.G., Reimers, J.L., Dufva, M.*, et al.*, Lab Chip, 2005. **5**(11): p. 1315.

135   Doyle, P.S., Bibette, J., Bancaud, A., and Viovy, J.L., Science, 2002. **295**(5563): p. 2237.

136   Slovakova, M., Minc, N., Bilkova, Z., Smadja, C.*, et al.*, Lab Chip, 2005. **5**(9): p. 935.

137   Bilkova, Z., Slovakova, M., Minc, N., Futterer, C.*, et al.*, Electrophoresis, 2006. **27**(9): p. 1811.

138   Park, J., Jung, S.H., Kim, Y.H., Kim, B.*, et al.*, Lab Chip, 2005. **5**(1): p. 91.

139   Xia, N., Hunt, T.P., Mayers, B.T., Alsberg, E.*, et al.*, Biomed. Microdevices, 2006. **8**(4): p. 299.

140   Siegel, A.C., Shevkoplyas, S.S., Weibel, D.B., Bruzewicz, D.A.*, et al.*, Angew. Chem. Int. Ed., 2006. **45**(41): p. 6877.

141   Lin, Y.A., Wong, T.-S., Bhardwaj, U., Chen, J.-M.*, et al.*, J. Micromech. Microeng., 2007. **17**(7): p. 1299.

142   Pamme, N. and Manz, A., Anal. Chem., 2004. **76**(24): p. 7250.

143   De Leonardis, F., Tarn, M.D., Pascali, G., Salvadori, P.A.*, et al.*, J. Labelled Compd. Radiopharm., 2011. **54**: p. S46.

144   De Leonardis, F., Pascali, G., Salvadori, P.A., Watts, P.*, et al.*, J. Chrom. A, 2011. **1218**(29): p. 4714.

145   Boyes, W., *Instrumentation reference Book*. Third edition ed. 2003: Butterworth-Heinemann. 1062.

146   Alexoff, D.L., Casati, R., Fowler, J.S., Wolf, A.P.*, et al.*, App. Radiat. Isot., 1992. **43**(11): p. 1313.

147   Shiue, C.Y., Fowler, J.S., Wolf, A.P., Alexoff, D.*, et al.*, J. Labelled Compd. Radiopharm., 1985. **22**(5): p. 503.

148   Nakao, R., Ito, T., Yamaguchi, M., and Suzuki, K., Nucl. Med. Biol., 2005. **32**(8): p. 907.

149   Nakao, R., Ito, T., Yamaguchi, M., and Suzuki, K., Nucl. Med. Biol., 2008. **35**(2): p. 239.

150   Fuechtner, F., Preusche, S., Maeding, P., Zessin, J.*, et al.*, Nucl. Med. Biol., 2008. **47**(3): p. 116.

151   Bogni, A., Pascali, C., Iwata, R., Cavalleri, A.*, et al.*, J. Radioanal. Nucl. Chem., 1998. **230**(1-2): p. 45.

152   Kuge, Y., Nishijima, K., Nagatsu, K., Seki, K.*, et al.*, Nucl. Med. Biol., 2002. **29**(2): p. 275.

153   Scott, P.J.H. and Kilbourn, M.R., Appl. Radiat. Isot., 2007. **65**(12): p. 1359.

154   Ma, Y., Huang, B.X., Channing, M.A., and Eckelman, W.C., Nucl. Med. Biol., 2002. **29**(1): p. 125.

155   Drumhiller, J.A., Laing, J.L. and Taylor, R.W., Anal. Chim. Acta, 1984. **162**(AUG): p. 315.

156   Fuchtner, F., Preusche, S., Mading, P., Zessin, J.*, et al.*, J. Nucl. Med., 2008. **47**(3): p. 116.

157   Coenen, H.H., Pike, V.W., Stocklin, G., and Wagner, R., Appl. Radiat. Isot., 1987. **38**(8): p. 605.

158   Channing, M.A., Huang, B.X. and Eckelman, W.C., Nucl. Med. Biol., 2001. **28**(4): p. 469.

159   Fuchtner, F., Steinbach, J., Mading, P., and Johannsen, B., Appl. Radiat. Isot., 1996. **47**(1): p. 61.

160   *Fludeoxyglucose (^{18}F) injection*, in *European Pharmacopeia*. 2002, European Directorate for the Quality of the medicines: Strasbourg, France. p. 2316.

161   Solin, O., Bergman, J., Haaparanta, M., and Reissell, A., Appl. Radiat. Isot., 1988. **39**(10): p. 1065.

162   Iwata, R., Ido, T., Brady, F., Takahashi, T.*, et al.*, Appl. Radiat. Isot., 1987. **38**(11): p. 979.

163   Pascali, G., D'Antonio, L., Bovone, P., Gerundini, P.*, et al.*, Nucl. Med. Biol., 2009. **36**(5): p. 569.

164   McCreedy, T., TrAC, Trends Anal. Chem., 2000. **19**(6): p. 396.

165   Fluigent. [accessed 2012 February]; Available from: http://www.azonano.com/article.aspx?ArticleID=2027.

166   Lee, J., Uhm, J., Lee, W., Lee, S.*, et al.*, Bull. Korean Chem. Soc., 2005. **26**(12): p. 1986.

167   Park, M.H., Jang, Y.J., Sung-Suh, H.M., and Sung, M.M., Langmuir, 2004. **20**(6): p. 2257.

168   Hartshorne, H., Backhouse, C.J. and Lee, W.E., Sens. Actuators, B, 2004. **99**(2-3): p. 592.

169   Roach, L.S., Song, H. and Ismagilov, R.F., Anal. Chem., 2005. **77**(3): p. 785.

170   Chen, Z.P., Xu, R.Z., Zhang, Y., and Gu, N., Nanoscale Res. Lett., 2009. **4**(3): p. 204.

171   Chuang, Y.-J., Huang, J.-W., Makamba, H., Tsai, M.-L.*, et al.*, Electrophoresis, 2006. **27**(21): p. 4158.

172   Oosterhof, J.J.H., Buijssen, K., Busscher, H.J., van der Laan, B.*, et al.*, Appl. Environ. Microbiol., 2006. **72**(5): p. 3673.

173   Arkles, B., Chemtech, 1977. **7**(12): p. 766.

174   Arkles, B., *Gelest Catalog for Silicon Compounds: Silanes and Silicones*. 2nd ed, ed. B. Arkles and G. Larson. 2008: Gelest.

175   Zagordini, A.A., *Ion Exchange Materials: Properties and Application*. 2007, Oxford: Elsevier.

176   De Leonardis, F., Pascali, G., Salvadori, P.A., and Pamme, N. *Microfluidic modules for [^{18}F-]activation – Towards an integrated modular lab on a chip for PET radiotracers synthesis.* in *Proceeding of the MicroTas*. 2010.

177   Pascali, G., Mazzone, G., Saccomanni, G., Manera, C., *et al.*, Nucl. Med. Biol., 2010. **37**(5): p. 547.

178   Peyman, S.A., Patel, H., Belli, N., Iles, A., *et al.*, Magnetohydrodynamics, 2009. **45**(3): p. 361.

179   Peyman, S.A., Iles, A. and Pamme, N., Lab Chip, 2009. **9**(21): p. 3110.

180   Vojtisek, M., Iles, A. and Pamme, N., Biosens. Bioelectron., 2010. **25**(9): p. 2172.

181   Tarn, M.D. and Pamme, N., Expert Review of Molecular Diagnostics, 2011. **11**(7): p. 711.

182   Tarn, M.D., Hirota, N., Iles, A., and Pamme, N., Science and Technology of Advanced Materials, 2009. **10**(1).

183   Tarn, M.D., Peyman, S.A., Robert, D., Iles, A., *et al.*, J. Magn. Magn. Mater., 2009. **321**(24): p. 4115.

184   Pamme, N., *Single Particle Analysis in Microfluidic Chips*. 2004, Imperial College London: London.

185   Kap-Soo, Journal of the Korean Institue of Chemicals Engineers, 1977. **15**(6): p. 422.

186   Kim, J., Ichimura, A.S., Huang, R.H., Redko, M., *et al.*, J. Am. Chem. Soc., 1999. **121**(45): p. 10666.

187   Peyman, S.A., Iles, A. and Pamme, N., Chem. Commun., 2008(10): p. 1220.